

Palladium complexes, nanoparticles and their use in coupling reactions of arylboronic acids in aqueous media

Azzedine Bouleghlimat

A thesis submitted for Degree of Doctor of Philosophy

School of Chemistry

Cardiff University

September 2013



DECLARATION

This work has not been submitted in substance for any other degree or award at this or any other university or place of learning, nor is being submitted concurrently in candidature for any degree or other award.

Signed Azzedine Z (candidate) Date 16/06/14

STATEMENT 1

This thesis is being submitted in partial fulfillment of the requirements for the degree of PhD (insert MCh, MD, MPhil, PhD etc, as appropriate)

Signed Azzedine Z (candidate) Date 16/06/14

STATEMENT 2

This thesis is the result of my own independent work/investigation, except where otherwise stated. Other sources are acknowledged by explicit references. The views expressed are my own.

Signed Azzedine Z (candidate) Date 16/06/14

STATEMENT 3

I hereby give consent for my thesis, if accepted, to be available for photocopying and for inter-library loan, and for the title and summary to be made available to outside organisations.

Signed Azzedine Z (candidate) Date 16/06/14

STATEMENT 4: PREVIOUSLY APPROVED BAR ON ACCESS

I hereby give consent for my thesis, if accepted, to be available for photocopying and for inter-library loans **after expiry of a bar on access previously approved by the Academic Standards & Quality Committee.**

Signed (candidate) Date

Acknowledgements

Whilst there are many people to thank for their help throughout these four years, it would be remiss of me not to thank those most responsible for getting me this far - my parents and brothers who never stopped supporting me even when I doubted myself.

First and foremost I would like to thank Niek for his guidance and encouragement - without his belief in me I doubt I would have been able to motivate myself to keep at it whenever failure seemed to be the only result of my research.

All researchers know how important it is to have others around to teach you and offer new viewpoints on your work, but they shouldn't underestimate how important a friendly work environment is, and so I would like to thank all of the members of the POC for making it a fun, helpful and friendly place to work, especially Jamie who was always there when I needed cheering up. You really made it some of the best years of my life.

I would like to thank everyone who has been involved in this research project, starting with Mazin who's own thesis laid the foundations for my work, and Alex, Ieuan and Pascaline who have all worked alongside me in the lab.

At times my project seemed more of a battle against faulty instruments than research, so I cannot forget to thank Rob, Robin, Alan and Steve for repairing or showing me how to repair myriad devices that were necessary for my work.

My project would likely have taken a very different route were it not for our group's collaborators - the group of Syuji in Osaka and the groups of Jorge, Pablo and Luis in Vigo. Special thanks are due to Patricia, Amane, Roberto and all of the others who made me welcome in Vigo, and to the Welsh Livery Guild and ESMI for funding my visit. I have never had a more enriching and enjoyable summer.

And finally, I should thank all of the rest of my friends for being there for me all of these years, and none more than Adam, who certainly made sure I completed this thesis on time with his constant encouragement and scolding. You really are always there for me when I need help.

Summary

This thesis is split into six chapters.

The first chapter introduces the homocoupling reaction of arylboronic acids, surfactants and aqueous solutions and nanoparticles.

The second chapter describes the synthesis of two different bisimidazolyl palladium catalysts, the characterisation of these catalysts, particularly the crystal structure, formation of aqua- and halogeno- complexes by NMR spectroscopy and the pK_a with varying halide concentration in both Laureth-10 and CTAB and the use of the of these catalysts in both Laureth-10 and CTAB to catalyse the homocoupling reaction of arylboronic acid and the pH rate profile in CTAB and in Laureth-10 at a variety of different halide concentrations, the origin of which is identified.

The third chapter describes the use of polystyrene-immobilised polypyrrole-palladium nanocomposite catalyst in the homocoupling reaction of arylboronic acids in aqueous solutions, with a particular interest in the effect of pH and halide addition on the reaction, and that the particles are recoverable and reusable with centrifugation.

The fourth chapter describes the use of a paper-immobilised palladium nanoparticle catalyst in the homocoupling reaction of arylboronic acids in aqueous and ethanolic aqueous solutions, and the Suzuki-Miyaura cross-coupling reaction in ethanolic aqueous solutions.

The fifth chapter describes the effect of nitric oxide release in the body and the synthesis of CTAB capped gold nanoparticles and their use in the release of nitric oxide from S-Nitrosothiols which will be measured using an NO selective probe.

The final chapter is an epilogue in which ideas for future experiments, or plans for experiments that were not accomplished are discussed.

Contents

Acknowledgements	i
Summary	ii
Chapter 1 - Introduction	1
1.1 - Carbon-Carbon Bond Formation	2
1.1.1 - Biaryl-containing Compounds	3
1.1.2 - Palladium-catalysed Coupling Reactions	5
1.1.3 - Suzuki-Miyaura Reaction	8
1.1.4 - Oxidative Homocoupling Reaction of Arylboronic Acids	14
1.2 - Environmental Considerations	17
1.2.1 - Boronic acid synthesis	17
1.2.2 - Water as a Reaction Medium	20
1.2.3 - Surfactants	21
1.3 - Nanoparticles	26
1.3.1 - Properties of nanoparticles	26
1.3.2 - Use of Nanoparticles in Antiquity	28
1.3.3 - Contemporary applications of nanoparticles	29
1.4 - Goals	30
1.5 - Bibliography	31
Chapter 2 - Synthesis of Bisimidazolyl-palladium Complexes	38
2.1 - Introduction	41
2.1.1 - Palladium Catalysts	41
2.1.2 - Bisimidazolyl catalysts	44
2.1.3 - Palladium-catalysed coupling reactions	46

for the homocoupling reaction of 6 in Laureth-10 solutions	118
2.2.3e - Effect of chloride concentration on the pH-rate profile for the homocoupling reaction of 6 in laureth-10 solutions	122
2.2.3f - MEGA-10 as a surfactant for the homocoupling reaction	127
2.3 - Conclusions	129
2.4 - Experimental	131
2.4.1 - General	132
2.4.2 - Synthesis of Bisimidazole 1	133
2.4.3 - Synthesis of Ligand 2	133
2.4.4 - Synthesis of Bisimidazole 3	134
2.4.5 - Synthesis of Ligand 4	135
2.4.6 - Synthesis of Ligand 5	136
2.4.7 - Synthesis of Catalyst PdCl ₂ -2	137
2.4.8 - Synthesis of Catalyst PdCl ₂ -4	138
2.4.9 - Synthesis of Catalyst PdCl ₂ -5	139
2.4.10 - XRD crystallography	140
2.4.11 - NMR experiments	140
2.4.12 – UV-visible titrations	140
2.4.13 - Kinetic experiments	141
2.5 - Bibliography	142
Chapter 3 - Kinetic Studies of the Homocoupling of Arylboronic acids by Pd-PPy Nanoparticles	145

3.1 - Introduction	147
3.1.1 - The homocoupling reaction and homogeneous catalysts.	147
3.1.2 - Heterogeneous catalysts and nanoparticles	148
3.1.3 - Polystyrene-immobilised Pd-PPy nanocomposites	150
3.2 - Results and Discussion	152
3.2.1 - Catalyst loading	152
3.2.2 - Pd-PPy-PS particle recovery	159
3.2.3 - Effect of halide on Pd-PPy-PS particle activity	165
3.3 - Conclusions	178
3.4 - Experimental	178
3.4.1 - Chemicals	178
3.4.2 - Techniques	179
3.4.3 - Kinetic experiments	180
3.4.4 - HPLC	181
3.4.5 - Catalyst Recovery	181
3.5 - Bibliography	182
Chapter 4 - Kinetic Studies of the Homocoupling of Arylboronic acids by Paper-Immobilised Pd Nanoparticles	183
4.1 - Introduction	185
4.1.1 - Nanoparticle Catalysts	185
4.1.2 - The Suzuki-Miyaura cross-coupling reaction	186
4.1.3 - Previous Work	187
4.1.4 - Objectives	192
4.2 - Results and Discussion	192
4.2.1 - Reproducing Homocoupling data "shaken, not stirred"	192

4.2.2 - pH dependence of the homocoupling reaction	203
4.2.3 - Effect of ethanol addition on the homocoupling reaction	206
4.2.4 - Suzuki-Miyaura Reaction	209
4.3 - Conclusions	228
4.4 - Experimental	229
4.4.1 - Chemicals	229
4.4.2 - Techniques	229
4.4.3 - Homocoupling and cross-coupling experiments	230
4.4.3 - HPLC	231
4.5 - Bibliography	232
Chapter 5 - Synthesis of gold nanoparticles for nitric oxide release	233
5.1 - Introduction	236
5.1.1 - Applications of Nanoparticles	236
5.1.2 - Nitric oxide release	238
5.1.3 - Use of Nanoparticles for NO release	242
5.1.4 - Previous Work and outline of Study	244
5.2 - Results and Discussion	245
5.2.1 - Effect of CTAB concentration on NO release from 15 nm gold nanoparticles	245
5.2.2 - Nitrosothiol binding with 60 nm gold nanoparticles	251
5.2.3 - Effect of Gold Particle concentration on NO release	254
5.3 - Conclusions and future work	257
5.4 - Experimental	258
5.4.1 - Chemicals	258
5.4.2 - Techniques	258

5.4.3 - Synthesis of 15 nm Nanoparticles	258
5.4.4 - Growth of 60 nm Nanoparticles	259
5.4.5 - NO release experiments - General procedures	260
5.5 - Bibliography	262
Chapter 6 - Epilogue	265
Appendix	269

Chapter 1

Introduction

The chemical industry is truly massive in both scale and importance to the modern world, and was worth globally in excess of \$4,000,000,000,000 in 2010 in the midst of the economic ‘crisis’.¹ This equates to roughly 400,000,000 tons of organic chemicals alone being produced every year² and in the process this generates a large amount of waste. This waste is a serious issue environmentally for two main reasons - it represents a waste of resources and energy and any waste must be properly treated and disposed of which can be costly. For these reasons, there is a big drive towards improving the environmental qualities of reactions, not just because it is the right thing to do, but there are also economic advantages from efficiency (and also from avoiding fines from Governments who are increasingly concerned with pollution and waste).

1.1 - Carbon-Carbon Bond Formation

Synthetic chemistry relies on a wide range of reactions in order to synthesise a broad spectrum of different chemicals - some are highly specific reactions and are used for making a small range of products, whilst others are much more general and are commonly used in the creation of incredibly varied products. Almost all organic molecules contain carbon-carbon bonds, and as such the ability to form carbon-carbon bonds is one of the most powerful tools an organic chemist can have. There is a multitude of reactions available for carbon-carbon bond formation, including aldol reactions,³ Diels-Alder reactions,⁴ Friedel-Crafts reactions⁵ and Grignard reactions⁶ all of which are suited for different purposes. Whilst many reactions are suitable for connecting alkyl components together, fewer are suitable for connecting aryl components together.

1.1.1 - Biaryl-containing compounds

The biaryl motif is a common one, both in nature and in chemical products, which is why the ability to synthesise biaryl compounds is so important. Pharmaceutically, there are many classes of drugs that contain biaryl functionalities. For example, one class are the Angiotensin II receptor antagonists, which are used to treat hypertension, kidney damage and migraines.⁷ There are many different Angiotensin II receptor agonists currently available, such as Valsartan,⁸ Losartan⁹ and Telmisartan¹⁰ (Figure 1), they all contain linked aryl systems which play a key role in binding to the target receptor. A second example of a compound that involves linked aryl rings to bind to target receptors is being tested by GSK for binding to dopamine D₃ receptors, which has potential applications for treating psychological disorders and drug addiction.¹¹ A third class of pharmaceuticals that make use of linked aryl rings are statins used for reducing cholesterol production, such as Atorvastatin (Figure 1) which is one of the most successful pharmaceuticals in history with annual sales exceeding \$10 billion.¹²

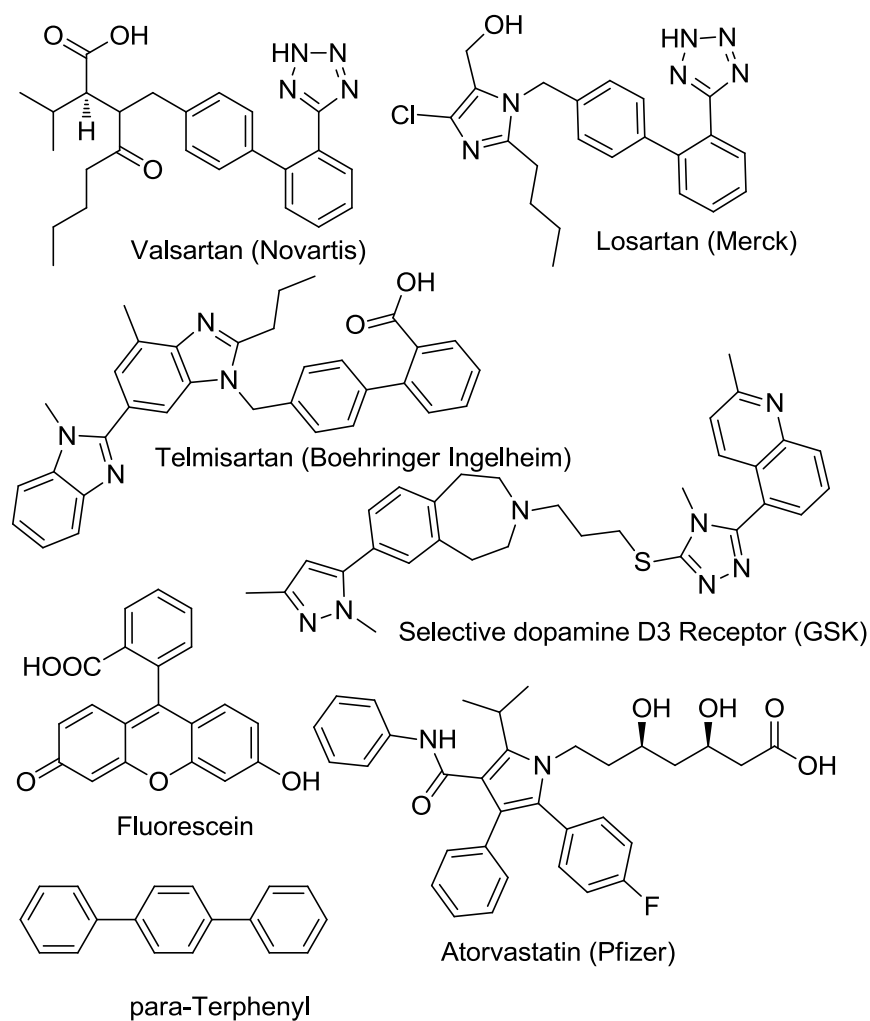


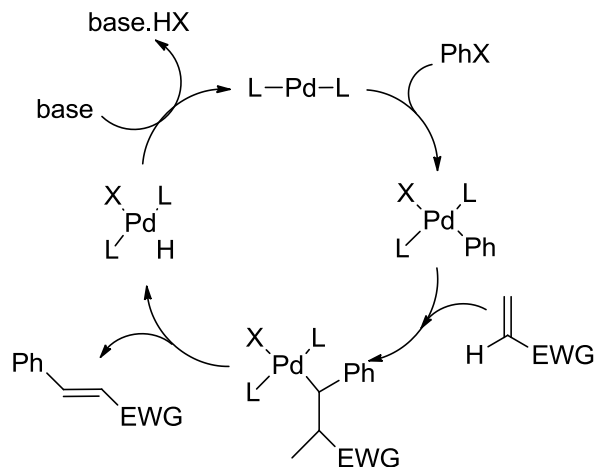
Figure 1 - Examples of biaryl containing pharmaceuticals and photocatalysts.

Linked aryl rings are not only used for binding to biological receptors. Due to the extended π -system present in most poly-aryl systems they are often chromophores and often get employed in photochemistry. For example, p-terphenyl (Figure 1) is a commonly used photocatalyst used to initiate photochemical processes by absorbing photons (as the triple aryl system is a good chromophore) and transferring the excitation energy to other species.¹³ Fluorescein (Figure 1) is

another compound where the extended π -system in the poly-aryl gives it useful photophysical properties, although it is less commonly used a photocatalyst and is more useful as a fluorescent dye.¹⁴ Dyes are also increasingly promising as components of organic solar cells, which would enable solar energy to be harvested without the use of expensive (such as silicon) or rare elements (such as indium or tellurium).¹⁵ The dyes can be added to the surface of titanium dioxide or zinc oxide¹⁶ nanowires in order to collect photons and pass the excitation into the nanowires, thus generating a current with an efficiency of ~10%.¹⁵

1.1.2 - Palladium-catalysed Coupling Reactions

The most important class of reactions for synthesising compounds containing aryl functionalities is probably that of catalysed coupling reactions. The first of these to be discovered was the Mizoroki-Heck reaction in 1971 (Scheme 1) that allows the coupling of an aryl halide with an alkene using a Pd [0] catalyst.¹⁷ Whilst not capable of producing a biaryl, the discovery was highly significant and was the precursor to a whole field of reactions that allowed the creation of bonded conjugated compounds from different precursors (no doubt one of the reasons for Heck being awarded the 2010 Nobel prize, amongst others).



Scheme 1 –Mechanism for a typical Mizoroki-Heck reaction.

The successor reactions are mainly based around substituting the alkene which allows for two things – 1) a wider range of organic groups that can be added and 2) a better leaving group for increased reactivity. These developments have propelled this class of reactions to being a synthetic staple.

Expanding Heck and Mizoroki's work lead to the development of the Sonogashira reaction, which, in addition to a palladium-based catalyst, usually uses a Cu co-catalyst and base to couple an alkyne to an aryl halide.¹⁸ The Cu catalyst increases the activity of the alkyne group by substituting the terminal proton with Cu and thus allows the reaction to proceed under much more gentle conditions than the Heck reaction. Recent advances have even used alternate bases¹⁹ and attuned substrates²⁰ to allow the reaction to proceed even in the absence of the Cu co-catalyst, but this is at the cost of harsher conditions or limited flexibility.

Ei-Ichi Negishi then discovered that organo-zinc-halo compounds could be used in place of the unfunctionalised aryl or alkenyl groups in conditions similar to the Heck reaction.²¹ The Negishi coupling however is not very widely employed, and as such there are relatively few references that discuss it (less than 2.5% of all papers published before 2013 on palladium-catalysed coupling reactions were about the Negishi Coupling). One of the reasons for the limited popularity of the Negishi coupling is the high degree of homocoupling of the phenyl-zinc compounds, even in the absence of air. Unlike the proposed mechanism for the aerobic homocoupling reaction of arylboronic acids (*vide infra*) the high degree of homocoupling is suggested to be due to a slow reductive elimination step. Before the cross-coupled product reductively eliminates from the palladium a second phenyl-zinc molecule can transmetallate and exchanges its phenyl group with the palladium which can result in the homocoupled product.²²

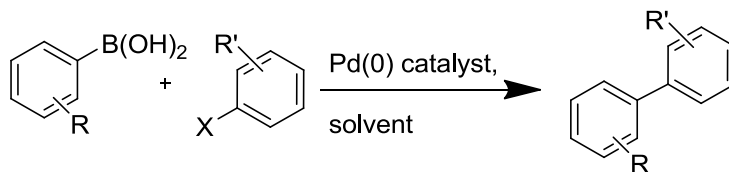
The next major advance in the field was the work of Stille.²³ The Stille coupling is still one of the most commonly used synthetic reactions due to its reputation of reliability across a wide range of substituents. However, the trialkylstannates used in the Stille coupling are highly toxic.²⁴ Whilst commonly used in the pharmaceutical industry, an alternative reaction that was equally robust but did not employ a reactant or leave a byproduct as toxic as an organotin compound would obviously be desirable.

One of the problems faced by many cross-coupling reactions is the potential for an aerobic side reaction that generates a homocoupled byproduct. The reason that the majority of the palladium-catalysed coupling reactions use aryl halides as one of the reactants is that they double as the stoichiometric oxidant in the reaction, and their oxidative addition to palladium⁰ initiates the

catalytic cycle. The formation of homocoupled side products is generally thought to be caused by the oxidation of the palladium catalyst by molecular oxygen as the stoichiometric oxidant to form a peroxo complex.²⁵ Once the palladium species is oxidised the non-halogenated reactant can homocouple by performing two successive transmetallations with the palladium centre followed by reductive elimination. Unless the two aryl substrates used in the cross-coupling reaction involve the same aromatic system, the additional homocoupling reaction results in two different biaryl products being formed. This not only directly decreases the yield of the process, separating two different biaryl systems is also less straightforward than separating biaryls from the other waste products from the reaction. For this reason palladium-catalysed coupling reactions are typically performed under inert atmosphere to limit the homocoupled product (although this is not sufficient for the prevention of homocoupling in the Negishi reaction).²²

1.1.3 - Suzuki-Miyaura Reaction

The most widely employed and heavily studied palladium-catalysed reaction is the Suzuki-Miyaura reaction (Scheme 2). Interest in the reaction has been steadily growing since its discovery in 1979 by Akira Suzuki, Norio Miyaura and Kinji Yamada.²⁶



Scheme 2 - The Suzuki Miyaura cross-coupling reaction.

Of late the number of papers published that study or employ the Suzuki-Miyaura reaction has been greater than on any other palladium-catalysed coupling reaction, and the rate of year on year growth is also greater than for other reactions (Figure 2).

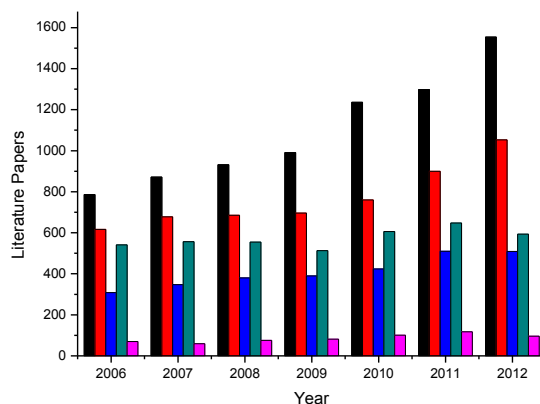
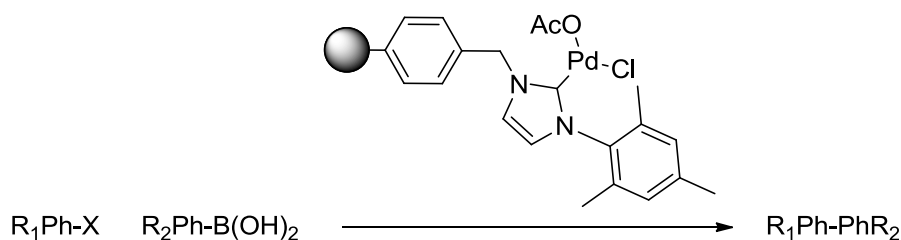


Figure 2 – The number of papers published between 2006 and 2012 which utilised Suzuki, Stille, Sonogashira, Heck and Negishi reactions.²⁷

The Suzuki-Miyaura reaction is of particular interest when compared to its counterparts because the substrate used is an arylboronic acid, which is far less toxic and environmentally damaging than other substrates such as stannates or organozinc compounds. In addition, the leaving group

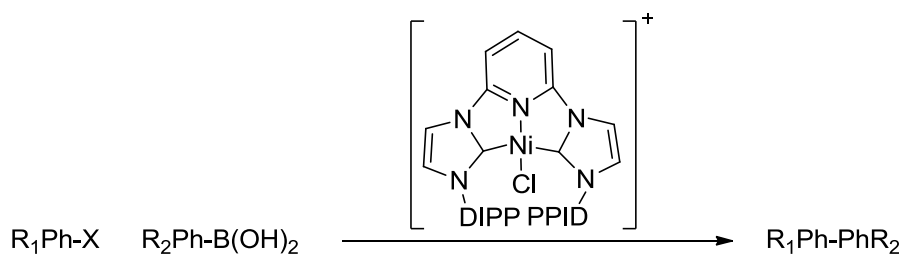
is far lighter than the corresponding stannates, so less mass is wasted in the reaction when compared to the Stille coupling. Additionally, arylboronic acids are far more soluble in water than the stannates, alkynes or alkenes used in other homocoupling reactions. The borate byproduct is readily removed by aqueous extraction (along with the halide salts from the aryl halide) whilst the products are typically hydrophobic and therefore remain in the non-polar phase.

Recent interest in the Suzuki-Miyaura reaction has been in a number of different areas. Three major avenues for investigation for any catalytic reaction are the catalyst, the substrate(s) and the conditions for the reaction. N-heterocyclic carbenes (NHCs) have attracted a great deal of attention since they make good ligands for a metal catalyst that remain stable even at high temperatures.²⁸ In addition, the energy level of the carbene lone pair can be modulated by changing the groups attached to the NHC's nitrogens. This in turn allows a great degree of control over the catalyst's properties. Additionally, the nitrogen groups of NHCs are a good position to attach the ligand to a solid support allowing the creation of a heterogeneous catalyst that can be easily recovered (an especially important concern given the value of both the metal and the ligands). Several groups have made progress in this area, such as the group of Lee *et al.* who synthesised polystyrene-immobilised palladium-NHC complexes that were both stable and reusable in the Suzuki reaction with aryl iodides, bromides and even chlorides at high temperatures (100 °C).²⁹



Scheme 3 – A polymer supported NHC-palladium catalyst used in the Suzuki reaction by Lee *et al.*²⁹

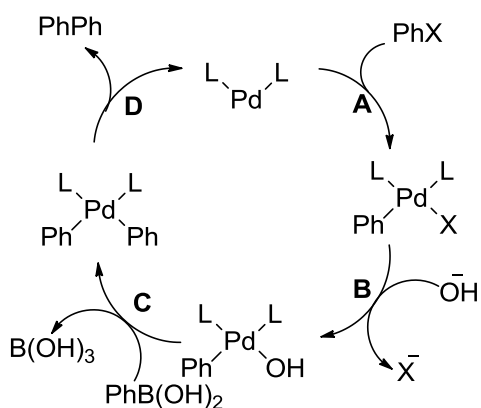
Another example uses an NHC-palladium catalyst bound to an iron oxide support by Gao *et al.* that achieved good yields and reusability in the Suzuki reaction of aryl iodides and bromides at 50 °C.³⁰ Palladium is expensive due to its low abundance, but fortunately it's not the only metal that can catalyse Suzuki coupling reactions. Nickel is generally a less active catalyst, but with the correct ligand system it can be a useful catalyst. Using a CNC pincer-type NHC-nickel catalyst Inamoto *et al.* were able to achieve yields of up to 94% depending on the boronic acid and aryl halide used (Scheme 4).³¹



Scheme 4 – A CNC pincer type NHC-nickel catalyst used in the Suzuki reaction by Inamoto *et al.*³¹

Another area of interest is in the substrate for the Suzuki reaction. Lloyd-Jones *et al.* have been investigating the use of the aryl trifluoroborates in the Suzuki reaction as a source of slow-released arylboronic acid.³² Since the boronic acid can homocouple under the reaction conditions (*vide infra*), having it slowly released keeps its concentration low which will inhibit the homocoupling pathway relative to the cross coupling pathway.

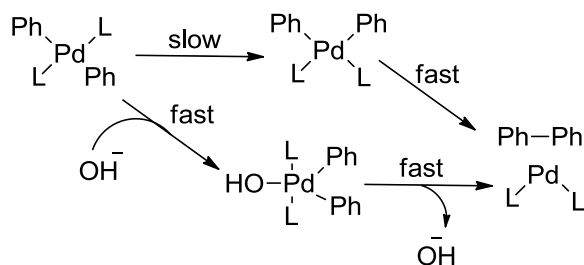
The mechanism of the Suzuki-Miyaura coupling reaction (Scheme 5) has been studied in depth by many authors, most notably by Amatore *et al.* who have probed the mechanism of the transmetallation step.³³



Scheme 5 – The currently accepted mechanism for the Suzuki Miyaura reaction comprising of (A) oxidative addition, (B) halide displacement, (C) transmetallation and (D) reductive elimination.

In particular Amatore *et al.* looked at the effect of base on the reaction and found it had three effects on the reaction. They found that the base plays two roles in the transmetallation step (Scheme 5.C). The primary role of the base is displacing the halide from the palladium to form a

hydroxo complex. This hydroxo complex, they suggested, was more reactive in the transmetallation step than the corresponding halide complex. In addition, increasing the amount of base leads to an increase in boronate formation, which they found to be less active in the transmetallation step than its boronic acid counterpart. The arylboronate slowing the reaction is contrary to the conventional wisdom that the arylboronate form is the active species in the transmetallation, which is often given as the reason that base accelerates the reaction.³⁴ In addition, Amatore *et al.* suggest that the base aids in the final reductive elimination by providing a faster alternative route to the slow cis-trans isomerisation required before reductive elimination can occur (Scheme 6).

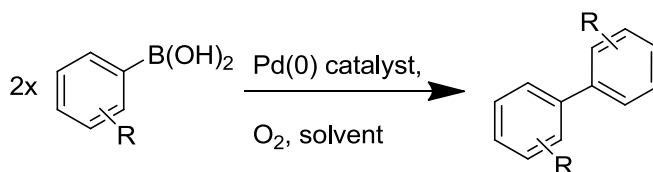


Scheme 6 – Base assistance in the reductive elimination step of the Suzuki Miyaura reaction.

Like other coupling reactions (*vide supra*) the Suzuki Miyaura reaction is typically performed under inert conditions as there is the potential for an oxidative homocoupling reaction of the arylboronic acids. In the Suzuki Miyaura reaction, this side reaction is obviously undesirable as it results in a loss of yield and a potentially non-trivial separation. However, this homocoupling could itself be employed in order to perform a palladium-catalysed coupling reaction that does not risk the production of multiple biaryl products or employ aryl halides.

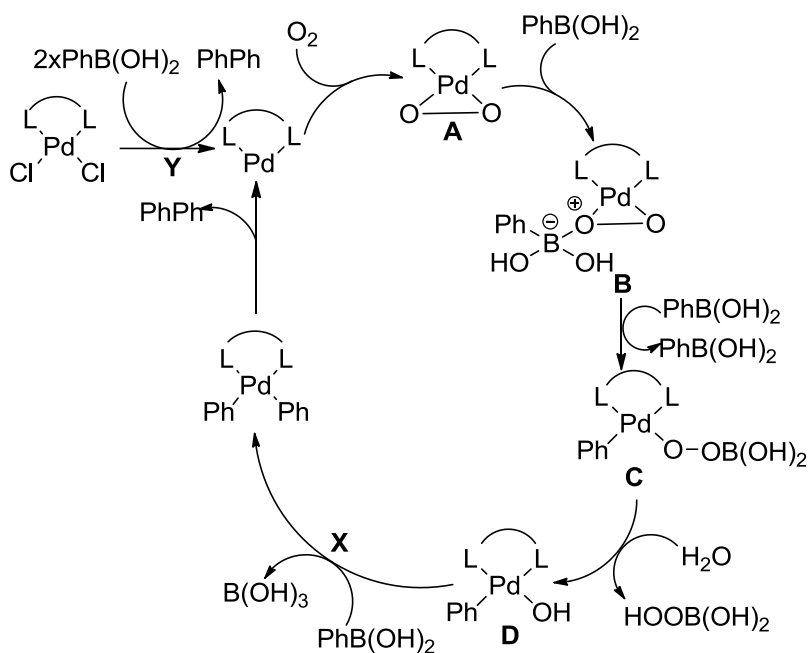
1.1.4 - Oxidative Homocoupling Reaction of Arylboronic Acids

The oxidative palladium-catalysed homocoupling reaction of arylboronic acids (henceforth 'the homocoupling reaction', Scheme 7) is very similar to the Suzuki Miyaura reaction in some respects, but has some key differences.



Scheme 7. The oxidative homocoupling reaction of arylboronic acids.

Since only arylboronic acids are used, the reactant is typically water soluble (unlike most aryl halides) and this would allow the reaction to be run in aqueous conditions. The elimination of arylhalides from the reaction makes it environmentally favourable (*vide infra*). The reaction no longer needs to be run under inert atmosphere (in fact that would be counterproductive as the system would be without an oxidant) which allows for simpler reaction conditions. The reaction is not without its drawbacks, however. The main drawback that is apparent in the homocoupling reaction is the production of phenol during the reaction.³⁵



Scheme 8. The proposed mechanism of the oxidative palladium catalyzed homocoupling reaction of arylboronic acids. (A) The peroxo Pd (0) species, (B) the first transmetalation and (C) the second transmetalation. The mechanism is based on work by Moreno-Manas³⁵ and Amatore²⁵ and is discussed in more detail in Chapter 2.

Amatore *et al.* and Moreno-Manas *et al.* both studied the homocoupling reaction and a mechanism based on their work has been derived (Scheme 8). The formation of the phenol is most likely due to the formation of peroxide species during the reaction. The peroxides form as a result of the reaction being initiated by the formation of the peroxopalladium complex **8.A** by molecular oxygen, as confirmed by Amatore *et al.*²⁵ Amatore then found that in substoichiometric additions of arylboronic acid to **8.A**, **8.B** formed that was replaced by the peroxoborate **8.C** upon addition of excess arylboronic acid. They suggest **8.B** is an intermediate for the first transmetalation. After the first transmetalation step the peroxide (Scheme **8.C**) is able to exchange with the solution and from there it is free to react with the arylboronic acid in a reaction which is known to produce phenols.³⁶ The second drawback is that by its nature the

reaction only reliably creates symmetrical biaryls, which would reduce its flexibility as a synthetic tool. It may be possible to employ the homocoupling as a cross-coupling reaction if two different boronic acids are used - purely statistically one would expect that in a 1:1 ratio the resultant product would be 50% cross-coupled and 50% the two different homocoupled products. If one boronic acid were far more precious than the other, the more available boronic acid could even be used sacrificially to improve the yield of the cross-coupled product with regards to the precious boronic acid. The usefulness of such a reaction would depend heavily on the ability to separate the cross-coupled product from the homocoupled product (although that may be easier in a 'real-world' application if the precious boronic acid was part of a much larger molecule than the abundant one). Alternatively, the reaction conditions and boronic acid choice may influence the cross-coupling vs. homocoupling ratio and if the relationship between these factors were better understood a cross-coupling reaction of boronic acids may be viable.³⁷

It often seems that it is impossible to declare a reaction strictly 'better' than another reaction, because frequently improvements in certain areas can only be made by paying costs in others. Balancing such costs and benefits is the essence of method development, since more often than not there are sacrifices that can be made that are much less of a cost compared to the gains you make. So, whilst there are clear gains to be made, one has to accept that there are limitations to the homocoupling reaction when compared to the Suzuki Miyaura reaction. Fortunately, the costs do not make the reaction pointless or useless since there is often a use for a more limited reaction if it performs better than the more broadly applicable reaction. This is especially true in industry; while a flexible reaction enables production to be set up easily, on large scale productions large efficiencies may be gained from using a more limited reaction if it is well

tailored for the task at hand. For example, if the homocoupling reaction allows the synthesis of a specific compound in water, the lower cost of disposing the waste (since neither the solvent nor the byproducts are toxic) may well save a lot of resources compared to the more generally applicable Suzuki Miyaura reaction.

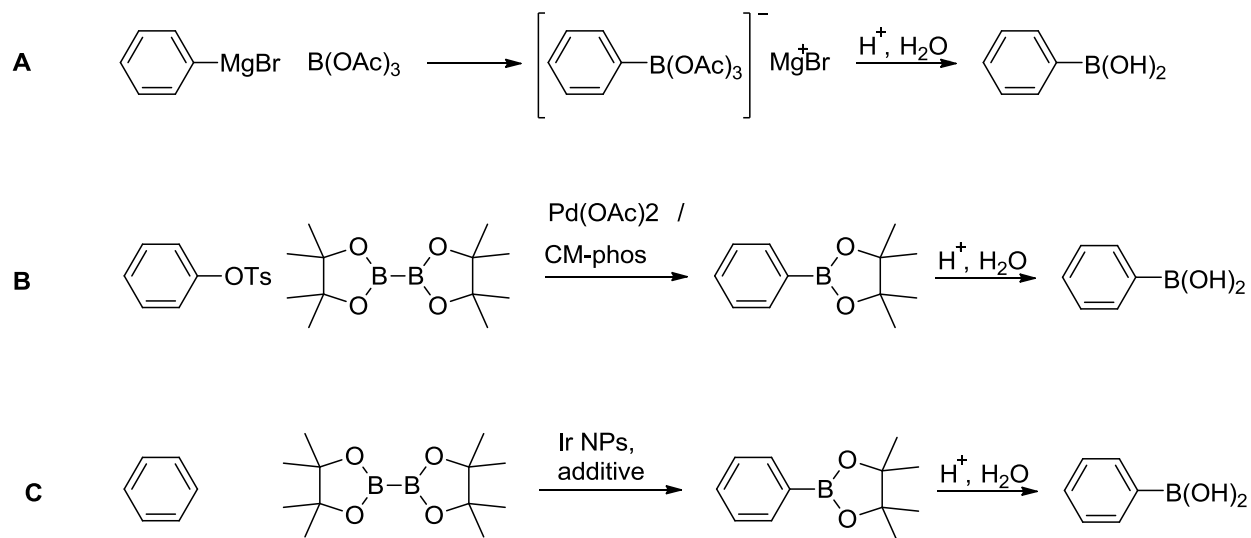
1.2 - Environmental Considerations

There is considerable interest from the pharmaceutical industry in reducing the need for organohalide compounds in industrial processes, due to the quantities of undesirable waste generated by their use.³⁸ Therefore, being able to replace the arylhalides in the Suzuki-Miyaura reaction, which is heavily used industrially, with arylboronic acids to in a homocoupling reaction would eliminate these undesirable halide waste products.

1.2.1 - Boronic acid synthesis

Unfortunately, the use of boronic acids does not necessarily remove the impact of organohalides from the overall production process. The reason for this is that, while the arylboronic acids may not cause environmental damage themselves, they are produced industrially from aryl halides via Grignard reagents (Scheme 9.A).³⁹ Fortunately, alternative syntheses that are more environmentally friendly are being explored. The main approach to replace the Grignard route to

arylboronic acids involves catalytic borylation of aryl compounds, inspired by Miyaura's work on cross-coupling aryl halides with bispinacolatodiborane.⁴⁰ One way to modify this reaction to be more environmentally friendly is to replace the halide with a pseudohalide leaving group, as used by Kwong *et al.* (Scheme **9.B**).⁴¹ They used tosylates and mesylates to replace the halides, and used the products in situ to perform a Suzuki reaction simply by adding the second substrate to the newly formed arylboronic ester. These sulfonates are still costly leaving groups compared to a proton, so to this end some researchers, including Yinghuai *et al.*⁴² have investigated direct C-H bond activation. Direct C-H bond activation would allow, for example, the direct synthesis of phenylboronic acid from benzene. To achieve this they used an Ir(0) nanoparticulate catalyst dissolved in an ionic liquid to react with bispinacolatodiborane (Scheme **9.C**), and the product could be extracted from the ionic liquid with ether, allowing the catalyst to be easily separated and reused. If the borylation can be directed to specific sites in substituted aryl compounds then this could be a suitable replacement for the current industrial synthesis of arylboronic acids.

Scheme 9. Synthetic routes to arylboronic acids.^{39, 41-42}

The elimination of the need for organohalides is not the only way to improve the environmental impact of coupling reactions. As mentioned before, increasing the recoverability and reusability of the palladium catalyst is very useful for financial reasons (given the value of palladium, and the cost of synthesising catalysts) and environmental reasons (as palladium is a toxic heavy metal and ideally it should not be disposed of as waste). Whilst it is possible to recover precious metals from chemical waste, it is far more efficient to recover functional catalysts from the reaction mixture and reuse them than to recover metal from waste and resynthesise the catalyst. Additionally, energy use is a big concern since energy prices are always rising and many countries are imposing regulation to discourage energy inefficiency. If a synthetic reaction can be performed at an appropriate rate at a low temperature then there will be a large energy saving, which reduces the impact of the process.

1.2.2 - Water as a Reaction Medium

Probably the most widely wasted class of chemicals are solvents, accounting for 75-80% of waste in the pharmaceutical industry.³⁸ Much chemistry is done in dilute systems to keep reactions under control and to ensure good yields, since concentrated reactions are susceptible to thermal effects that can cause unwanted side reactions. This means that the solvent can be considered a necessary evil, a price that one has to pay to perform the desired reaction, but that solvent does not contribute directly to the yield of the reaction. Solvent-free reactions, such as reactions where one or more of the reagents also doubles as the reaction solvent,⁴³ or where the whole reaction is performed in solid-phase,⁴⁴ are being explored due to their lower waste generation. Unfortunately, however, exclusion of solvent is not always possible.

Instead of removing the solvent altogether, changing the solvent can be an easier approach. Palladium-catalysed coupling reactions typically use organic solvents, such as toluene or DMF, which are flammable and toxic (especially DMF) and costly to purchase and dispose of. Water is a very desirable solvent since it is typically cheap and plentiful, non-toxic and non-flammable which makes it safer to use and dispose of. Additionally, water allows for far more predictable control of pH in solution since K_w is well-understood. However, the use of water as a solvent brings its own complications to a reaction that need consideration. Many chemicals (such as Grignard reagents that are often used in C-C bond forming reactions) are water-sensitive and hydrolyse in aqueous conditions (sometimes violently), and if reagents of this kind are needed for a reaction then water cannot be a suitable solvent. The second complication is solubility, since the most common catalysts for aryl-aryl coupling reactions, such as $\text{Pd}(\text{PPh}_3)_4$, are

insoluble in water this would be a problem. There are two solutions to this – change the catalyst or change the solvent system.

1.2.3 - Surfactants

Surfactants, such as cetyltrimethylammonium bromide (CTAB) and decaethylene glycol monododecyl ether (Laureth-10) (Figure 3), are comprised of two parts - a polar head group and a non-polar tail.

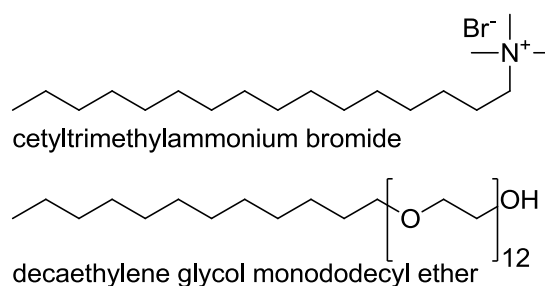


Figure 3 – The surfactants CTAB and Laureth-10.

The dual nature of the molecule means that they can be used to solubilise non polar compounds in a polar solvent (or conversely for solubilising a polar compound in a non polar solvent⁴⁵). The surfactants order themselves around non-polar compounds so that these interact with the non-polar tail, whilst the polar head group faces into the bulk polar solvent (Figure 4).

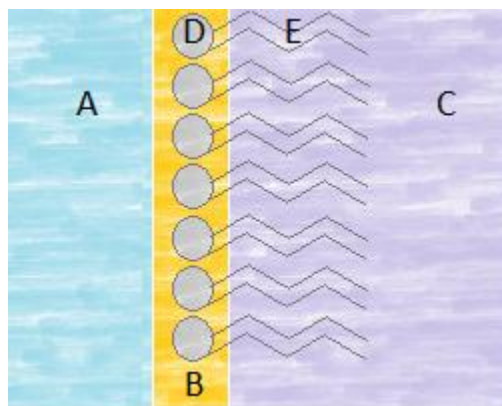


Figure 4 - Surfactant structure. **A** Aqueous region, **B** Stern region, **C** Non-polar region, **D** Polar headgroup, **E** Non-polar tail.

Above the critical micelle concentration (CMC) this ordering of the surfactants results in the formation of transient microscale structures called micelles. A single layer of surfactants forms a sphere (or depending on conditions a rod) where all the head groups face out to interact with the solvent, and the interior is a non-polar environment available for solubilising non-polar compounds (Figure 5). The area around the polar head groups at the interface of the aqueous phase and the non-polar internal area is the so-called Stern region.

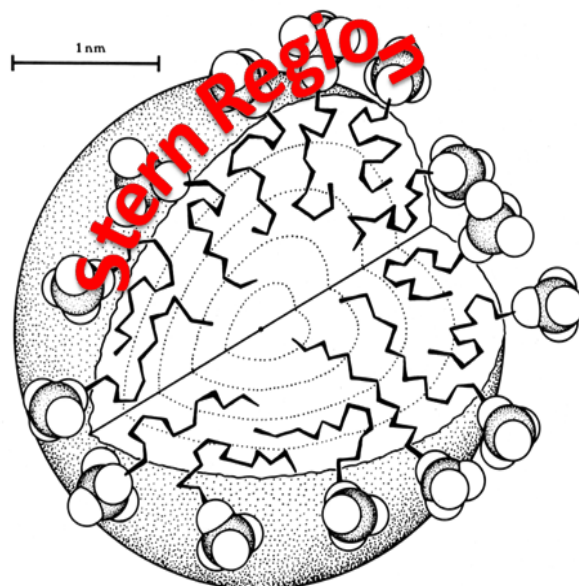


Figure 5. Schematic of a spherical micelle with the Stern region indicated.

The Stern region is where the high concentration of non-polar compounds inside the micelle and polar compounds in the aqueous phase can come into contact and has a drastically higher surface area of the non-polar/polar interface compared to conventional biphasic solvent systems such as toluene-water. The increased interface aids the rate of reaction. This effect is one of the reasons for the documented rate enhancement that is often found when adding surfactants to an aqueous reaction.⁴⁶ High local concentrations of reactants in the Stern region can induce high reaction rates, the so-called surfactant-induced rate acceleration, that can result in higher rates than one would get if the reaction was performed in a monophasic system at the same overall concentration.⁴⁷ In ionic micelles (where the head group is either positively or negatively charged) the high density of head groups in the Stern Region (the interface) results in a very high charge density, and

therefore causes a concentration of counter-ions in the Stern region. If the reactants are negatively charged, they will therefore be concentrated in the Stern region of the cationic surfactants, and the same is true of positively charged reactants in the Stern region of micelles formed by anionic surfactants. Since the concentration of non-polar compounds is also very high in the Stern region (as the internal volume of the micelles where they are present is very small) this results in much higher local concentrations in the Stern region than if species were evenly distributed across the reaction medium. This increased local concentration in the Stern region is a second reason for micellar rate enhancement effect. Local medium effects can also affect kinetics in micellar solutions/ For example where the polarity of the Stern region decreases the reaction rate can also decrease depending on the extent and type of charge formation in the activated complex of the reaction⁴⁸

The rate effect of high local reactant concentrations can make micellar catalysis very effective in supporting catalysis as a small amount of catalyst can result in a very high effective concentration in the Stern region, which can result in a very fast reaction if this is where the reactants bind as well. However, if the reaction involves both anions and cations, then concentrating one in the micelles and repelling the other may not be conducive to a rapid reaction as the two components will be electrostatically segregated. Nonionic surfactants are those where the head group is not charged and so uses a series of polar groups (usually ethers, but also alcohols, sugars and aldehydes are used) and as such they typically are much larger molecules. Since neither anions nor cations are electrostatically repelled or attracted to the nonionic surfactants there will not be a rate acceleration due to the localisation of ions in the

Stern region. If the reaction depends on both anions and cations then non-ionic surfactants are preferred.

The nonpolar tail of all types of surfactants is a lot simpler, usually consisting of a hydrocarbon chain, the length of which has an effect on the diameter and CMC of the resulting micelles, but otherwise there is not much that can be done to change its nature and effect on the reaction.

The effect of the surfactant head group on pH in the Stern region is less obvious than of the effects on local concentrations of anions and cations, but it must be considered for a reaction that involves acids or bases.⁴⁹ pH quantifies the concentration (or actually the activity) of hydroxonium ions in solution which is related to the concentration of hydroxide through the self-ionisation equilibrium constant K_w . In cationic micelles the hydroxide ions will be present in a much higher concentration in the Stern region due to their attraction to the positive charges of the headgroups, and conversely hydroxonium ions will be repelled by those same positive charges. These two effects mean that the local pH experienced by reactions and compounds in the Stern region of cationic micelles will be higher than the pH of the bulk solution (and the bulk solution will be largely unaffected due to its volume compared to that of the micelles). The opposite is true for anionic surfactants.

The local pH in the Stern Region of CTAB can be calculated using the Poisson-Boltzmann equation which relates the pK_a of a species in the bulk solution to its pK_a in the Stern region (pK_i)

via the micelle's interfacial potential (ψ). Applying this to CTAB gives an effective pH in the Stern region that is 1.4 units higher than the bulk solvent.⁵⁰

$$pK_a - pK_i = \frac{-F\psi}{2.3RT} \quad \text{Poisson-Boltzmann Equation}$$

1.3 - Nanoparticles

1.3.1 - Properties of nanoparticles

Nanoscience is an increasingly studied field due to the unique properties possessed by particles with sizes of the order of nanometers. In many respects nanoparticles share many of the advantages of both individual molecules and of larger macrostructures. The larger a structure is, the easier it is to manipulate and handle, which is very useful for recovering them. But as the particles get larger the surface area decreases relative to its volume and proportionally more of the material is trapped beneath the surface where it is inactive, reducing the total activity of the system. This reduced relative surface area is of particular concern for precious metals, as for something both rare and costly, having the majority of the metal unable to react is wasteful. Individual molecules, on the other hand, have the opposite problem- they can be incredibly active since none of the atoms/molecules are buried under a surface, but manipulating individual atoms or molecules/complexes can be tricky since the means to do so vary greatly with the properties of the molecules. Typically the molecules would be freely dispersed in solution during a reaction and then would be concentrated to retrieve them. Unfortunately, with few exceptions,

the reaction mixture will contain a mixture of chemicals and in order to recover the desired compounds they need to be separated before they can be recovered, and the more similar the chemicals are in properties, the more difficult the separation will be.

Nanoparticles are defined as being particles or materials the dimensions of which are measured in nanometers, although it is typical to only consider particles with dimensions in the 1-100 nm range.⁵¹ In this range even spherical particles (which have the lowest possible surface area for a given volume) have extremely high surface areas compared to their volumes. For example, palladium has a molar volume of 8.85 cm^3 at room temperature, but for spherical particles with a radius of 20 nm the molar surface area is approximately 242 m^2 . Therefore, whilst having a large surface area which is beneficial for reactivity, metallic nanoparticles are also large enough to be separated from individual molecules by centrifugation or sedimentation, allowing the particles to be recovered from a reaction mixture.

High surface area is not the only reason for the difference between the activity of nanoparticles and their bulk materials or individual atoms. The electronic nature of nanoparticles is dominated by the surface atoms since the smaller the particle the greater the proportion of atoms on the surface relative to the core of the particle. Since the properties of the surface atoms are different to the core atoms (since the core atoms are entirely surrounded by metal atoms whilst the surface is only partially covered in metal atoms) changing the ratio of surface to core atoms changes the electronic properties of the particle.⁵¹ The most visible change is in the band gap, which decreases as the particle size increases, which results in the absorption wavelength changing with particle size.

1.3.2 - Use of Nanoparticles in Antiquity

Even before the nature of atoms was discovered there were already a number of examples of materials with what at the time must have seemed ‘mystical’ properties. Unknown to their creators, the properties of these materials were down to the nanoparticles contained within them. The most famous of these is the Lycurgus Cup, a chalice made in the 4th century AD from glass containing trace quantities of gold and silver nanoparticles, giving it dichroic properties. The nanoparticles were added using ‘soluble gold’ which was discovered by accident in antiquity. Soluble gold was probably a preparation of colloidal gold (although, obviously its colloidal nature was unknown at the time) that was also used medicinally.⁵² Roman glass blowers used the dichroic ‘rose glass’ for special items due to its unusual properties. When the light reflects off the glass it appears green, but when the light source is moved to transmit through the glass it instead appears red due to the blue light being scattered by the nanoparticles.⁵³ Another example of the early use of nanomaterials is the ‘Damascus’ steel from the 3rd century that Arab weaponsmiths were famed for, and which their European counterparts could never replicate. ‘Damascened’ blades not only had a distinctive wavy pattern in the steel (similar to Japanese folded steel) they were also stronger, more shatter resistant and kept their edge better than conventional steel. Despite the fact that modern metallurgy has eclipsed the properties of Damascus steel, the legend of Damascus steel, especially given the loss of the technique in the 18th century, drives many to investigate the matter and attempt to reproduce it. Recently, it was discovered that the steel contains carbon nanotubes and nanowires, either from the specific Indian ore that was used or

from the wood that was used to provide the carbon for the steel, and this is likely what made the Damascus steel so unique.⁵⁴

1.3.3 - Contemporary applications of nanoparticles

There are many more examples of applications of nanoparticles being developed, nowadays *with* knowledge of the existence of nanoparticles, that illustrate the potential benefits their use could bring. These benefits could be structural, such as imbuing magnesium metal with SiC nanocrystals to strengthen the material without greatly increasing the weight of the metal.⁵⁵ The benefits could also be electronic, such as the tuning of a semiconductor's band gap by altering the size of the nanoparticle, for example by varying the diameter of a quantum dot,⁵⁶ which is a tool that can be used to improve the quantum yield of solar cells.

As with many new technologies and discoveries, in popular culture there is an undercurrent of distrust of nanoparticles. In particular the idea that they may be hazardous has led to personal condemnation from the Prince of Wales.⁵⁷ However, it appears that whilst nanoparticles, like any novel chemicals, could be harmful, there are many potential applications in biology and medicine which would be highly beneficial. In fact, many of the nanoparticles in use currently are less harmful than the alternatives since they are often active in much lower concentrations.⁵⁸ The applications of nanoparticles fall into three broad categories, viz. nanoprobe and contrast agents,⁵⁹ nanoparticle-based delivery methods⁵⁸ and biologically active nanoparticles.'

Nanoparticles make good probes due to the aforementioned electronic properties that can make them extremely strong chromophores with highly tunable absorption properties. In addition they are typically considerably more photostable and biostable than organic fluorophores and as such nanoparticle-based probes can last much longer in use. A photo-active nanoparticle can be surface functionalised to introduce an attachment point, such as a carboxyl, thiol or amino group. These attachment points can then be used to attach a biological probe, such as a protein or nucleic acid that will bind to a target in the body. The binding site can then be visualised by fluorescence even in low concentrations and since the wavelength of fluorescence can be easily controlled by modifying the size of the nanoparticles, multiple different analyses can be performed simultaneously in a single subject.⁶⁰ Further examples of the use of nanoparticles can be found in Chapter 7.

1.4 - Goals

The main goal of the work presented in Chapters 2-4 is to study the palladium-catalysed homocoupling reaction of arylboronic acids as an alternative to the Suzuki-Miyaura and other related coupling reactions. In particular the use of surfactant-solubilised or heterogeneous nanoparticle-based palladium catalysts will be studied in order to allow the use of water as the bulk solvent, in place of less environmentally-friendly solvents. Additionally, the effect of reaction conditions, particularly the pH, on the rate of reaction and product yield will be studied since these are important parameters for the synthetic reactions. In Chapter 5 gold nanoparticles will be studied as catalysts for the release of nitric oxide from nitrosothiols to see if the release

can be controlled, which would enable the use of such nanoparticles as a means of targeting nitric oxide release *in vivo*.

1.5 - Bibliography

1. UNEP Global Chemicals Outlook - Towards Sound Management of Chemicals. http://www.unep.org/pdf/GCO_Synthesis_Report_CBDTIE_UNEP_September5_2012.pdf (accessed 15/09).
2. Commission, I. P. INDIAN CHEMICAL INDUSTRY Five Year Plan – 2012-2017. http://planningcommission.nic.in/aboutus/committee/wrkgrp12/wg_chem0203.pdf.
3. Franklin, A. S.; Paterson, I., Recent developments in asymmetric aldol methodology. *Contemporary Organic Synthesis* **1994**, *1* (5), 317-338.
4. Weinreb, S. M.; Staib, R. R., Synthetic aspects of diels-alder cycloadditions with heterodienophiles. *Tetrahedron* **1982**, *38* (21), 3087-3128.
5. Rueping, M.; Nachtsheim, B. J., A review of new developments in the Friedel–Crafts alkylation – From green chemistry to asymmetric catalysis. *Beilstein Journal of Organic Chemistry* **2010**, *6*, 6.
6. Franzén, R. G., Utilization of Grignard Reagents in Solid-phase Synthesis: A Review of the Literature. *Tetrahedron* **2000**, *56* (5), 685-691.
7. Gales, B. J.; Bailey, E. K.; Reed, A. N.; Gales, M. A., Angiotensin-Converting Enzyme Inhibitors and Angiotensin Receptor Blockers for the Prevention of Migraines. *Annals of Pharmacotherapy* **2010**, *44* (2), 360-366.
8. Schrader, J.; Salvetti, A.; Calvo, C.; Akpınar, E.; Keeling, L.; Weisskopf, M.; Brunel, P., The combination of amlodipine/valsartan 5/160 mg produces less peripheral oedema than amlodipine 10 mg in hypertensive patients not adequately controlled with amlodipine 5 mg. *International Journal of Clinical Practice* **2009**, *63* (2), 217-225.
9. Gradman, A. H.; Arcuri, K. E.; Goldberg, A. I.; Ikeda, L. S.; Nelson, E. B.; Snively, D. B.; Sweet, C. S., A Randomized, Placebo-Controlled, Double-Blind, Parallel Study of Various

Doses of Losartan Potassium Compared With Enalapril Maleate in Patients With Essential Hypertension. *Hypertension* **1995**, *25* (6), 1345-1350.

10. Zhu, D. L.; Bays, H.; Gao, P.; Mattheus, M.; Voelker, B.; Ruilope, L. M., Efficacy and Tolerability of Initial Therapy With Single-Pill Combination Telmisartan/Hydrochlorothiazide 80/25 mg in Patients With Grade 2 or 3 Hypertension: A Multinational, Randomized, Double-Blind, Active-Controlled Trial. *Clinical therapeutics* **2012**, *34* (7), 1613-1624.

11. Micheli, F.; Bonanomi, G.; Braggio, S.; Capelli, A. M.; Celestini, P.; Damiani, F.; Fabio, R. D.; Donati, D.; Gagliardi, S.; Gentile, G.; Hamprecht, D.; Petrone, M.; Radaelli, S.; Tedesco, G.; Terreni, S.; Worby, A.; Heidebreder, C., New fused benzazepine as selective D3 receptor antagonists. Synthesis and biological evaluation. Part one: [h]-fused tricyclic systems. *Bioorganic & Medicinal Chemistry Letters* **2008**, *18* (3), 901-907.

12. Pfizer *Doing things differently -Pfizer Annual Review 2008*; Pfizer: 2009.

13. Richardson, R. D.; Holland, E. J.; Carpenter, B. K., A renewable amine for photochemical reduction of CO₂. *Nat Chem* **2011**, *3* (4), 301-303.

14. Chen, F.; Zou, W.; Qu, W.; Zhang, J., Photocatalytic performance of a visible light TiO₂ photocatalyst prepared by a surface chemical modification process. *Catalysis Communications* **2009**, *10* (11), 1510-1513.

15. Grätzel, M., Recent Advances in Sensitized Mesoscopic Solar Cells. *Accounts of Chemical Research* **2009**, *42* (11), 1788-1798.

16. Baxter, J. B.; Aydil, E. S., Nanowire-based dye-sensitized solar cells. *Applied Physics Letters* **2005**, *86* (5), -.

17. Heck, R. F.; Nolley, J. P., Palladium-catalyzed vinylic hydrogen substitution reactions with aryl, benzyl, and styryl halides. *The Journal of Organic Chemistry* **1972**, *37* (14), 2320-2322.

18. Sonogashira, K.; Tohda, Y.; Hagihara, N., A convenient synthesis of acetylenes: catalytic substitutions of acetylenic hydrogen with bromoalkenes, iodoarenes and bromopyridines. *Tetrahedron Letters* **1975**, *16* (50), 4467-4470.

19. Liang, B.; Dai, M.; Chen, J.; Yang, Z., Copper-Free Sonogashira Coupling Reaction with PdCl₂ in Water under Aerobic Conditions. *The Journal of Organic Chemistry* **2004**, *70* (1), 391-393.

20. Yi, C.; Hua, R., Efficient Copper-Free PdCl₂(PCy₃)₂-Catalyzed Sonogashira Coupling of Aryl Chlorides with Terminal Alkynes. *The Journal of Organic Chemistry* **2006**, *71* (6), 2535-2537.
21. King, A. O.; Okukado, N.; Negishi, E.-i., Highly general stereo-, regio-, and chemo-selective synthesis of terminal and internal conjugated enynes by the Pd-catalysed reaction of alkynylzinc reagents with alkenyl halides. *Journal of the Chemical Society, Chemical Communications* **1977**, (19), 683-684.
22. Liu, Q.; Lan, Y.; Liu, J.; Li, G.; Wu, Y.-D.; Lei, A., Revealing a Second Transmetalation Step in the Negishi Coupling and Its Competition with Reductive Elimination: Improvement in the Interpretation of the Mechanism of Biaryl Syntheses. *Journal of the American Chemical Society* **2009**, *131* (29), 10201-10210.
23. Milstein, D.; Stille, J. K., A general, selective, and facile method for ketone synthesis from acid chlorides and organotin compounds catalyzed by palladium. *Journal of the American Chemical Society* **1978**, *100* (11), 3636-3638.
24. Aldrich, S. MSDS for Tributylphenylstannane (960-16-7). http://www.sigmaaldrich.com/MSDS/MSDS/PrintMSDSAction.do?name=msdspd_1310293165605671.
25. Adamo, C.; Amatore, C.; Ciofini, I.; Jutand, A.; Lakmini, H., Mechanism of the palladium-catalyzed homocoupling of arylboronic acids: Key involvement of a palladium peroxo complex. *Journal of the American Chemical Society* **2006**, *128* (21), 6829-6836.
26. Miyaura, N.; Yamada, K.; Suzuki, A., A new stereospecific cross-coupling by the palladium-catalyzed reaction of 1-alkenylboranes with 1-alkenyl or 1-alkynyl halides. *Tetrahedron Letters* **1979**, *20* (36), 3437-3440.
27. Number was derived from searching for papers containing the reaction name using Scifinder, and then filtered by publication date.
28. Ranganath, K. V. S.; Onitsuka, S.; Kumar, A. K.; Inanaga, J., Recent progress of N-heterocyclic carbenes in heterogeneous catalysis. *Catalysis Science & Technology* **2013**, *3* (9), 2161-2181.
29. Lee, D.-H.; Kim, J.-H.; Jun, B.-H.; Kang, H.; Park, J.; Lee, Y.-S., Macroporous Polystyrene-Supported Palladium Catalyst Containing a Bulky N-Heterocyclic Carbene Ligand for Suzuki Reaction of Aryl Chlorides. *Organic Letters* **2008**, *10* (8), 1609-1612.

30. Stevens, P. D.; Li, G.; Fan, J.; Yen, M.; Gao, Y., Recycling of homogeneous Pd catalysts using superparamagnetic nanoparticles as novel soluble supports for Suzuki, Heck, and Sonogashira cross-coupling reactions. *Chemical Communications* **2005**, (35), 4435-4437.
31. Inamoto, K.; Kuroda, J.-i.; Kwon, E.; Hiroya, K.; Doi, T., Pincer-type bis(carbene)-derived complexes of nickel(II): Synthesis, structure, and catalytic activity. *Journal of Organometallic Chemistry* **2009**, 694 (3), 389-396.
32. (a) Butters, M.; Harvey, J. N.; Jover, J.; Lennox, A. J. J.; Lloyd-Jones, G. C.; Murray, P. M., Aryl Trifluoroborates in Suzuki–Miyaura Coupling: The Roles of Endogenous Aryl Boronic Acid and Fluoride. *Angewandte Chemie* **2010**, 122 (30), 5282-5286; (b) Lennox, A. J. J.; Lloyd-Jones, G. C., Transmetalation in the Suzuki–Miyaura Coupling: The Fork in the Trail. *Angewandte Chemie International Edition* **2013**, 52 (29), 7362-7370.
33. Amatore, C.; Jutand, A.; Le Duc, G., Kinetic Data for the Transmetalation/Reductive Elimination in Palladium-Catalyzed Suzuki–Miyaura Reactions: Unexpected Triple Role of Hydroxide Ions Used as Base. *Chemistry – A European Journal* **2011**, 17 (8), 2492-2503.
34. Matos, K.; Soderquist, J. A., Alkylboranes in the Suzuki–Miyaura Coupling: Stereochemical and Mechanistic Studies. *The Journal of Organic Chemistry* **1998**, 63 (3), 461-470.
35. Moreno-Mañas, M.; Pérez, M.; Pleixats, R., Palladium-Catalyzed Suzuki-Type Self-Coupling of Arylboronic Acids. A Mechanistic Study. *The Journal of Organic Chemistry* **1996**, 61 (7), 2346-2351.
36. Kuivila, H. G.; Armour, A. G., Electrophilic Displacement Reactions. IX. Effects of Substituents on Rates of Reactions between Hydrogen Peroxide and Benzeneboronic Acid¹⁻³. *Journal of the American Chemical Society* **1957**, 79 (21), 5659-5662.
37. Othman, M. A. The palladium-catalysed aerobic oxidative homocoupling reaction of arylboronic acids in aqueous micellar medium kinetic and mechanistic studies. Cardiff University, Cardiff University, 2011.
38. Constable, D. J. C.; Dunn, P. J.; Hayler, J. D.; Humphrey, G. R.; Leazer, J. J. L.; Linderman, R. J.; Lorenz, K.; Manley, J.; Pearlman, B. A.; Wells, A.; Zaks, A.; Zhang, T. Y., Key green chemistry research areas-a perspective from pharmaceutical manufacturers. *Green Chemistry* **2007**, 9 (5), 411-420.

39. Hessel, V.; Hofmann, C.; Löwe, H.; Meudt, A.; Scherer, S.; Schönfeld, F.; Werner, B., Selectivity Gains and Energy Savings for the Industrial Phenyl Boronic Acid Process Using Micromixer/Tubular Reactors. *Organic Process Research & Development* **2004**, *8* (3), 511-523.
40. Ishiyama, T.; Murata, M.; Miyaura, N., Palladium(0)-Catalyzed Cross-Coupling Reaction of Alkoxydiboron with Haloarenes: A Direct Procedure for Arylboronic Esters. *The Journal of Organic Chemistry* **1995**, *60* (23), 7508-7510.
41. Chow, W. K.; So, C. M.; Lau, C. P.; Kwong, F. Y., Palladium-Catalyzed Borylation of Aryl Mesylates and Tosylates and Their Applications in One-Pot Sequential Suzuki–Miyaura Biaryl Synthesis. *Chemistry – A European Journal* **2011**, *17* (25), 6913-6917.
42. Yinghuai, Z.; Chenyan, K.; Peng, A. T.; Emi, A.; Monalisa, W.; Kui-Jin Louis, L.; Hosmane, N. S.; Maguire, J. A., Catalytic Phenylborylation Reaction by Iridium(0) Nanoparticles Produced from Hydrido-iridium Carborane. *Inorganic Chemistry* **2008**, *47* (13), 5756-5761.
43. Bakherad, M.; Keivanloo, A.; Samangoeei, S.; Omidian, M., A phenyldithiocarbamate-functionalized polyvinyl chloride resin-supported Pd(II) complex as an effective catalyst for solvent- and copper-free Sonogashira reactions under aerobic conditions. *Journal of Organometallic Chemistry* **2013**, *740* (0), 78-82.
44. Klingensmith, L. M.; Leadbeater, N. E., Ligand-free palladium catalysis of aryl coupling reactions facilitated by grinding. *Tetrahedron Letters* **2003**, *44* (4), 765-768.
45. Riter, R. E.; Kimmel, J. R.; Undiks, E. P.; Levinger, N. E., Novel Reverse Micelles Partitioning Nonaqueous Polar Solvents in a Hydrocarbon Continuous Phase. *The Journal of Physical Chemistry B* **1997**, *101* (41), 8292-8297.
46. Balakrishnan, V. K.; Han, X.; VanLoon, G. W.; Dust, J. M.; Toullec, J.; Buncel, E., Acceleration of Nucleophilic Attack on an Organophosphorothioate Neurotoxin, Fenitrothion, by Reactive Counterion Cationic Micelles. Regioselectivity as a Probe of Substrate Orientation within the Micelle†. *Langmuir* **2004**, *20* (16), 6586-6593.
47. Khan, M. N., Unusual Rate Enhancement in the Hydroxide-Ion-Catalyzed Cleavage of Acetyl Salicylate Ion (Aspirin Anion) in the Presence of Anionic Micelles. *Journal of Colloid and Interface Science* **1995**, *170* (2), 598-601.

48. Cabaleiro-Lago, C.; García-Río, L.; Hervés, P.; Pérez-Juste, J., Nonionic microemulsions: Effects of the interface on metal–ligand reactions. *Colloids and Surfaces A: Physicochemical and Engineering Aspects* **2007**, *309* (1–3), 286-291.
49. Buurma, N. J.; Serena, P.; Blandamer, M. J.; Engberts, J. B. F. N., The Nature of the Micellar Stern Region As Studied by Reaction Kinetics. 2†,1. *The Journal of Organic Chemistry* **2004**, *69* (11), 3899-3906.
50. Fernandez, M. S.; Fromherz, P., Lipoid pH indicators as probes of electrical potential and polarity in micelles. *The Journal of Physical Chemistry* **1977**, *81* (18), 1755-1761.
51. Eustis, S.; El-Sayed, M. A., Why gold nanoparticles are more precious than pretty gold: Noble metal surface plasmon resonance and its enhancement of the radiative and nonradiative properties of nanocrystals of different shapes. *Chemical Society Reviews* **2006**, *35* (3), 209-217.
52. Amatore, C.; Jutand, A., Anionic Pd(0) and Pd(II) Intermediates in Palladium-Catalyzed Heck and Cross-Coupling Reactions. *Accounts of Chemical Research* **2000**, *33* (5), 314-321.
53. Barber, D. J.; Freestone, I. C., AN INVESTIGATION OF THE ORIGIN OF THE COLOUR OF THE LYCURGUS CUP BY ANALYTICAL TRANSMISSION ELECTRON MICROSCOPY. *Archaeometry* **1990**, *32* (1), 33-45.
54. Reibold, M.; Paufler, P.; Levin, A. A.; Kochmann, W.; Patzke, N.; Meyer, D. C., Materials: Carbon nanotubes in an ancient Damascus sabre. *Nature* **2006**, *444* (7117), 286-286.
55. Ferkel, H.; Mordike, B. L., Magnesium strengthened by SiC nanoparticles. *Materials Science and Engineering: A* **2001**, *298* (1–2), 193-199.
56. Khare, A.; Wills, A. W.; Ammerman, L. M.; Norris, D. J.; Aydil, E. S., Size control and quantum confinement in Cu₂ZnSnS₄ nanocrystals. *Chemical Communications* **2011**, *47* (42), 11721-11723.
57. News, B., Prince warns of science 'risks'. 2004.
58. Zhang, L.; Gu, F. X.; Chan, J. M.; Wang, A. Z.; Langer, R. S.; Farokhzad, O. C., Nanoparticles in Medicine: Therapeutic Applications and Developments. *Clin Pharmacol Ther* **2007**, *83* (5), 761-769.
59. Jain, P. K.; Huang, X.; El-Sayed, I. H.; El-Sayed, M. A., Noble Metals on the Nanoscale: Optical and Photothermal Properties and Some Applications in Imaging, Sensing, Biology, and Medicine. *Accounts of Chemical Research* **2008**, *41* (12), 1578-1586.

60. Wang, L.; Wang, K.; Santra, S.; Zhao, X.; Hilliard, L. R.; Smith, J. E.; Wu, Y.; Tan, W., Watching Silica Nanoparticles Glow in the Biological World. *Analytical Chemistry* **2006**, 78 (3), 646-654.

Chapter 2

Bisimidazolyl-palladium Complexes and their use in the Oxidative Homocoupling of Arylboronic acids

Abstract: Two catalysts, *viz.* bis(1-methylimidazol-2-yl)methylenepalladium dichloride and bis(1-methylimidazol-2-yl)butanepalladium dichloride, were synthesised as alternatives to bis(1-methylimidazol-2-yl)propyl methyl thioetherpalladium dichloride for the homocoupling reaction of arylboronic acids. These catalysts were analysed to determine how their properties differed from the bisimidazolyl palladium catalyst previously used in the homocoupling reaction of arylboronic acids. The lengths of the Pd-N and Pd-Cl bonds from the crystal structure appear unchanged by the substituents attached to the bisimidazole ligand, but the bite angle was found to be smaller for ligand bis(1-methylimidazol-2-yl)methylene than for bis(1-methylimidazol-2-yl)butane. The exchange of ligands from the palladium in bis(1-methylimidazol-2-yl)methylenepalladium dichloride was investigated by NMR in acetonitrile and water was shown to readily displace the chloride ligands. Addition of bromide ions to the catalyst in water and acetonitrile was shown to create a new species, which is thought to be the result of the water ligands being substituted by bromide ligands. In non-ionic surfactant laureth-10 no pK_a was found for Bis(1-methylimidazol-2-yl)methylenepalladium dichloride until halide ions were added to the system. The pK_a of the catalyst was shown to vary linearly with $[Br^-]$ and $[Cl^-]$, with the $[Br^-]$ having the more marked effect on the pK_a . The pK_a of Bis(1-methylimidazol-2-yl)butanepalladium dichloride was also shown to vary linearly with $[Br^-]$ in laureth-10. In CTAB the pK_a of bis(1-methylimidazol-2-

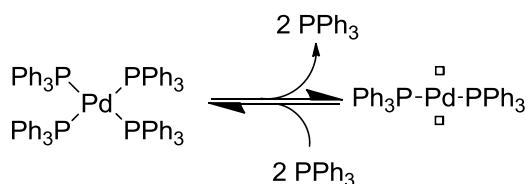
yl)methylenepalladium dichloride was shown to change linearly with CTAB concentration. These catalysts were then also tested as pre-catalysts in the homocoupling reaction of 4-carboxyphenylboronic acid in three different aqueous surfactant solutions - CTAB, laureth-10 and MEGA-10. Laureth-10 was shown to oxidise in solution over two weeks and the oxidation product caused destruction of phenylboronic acids and inhibition of the homocoupling reaction. The homocoupling reaction in laureth-10 was found to have a broad optimal pH of 9.09 for the reaction with unactivated catalyst and 8.75 for the reaction with activated catalyst. Adding bromide or halide ions to the system in laureth-10 caused a sharper pH maximum that increased in pH with halide concentration, although the maximum observed rate constant also decreased with halide concentration. The pH rate profile for both catalysts in CTAB was determined and for the catalyst with no alkyl groups attached to the bisimidazolyl bridge the optimal pH was found to be higher than for the corresponding reaction with the catalyst with a propyl group attached to the bisimidazolyl bridge. Increasing the CTAB concentration was also shown to increase the optimal pH, as the concentration of bromide relative to the catalyst in the Stern region was increased. MEGA-10 was shown to be extremely inactive in the homocoupling reaction, failing to react to completion in the experiment time frame.

2.1 - Introduction

2.1.1 - Palladium Catalysts

Palladium is widely used as a catalyst or component of catalysts, both in chemical synthesis and in automobile catalytic converters with the latter accounting for 80% of worldwide palladium consumption.¹ Use of palladium in the chemical industry is continually increasing and in 2012 16.5 tonnes were used for a variety of different processes. The structure of the catalyst is very important to its activity and there are a wide variety of different palladium catalysts and palladium complexes available that are optimised for different reactions.²

For palladium-catalysed coupling reactions homogeneous palladium (0) catalysts are most often used, with the most popular being tetrakis(triphenylphosphine)palladium (0) ($\text{Pd}(\text{PPh}_3)_4$, see Scheme 1), which is a particularly efficient and readily available catalyst.



Scheme 1. Tetrakis(triphenylphosphine)palladium (0).

The main reason for this preference is the simplicity of the catalyst and its high reactivity due to its phosphine ligands. Tetrakis(triphenylphosphine)palladium (0) readily loses phosphine ligands

to allow for a substrate to oxidatively add and initiate a catalytic cycle. The mass adoption of palladium carrying phosphine-based ligands has led to widespread availability and a low cost of these complexes (as low as £17 per gram³). However, the readiness of displacing the ligands is also one of the weaknesses of Pd(PPh₃)₄ as it is quite unstable in solution; if all the ligands are removed from the palladium centre, the palladium precipitates as palladium black. This decomposition reduces the amount of catalytically active palladium, and thus makes kinetic measurements unreliable as the catalyst concentration is not constant or reproducible. In fact, Pd(PPh₃)₄ is typically stored in cool, dark and anaerobic conditions to prevent the catalyst decomposing.

Previous work in the group had started using tetrakis(triphenylphosphine)palladium (0) (Pd(PPh₃)₄) as a catalyst for studying Suzuki Miyaura reactions and the oxidative homocoupling reaction of arylboronic acids (*vide infra*).⁴ Whilst Pd(PPh₃)₄ was a very reactive catalyst, it does not make a good catalyst for kinetic studies due to the complex's aforementioned instability. The instability in solution means that the kinetics of reactions catalysed by Pd(PPh₃)₄ are rarely reproducible even when using catalyst from the same stock solution. To circumvent the problems resulting from poor reproducibility, a more stable pre-catalyst was identified in the form of palladium (II) complexes.

Palladium (II) complexes, such as palladium (II) chloride and palladium (II) acetate, are far less susceptible to decomposition than Pd(PPh₃)₄ and as such can be stored in air at room temperature for long time periods without adverse effects, making them better catalysts for kinetic measurements. This resilience comes at a cost, though, as palladium (II) complexes would be

more correctly referred to as pre-catalysts, since they must typically first be reduced to Palladium (0). In fact, palladium (II) complexes are more commonly used as precursors to palladium (0) catalysts that are formed *in situ* or shortly before use; it is in actuality more appropriate to refer to such palladium (II) complexes as pre-catalysts. This can be done by reduction of the Palladium (II) catalyst to form a Palladium (0) catalyst *in situ* immediately prior to use, but in cross-coupling reactions it is more typical for the Palladium (II) catalyst to be reduced in a slow induction step that leads to generation of Palladium (0).⁵

The second consideration that needs to be made about the pre-catalyst, beyond the oxidation state, is the ligand used. The effect of the ligand on the stability of the pre-catalyst, both in storage and during reactions, can be marked. Palladium acetate is very stable in its +2 oxidation state, but once the catalyst is in its active +0 oxidation state this is a different matter and the acetate ligand does little to stabilise the palladium (0). The reason palladium complexes with poor ligands can be used catalytically at all is that at low palladium loading the oxidative addition that initiates the catalytic cycle is typically much faster than the palladium aggregation process that forms palladium black⁶. If the palladium loading is too high then the aggregation will be fast enough to start decomposing the catalyst before the reaction can finish. Obviously, the catalyst decomposition is bad synthetically, as the catalyst may decompose before the reaction is complete, but precipitation of unstabilised palladium (0) is also a hindrance to the development of reusable catalysts as at completion of the reaction there is no competing reaction to prevent the decomposition of the complex. Using a ligand that is strongly bound to the palladium can therefore be very beneficial as it will prevent the palladium aggregating as long as it remains bound. The presence of bound ligands also allows for control over the catalytic

properties of palladium by influencing its electronic properties and also by using steric properties to influence the reactants (a common route to stereoselective catalysts).⁷

2.1.2 - Bisimidazolyl catalysts

Since the most commonly used catalyst for aryl-aryl coupling reactions, tetrakis triphenylphosphine palladium (0) ($\text{Pd}(\text{PPh}_3)_4$) (*vide supra*), is not a very good catalyst for studying reaction kinetics as it is not stable in solution (which is why it is stored at -8°C), an alternative catalyst is necessary. In previous work, a variety of catalysts were therefore sought and the catalyst eventually settled on was a Palladium (II) pre-catalyst PdCl_2 -**4** synthesised by Dr Mandeep Sidhu (Figure 1).⁴

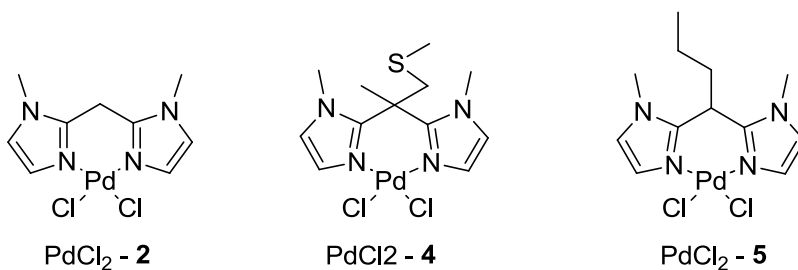


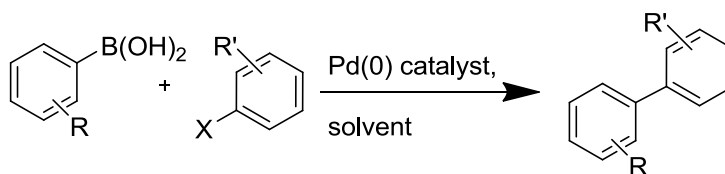
Figure 1. The molecular catalysts PdCl_2 -**4** and analogues PdCl_2 -**2** and PdCl_2 -**5**.

binding to a palladium centre, which would prevent the substrates coordinating to the catalyst. Finally, there is no need for the reaction intermediate to cis-trans isomerise prior to reductive elimination (*vide infra*).

To ascertain whether the stability of PdCl₂-**4** is due to the steric hindrance of the side chain, interaction with the sulfur or merely common to bisimidazolyl ligands two additional precatalysts, PdCl₂-**2** and PdCl₂-**5** also shown in Figure X will be investigated (*vide infra*).

2.1.3 - Palladium-catalysed coupling reactions

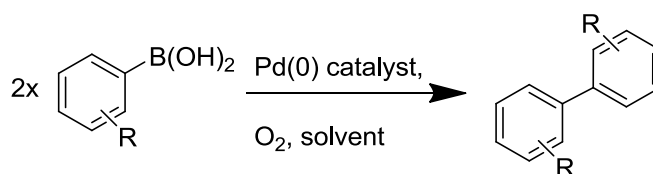
The carbon-carbon bond is arguably the most important bond in organic chemistry, and there are myriad ways to form these bonds. When it comes to forming an aryl-aryl bond, one of the most commonly employed and famous reactions is the Suzuki-Miyaura cross-coupling (Scheme 3).



Scheme 3. The Suzuki-Miyaura cross-coupling reaction.

The Suzuki-Miyaura reaction is popular due to the availability and benign nature of the arylboronic acids used as a substrate, especially in comparison with the toxic stannates required for the related Stille cross-coupling. Whilst typical conditions for the Suzuki-Miyaura reaction compare favourably with the conditions required for other commonly employed coupling reactions, there is still scope for improvement in several areas. For example, the organohalides required in the Suzuki-Miyaura reaction are undesirable precursors in the pharmaceutical industry and are also not environmentally friendly, so a method for performing coupling reactions easily without these reactants would be beneficial.

The main problem with the Suzuki-Miyaura reaction, and with other palladium catalysed crosscoupling reactions, is that they must be performed under inert atmosphere as oxygen causes a side reaction where the arylboronic acids homocouple (Scheme 4).



Scheme 4. The oxidative homocoupling reaction of arylboronic acids.

This oxidative homocoupling reaction of arylboronic acids (from now on simply the homocoupling reaction) is one of the greatest weaknesses of the Suzuki-Miyaura reaction, but it may also be key to an alternative. Whilst the homocoupling can cause the biaryl product of a

cross-coupling reaction to be contaminated by a biaryl impurity that can be hard to remove, there is no scope for a biaryl impurity in the homocoupling reaction as only one aryl compound would be present. Additionally, using the homocoupling reaction eliminates the need to use aryl halides in the reaction and remove one of the barriers to running the reaction in water which would be stepping in the right direction as far as its environmental qualities go. The major disadvantage of the homocoupling reaction is that by its very nature it results in symmetrical biaryl products, which reduces the number of possible applications.

Another way to improve the environmental characteristics of cross-coupling reactions would be to cut down on the hazardous waste generated. The vast majority of coupling reactions are run in either an organic solvent like toluene or xylene, which must be disposed of by burning (releasing CO₂), or a mixture of water and DMF where the toxic solvents are not trivial to dispose of. If one could change the solvent used for C-C bond-forming reactions to water, then this would result in appreciable environmental advantages. Additionally, water is cheaper (even after accounting for the cost of deionising water it costs less than £0.50 a litre), non-flammable, non-toxic and typically readily available, which are all advantages for its use. The usual two barriers to the use of water in a reaction are its reactivity and the lack of solubility of typical organic compounds in water. Reactivity is a hard line as far as suitability goes - if a reaction involves chemicals that are water sensitive then water would obviously be unsuitable (such as organolithium or grignard reagents). Solubility is a lot more of a flexible requirement as reactants and reaction conditions can be modified to reduce solubility problems.

For molecular palladium catalysts solubility is a large concern, as commonly used palladium catalysts (such as tetrakis(triphenylphosphine) palladium, palladium acetate and palladium chloride) are insoluble or sparingly soluble in water. This lack of solubility would pose a problem, as these kinds of catalysts are not really suitable for heterogeneous use, and so efforts must be made in order to solubilise the catalyst. Whilst the solubility could be increased by modification of the catalyst, such catalysts are not as readily available so a way of solubilising the existing catalysts would be preferred, and the easiest way of doing that is through the use of surfactants.

2.1.4 - Surfactants

Surfactants form micelles in aqueous solution and can be used to solubilise non-polar compounds in water to allow them to react with polar compounds. This occurs at the interface between the non-polar interior of the micelle and the aqueous solution, the Stern region (Figure 2).

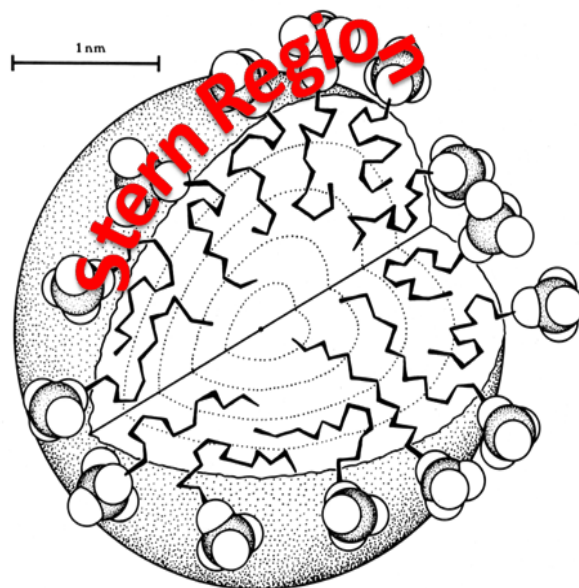


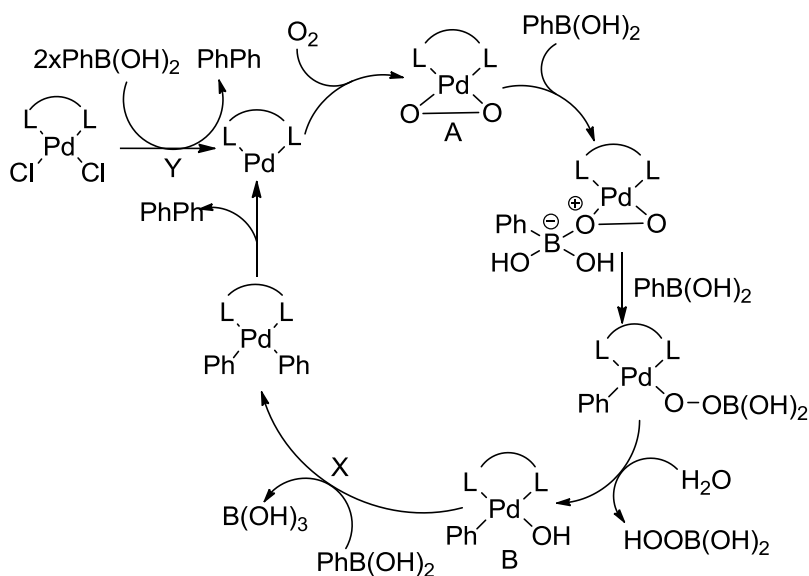
Figure 2. Schematic of a spherical micelle with the Stern region indicated.

But surfactants do not just allow for the solubilising of non-polar and polar molecules in the same system, they can also increase the rate of reaction due to the micellar system's properties. The first is that, unlike more usual biphasic systems, the interface between the interior of the micelles and the aqueous solution has a very high surface area, allowing for a much greater likelihood of interaction between the non-polar contents of the micelles and the polar molecules in the bulk solution. Additionally, the charge density of the polar head groups in ionic surfactants results in reactants of the opposite charge to the head group being localised in the Stern region of the micelles, and in a much higher concentration than in the bulk solution. The interior volume of the micelles is far smaller than the total volume of the solution, and as such the concentration of non-polar species within can be extremely high both inside the micelles and the Stern region.

The concentration of both non-polar and polar species in the Stern region can accelerate the rate of reaction (See Chapter 1) . However, the charged counter ion in many cationic surfactants is a halide and these halide ions are also highly concentrated in the Stern region and as such could be a hindrance to catalytic reactions (*vide infra*).

2.1.5 - Mechanistic Studies

The proposed mechanism for the homocoupling reaction (Scheme 5) is based upon the studies of Amatore who studied the reaction in organic solvents using $\text{Pd}(\text{PPh}_3)_4$.⁹



Scheme 5 - The originally proposed catalytic scheme.

In particular Amatore and co-workers focussed on the first step of the cycle, the reaction of oxygen with the palladium (0) catalyst to form peroxo complex A. By isolating the peroxo complex and using it as the catalyst they confirmed that the reaction proceeded from that point, showing that the formation of the peroxo complex is the starting step of the catalytic cycle.

However, this peroxide formation is also the cause of one of the major weaknesses in the reaction. In the presence of peroxides arylboronic acids are known to break down to form boric acids and phenols.¹⁰ Because the first transmetallation of the palladium peroxo species forms peroxoborates at the palladium, that are then released into solution, there is a high degree of phenol formation during the reaction. This is because there is too high a concentration of the substrate near the site of peroxide formation so the likelihood of peroxides breaking down before encountering an arylboronic acid is low. This means the homocoupling reaction typically produces a 1:1 biphenyl : phenol product ratio. Although the phenol involves a significant amount of reactant (up to 1/3 of the reactant), this does have one advantage compared to the Suzuki-Miyaura reaction; since the byproduct is not a biphenyl and is likely more polar, therefore separating it from the product after the reaction should be a lot simpler. Since the product ratio is so close to one, it would imply that the rate of the peroxide reaction to form phenol is at least as fast as the rate of the coupling reaction.

Suzuki-Miyaura reactions are usually carried out in the presence of a high concentration of a base, such as K_2CO_3 but the role of the base is not fully understood. Since the reaction is

considered to be base accelerated, the common expectation is that the effect of the base reaches a plateau as one increases the pH. The homocoupling reaction of phenylboronic acids catalysed by $\text{PdCl}_2\text{-4}$ in CTAB was previously shown to display a bell-shaped pH-rate profile and several reasons for this observation were suggested (Figure 3).

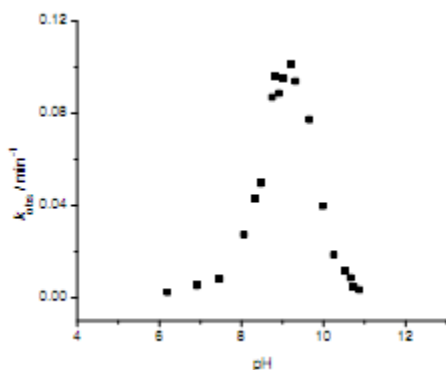
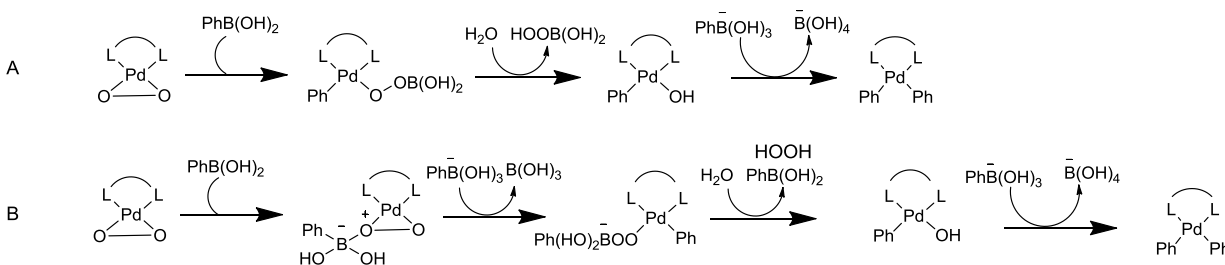


Figure 3. The pH rate profile for the homocoupling reaction of 0.1 mM phenylboronic acid with 27 μM $\text{PdCl}_2\text{-4}$ in 10 mM CTAB at 30 $^{\circ}\text{C}$.⁴

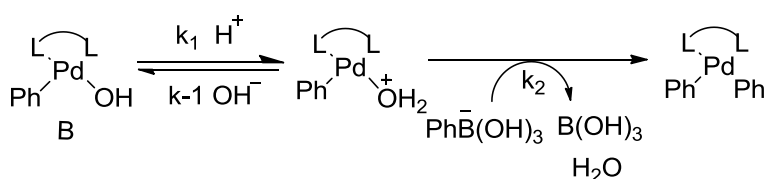
The pH maximum was shown to change when different phenylboronic acids were used, with the maximum following the same trend as the $\text{p}K_{\text{a}}$ of the phenylboronic acid. It was therefore assumed that the protonation state of the phenylboronic acid must be relevant to the rate-determining step. In order to get a bell-shaped pH rate profile (at least) two protonation equilibria must be involved and two possible reaction mechanisms were proposed, based on earlier work by Adamo (Scheme 1).⁹

The first mechanism would involve the boronic acid being required in both its acidic and its conjugate boronate form during the reaction, with the different forms being needed in the first and second transmetallation steps. Since the second transmetallation is analogous to the transmetallation step in the Suzuki Miyaura reaction (Scheme 5, step X), it was expected to be base-catalysed. For the pH maxima to be solely due to the boronic acid there are two possible explanations. Either there are two steps that require the acidic and basic forms of the phenylboronic acid and as such the pH maximum originates from a change in the rate determining step (Scheme 6.A); or the first transmetallation (as the second is thought to be analogous to the transmetallation in the Suzuki Miyaura reaction and therefore base catalysed) requires both the acidic and basic forms of the phenylboronic acid and so the pH maximum isn't caused by a change in rate determining step (Scheme 6.B). Instead the pH maximum would be caused by a change in which form is in excess.



Scheme 6. Two possible pathways where the pH maximum is caused by the phenylboronic acid protonation equilibrium alone. (A) Where the initial transmetallation is acid catalysed and the second is base catalysed and (B) the initial transmetallation requires the phenylboronic acid to be present in both its acidic and basic forms.

The second proposed explanation for the pH maximum is that there are two separate protonation equilibria involved in the rate-determining step. It was suggested that the palladium complex itself needed to be protonated in order to facilitate attack by the basic boronate, generating water as a leaving group rather than hydroxide (Scheme 7).

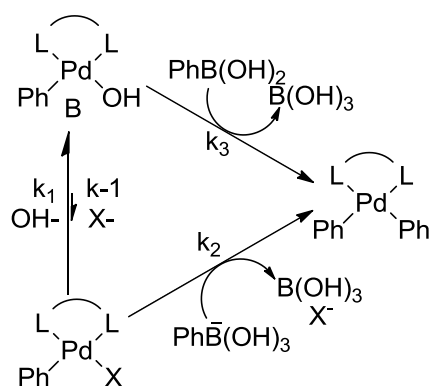


Scheme 7. The second proposed effect of pH on the homocoupling reaction.

This mechanism would obviously only give a pH maximum if the pK_a of the catalyst was close to the observed pH maximum. Experiments showed that the (apparent) pK_a of $\text{PdCl}_2\text{-4}$ was 8.0 in CTAB (cetrimonium bromide). The pK_a of a palladium hydroxo compound to form an aqua complex (k_1, k_{-1}) is typically much lower than this¹¹ (hence why van Eldik *et al* studied the substitution of water ligands by halide at low pH in order to prevent the formation of the hydroxyl complex. Therefore under the reaction conditions involving a pH of 7-10 the aqua complex is unlikely to be present so this cannot be the cause of the pH dependence.

However, an alternative explanation that was previously dismissed was that the one of the pK_a s leading to the bell-shaped pH-rate profile was not a protonation equilibrium at all, but was in fact

the equilibrium for the displacement of halide by hydroxyl groups on the palladium complex in solution (Scheme 4). This equilibrium had initially been dismissed because it was considered unlikely that the concentration of halide in the system would coincidentally be exactly the concentration leading to an apparent pK_a equal to the pK_a one would expect for the palladium-aqua complex. For the Suzuki-Miyaura reaction, there are three hypotheses for why base is required in the transmetallation step **X** of the reaction that invokes a halide equilibrium (Scheme 5), summarised in Schemes 8 and 9,¹² as well as one for the reductive elimination step.^{12c}

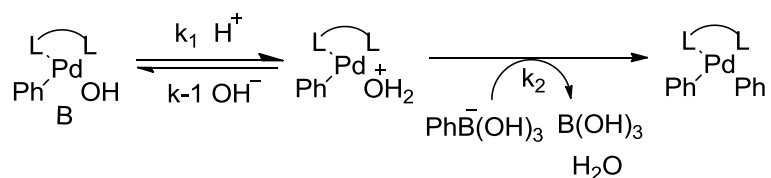


Scheme 8 - The proposed role for the base in the Suzuki-Miyaura reaction involving the displacement of halide from the palladium

Step **X** of the mechanism of the homocoupling reaction (Scheme 5) is broadly analogous to the transmetalation step of the Suzuki reaction. The transmetalation step is the step on which most investigation of the effect of base on the Suzuki-Miyaura reaction has been focussed. Matos and Soderquist^{12a} considered possible effects of the base in the reaction including whether it was

necessary to convert the boronic acid to its basic boronate form before reaction, or whether it was necessary to displace the halide from the intermediate palladium complex by hydroxide (Scheme 8). The main difference in the Suzuki-Miyaura reaction is that by its very nature the catalyst will be bound to a halide after the first oxidative addition of an aryl halide, whilst that is not necessarily true for the homocoupling reaction. Therefore, if the addition of arylboronic acid to the palladium is slowed by halide then this would be less of a concern in the homocoupling reaction.

A second possible reason for the pH dependence is the pH-dependent equilibrium between palladium aqua complexes and palladium hydroxo complexes. If only the aqua complex reacts with the boronate, this would explain why a pH maximum forms (Scheme 9).^{12b}



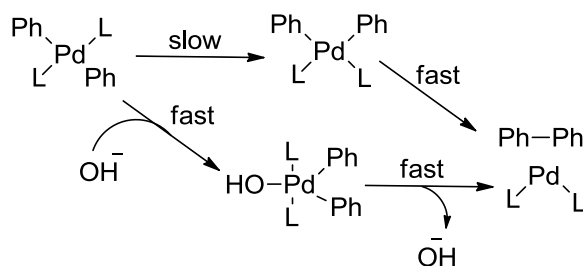
Scheme 9 - The proposed role for the base in the homocoupling or Suzuki-Miyaura reaction involving the formation of the palladium aqua complex

Too low a pH would prevent the formation of the boronate, whilst too high a pH would deprotonate the palladium aqua complex and prevent it from reacting with the boronate. This

pathway is unlikely to be the major pathway for a number of reasons. The aqua complex requires an aqueous medium to form in order to supply the proton and to stabilise the charges, meaning that this pathway would only be valid in water or a highly aqueous solvent. This is not necessarily the only factor, though, as Suzuki-Miyaura reactions are known to occur in organic solvents. Whilst the aqua-palladium mechanism would imply that the pH dependence of the Suzuki-Miyaura reaction and the homocoupling would be the same, it could be that the halide being bound to the palladium in the Suzuki-Miyaura reaction inhibits formation of both the hydroxo and aqua palladium complexes at low pH. This would also result in a relatively high pH required for optimum reactivity.

The third possibility is that the pH maximum results from the rate-determining step being switched from the transmetallation step **X** to the earlier transmetallation where the peroxide is displaced by an aryl group. If the earlier transmetallation is acid-catalysed, or at least requires the boronic acid as claimed by Adamo et al., and the latter transmetalation base-catalysed, then changing the pH would change the rate-determining step, and further changing the pH away from this point could only decrease the rate. If the rate-determining step is changing it could be due to the first transmetallation requiring the acidic form of the boronic acid, and the second step requiring the basic form. The pH effects on the two transmetallations would then explain why the pH maximum occurs on or around the pK_a of the boronic acid as each cycle would require one molecule in each form.

Recently Amatore considered the effect of base on the transmetallation step of the Suzuki-Miyaura reaction (the analogous step to step **X**, Scheme 5).^{12c} They found that the base plays two roles in this step, its primary role is displacing the halide from the palladium to form a hydroxo complex **B** (Scheme 10). This hydroxo complex, they suggested, was more reactive in the transmetallation than the corresponding halide complex. In addition, they suggested that increasing the amount of base leads to an increase in boronate formation, which they found to be less active in the transmetallation step than its boronic acid counterpart. This could be due to the favourable dative interaction between the hydroxides and the empty p-orbital in the borate which could assist the transmetallation step.



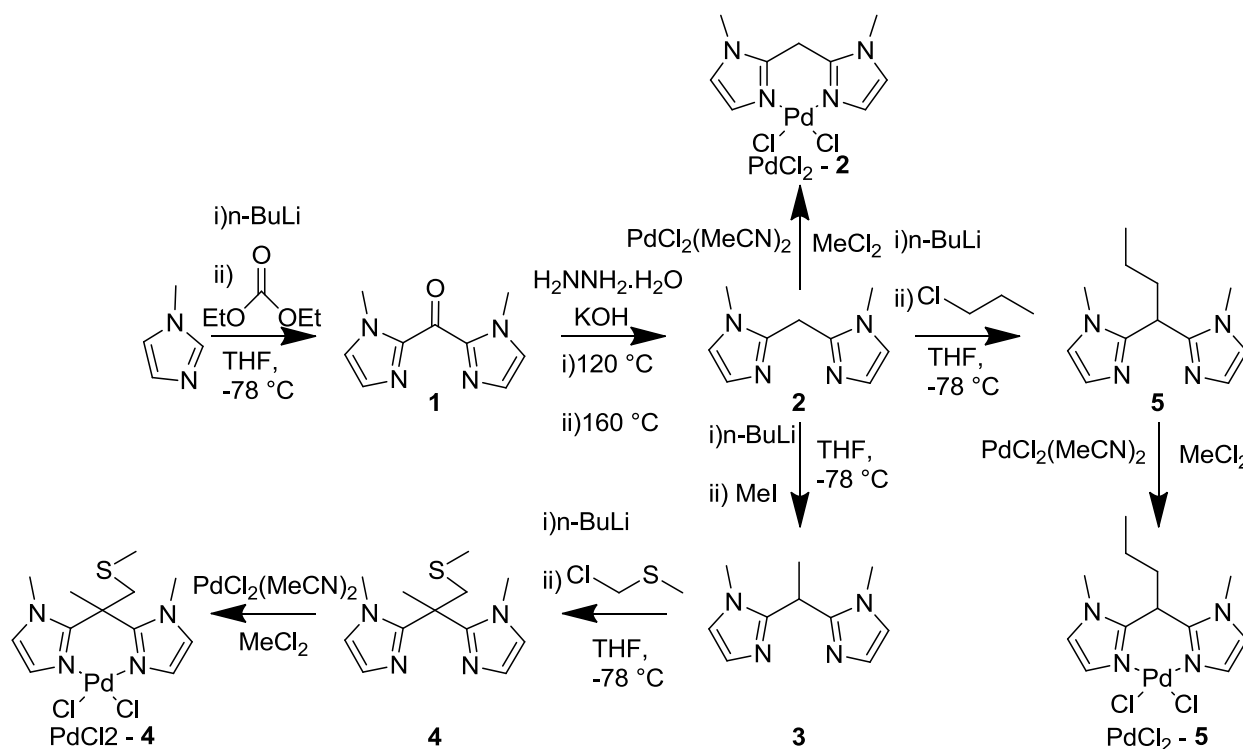
Scheme 10 - The proposed role for the base in the Homocoupling or Suzuki-Miyaura reaction in the reductive elimination step.

The idea that formation of the arylboronate slows down the reaction is contrary to the conventional wisdom that the arylboronate form is the active species in the transmetallation,^{12a} which is often given as the reason that base accelerates the reaction. In addition, Amatore *et al.*

suggest that the base aids in the final reductive elimination by providing a faster alternative route to the slow cis-trans isomerisation required before reductive elimination can occur (Scheme 7), which is, of course, irrelevant for a chelated ligand system such as our bisimidazoles.

2.1.6 - Aims

Supply of catalyst PdCl₂-**4** had run out and a reproduction of the previous synthesis⁸ of Catalyst PdCl₂-**4** was required not only for the product but also to clarify the original procedure which lacked detail. In addition the effect of the sulfur was of interest in more detailed studies. Three catalysts were selected for synthesis. The first catalyst for synthesis, catalyst PdCl₂-**2**, has no groups attached to the methylene bridge and is synthesised by attaching ligand **2** to a palladium centre. For the second complex, catalyst PdCl₂-**4**, the central methylene bridge was modified twice, once with a methyl group and then again with a methylthiomethyl group, forming ligand **4** before addition to the palladium centre. For the final complex, catalyst PdCl₂-**5**, the central methylene bridge was modified with a propyl group forming ligand **5**. The propyl group mimics the steric effect of the sulfide-containing chain of ligand **4** without the potentially coordinating sulfur atom (Scheme 11).



Scheme 11 - The synthetic pathway taken to create the three molecular catalysts PdCl₂-2, PdCl₂-4, and PdCl₂-5.

Catalyst PdCl₂-4 is not soluble in water, and neither are many of the biphenyl products of the homocoupling reaction, and so the reaction was studied with cetyltrimethylammonium bromide (CTAB), a cationic surfactant, to help solubilise the non-polar molecules in water. A cationic surfactant was chosen because the Suzuki-Miyaura reaction is base-catalysed, and the mechanism for the homocoupling was expected to bear similarities to the Suzuki-Miyaura reaction. If this expectation is borne out in practice, then the higher local pH of the Stern region, even under neutral bulk conditions, would accelerate the reaction. The local concentration of

bromide in the CTAB Stern region is high at approximately 1 mol dm^{-3} ,¹³ and because halide concentration does affect the reaction, the effect of halide on the catalyst needs to be investigated.

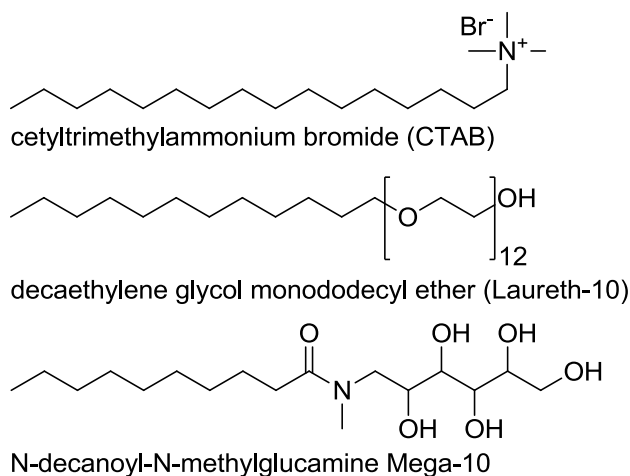


Figure 4 - The surfactants cetyltrimethylammonium bromide (CTAB), decaethyleneglycol monododecyl ether (Laureth-10) and N-Decanoyl-N-methylglucamine (MEGA-10).

By using non-ionic surfactants such as Laureth-10 and MEGA-10 (Figure 4) the effect of halide concentration on the state of the palladium complex can be studied because these non-ionic surfactants do not necessarily lead to high local halide concentrations. The halide concentration can then be adjusted by addition of halide to the system.

As the second aim, in the place of catalyst $\text{PdCl}_2\cdot 4$, catalyst $\text{PdCl}_2\cdot 2$ and $\text{PdCl}_2\cdot 5$ (Figure 3) will be explored as catalysts in the oxidative homocoupling reaction, as they are much simpler to synthesise than $\text{PdCl}_2\cdot 4$. $\text{PdCl}_2\cdot 2$ is of interest because it has less steric bulk than $\text{PdCl}_2\cdot 4$, and

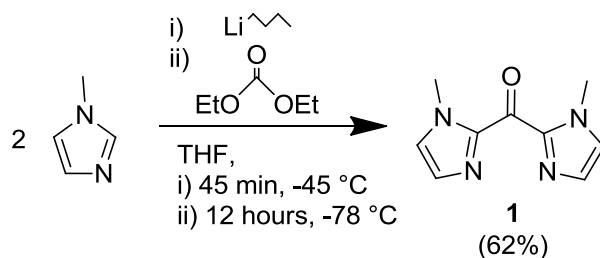
this complex will give insight into whether the bisimidazole functionality itself results in stability. PdCl₂-**5** is another analogue for PdCl₂-**4**, but will reflect whether the steric bulk of the thiol chain has any effect on the catalyst stability; the propyl group mimicks the methylthiomethyl group but does not include the thioether.

The facet of the homocoupling reaction that has caught our interest is its pH dependence. For the homocoupling reaction it was found that the rate reached its maximum around pH 9 and then sharply dropped (Figure 4).⁴ This maximum in the pH rate profile indicates that the pH effect is more than just base catalysis (as then one would not predict increasing the pH to cause a decrease in the reaction rate). Additionally, this pH maximum was found to change according to the pK_a of the boronic acid in use. Since the function of the base in both the Suzuki-Miyaura reaction and the homocoupling reaction are thought to be related to the substitution of halide ions rather than a true pK_a, the third aim is to investigate the effect of halide concentration on the pH rate profile of the homocoupling reaction.

2.2 -Results and discussion

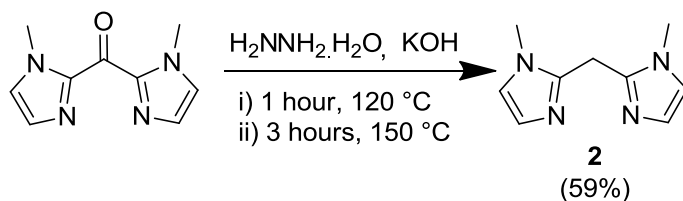
2.2.1 - Synthesis

2.2.1a - Bisimidazole 1

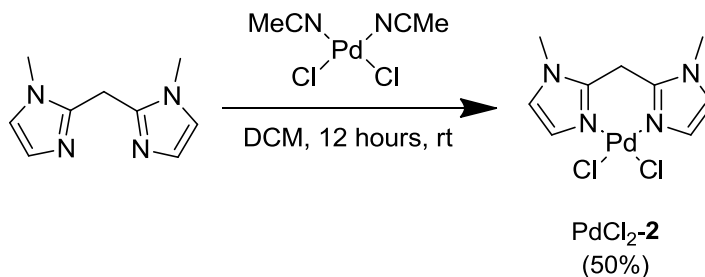


Scheme 12 - Synthesis of bisimidazole **1**

The synthesis of bisimidazole **1** is a straightforward lithiation reaction, carried out following the procedure from Dr. Sidhu's thesis exactly, giving the product quite readily in 62% yield (Scheme 12). As was previously reported, in ^1H NMR spectra the two imidazolyl protons appear as a singlet and not a doublet as one would normally have expected indicating a very small coupling constant. The singlet imidazolyl protons are a feature common to all imidazolyl compounds in this chapter.

2.2.1b - Ligand **2**Scheme 13 - Synthesis of ligand **2**

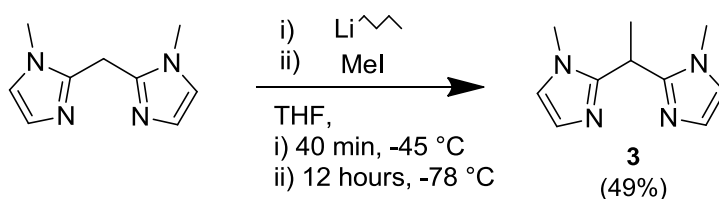
Similarly, the second step, involving a standard Wolff-Kishner procedure to synthesise ligand **2** proceeds smoothly giving the product in 59% yield (Scheme 13).

2.2.1c - Catalyst $\text{PdCl}_2\text{-2}$ Scheme 14 - Synthesis of Catalyst $\text{PdCl}_2\text{-2}$

Since ligand **2** is easily synthesised in good yields, it forms a perfect starting point for making a new catalyst that does not contain a sulfide group. Ligand **2** was added to palladiumbisacetonitrile dichloride in dichloromethane and stirred in solution resulting in precipitation of catalyst $\text{PdCl}_2\text{-2}$ as an orange powder. The literature work-up⁸ described for similar catalysts was not viable as the powder was not appreciably soluble in either hexane or

dichloromethane. No $^1\text{H-NMR}$ spectrum could be recorded in chloroform, and instead the $^1\text{H-NMR}$ spectrum was recorded in acetonitrile in which catalyst $\text{PdCl}_2\text{-2}$ was slightly soluble (^{13}C was not obtained as the catalyst was not sufficiently soluble for the peaks to be discerned from the background noise, even in acetonitrile). The powder was dissolved in hot acetonitrile, with the assistance of ultrasound in dissolving the powder, which gave the product as a pure orange powder in 50% yield (Scheme 14). Storing the mother liquor in a freezer eventually yielded large needle-like crystals that were used to obtain a crystal structure (Figure 5) *vide infra*. Catalyst $\text{PdCl}_2\text{-2}$ was dissolved in acetonitrile in order to make a stock solution (0.17 mM) which appears to be near the catalyst's solubility limit - solutions with a concentration of 0.22 mM left a fine powder in suspension that would not dissolve at room temperature. Catalyst $\text{PdCl}_2\text{-2}$ appears to be insoluble in 50:50 acetonitrile:water unlike the sample of catalyst $\text{PdCl}_2\text{-4}$ previously provided by Dr. Sidhu. The synthesis of the ligands to create catalysts $\text{PdCl}_2\text{-4}$ and $\text{PdCl}_2\text{-5}$ uses ligand **2** as a starting point and involves its functionalisation via lithiation.

2.2.1d - Bisimidazole **3**

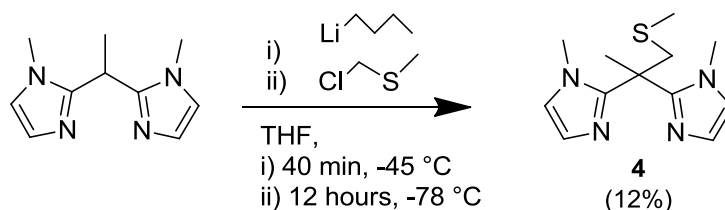


Scheme 15 - Synthesis of Bisimidazole **3**

The synthesis of bisimidazole **3** (Scheme 15) proceeded as anticipated, lithiating the bridging methylene using *n*-butyl lithium and substituting with iodomethane. The reaction appeared to be

particularly sensitive to the addition rate of the iodomethane which should be kept to one drop every thirty seconds - too hasty addition would turn the mixture a dark colour and form an impurity that complicated the purification of the product. However, the amount of iodomethane did not adversely affect the reaction as long as it was in excess, and the remaining iodomethane was removed along with the solvent in the work-up. Purity of the starting materials at this step is important, since the lithiation reaction is sensitive even under ideal conditions often leading to low yields or worse the complete failure of the reaction. If bisimidazole **3** cannot be crystallised to purity, the impurity can be removed by flash column chromatography as described for ligand **4**. The yield varied from 5% - 50% with an addition rate of the iodomethane of one drop every thirty seconds giving the best yield.

2.2.1e - Ligand 4

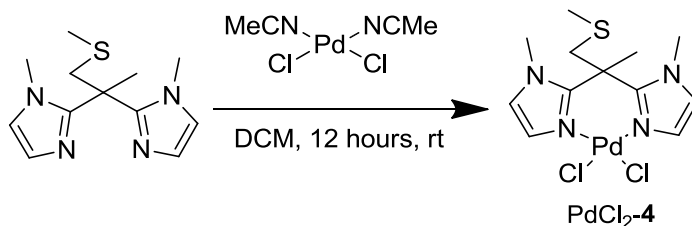


Scheme 16 - Synthesis of Ligand **4**

The synthesis of ligand **4** is rather difficult. As previously mentioned, the purity of the reagents is important, since the reaction seems very sensitive to adverse reactions. It may be that the final proton on the methylene bridge is difficult to abstract, but the reaction is certainly not made easier by the nature of the reactant chloromethylmethyl sulfide which, apart from the stench, is likely hazardous to health based on its similarity to sulfur mustards (despite the MSDS only

warning of its flammability).¹⁴ When the reaction did yield product the work up was usually more successful if the solvent was removed at room temperature, but even still the product was impure and formed an oil with a moderate sulfur odour. Crystallisation never succeeded (it is possible that breaking the planarity of the molecule by adding this chain makes crystallisation less favourable). The only method that successfully purified ligand **4** was flash column chromatography over silica. The polarity of the eluent (up to 30% methanol in ethyl acetate, although this is already high enough that some silica may be brought through) is far higher than would normally be used. Due to the coordinating nitrogen atoms, 1% triethylamine was added to prevent streaking, and a gradient from 4% to 30% methanol in ethyl acetate seemed to work better than a constant ratio. When the reaction worked, the yield was low (12% was the highest recorded) (Scheme 16).

2.2.1f - PdCl₂-4

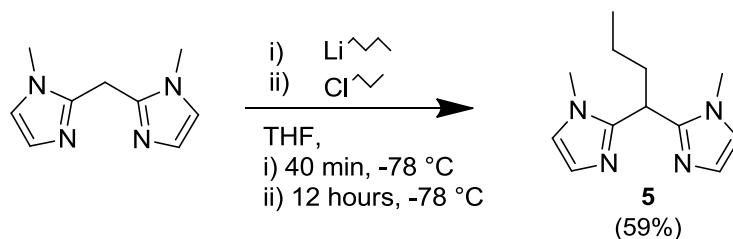


Scheme 17 - Synthesis of Catalyst PdCl₂-4

The small amount of ligand **4** that had been successfully synthesised was added to bisacetonitrilepalladium dichloride following the same procedure as described for catalyst **1**, which yielded a small quantity of rusty brown powder. This powder was also insoluble in hexane

or dichloromethane, so recrystallising as described in previous reports was not possible.⁸ Instead the powder was dissolved in acetonitrile and the ¹H NMR spectrum was recorded which revealed that the powder did not contain catalyst PdCl₂-**4** (or any trace of the bisimidazolyl compound). Due to this loss of the ligand **4** and the difficulty faced in synthesising it, PdCl₂-**4** was not successfully resynthesised. (Scheme 17)

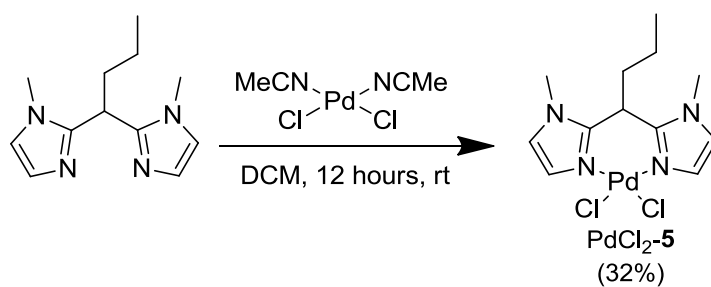
2.2.1g - Ligand **5**



Scheme 18 - Synthesis of ligand **5**

Ligand **5** was straightforward to synthesise by comparison, seeing as it used a far less offensive reagent and was only one step from ligand **2** rather than two. Removing the reaction solvent during the work up left an oil that would not crystallise. The oil was also purified by flash column chromatography, in a similar manner to ligand **4** but instead using a constant 15% methanol and 1% triethylamine in ethyl acetate eluent giving the product in 59% yield (Scheme 18).

2.2.1h - Catalyst PdCl₂-**5**

Scheme 19 - Synthesis of Catalyst PdCl₂-5

The ligand was attached to palladium using the same procedure as for catalyst PdCl₂-2, giving catalyst PdCl₂-5 as a rusty brown powder. (Scheme 19) The powder was recrystallised from acetonitrile to form a pale brown powder. Leaving the mother liquor in a freezer eventually formed sharp needle crystals which were used to obtain crystal structures. Again, a ¹H NMR spectrum was obtained in acetonitrile, but the catalyst was not sufficiently soluble to record a ¹³C NMR. Unusually, the crystal appears to be a co-crystal with two components - the expected structure and also the structure with chloride substituted by what could be a carbonyl or cyanide group (*vide infra*).

2.2.2 - Catalyst Characterisation

2.2.2a - Crystal Structures

First, the environment of the palladium centre as offered by the ligand was studied, since changes to that environment may affect the catalytic activities of the formed complexes. Whilst not necessarily reflective of the palladium species as it exists in solution during the reaction, the crystal structure of the palladium (II) pre-catalyst illustrates the steric and electronic effects of the ligand on the palladium centre. The crystal structure for PdCl₂-**2** was determined (Figure 5).

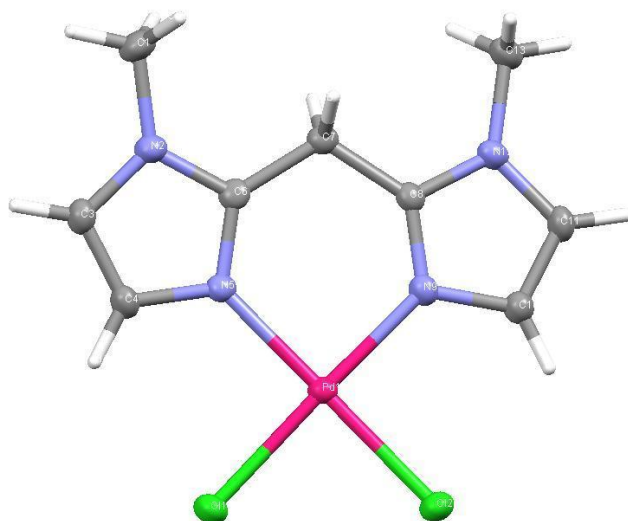


Figure 5 - The crystal structure of PdCl₂-**2** obtained by XRD of crystals grown from acetonitrile.

Figure 5 and the accompanying crystallographic data (Table 1 and Appendix A.1) show that the crystal structure of PdCl₂-**2** is only slightly different from that previously found for PdCl₂-**4** (Figure 4).⁸ The length of the Pd-Cl bonds and the Pd-N bonds do not appear to be affected by the change in ligand, with both Pd-Cl bonds being approximately 2.3 Å in length and both Pd-N bonds being approximately 2.0 Å. There are bigger changes in the bond angles, however, with the N-Pd-N angle being 4.5° larger in PdCl₂-**2**, and the Cl-Pd-Cl angle is 3.75° smaller compared to PdCl₂-**4**. This difference in bond angles indicates that the removal of the side chains on the bridging carbon of ligand **2** has increased the bite angle compared to ligand **4**.

The crystal structure for PdCl₂-**5** was similarly determined and found to be a co-crystal (Figure 6).

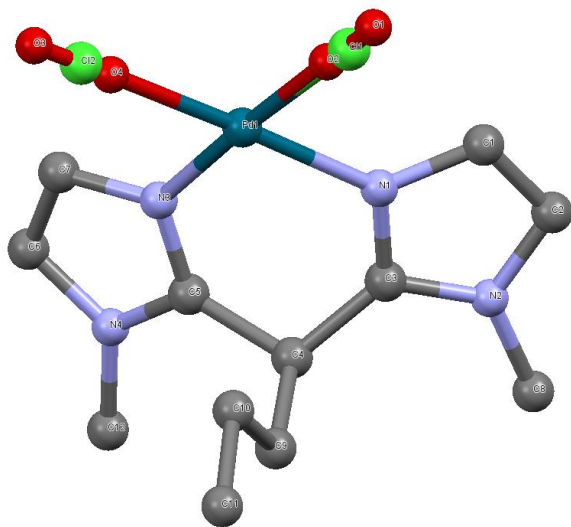


Figure 6 - The crystal structure of PdCl₂-**5**/PdR₂-**5** obtained by XRD of co-crystals grown from acetonitrile, where R could be MeCN.

Figure 6 and the accompanying crystallographic data (Table 1 and Appendix A.2) show that the crystal structure obtained from the XRD analysis of PdCl₂-**5** identified the structure of the bisimidazolyl ligand, but the remaining ligands attached to the palladium were less certain. The diffraction pattern suggested that, along with the chloride anions, there were also diatomic species around the palladium centre with electron densities corresponding to late second-row elements. This finding indicates that the crystal was a mixture of at least two different complexes where one or both of the chloride anions had been displaced by a diatomic molecule or ion. The distance between the two atoms of the diatomic species is 1.1 Å, so it appears that a diatomic molecule has displaced the chlorides, although why it should appear in the PdCl₂-**5** crystal and not the PdCl₂-**2** or PdCl₂-**4** is not clear. The diatomic bond length is too short to be molecular oxygen (~1.4 Å) and the proton in hydroxide would be too small to be visible in XRD. The diatomic bond length is much closer in length to the C-N triple bond length in a cyanide ligand or the C-O triple bond length in a carbon monoxide ligand which are both (~1.1 Å). The Pd-Cl bond length is not unusual at approximately 2.34 Å, which is slightly longer than found for PdCl₂-**2** or PdCl₂-**4**. The bond length of the Pd-N bonds is again approximately 2.0 Å, just as for PdCl₂-**2** and PdCl₂-**4**. The bond angles are also much closer to those found for PdCl₂-**4**, with the N-Pd-N bond angle only being 1.5° wider and the Cl-Pd-Cl bond angle being only 0.5° wider. The similarity in bond angles and bond lengths makes sense with what was found for PdCl₂-**2** as the bridging carbon is more sterically hindered, but less so than PdCl₂-**4** which has a bulkier S atom on the chain and a second methyl group. The sum of the bond angles of all the groups attached to PdCl₂-**2** is 360.24° and for PdCl₂-**5** is 359.97° meaning they are both square planar complexes (as is PdCl₂-**4** which has a sum of exactly 360°). The crystal structures thus imply that the change in geometry is caused by the steric effect of groups on the side chain constricting the

bite angle of the chelating bisimidazolyl ligand. Additionally, since there is little difference in the bond lengths around the palladium, it would imply that the change in the ligand structure has not significantly affected the electronic structure of the palladium centre. The lack of change in electronic structure of the complex should be reflected by similar activity of all the catalysts in the homocoupling reaction, although the larger bite angle of ligand **2** could affect the rate constants of the reaction given the bulk of the phenyl groups in the reactant. Whether this steric effect is a positive or negative effect would depend on whether the rate-determining step is the addition of phenyl groups to the palladium (which would be slowed by the larger bite angle) or the elimination of biphenyl (which would be accelerated).

Table 1 - Selected bond lengths and bond angles around the palladium centre from the XRD crystal structures of PdCl₂-4,⁸ PdCl₂-2 and PdCl₂-5. Errors are given where available and are calculated by

	Bond Length (Å)		Bond Angles (°)	
	Pd-Cl3	2.284	N2-Pd-N3	85.69
PdCl ₂ -4	Pd-Cl4	2.308	Cl3-Pd-Cl4	91.17
	Pd-N2	1.998	Cl3-Pd-N2	91.43
	Pd-N3	2.004	Cl4-Pd-N3	91.71
	Pd-Cl3	2.296 ± 0.003	N2-Pd-N3	90.00 ± 0.36
PdCl ₂ -2	Pd-Cl4	2.312 ± 0.003	Cl3-Pd-Cl4	87.43 ± 0.09
	Pd-N2	2.032 ± 0.009	Cl3-Pd-N2	91.00 ± 0.27
	Pd-N3	2.034 ± 0.009	Cl4-Pd-N3	91.81 ± 0.24
	Pd-Cl3	2.374 ± 0.012	N2-Pd-N3	87.22 ± 0.33
PdCl ₂ -5	Pd-Cl4	2.323 ± 0.006	Cl3-Pd-Cl4	91.61 ± 0.33
	Pd-N2	2.002 ± 0.009	Cl3-Pd-N2	89.41 ± 0.36
	Pd-N3	2.035 ± 0.009	Cl4-Pd-N3	91.73 ± 0.30

2.2.2b – ^1H -NMR spectroscopic studies of catalyst $\text{PdCl}_2\text{-2}$

Crystal structures do not necessarily reflect the state of chemicals in solution so the NMR spectra of the catalyst in different solutions were recorded in order to see the effect of the solution on the ligands attached to the palladium centre. Changes in the complexation environment of the palladium centre are most likely to affect the chemical shift of the imidazolyl protons, since they are part of the π -system containing the co-ordinating nitrogens.

Complex $\text{PdCl}_2\text{-2}$ is sparingly soluble in MeCN and D_2O , but it is possible to detect changes in the ^1H -NMR spectrum of the complex as the solvent conditions are changed (Figures 7-12).

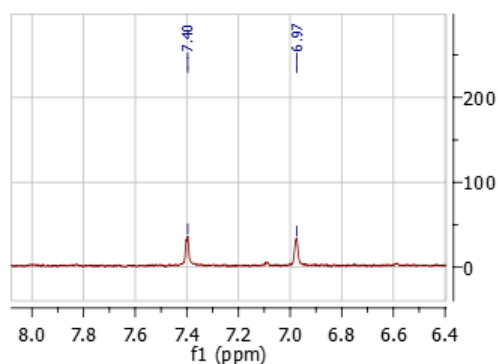


Figure 7. The portion of the ^1H NMR spectrum corresponding to the imidazolyl protons of catalyst $\text{PdCl}_2\text{-2}$ in $\text{d}_3\text{-MeCN}$.

The ^1H -NMR spectrum for $\text{PdCl}_2\text{-2}$ in dry acetonitrile shows a single pair of peaks at δ 7.40 and δ 6.97 (Figure 7).

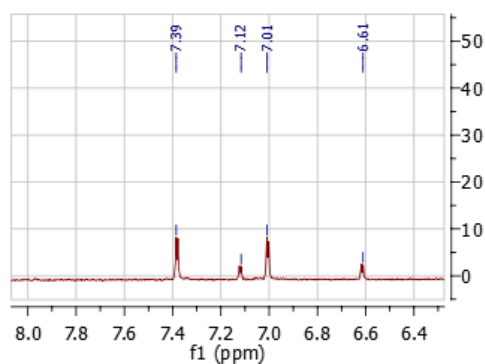


Figure 8. The portion of the ¹H NMR spectrum corresponding to the imidazolyl protons of catalyst PdCl₂-2 in d₃-MeCN with a single drop of D₂O added.

Adding a drop of D₂O to the solution (making a 1:20 water:acetonitrile volume ratio) causes the formation of two new peaks at δ 7.12 and δ 6.61 which are likely due to the formation of either the Pd-aqua or Pd-hydroxyl complex (Figure 8).

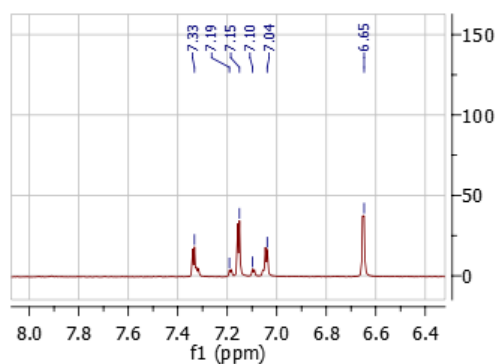


Figure 9. The portion of the ¹H NMR spectrum corresponding to the imidazolyl protons of catalyst PdCl₂-2 in d₃-MeCN with a second drop of D₂O added.

Adding a further drop of D₂O (making the water:acetonitrile volume ratio 1:10) causes the reduction of the peaks at δ7.33 and δ 7.04 and the heightening of peaks at δ7.15 and δ6.65, as well as the appearance of small peaks at δ 7.19 and δ 7.10 (Figure 9).

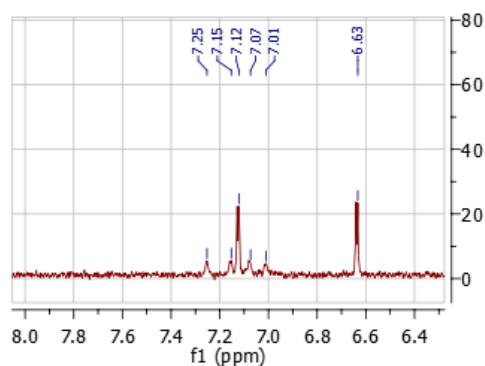


Figure 10. The portion of the ¹H NMR spectrum corresponding to the imidazolyl protons of catalyst PdCl₂-2 in 1:1 d₃-MeCN:D₂O.

Increasing the volume ratio of D₂O:MeCN in the solution to 1:1 completely eliminates the original δ 7.40 and δ 6.97 peaks leaving the δ 7.12 and δ 6.63 peaks, as well as four very small peaks between δ 7.00-7.25 (Figure 10). We assign the original pair of peaks at δ 7.4 ppm and δ 7.0 ppm to the PdCl₂-**2** species and the pair at δ 7.1 ppm and δ 6.6 ppm to either the PdCl(OH)₂-**2** or Pd(OH)₂-**2** species. The four small peaks do not appear to correspond to any of the previously observed complexes, so it is not clear what is causing them. Since it is not in rapid exchange on the NMR timescale, it is unlikely to be an aqua-hydroxo equilibrium. Perhaps it could be an oxo-bridged di-palladium species.

Since addition of water to the complex has caused the halide ligands to be displaced, it should be possible to push the equilibrium back towards the original complex by addition of chloride ions to the solution (Figure 11).

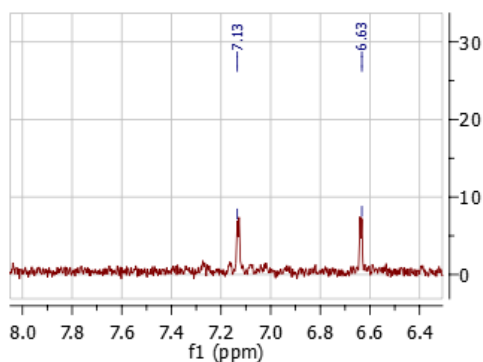


Figure 11. The portion of the ¹H NMR spectrum corresponding to the imidazolyl protons of catalyst PdCl₂-**2** in 1:1 d₃-MeCN:D₂O and 0.4 M NaCl.

Addition of chloride to the system in 1:1 D₂O:d₃-acetonitrile does not appear to have much effect on the equilibrium between the palladium-aqua and palladium-chloride species as the peaks appear unchanged. The four small unidentified peaks that were visible in Figure 9 are no longer visible. Since chloride does not seem to have had much of an effect on the complex, the experiment was repeated with an equal concentration of bromide ions to see if this would change the complex's state (Figure 12).

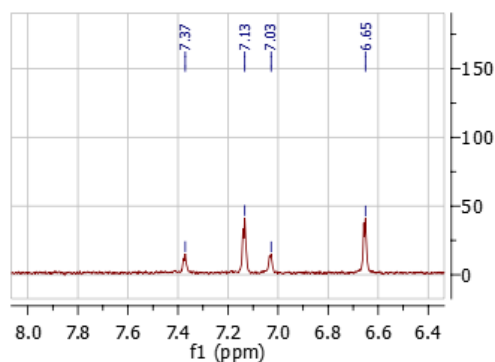


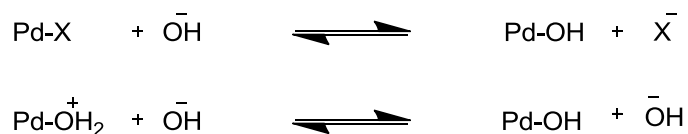
Figure 12. The portion of the ¹H NMR spectrum corresponding to the imidazolyl protons of catalyst PdCl₂-2 in 1:1 d₃-MeCN:D₂O and 0.4 M NaBr.

If instead of chloride an equivalent amount of bromide is added, then a change is visible, with the peaks at δ 7.4 ppm and δ 7.0 ppm being restored and the peaks at δ 7.13 and δ 6.65 diminished. This observation implies that there is a stronger interaction between the palladium and the bromide than there is with the chloride, as the equilibrium lies further towards the halogenated complex when bromide is used at the same concentration as chloride. If the

halogenated complex is not active in the catalytic cycle then this interaction with bromide would significantly slow the reaction by pushing the equilibrium towards the halo-complex.

2.2.2c - pK_a s of catalyst PdCl₂-2 in Laureth-10

The pK_a of PdCl₂-4 was previously determined to be 8.0 in 10 mM CTAB. This value was thought to match the assumed mechanism involving a Pd-aqua Pd-hydroxyl equilibrium (*vide supra*) but this pK_a may not have been a true pK_a in light of the effect of halide ions on the catalyst. Rather it may have reflected the equilibrium for the displacement of halide from the palladium by hydroxide that appeared as a pK_a because pH is inversely proportional to the concentration of hydroxide in water (Scheme 20).



Scheme 20. The two possible equilibria that could give rise to the apparent pK_a observed for PdCl₂-4.

If the observed pK_a of the catalyst is changed by the halide concentration then it is not a true pK_a but rather a halide - hydroxyl equilibrium which will be referred to as an apparent pK_a . If the catalyst is in equilibrium between its hydroxyl and halide bound forms under the reaction

conditions, rather than between aqua and hydroxyl forms, then some of the assumptions previously made about the mechanism are likely to have been wrong. In order to test if the pK_a is affected by halide the pK_a will be determined with varying halide concentrations. The UV absorbances are used as an approximation for the concentration, since the concentration of a species is directly related to its absorbance at a given wavelength by a factor called its extinction coefficient by the Beer-Lambert law. UV-visible absorbances are recorded as a function of pH and these are analysed in terms of Equation 1. Since the two species will have different extinction coefficients, but the total concentration of palladium is constant, the absorbance at any given pH can be used to approximate the proportion of each species giving an absorbance factor which is equivalent to the extinction coefficient multiplied by the palladium concentration. Equation 1 has two components that approximate the absorbance, which assumes that the top and bottom of the sigmoidal plot correspond to the absorbance ~100% of each species respectively. The concentration of each species is modeled as an exponential, one which increases as the pH does, and the other which decreases over the same period, and as such the total concentration of both species is constant. These concentrations are multiplied by the absorbance factor for the species and these two absorbances added to give the total absorbance at that pH. Plotting the range of absorbances will therefore give rise to a sigmoidal graph. It should be noted, that this model does assume that there will be a single pK_a over the studied range. A second pK_a could be modelled in the same way, by adding a third concentration, but would be much harder to analyse, as the proportion of the second species would not reach ~100%, so this would not give rise to the absorbance factor.

$$A_{\text{obs}} = \frac{1}{1 + 10^{(\text{pH}-\text{p}K_a)}} \cdot A_{\text{low pH}} + \frac{1}{1 + 10^{(\text{p}K_a-\text{pH})}} \cdot A_{\text{high pH}}$$

Equation 1

The UV-Vis absorbance of catalyst PdCl₂-2 was recorded in the absence and presence of halide ions to see if the change in catalyst could be observed by UV-Vis spectrometry (Figure 13)

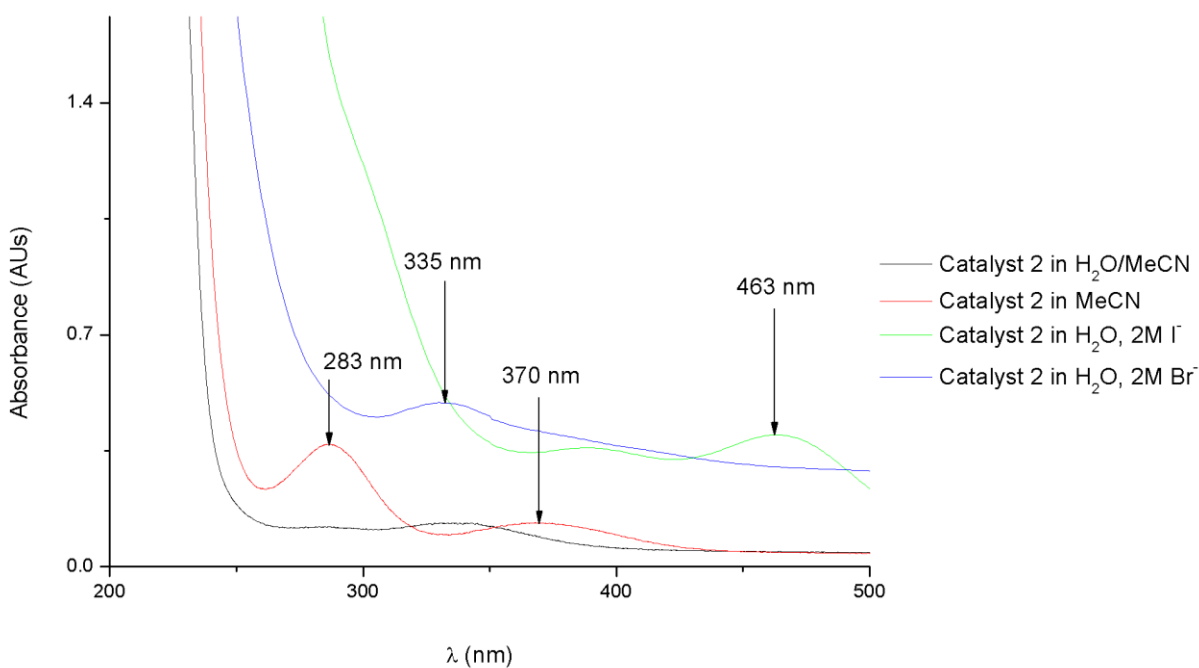


Figure 13. The spectra of catalyst PdCl₂-2 (10 μM) in various solutions.

The UV-visible spectrum of catalyst PdCl₂-2 in acetonitrile changes upon addition of water to the catalyst solution (Figure 13). This change in UV-visible spectrum can be attributed to the

same process that leads to the change in the observed $^1\text{H-NMR}$ spectra (See section 3.2.2). The peaks at 283 nm and 370 nm in the spectra in pure acetonitrile (red line) vanish and are replaced by a single broad absorbance at 335 nm (navy blue line). This absorbance is likely due to the displacement of the chloride by water to either form the palladium-hydroxo or palladium-aqua complex. Figure 12 also shows that addition of halide to the complex $\text{PdCl}_2\text{-2}$ has an effect on the catalyst absorbance. Addition of 2 M sodium iodide caused the peak to shift to a longer wavelength of 463 nm and the absorbance below 350 nm was much higher (well above 1 unit). Addition of 2 M sodium bromide does not shift the position of the peak relative to the presumed aqua-complex, however there is a large increase in the absorbance below 285 nm. Both the halide containing solutions have an elevated base line, which is due to the absence of acetonitrile to solubilise the catalyst causing precipitation.

In order to find the $\text{p}K_a$ of the complex without causing precipitation, surfactants CTAB and laureth-10 were used (Figure 1). If the observed $\text{p}K_a$ of the catalyst is due to the halide displacement equilibrium one would expect a low $\text{p}K_a$ in the absence of added halide and when using laureth-10 (which contains no halide counterions) as the solubilising surfactant. However, sigmoidal pH rate profile was not observed until halide was added to the system. A system with 2 M NaBr (Figure 14) in laureth-10 was tested as this concentration is similar to the bromide concentration in the Stern region of CTAB.

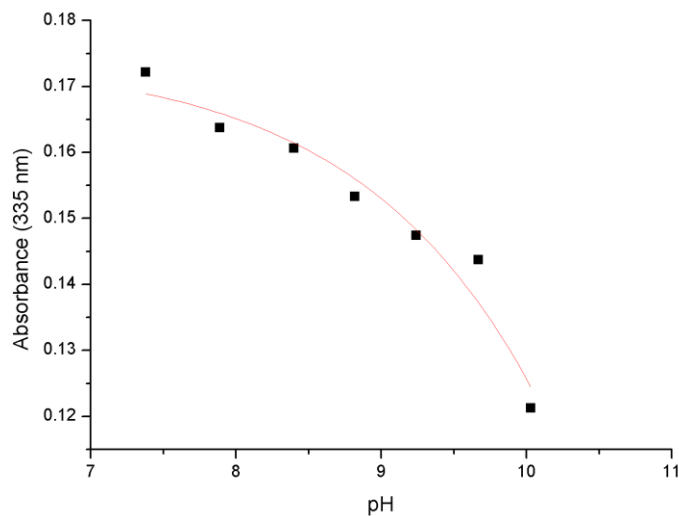


Figure 14. The absorbance at 335 nm of catalyst PdCl₂-2 (10 μM) at various pHs in laureth-10 (100 mM) in the presence of 2 M NaBr.

Addition of bromide ions to the solution does cause it to exhibit an apparent pK_a . At 2 M bromide the apparent pK_a is high, beyond the buffering range of the borate buffers, but the start of the slope is visible around pH 10 (Figure 14). The bromide concentration was reduced to 0.5 M and the pK_a was determined (Figure 15).

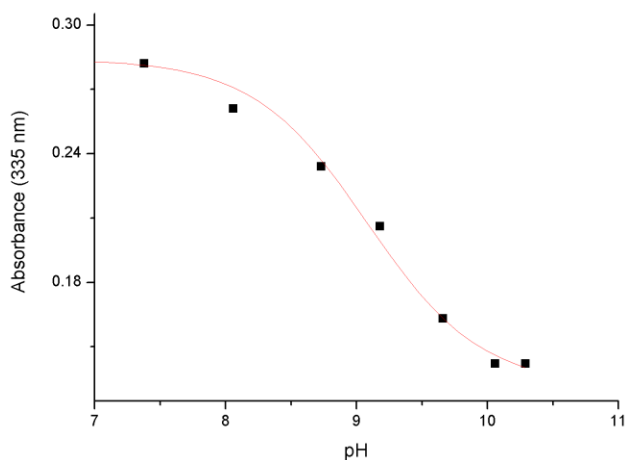


Figure 15. The change in absorbance at 335 nm of catalyst PdCl₂-2 (10 μM) at various pHs in laureth-10 (100 mM) in the presence of 0.5 M NaBr.

Decreasing the bromide concentration to 0.5 M gives rise to an apparent pK_a of 9.08 ± 0.07 (Figure 15). This is a higher pK_a than was found for catalyst PdCl₂-4 in CTAB, despite the bromide concentration of the solution being lower than in the Stern region of CTAB. This difference could be due to the fact that the local pH is also higher in the Stern region of cationic surfactants than in the bulk solution, which reduces the apparent pK_a of the catalyst. This difference in local pH means that results in the different surfactant systems are not directly comparable.

The bromide concentration was further reduced to 0.05 M and the pK_a was measured again to see if it would again decrease (Figure 16).

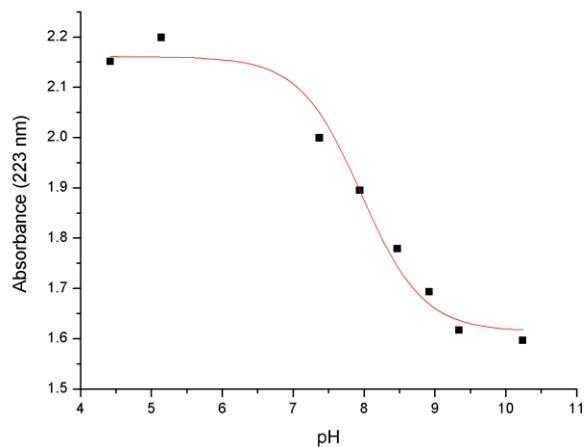


Figure 16. The change in absorbance at 223 nm of catalyst PdCl₂-2 (10 μM) at various pHs in laureth-10 (100 mM) in the presence of 0.05 M NaBr.

Despite the fact that there is a peak at 335 nm in the UV, the largest change in absorbance with pH was actually at 223 nm, which is in the shoulder of the large peak that is at or below 200 nm. At a bromide concentration of 0.05M bromide this gives a p*K*_a of 7.96, which is approximately the same as the p*K*_a of PdCl₂-4 in CTAB.

Repeating these experiment in D₂O yields observed p*K*_a^{*} values at all bromide concentrations that are higher by approximately 0.4. This increase in apparent p*K*_a^{*} value is as expected, given that the pD of a solution is typically 0.41 units higher than the pH* measured by a conventional glass electrode (and hence the p*K*_a of the catalyst).¹⁵

The pK_a and pK_a^* values recorded in D_2O and H_2O in the presence of varying concentrations of Br^- are summarised in Figure 16.

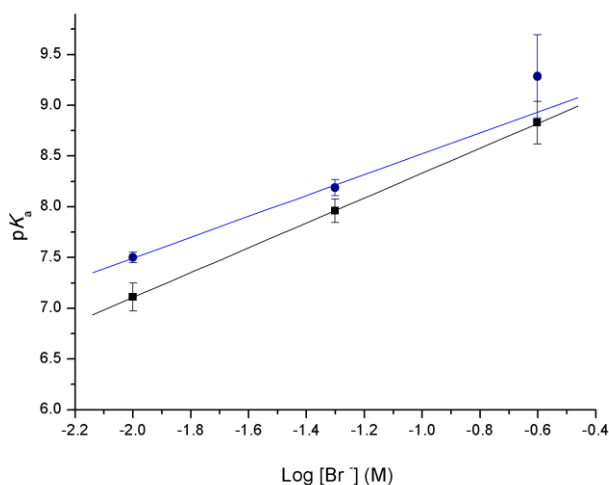


Figure 17. The change in apparent pK_a of catalyst $PdCl_2-2$ ($10 \mu M$) at various Br^- concentrations in H_2O (■) and D_2O (●) in Laureth-10 (100 mM).

Figure 17 shows that in both H_2O and D_2O the pK_a changes linearly with $\log[Br^-]$ which is exactly what would be expected for the halide dissociation equilibrium in Scheme 5. Both relationships have a similar gradient (1.20 ± 0.17 for H_2O compared to 1.02 ± 0.13 for D_2O). This observed pK_a is the result of halide-hydroxide exchange at the palladium (Equation 2.i). Equation 2.ii shows an equilibrium constant for an acid-base dissociation, K_a . Equation 2.iii shows the equilibrium constant for the halide exchange, K , which can be rearranged to give Equation 2.iv. Since the acidic form $PdOH_2$ in equation 2.ii is actually $PdBr$, then substituting Equation 2.iv into Equation 2.ii gives Equation 2.v, which gives the acid-base dissociation constant in terms of K . Therefore if you convert it into a pK_a (Equation 2.vi) it shows the gradient of this relationship

should be linear with a gradient of 1 as the observed pK_a would be directly proportional to $\log [Br^-]$.



$$\text{ii} \quad K_a = \frac{[PdOH] \cdot [H_2O]}{[OH^-] \cdot [PdOH_2]^+}$$

$$\text{iii} \quad K = \frac{[PdOH] \cdot [X^-]}{[OH^-] \cdot [PdX]}$$

$$\text{iv} \quad \frac{[PdOH]}{[PdX]} = K \frac{[OH^-]}{[X^-]}$$

v

$$\text{vi} \quad K_a = \frac{K}{[X^-]}$$

Equation 2

$$pK_a = pK + \text{Log}[X^-]$$

The effect of chloride on the catalyst pK_a was then investigated under similar conditions, to see if the effect on the apparent pK_a differed from the effect exerted by bromide. The absorbance was measured at high and low pH at a chloride concentration of 50 mM in order to find the wavelength of greatest change (Figure 18).

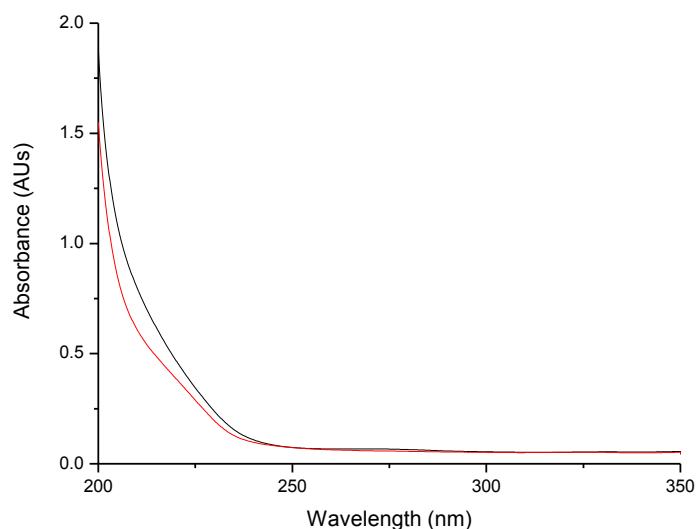


Figure 18. The spectra of catalyst PdCl₂-2 (10 μM) in Laureth-10 (10 mM), chloride (0.05 M) - and pH 5.43 and - pH 9.33.

In the presence of 50 mM chloride there is only one clear peak that has a λ_{max} below 200 nm and the biggest change in absorbance with pH occurs at 212 nm. This difference in UV-visible spectra between the bromo and chloro complexes is in agreement with the similar difference between bromo- and iodo-complexes (vide supra) and suggests significantly different electronic effects in the different complexes. The pK_a was determined by plotting the absorbance at 212 nm as a function of pH (Figure 19).

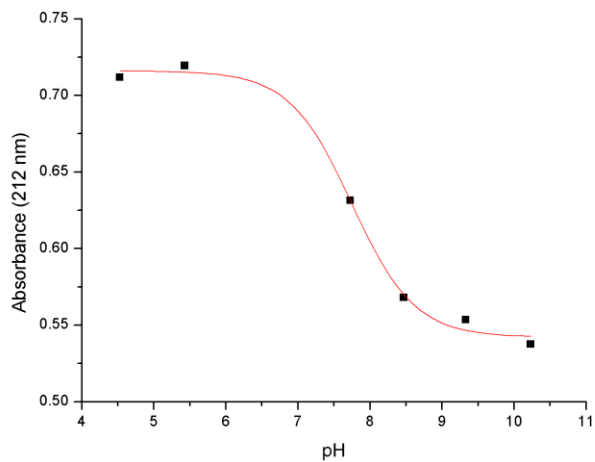


Figure 19. The change in absorbance at 212 nm of catalyst PdCl₂-2 (10 μM) at various pHs in laureth-10 (100 mM) with 0.05 M NaCl.

The pK_a of PdCl₂-2 at 0.01 M chloride is the same as the pK_a for 0.01 M bromide (7.1), but increasing the chloride concentration to 0.05 M only leads to a pK_a of 7.7 (Figure 19) whereas at the corresponding bromide concentration the pK_a is 7.96.

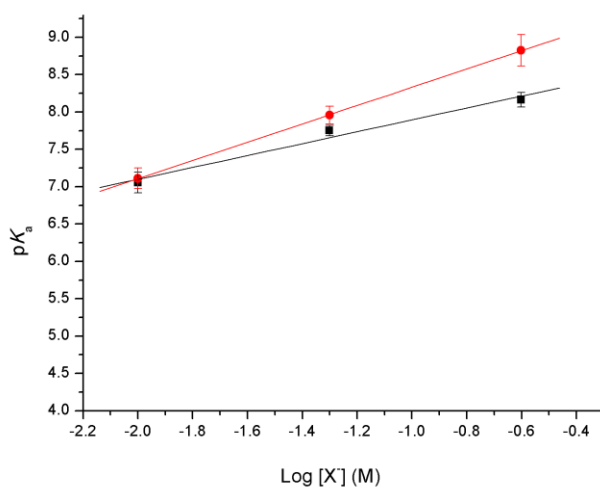


Figure 20. The change in apparent pK_a of catalyst $\text{PdCl}_2\text{-2}$ ($10\ \mu\text{M}$) at various Br^- (● $R^2=0.99991$) or Cl^- (■ $R^2=0.95838$) concentrations in H_2O and laureth-10 ($100\ \text{mM}$).

Figure 20 shows the gradient of absorbance at $212\ \text{nm}$ as a function of chloride concentration is 0.8 ± 0.12 which is shallower than for the bromide. This indicates that at a given concentration of chloride and pH the equilibrium lies further towards the hydroxyl form of the complex than for the same concentration of bromide. This would imply that if halide affects the rate of the homocoupling reaction, then chloride would have not increase the pH maximum as much as bromide would. This is not as expected, since according to equation 2 the gradient should be 1.

The recorded pK_a s in H_2O and D_2O with Br^- and Cl^- are summarised in Table 2.

Table 2. The change in pK_a of catalyst $PdCl_2-2$ ($10 \mu M$) at various concentrations of NaBr and NaCl in laureth-10 (10 mM), H_2O and D_2O .

Halide concentration (M)	pK_a Br (H_2O)	pK_a Br (D_2O)	pK_a Cl (H_2O)
1×10^{-2}	7.1 ± 0.14	7.5 ± 0.05	7.1 ± 0.14
5×10^{-2}	7.96 ± 0.12	8.2 ± 0.08	7.7 ± 0.07
2.5×10^{-1}	8.8 ± 0.21	9.3 ± 0.41	8.2 ± 0.10

2.2.2d - pK_a of catalyst $PdCl_2-2$ in aqueous CTAB solutions

The effect of pH and halide concentration in the bulk solvent on local conditions in the Stern region is not directly analogous between non-ionic and cationic surfactants. To allow comparison of the effect of the catalyst structure on the apparent pK_a with the results for $PdCl_2-4$ in CTAB, the pK_a of $PdCl_2-2$ in CTAB was determined. The wavelength where the greatest change in absorbance occurred with changing pH in CTAB was 223 nm, and in CTAC this wavelength was 227 nm. Therefore, absorbances at these wavelengths were used for the pK_a determinations.

The pK_a of $PdCl_2-2$ in the presence of 0.01 M CTAB was found to be 6.8 ± 0.2 , which is considerably less than the 8.0 ± 0.1 which was found for $PdCl_2-4$ at the same catalyst and CTAB concentrations. This decrease in the apparent pK_a upon changing the ligand could be a result of the change in the bite angle of the ligand (*vide supra*). Since bromide ions are larger than hydroxide groups, the fact they are pushed closer together by the larger bite angle of the ligand

may destabilise the halide complex and as such favour the displacement of halide by base. If this were the case then it would be expected that the maximum in the pH-rate profile for the homocoupling reaction would occur at a lower pH for PdCl₂-**2** than for PdCl₂-**4**.

The effect of the bromide concentration on the apparent pK_a of the pre-catalyst in CTAB cannot simply be tested by adding bromide ions to the reaction for two reasons. First the concentration of bromide in the Stern region of the micelles is already high, and bromide will localise itself in the Stern region due to attraction to the cationic head groups. This means that adding even a small amount of bromide to the system will have a large effect on the local bromide concentration in the Stern region, and the Stern region will be quickly saturated in bromide. Also, the addition of halide can alter the size and shape of the micelles, and this is not conducive to monitoring trends, as the change in the Stern region may reflect more than simply the change in local halide concentration.

Instead, the bromide concentration was varied by changing the concentration of CTAB, which would have the effect of increasing the effective concentration of bromide in the system as the volume of the micellar pseudophase is increased. This increase in volume will dilute the catalyst and will also require a larger change in the pH of the bulk solvent in order to have an equivalent effect on the Stern region. Contrary to the effect of added bromide on the pK_a in the non-ionic surfactant, equation 2 is not expected to hold for these systems. The apparent pK_a of PdCl₂-**2** is presented as a function of CTAB and CTAC concentration in Figure 21.

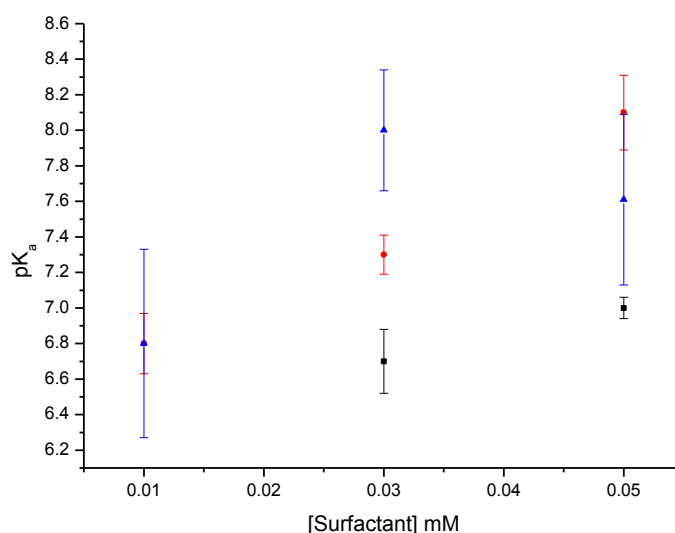


Figure 21. The change in apparent pK_a of catalyst $\text{PdCl}_2\cdot 2\text{H}_2\text{O}$ ($10\ \mu\text{M}$) at various CTAB (●) or CTAC (■) in H_2O or CTAB in D_2O (▲) concentrations in H_2O .

Figure 21 shows that increasing the concentration of CTAB causes a general increase in the apparent pK_a , (although not with the logarithm of the bromide concentration). The general trend of increasing pK_a with increasing bromide concentration is in line with what was found for the laureth-10 system. The relationship may not be linear with the logarithm of the concentration because increasing the volume of the micellar pseudophase will not cause a linear increase in the effective local bromide concentration.

The experiments were repeated using CTAC, the chloride-containing analogue of CTAB. A pK_a could not be determined from the data for the system at 0.01 M CTAC. This could be due to the

lower CMC of CTAC, meaning the complex may not be sufficiently solubilised. At 0.03 and 0.05 M CTAC, pK_a s were derived from the data and they were lower than for the equivalent concentration of CTAB. The lower pK_a values indicate that the binding of chloride to palladium is weaker than binding of bromide to palladium, which is in line with what was found in laurth-10. This finding is in line for the trends that de Jong *et al.* calculated for the addition of HBr and HCl to palladium.¹⁶

The apparent pK_a s were also determined in CTAB solutions in D₂O. In D₂O the relationship between CTAB concentration and pK_a is not linear. Instead of continuously increasing, the pK_a of PdCl₂-2 actually drops as the bromide concentration is increased from 0.03 to 0.05 M. However, given the large error margins for the analysis of the data for D₂O-based solutions, reliably identifying a trend would be difficult.

The recorded pK_a s in H₂O and D₂O with CTAB and CTAC are summarised in Table 3.

Table 3. The apparent pK_a of catalyst PdCl₂-**2** (10 μM) at various concentrations of CTAB and CTAC in H₂O and D₂O.

Surfactant Concentration (M)	pK _a CTAB (H ₂ O)	±	pK _a CTAB (D ₂ O)	±	pK _a CTAC (H ₂ O)	±
1x10 ⁻²	6.8	0.17	6.8	0.53	-	-
3x10 ⁻²	7.3	0.11	8.0	0.34	6.7	0.18
5x10 ⁻²	8.1	0.21	7.61	0.48	7.0	0.06

2.2.2e – apparent pK_a of catalyst PdCl₂-**5**

Since the pK_a of PdCl₂-**2** and PdCl₂-**4** were not the same under the same conditions, it would not be surprising to find that PdCl₂-**5** had a different pK_a as well. Since **5** was shown to have a larger bite angle than **2** (*vide supra*), it would be expected that PdCl₂-**5** would have a higher pK_a than PdCl₂-**2** under the same conditions if the change in the apparent pK_a is due to the change in the ligand bite angle.

PdCl₂-**5** was dissolved in Laureth-10 and 0.5 mM bromide was added at pH 6.01 and pH 10.50 to see how the absorbance changes with pH (Figure 22).

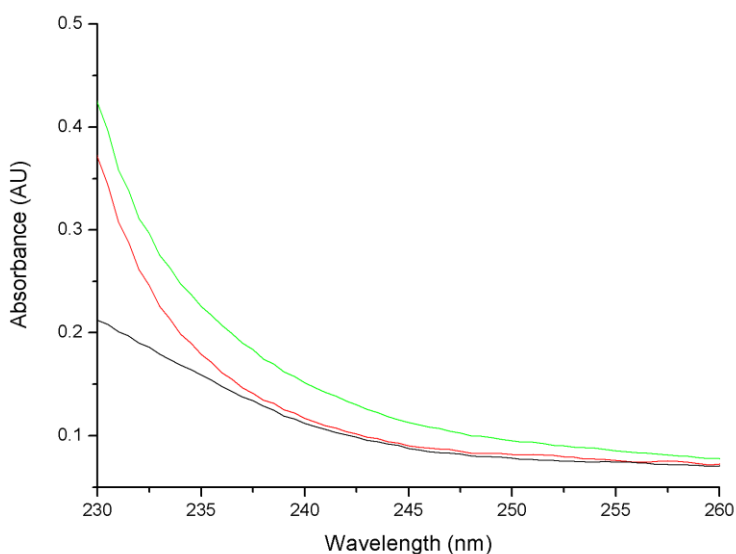


Figure 22. The spectra of catalyst PdCl₂-**5** (10 μM) in Laureth-10 (10 mM) and - no bromide, - bromide (50 mM) and pH 6.01 and - bromide (50 mM) and pH 10.5.

Unlike the spectra for PdCl₂-**2** there is only a single visible peak in the UV spectrum of PdCl₂-**5**, and it is an extremely strong absorbance around 200 nm. The wavelength of largest change in absorbance between the acidic and basic forms of the PdCl₂-**5** is 234 nm, so this wavelength was used to determine the p*K*_a (Figure 23).

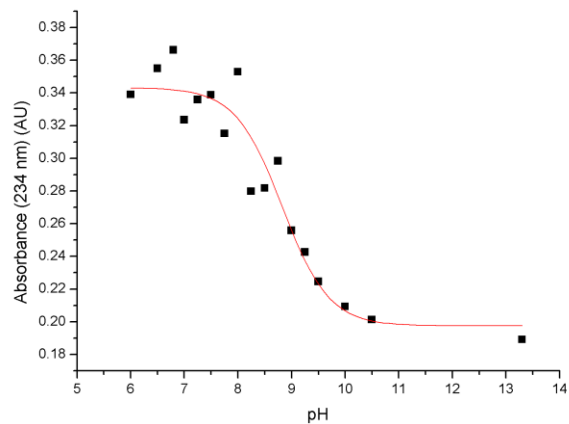


Figure 23. The change in absorbance at 234 nm of catalyst PdCl₂-**5** (10 μM) at various pHs in laureth-10 (100 mM) with 0.05 M NaBr.

The pK_a of complex PdCl₂-**5** in 0.05 M bromide is 8.83 ± 0.14 , which is 0.87 pK_a units higher than was found for PdCl₂-**2** under the same conditions. The pK_a of complex PdCl₂-**5** was measured at bromide concentrations between 0.1 M and 0.01 M and the experimentally determined values are presented as a function of log [Br] in Figure 24.

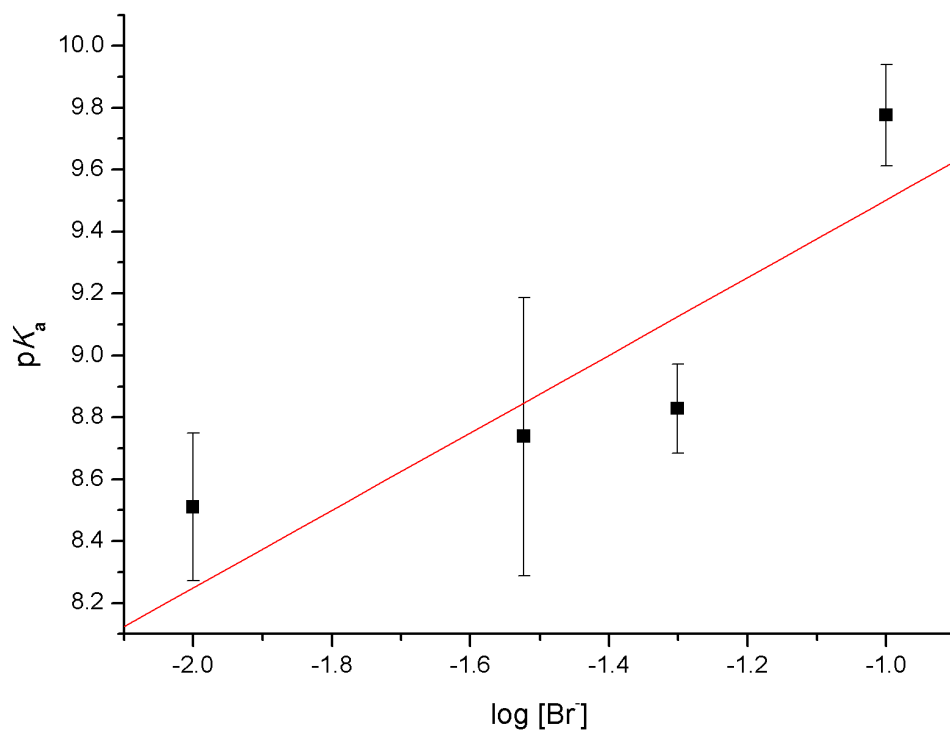


Figure 24. The change in apparent pK_a of catalyst $\text{PdCl}_2\text{-5}$ ($10\ \mu\text{M}$) at various NaBr concentrations in H_2O and Laureth-10 ($100\ \text{mM}$). $R^2=0.7378$

Although the error margins on the data are significant, the apparent pK_a increases with increasing $\log [\text{Br}]$ with a gradient of 1.25 ± 0.29 . This gradient is also in agreement with that found for $\text{PdCl}_2\text{-2}$ as the gradient is approximately 1 which is in agreement with Equation 2. This shows that both $\text{PdCl}_2\text{-5}$ and $\text{PdCl}_2\text{-2}$ are affected in a similar manner by added bromide ions, indicating that the effect of bromide on the pH optimum of the homocoupling reaction would also be expected to be similar (if bromide does indeed affect the rate of the homocoupling reaction). These pK_a values are summarised in Table 4.

Table 4. The change in pK_a of catalyst PdCl₂-5 (10 μ M) at various pHs in Laureth-10 (100 mM) with 0.05 M NaBr.

Halide concentration (M)	pK_a Br (H ₂ O)
1×10^{-2}	8.51 ± 0.24
3×10^{-2}	8.74 ± 0.45
5×10^{-2}	8.83 ± 0.14
1×10^{-1}	9.78 ± 0.16

Whilst these are not direct analyses of the catalytically active species, the Pd^{II} form of the catalyst as it occurs during the catalytic cycle likely follows the same trends as the pre-catalyst with respect to its pK_a . This is because the difference in the strength of binding to the palladium between hydroxide and bromide will not be affected by the change in the other ligands to the palladium. The lower pK_a of PdCl₂-2 when compared to PdCl₂-4 may well be an advantage as far as reactivity goes, since it could move the pH maximum to a lower value than was previously found, and in doing so increase the maximum rate constant. The optimal rate will be at the point where the highest concentrations of both the active components are present. If the hydroxyl form of the catalyst and the acidic form of the boronic acid are the active species in the homocoupling reaction then reducing the apparent pK_a of the catalyst will result in a higher effective concentration of the active species at the optimal rate. This is shown in Figure 25, where moving the sigmoidal curve representing the catalyst to the left results in both a lower optimum pH (the place where the curves cross) and higher concentrations of the active species at that optimum.

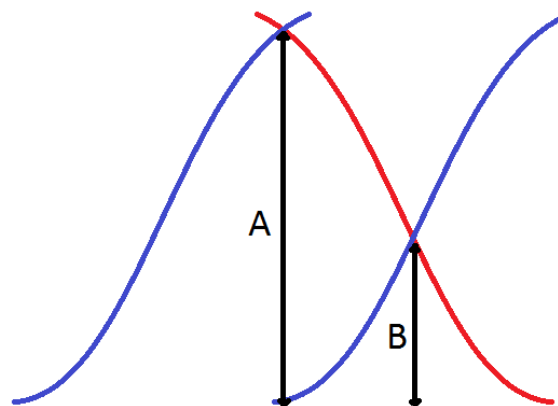
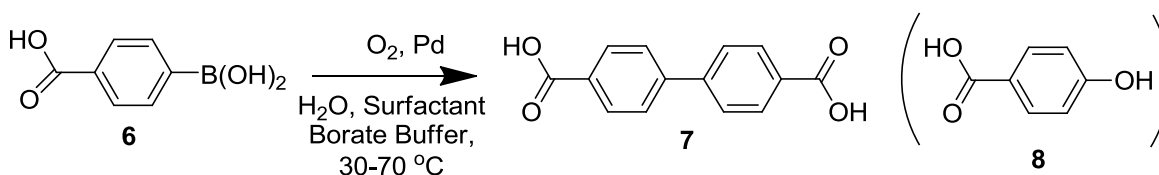


Figure 25. Reducing the pK_a of a species could increase the overall rate.

2.2.3 - Kinetic Studies

The reaction under study (Scheme 21) is the homocoupling reaction of 4-carboxyphenylboronic acid **6**, yielding 4,4'-dicarboxybiphenyl **7** as the product. This reaction was selected because 4,4'-dicarboxybiphenyl **7** is more soluble in water than other alternative biphenyls, thus giving more flexibility for kinetic studies because product solubility should not be an issue.



Scheme 21 - The palladium catalysed oxidative homocoupling reaction of 4-carboxyphenylboronic acid (6) to form 4,4'-dicarboxybiphenyl (7) and 4-hydroxybenzoic acid (8).

The pseudofirst-order rate constant k_{obs} is calculated by fitting Equation 3 to the absorbances measured by UV spectroscopy. The equation assumes that the reaction goes to completion and uses the final absorbance as the end point of the exponential curve and that the absorbance at a species' λ_{max} is directly proportional to the concentration of that species. The absorbance at any given time is a function of an exponential curve where the exponent is the time and the pseudofirst-order rate constant.

$$A = A_{\text{final}} - \Delta A e^{-k_{\text{obs}}t} \quad \text{Equation 3}$$

2.2.3a - Effect of Laureth-10 on Product Formation

Laureth-10 is a very different surfactant to CTAB, so we first ascertained whether the kinetics for the homocoupling reaction are measurable and reproducible. Therefore, the homocoupling reaction of **6** was performed with various concentrations of catalyst PdCl₂-**2** and using both CTAB and laureth-10 as the surfactant, and the spectra of the final products were compared (Figure 26).

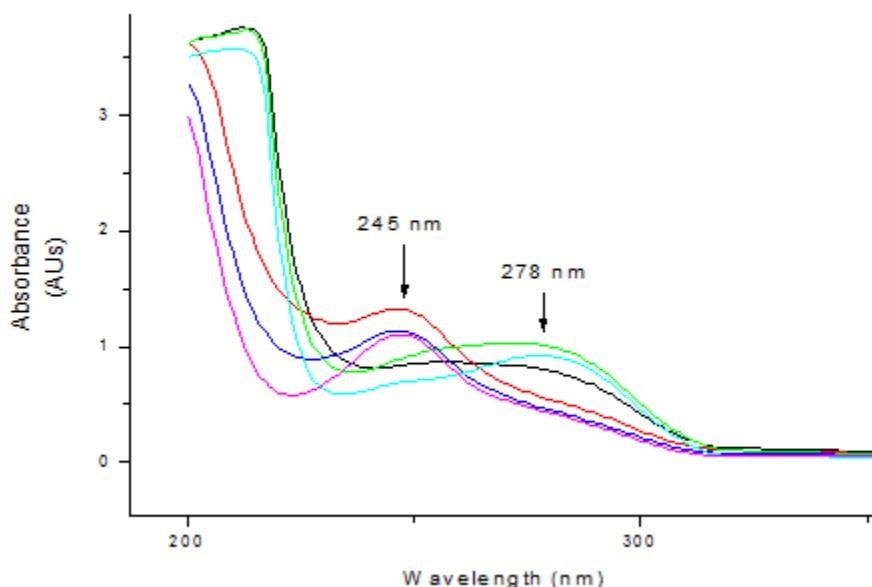


Figure 26 - Final spectrum of the homocoupling reaction of 150 μM **6** at pH 8 with 10 mM borate buffer, 10 mM CTAB or laureth-10 at varying concentrations of catalyst PdCl₂-**2** at 30 °C. - 67.2 μM PdCl₂-**2** in CTAB, - 67.2 μM PdCl₂-**2** in Laureth-10, - 33.6 μM PdCl₂-**2** in CTAB, - 33.6 μM PdCl₂-**2** in Laureth-10, - 6.7 μM PdCl₂-**2** in CTAB, - 6.7 μM PdCl₂-**2** in Laureth-10,

Figure 26 shows that there is a distinct difference between the reactions performed in CTAB and those performed in laureth-10. The reactions in laureth-10 tended to give a λ_{max} of 245-255 nm rather than the 278 nm found in reactions carried out in CTAB solutions. This indicates that over time the experiments generate more and more of the phenol byproduct **8**, even if the reaction is carried out under the same conditions. This only affected reactions in laureth-10 not CTAB. Qualitatively testing the stock solution of laureth-10 with KI and starch solution indicates that the surfactant had become peroxidised over time.

A more quantitative approach compared the reaction profiles of the homocoupling reaction with newly prepared laureth-10 solutions against two week old solutions both with and without palladium (Figure 27). At 253 nm, the formation of **8** was tracked whilst at 278 nm the formation of **7** was tracked.

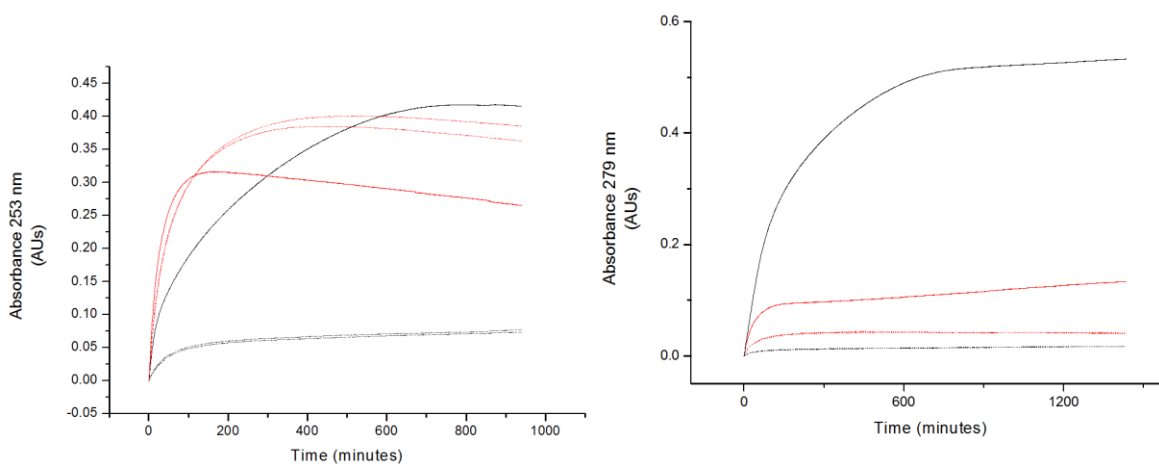


Figure 27 - Kinetic traces at 253 and 278 nm comparing formation of **7** (l) and **8** (r) from 150 μM **6** in old and new Laureth-10 solutions at pH 8 with borate buffer 10 mM at 30 $^{\circ}\text{C}$. (New surfactant 33.6 μM catalyst $\text{PdCl}_2\cdot 2\text{H}_2\text{O}$: —, Old surfactant 33.6 μM catalyst $\text{PdCl}_2\cdot 2\text{H}_2\text{O}$: —, New surfactant no catalyst: ---, Old surfactant no catalyst: ---)

The dashed lines in Figure 27 show there is some formation of **8** by the laureth-10 alone, and both the rate of formation, and the total amount of **8** formed, were much higher for the old surfactant stock solution. The solid lines show that in the presence of catalyst the formation of phenol is much faster than in the absence of it, but in the two-week old surfactant solution the total phenol generation is less than in the absence of catalyst, whilst the opposite is the case for the fresh surfactant. Looking at the reaction profile at 278 nm, despite the fact that no biphenyl **7** is formed in the absence of catalyst, the dashed lines still show some increase in the absorbance at 278 nm, indicating that at least part of the absorbance at 278 nm is due to the phenol **8**. The reaction giving rise to the absorbance at 278 nm is more interesting in the presence of the catalyst, as the reaction terminates in the old surfactant with roughly 1/5 (ΔA_{278} 0.09125/0.47505) of the formation of biphenyl compared to the fresh surfactant. Considering that

the ΔA is higher in the fresh surfactant at both 253 nm and 278 nm, it would imply that the catalysed homocoupling reaction does not go to completion with the old surfactant. If that is the case, the peroxidation or the production of **8** may be interfering with the homocoupling reaction and preventing it from going to completion. The degradation of **6** by laureth-10 is more clearly shown when one varies the concentration of laureth-10 (Figure 28). Figure 28 shows that at the end of the reaction a much lower concentration of **7** is formed at high surfactant concentrations, although the reaction itself finishes more quickly. At high surfactant concentrations the rate of peroxide decomposition of starting material **6** is increased, and the homocoupling reaction terminates swiftly.

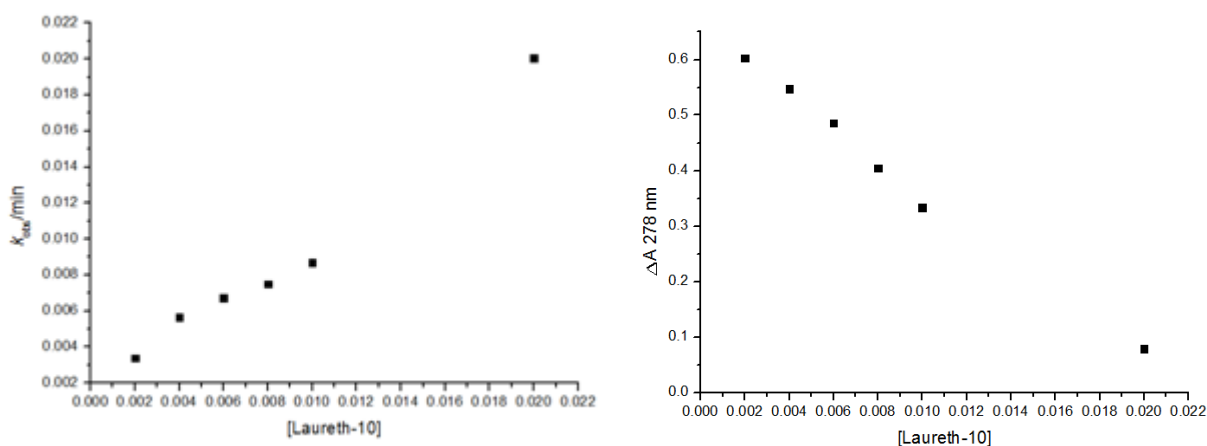


Figure 28 - Change in observed reaction rate (k_{obs}) and final product **7** concentration (r) as [laureth-10] is varied in the homocoupling reaction of **6** (15 μM) by catalyst $\text{PdCl}_2\text{-2}$ (33.6 μM) at pH 8 borate buffer (10 mM) at 30 $^\circ\text{C}$.

The likely cause of the significant formation of phenol is the peroxidation of the ether functional groups in laureth-10. Typical experiments involve a laureth-10 concentration of 10 mM which,

together with the fact that there are twelve ether linkages per molecule, leads to a concentration of ether groups of 120 mM. At a typical concentration of **6** of 150 μM (chosen so the maximum absorbance of the product **7** would remain below 1.5 AU of absorbance in a 1 cm path length cuvette), only a 0.125% peroxidation of the surfactant would therefore be sufficient to destroy all of the starting boronic acid. Based on the fact that the two-week-old surfactant still did not reach 100% conversion into the phenol **8**, the degree of peroxidation is somewhat less than that mark. Still, in order to limit the effect this peroxidation of the surfactant can have on the kinetics, the laureth-10 was stored in darkened containers and prepared freshly every week for subsequent experiments.

2.2.3b - pH rate profile for catalyst PdCl₂-2 in Laureth-10

The rate observed constant k_{obs} was calculated for the homocoupling reaction of **6** by catalyst PdCl₂-2 at varying pH in order to determine the pH rate profile for the reaction for the first and second use cycle of the catalyst (Figure 29). A representative trace is given in Figure 30.

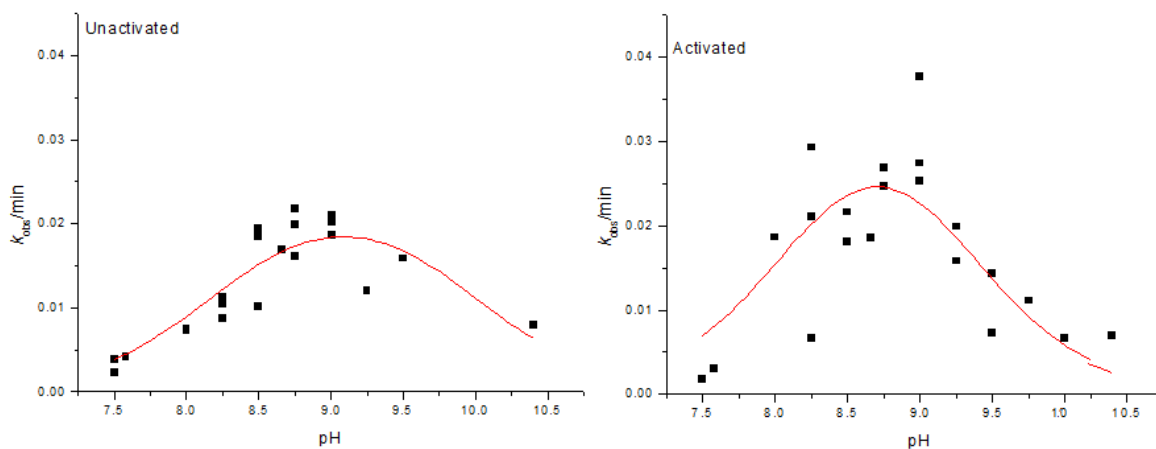


Figure 29 - pH rate profile for the homocoupling of **6** (150 μ M) with unactivated and activated catalyst PdCl₂-**2** (33.6 μ M) in laureth-10 (10 mM) and borate buffer (10 mM) at 30 °C.

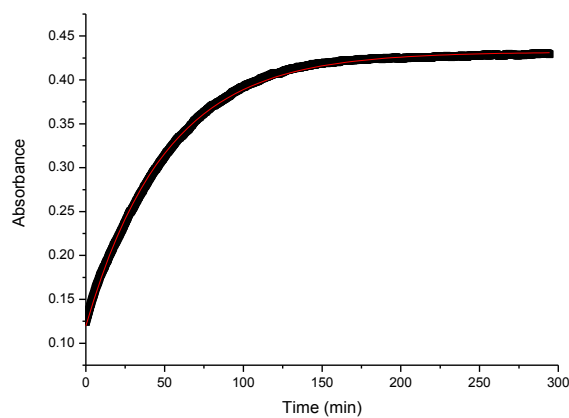


Figure 30 - UV absorbance at 278 nm measured during the homocoupling of **6** (150 μ M) with unactivated PdCl₂-**2** (33.6 μ M) in laureth-10 (10 mM) and borate buffer (10 mM) at 30 °C and pH 8.75. Absorbances are given in black and the exponential fit is given in red, which calculated the rate k_{obs} to be 0.0198 min⁻¹.

The pH maximum was calculated by fitting equation 4 to the pH rate profile which makes the assumption that the maximum is the result of two different pK_a s, one for the phenylboronic acid **6** and one that may be for the Pd complex. The sigmoidal curves overlap to give a pH maximum where they cross (figure 25).

$$k_{\text{obs}} = k_{\text{catPd}} \left(\frac{1}{1+10^{(\text{pH}-pK_a^{\text{PhB}})}} \right) \left(\frac{1}{1+10^{(pK_a^{\text{Pd}}-\text{pH})}} \right) \quad \text{Equation 4}$$

The pK_a of **6** is known ($pK_a = 8.0$) and is assumed to be the same in the surfactant solution. The pK_a is therefore fixed in the analysis, and the second pK_a is found by fitting equation 2 to the kinetic data. If the second pK_a matches up with the pK_a of the Pd complex that was previously determined (*vide supra*), then the pH maximum is likely the result of the required state of both the palladium complex and the arylboronic acid. Otherwise it may be that the pK_a is that of **6** which would indicate the pH maximum is entirely down to the state of the phenylboronic acid required for the reaction.

For the unactivated palladium complex, a broad pH maximum was found at $\text{pH } 9.09 \pm 2.73$ by fitting equation 2 to the pH rate data. This optimum pH is higher than the pH 8.7 that was previously found for the reaction in CTAB (although the highest individual point is at pH 8.5). In

this analysis the pK_a of the palladium complex was estimated to be 10.20. However, once activated, the results were much less reproducible and gave a less defined pH-rate profile. Regardless, this shows there is still a pH maximum for the reaction even though there is no bromide in the solution, and the maximum concentration of chloride in solution is 67.2 μM , which is far below either the absolute concentration of bromide in an analogous CTAB reaction (10 mM) or the concentration of bromide in the CTAB Stern region ($\sim 1 \text{ M}$).¹³

For Pd (II) catalysts used in the palladium-catalysed coupling reactions there is a slow induction step to the reaction.¹⁷ In the induction step, the Pd (II) pre-catalyst loses the chloride ligands that are bound to it in the stock solution and two transmetalation steps involving **6** in solution and subsequent reductive elimination generates the palladium (0) catalyst and one molecule of **7** (Scheme 4). Due to this induction step, the first time the catalyst is used in a reaction may not reflect the pH dependence of the catalytic cycle depending on how fast this induction step is. To check for the effect of the induction step on the pH dependence of the reaction, the kinetics were measured for both the first and second addition of **6** to the same cuvette. The reaction kinetics for the second addition of **6** should only reflect the pH dependence of the catalytic cycle as long as all the pre-catalyst has been activated following the first addition of **6**. Equation 2 was fitted to the pH rate profile of the reaction catalysed by the activated palladium complex which gives a maximum of 8.75, but the fit is a lot less reliable. In this case the pK_a of the Pd complex was estimated to be 9.49. As expected the pH maximum is higher in laureth-10 than it is in CTAB as the pH in the Stern region of laureth-10 should be approximately the same as the bulk pH (unlike CTAB where the Stern region should have a higher pH than the bulk pH).

As such, the pH maximum should be higher in laureth-10 than in CTAB. However, since there is also no bromide, and the concentration of chloride in the solution is equal to twice the concentration of the catalyst, the pK_a of the catalyst should also lower and this effect may reduce the pH maximum. As was also noted for the experiments carried out in CTAB, the pH maximum appears lower for the activated catalyst. This suggests that the induction step benefits from higher pH more than the catalytic cycle. The fact that the pH maximum is higher in laureth-10 is an interesting result, as the pK_a s calculated in Chapter 3 showed that the bromide content of the CTAB caused a higher catalyst pK_a than in laureth-10. If the optimum pH was reflecting the need to displace halide from the palladium then one would have expected CTAB to cause a higher pH optimum as higher pHs would be necessary to displace the bromide ions. It may be that the effect of the increased pH in the Stern region of the micelles compared to the pH in the bulk solution more than compensates the rate retardation caused by the bromide ions in the CTAB solution. Therefore, despite the bromide displacement from the palladium increasing the effective pK_a of the catalyst, since the pH experienced in the Stern region is much higher than the bulk water, the pH optimum appears lower.

2.2.3c - pH rate profile for catalyst PdCl₂-2 and PdCl₂-5 in CTAB

If the thioether group on the ligand has no influence on the reaction, then one would expect that under the same conditions catalysts PdCl₂-2 and PdCl₂-5 should exhibit the same maxima in the pH-rate profiles in CTAB as was previously found for thioether-containing PdCl₂-4. If the

behaviour of PdCl₂-2 differs from PdCl₂-4 and PdCl₂-5, then it is possible that the steric crowding around the bridging carbon in the ligand plays some part in the catalyst's behaviour. To test this the pH rate profile for catalyst PdCl₂-2 was determined under the same conditions as were previously used for PdCl₂-4 to ascertain if the ligand structure affected the pH optimum of the process (Figure 30).

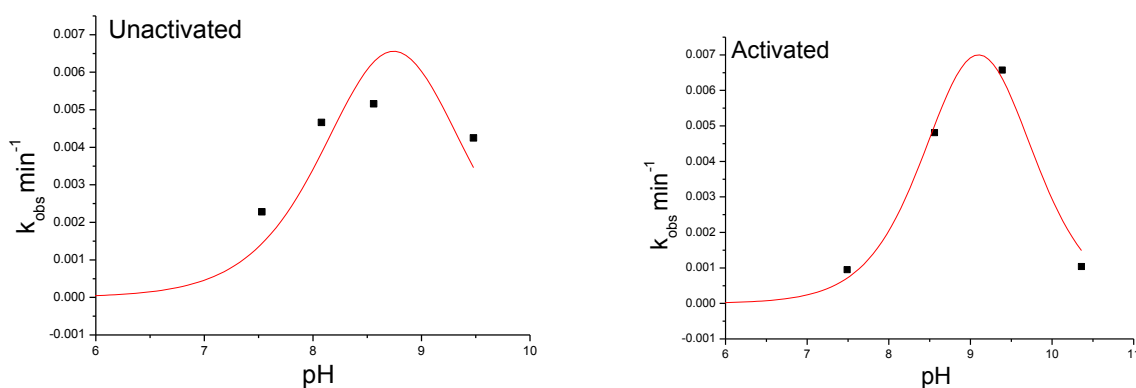


Figure 30 - pH rate profile for the homocoupling of **6** (150 μM) with unactivated (left) and activated (right) catalyst PdCl₂-2 (10 μM) in CTAB (10 mM) and borate buffer (10 mM) at 30 $^{\circ}\text{C}$.

Figure 30 shows that the optimum pH for both the homocoupling reaction performed with unactivated PdCl₂-2 is the same as for PdCl₂-4, although the same was not true for the activated catalyst. At 10 mM CTAB and 30 $^{\circ}\text{C}$, the optimum pH for the reaction is estimated to be 8.76 ± 0.23 for unactivated PdCl₂-2, with the $\text{p}K_{\text{a}}$ of the catalyst estimated to be 8.65 ± 0.23 when equation 2 is fitted to the data with the $\text{p}K_{\text{a}}$ of the boronic acid set to 8.0. This pH optimum is exactly in line with what was previously observed for catalyst PdCl₂-4 (pH 8.7). However, after activation, the second run of the reaction leads to a higher optimum pH for the reaction of $9.07 \pm$

0.05, and an estimated pK_a for the palladium complex of 9.48 ± 0.05 . Why the optimum pH for the activated palladium complex should be higher, when catalyst PdCl₂-**4** had a lower optimum pH after activation under the same conditions, we do not understand. Additionally, catalyst PdCl₂-**2** appears to be a less effective catalyst than PdCl₂-**4**, as the highest rate constant is a quarter of the rate constant for the sulphide-containing catalyst under the same conditions (0.007 min^{-1} as compared to 0.030 min^{-1}).

The experiment was repeated at a higher concentration of CTAB, 30 mM CTAB, to determine if the concentration of surfactant (and therefore the concentration of catalyst in the micellar pseudophase) had an effect on the optimum pH (Figure 31).

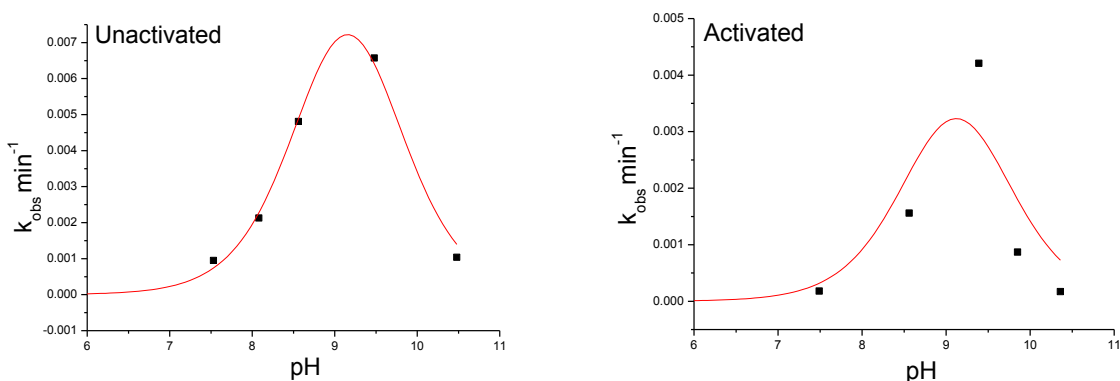


Figure 31 - pH rate profile for the homocoupling of **6** ($150 \mu\text{M}$) with unactivated (l) and activated (r) catalyst PdCl₂-**2** ($10 \mu\text{M}$) in CTAB (30 mM) and borate buffer (10 mM) at $30 \text{ }^\circ\text{C}$.

Using a higher concentration of CTAB will result in a higher concentration of bromide anions in the Stern region, relative to the palladium (as the palladium will be dispersed across more micelles). The maximum in the pH-rate profile for PdCl₂-**2** for the first addition of **6** is $9.10 \pm$

0.08 in 30 mM CTAB, which is higher than for the same catalyst in 10 mM CTAB. The estimated pK_a of the palladium complex is 9.37 ± 0.08 under these conditions. This is in line with what one would expect because the higher bromide concentration would push the pH optimum higher, as a higher concentration of hydroxide anions is needed to displace the halide from the palladium centre. However, for the second addition of the boronic acid, the pH optimum for the reaction appears relatively unchanged at 9.14 ± 0.39 , giving an estimated pK_a for the palladium complex of 9.41 ± 0.39 . Again the fastest reaction with activated $PdCl_2\text{-2}$ is slower at this higher CTAB concentration than with activated $PdCl_2\text{-4}$ under otherwise identical conditions (0.007 min^{-1} as compared to 0.030 min^{-1}).

The pH rate profile for the homocoupling reaction of **6** catalysed by catalyst $PdCl_2\text{-5}$ was also determined in CTAB to see if the propyl group also affected the pH optimum in the same manner as it affected the pK_a of the complex in Chapter 3 (Figure 32).

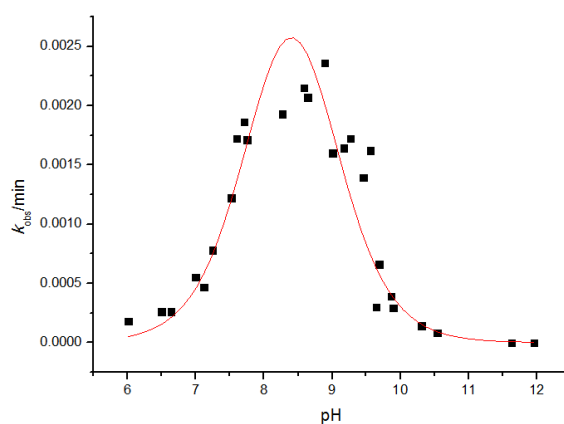


Figure 32 - pH rate profile for the homocoupling of **6** (100 μM) with catalyst $PdCl_2\text{-5}$ (30 μM) in CTAB (10 mM) and borate buffer (10 mM) at 30 °C.

For catalyst PdCl₂-**5** the maximum in the pH-rate profile is at pH 8.49 ± 0.76 , with a fitted pK_a for the palladium complex of 8.97 ± 0.09 . The optimum pH for PdCl₂-**5** is not in agreement with what was found for catalyst PdCl₂-**4**, as the optimum pH is 0.25 units lower than for the thioether containing complex. This pK_a difference suggests that the propyl chain probably does have an effect on the pK_a of the catalyst. It is not exactly obvious why the homocoupling with catalyst PdCl₂-**2** and PdCl₂-**4** should exhibit similar optimal pHs whilst the homocoupling reaction with PdCl₂-**5** does not. It may be that the steric effect of the additional alkyl chain in catalysts PdCl₂-**4** and PdCl₂-**5** reduces the optimum pH, but the interaction of the thioether group with the palladium centre in PdCl₂-**4** increases the optimum pH. Interestingly, the observed rate constant for the reaction is much lower for PdCl₂-**5** than found for PdCl₂-**4**; the highest rate constant recorded for the PdCl₂-**5**-catalysed reaction is 0.024 min^{-1} , but this rate constant is found at three times higher catalyst loading of PdCl₂-**5** compared to PdCl₂-**4** where the highest rate recorded was 0.030 min^{-1} . This gives it a similar activity to PdCl₂-**2** which has a highest recorded rate of 0.007 min^{-1} but at a third of the concentration of PdCl₂-**5**.

To test if the reaction is first order with respect to PdCl₂-**5** in this range of concentrations, the rate constant was determined with increasing catalyst concentration (Figure 33).

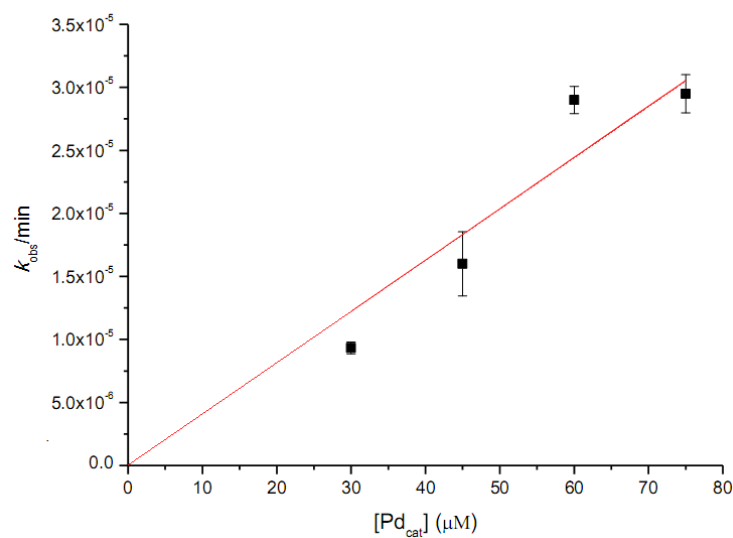


Figure 33 – Rate constant for the homocoupling of **6** (100 μM) with varying concentrations of catalyst PdCl₂-**5** in CTAB (10 mM) and pH 9.00 borate buffer (10 mM) at 30 °C. R² = 0.9084

Figure 33 shows that the rate constant increases with catalyst concentration, so saturation of catalyst PdCl₂-**5** cannot be the cause of the low rate constant with respect to PdCl₂-**4**.

2.2.3d - Effect of bromide concentration on the pH-rate profile for the homocoupling reaction of **6** in Laureth-10 solutions

The apparent pK_a of $PdCl_2\cdot 2$ varies with halide concentration (*vide supra*). Therefore, if the maximum in the pH-rate profile for the homocoupling reaction is affected by the $Pd-OH \rightleftharpoons Pd-X$ equilibrium then this can be probed by altering the halide concentration in the laureth-10 system. The pH rate profiles for the homocoupling reaction of **6** in laureth-10 at 10 mM bromide concentration was determined (Figure 34).

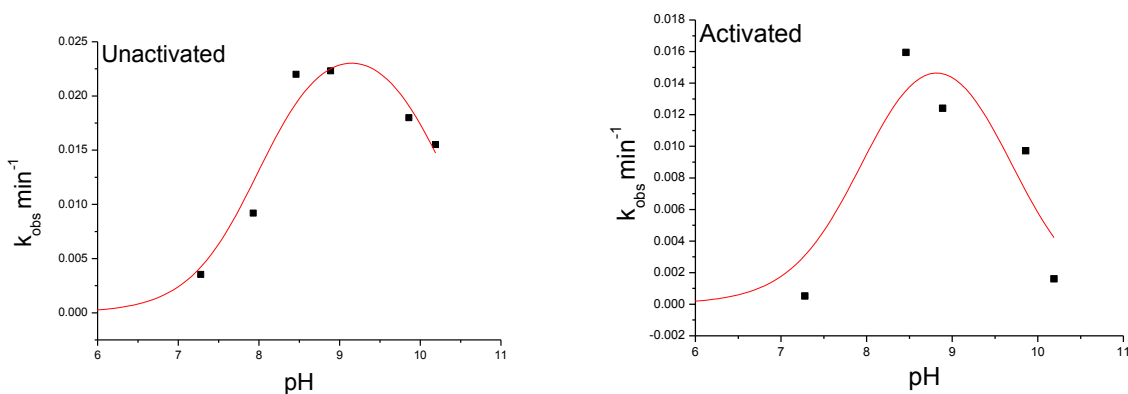


Figure 34 - pH rate profile for the homocoupling of **6** (150 μ M) with unactivated (l) and activated (r) catalyst $PdCl_2\cdot 2$ (10 μ M) in laureth-10 (10 mM), NaBr (10 mM) and borate buffer (10 mM) at 30 $^{\circ}$ C.

Figure 34 shows that addition of 10 mM of bromide ions to the system results in a maximum in the pH-rate profile of 9.15 ± 0.13 and a pK_a of 10.30 ± 0.14 for the unactivated reaction. The

optimum pH drops to 8.83 ± 0.7 and a pK_a 9.64 ± 0.26 of for the second addition, which again indicates that the induction reaction is more base accelerated than the rest of the catalytic cycle.

The bromide concentration was raised to 50 mM and the pH rate profile was again determined to see if it would shift further in a higher concentration of bromide (Figure 35).

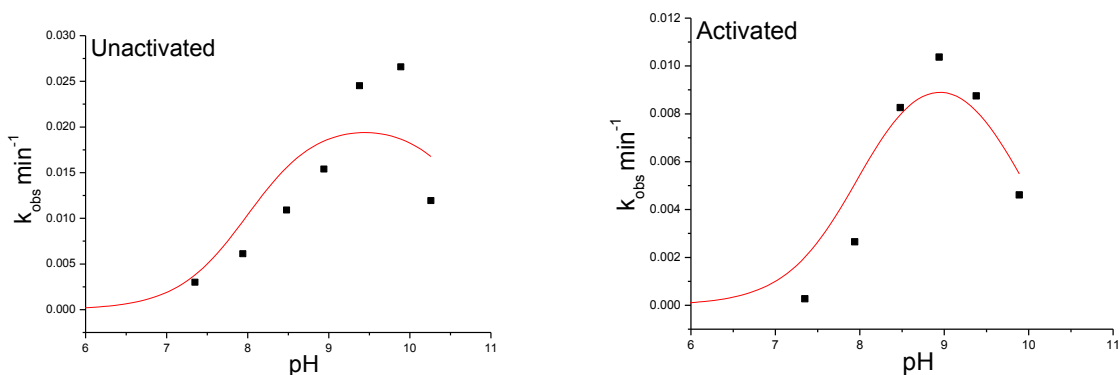


Figure 35 - pH rate profile for the unactivated (l) and activated (r) homocoupling of **6** (150 μM) with catalyst $\text{PdCl}_2\cdot\mathbf{2}$ (10 μM) in laureth-10 (10 mM), NaBr (50 mM) and borate buffer (10 mM) at 30 $^\circ\text{C}$.

Figure 35 shows that increasing the bromide concentration to 50 mM results in a maximum on the pH-rate profile at a pH of 9.43 ± 0.89 and a pK_a of 10.89 ± 0.89 for the unactivated reaction. The optimum pH has increased as one would expect for an increased bromide concentration if the $\text{Pd-Br} \rightleftharpoons \text{Pd-OH}$ equilibrium does have an effect on the rate. The optimum pH of 9.0 ± 0.29

and a pK_a of 9.90 ± 0.29 for the activated reaction has again dropped relative to the unactivated reaction, which is in agreement with the pattern in CTAB.

The pH rate profile of the reaction after further increasing the bromide concentration to 250 mM was determined to see how far the optimum pH could be increased (Figure 36).

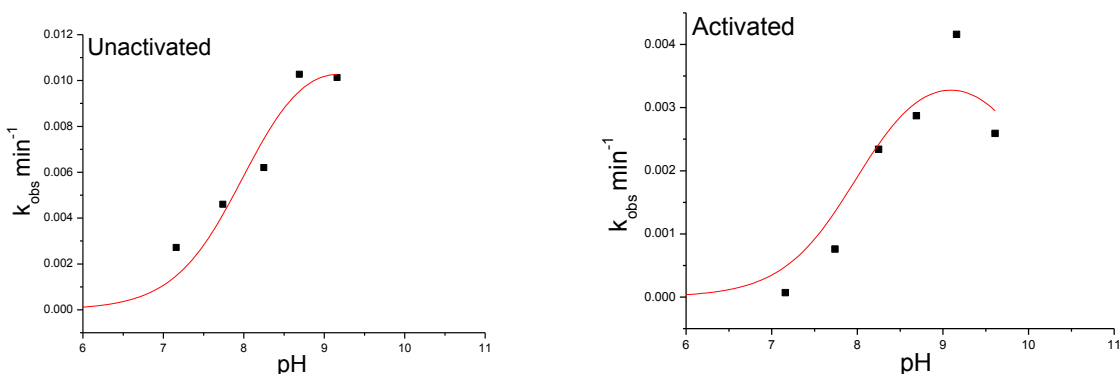


Figure 36 - pH rate profile for the homocoupling of **6** (150 μM) with unactivated (l) and activated (r) catalyst $\text{PdCl}_2\text{-2}$ (10 μM) in laureth-10 (10 mM), NaBr (250 mM) and borate buffer (10 mM) at 30 $^\circ\text{C}$.

Figure 36 shows that the optimum pH for the homocoupling reaction with the unactivated catalyst has been further increased. Data analysis in terms of equation 4 indicated an optimum pH of 9.13 ± 0.27 and a pK_a of 10.31 ± 1.09 for the reaction using the unactivated catalyst and an optimum pH of 9.10 ± 0.54 and a pK_a of 10.18 ± 0.55 for the reaction involving the activated catalyst.

Collecting the optimum pHs and the catalyst pK_a s that have been calculated and plotting them as a function of halide concentration shows the effect of changing the halide concentration (Figure 37).

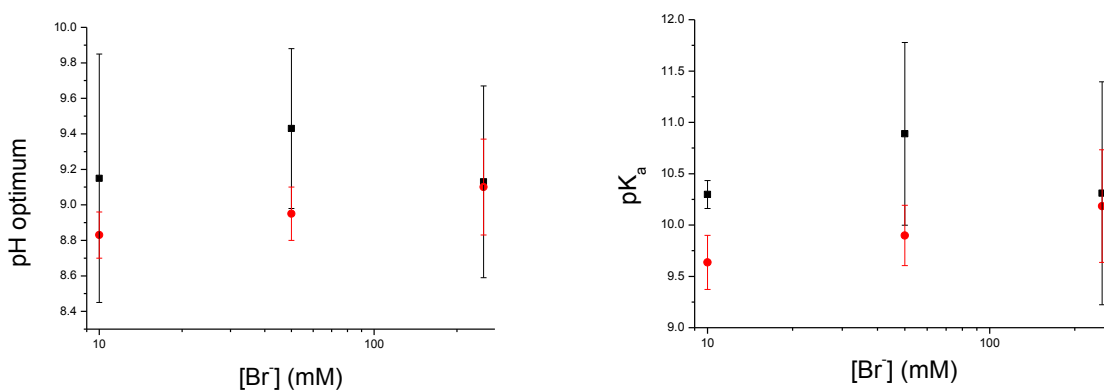


Figure 37 - Change in pH optimum (l) and pK_a (r) with bromide concentration for the homocoupling reaction of **6** (100 mM) with unactivated (■) and activated (●) catalyst $\text{PdCl}_2\cdot 2$ (10 μM) in laureth-10 (10 mM) and borate buffer (10 mM) at 30 °C.

Figure 37 shows that the optimum pH for the reaction using the activated catalyst increase in a linear fashion with $\log [\text{Br}^-]$, which definitely agrees with the suggestion that the optimum pH involves the $\text{Pd-X} \rightleftharpoons \text{Pd-OH}$ equilibrium. However, given the large error margins it is hard to tell if the slope is 1 or not (as the pK_a s of the catalysts did earlier). The pH maximum for the reaction using the activated catalyst does not show a conclusive trend, although this may simply be because the pH-rate profile for the error margins are even larger than for the unactivated

reaction. The maximum rate constant of the reaction using the activated catalyst drops as the bromide concentration increases. As only the pK_a of the palladium complex is changing and the pK_a of **6** is stationary this will result in the maximum (the point that the two sigmoidal curves cross) being further along the right-hand sigmoidal and a lower observed maximum rate constant.

2.2.3e - Effect of chloride concentration on the pH-rate profile for the homocoupling reaction of **6 in laureth-10 solutions**

Since the bromide concentration was shown to increase the pH maximum of the homocoupling reaction, then the response to increasing chloride ion concentration should have a lower offset as the pK_a of the catalyst changes less in response to added chloride than it does in response to bromide ions (*vide supra*).

The pH rate profile in the presence of 10 mM chloride ions was determined for the homocoupling reaction of **6** in laureth-10 (Figure 38).

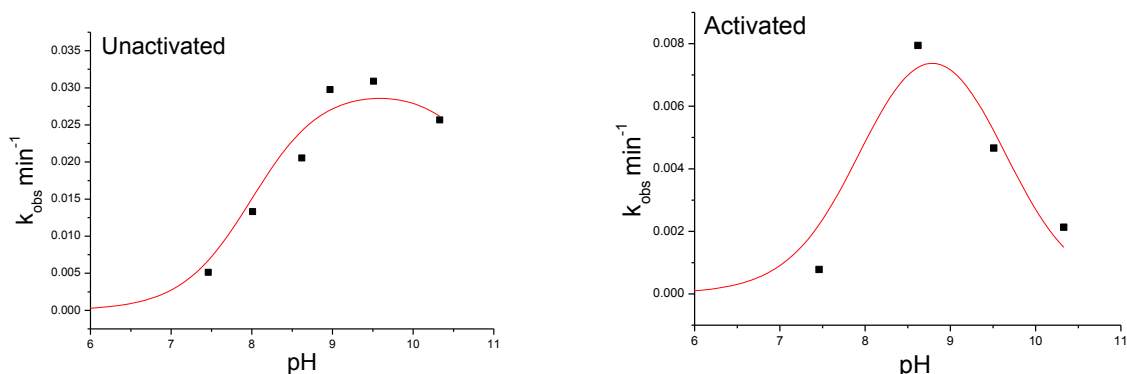


Figure 38 - pH rate profile for the unactivated (l) and activated (r) Homocoupling of **6** (150 μM) with catalyst $\text{PdCl}_2\text{-2}$ (10 μM) in Laureth-10 (10 mM), NaCl (10 mM) and borate buffer (10 mM) at 30 $^\circ\text{C}$.

Figure 38 shows that addition of 10 mM of chloride ions to the reaction mixture results in a pH optimum of 9.59 ± 0.45 and a $\text{p}K_a$ of 11.17 ± 0.44 for the reaction following the first addition of the boronic acid, and 8.77 ± 0.23 and a $\text{p}K_a$ of 9.58 ± 0.23 for the reaction following the second addition of the boronic acid. The increase in the optimum pH for the reaction involving the unactivated catalyst upon addition of chloride relative to the optimum pH for the reaction in the presence of bromide at the same halide concentration is unexpected; one would expect the optimum pH to be the same (as the $\text{p}K_a$ of catalyst $\text{PdCl}_2\text{-2}$ are the same at 10 mM halide – see Chapter 3). The maximum in the pH-rate profile for the reaction catalysed by the activated catalyst in the presence of 10 mM chloride, on the other hand, is very close (0.04 pH units difference) to the optimum pH for the analogous reaction in the presence of bromide.

The chloride concentration was raised to 50 mM and the pH rate profile was again determined to see if it would shift further in the presence of a higher concentration of chloride (Figure 39).

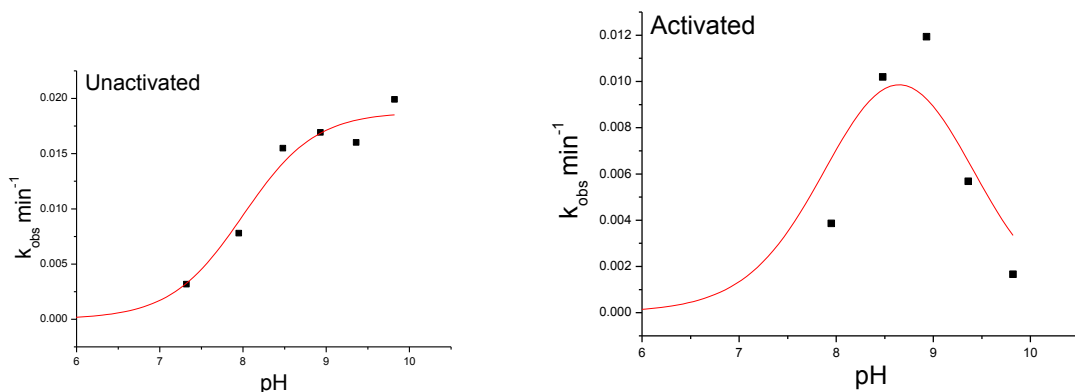


Figure 39 - pH rate profile for the homocoupling of **6** (150 μM) with unactivated (l) and activated (r) catalyst $\text{PdCl}_2\text{-2}$ (10 μm) in laureth-10 (10 mM), NaCl (50 mM) and borate buffer (10 mM) at 30 $^\circ\text{C}$.

Figure 39 shows that increasing the chloride concentration to 50 mM also increases the optimum pH for the reaction following the first addition of boronic acid to 9.83 ± 21.4 , whilst the for the reaction following the second addition of boronic acid the optimum pH decreases to 8.63 ± 0.29 . The optimum pH for the reaction involving the unactivated palladium complex has clearly increased, but the error in the calculation is too high to trust as the maximum falls outside the experimental range. However the optimum pH of the reaction involving the activated catalyst seems to have decreased, which is not as expected.

The chloride concentration was further raised to 250 mM and the pH rate profile was again determined to see if it would shift further in the presence of a higher concentration of chloride (Figure 40).

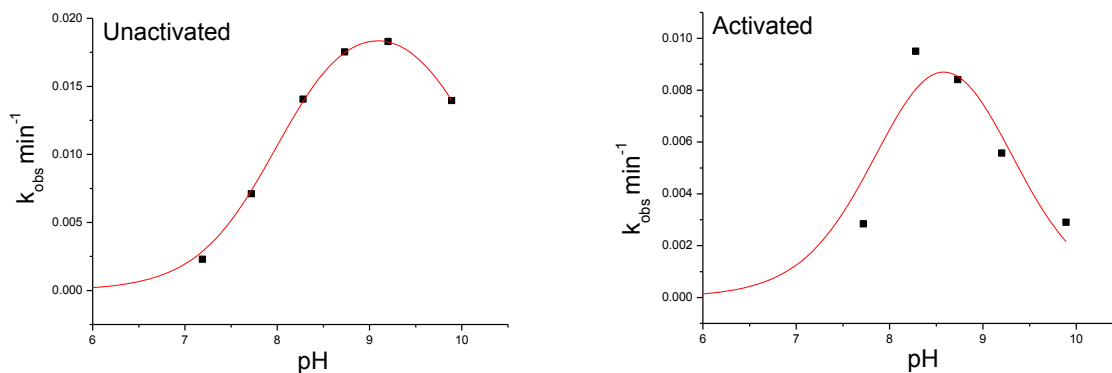


Figure 40 - pH rate profile for the homocoupling of **6** (150 μM) with unactivated (l) and activated (r) catalyst $\text{PdCl}_2\cdot 2$ (10 μM) in laureth-10 (10 mM), NaCl (250 mM) and borate buffer (10 mM) at 30 $^\circ\text{C}$.

Figure 40 shows that at the highest chloride concentration used in our experiments (250 mM) the pH maximum for the reaction following the first addition of boronic acid has dropped to 9.11 ± 0.03 . This is a substantial decrease from the pH maxima for the lower chloride concentrations. For the reaction following the second addition of the boronic acid, the pH maximum has also dropped to 8.58 ± 0.21 .

Taking the optimum pHs and the catalyst pK_a s that have been calculated and plotting them as a function of halide concentration shows the effect of changing the halide concentration (Figure 41).

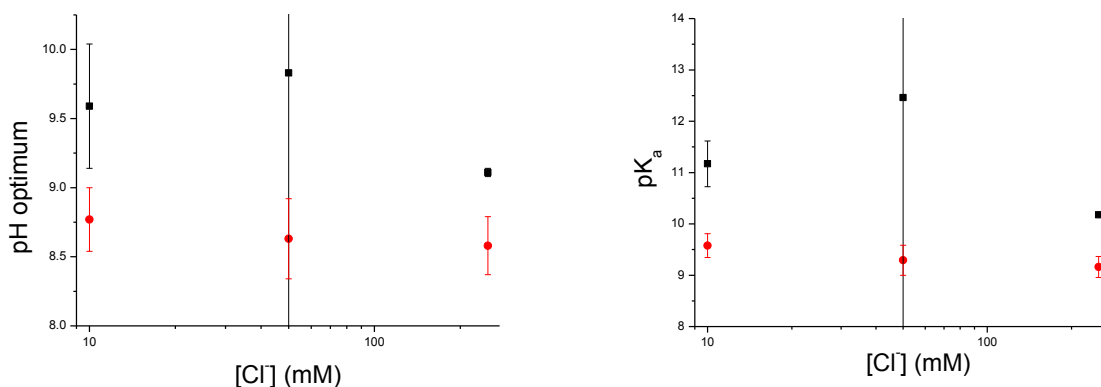


Figure 41 - Change in optimum pH (l) and k_{\max} (r) with chloride concentration for the homocoupling reaction of **6** (100 mM) with unactivated (■) and activated (●) catalyst PdCl₂-**2** (10 μm) in laureth-10 (10 mM) and borate buffer (10 mM) at 30 °C.

The results for the reaction involving the unactivated palladium complex are unusual as they appear to show a downwards trend (although, the error on the 50 mM optimum is clearly too large to consider). For the reaction involving the activated palladium complex, both bromide and chloride concentration follow a linear trend with pH optimum and k_{obs} . The trend, however, is the opposite: the optimum pH increases linearly with log [Br⁻] but decreases linearly with log [Cl⁻] (Figure 41). Exactly why this would be is unclear, since the apparent pK_a of the catalyst does increase with chloride concentration (although not as severely). Perhaps the pH maximum is also

influenced by the ionic strength of the reaction medium, and this effect may be greater in magnitude than the increase in pK_a caused by the chloride (but less than that caused by bromide). All of the pH maxima and k_{max} values found for varying halide concentrations are summarised in Table 5.

Table 5 - pH maxima and k_{max} values for the homocoupling of 6 (150 μ M) by both unactivated and activated PdCl₂-2 in laureth-10 (10 mM) and borate buffer (10 mM) at 30 °C at varying concentrations of bromide and chloride.

	10 mM [Br ⁻]	50 mM [Br ⁻]	250 mM [Br ⁻]	10 mM [Cl ⁻]	50 mM [Cl ⁻]	250 mM [Cl ⁻]
1st pH maximum	9.15	9.43	9.13	9.59	9.83	9.11
1st k_{max}	0.02232	0.02659	0.01027	0.03088	0.01992	0.01830
2nd pH maximum	8.83	8.95	9.10	8.77	8.63	8.58
2nd k_{max}	0.01594	0.01037	0.00416	0.00794	0.01163	0.0095

2.2.3f - MEGA-10 as a surfactant for the homocoupling reaction

The major problem with using laureth-10 as a surfactant to support the homocoupling of boronic acids is the peroxidation of the ether linkages in the polar head group. N-Decanoyl-N-methylglucamine (Mega-10) is an alternative surfactant that replaces the poly-ether motif that most non-ionic surfactants use for their polar component with a sugar-derived moiety.

The rate constant for the homocoupling reaction was determined as a function of concentration of catalyst PdCl₂-**5** in order to determine if the surfactant structure interferes with the catalyst activity, relative to laureth-10 or CTAB (Figure 42).

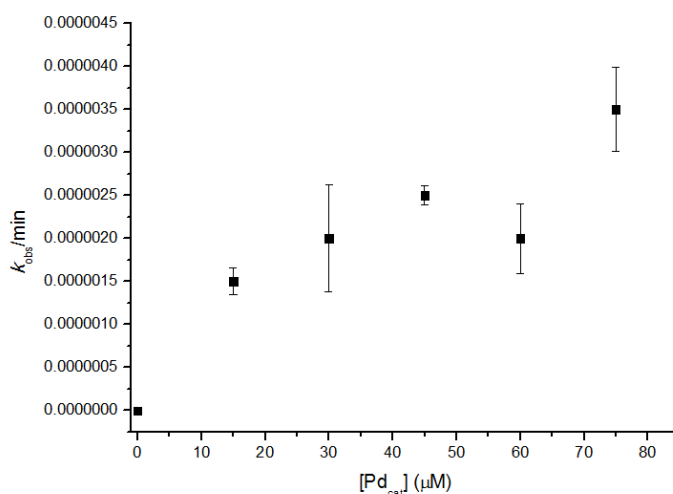


Figure 42 - Change in k_{obs} with catalyst PdCl₂-**5** concentration for the homocoupling reaction of **6** (100 μM) with catalyst PdCl₂-**5** (10 μM) in MEGA-10 (10 mM) and pH 9.00 borate buffer (10 mM) at 30 °C.

Figure 42 shows that the rate constant of the reaction was extremely low in MEGA-10. Whilst the reaction proceeds with low phenol generation, the highest completion attained was 24%, indicating that MEGA-10 is not a very good medium for the homocoupling reaction. This low conversion suggests that the rates constants in Figure 22 may mainly reflect the induction step of the reaction. In addition, these rate constants are very low in comparison to the rate constants for the analogous reaction in laureth-10 or CTAB (at 80 μM Pd-Cl₂ the observed rate constant is an order of magnitude greater in CTAB). It may be because the surfactant concentration is too close

to the CMC (6-7 mM for MEGA-10, as opposed to <1 for CTAB and Laureth-10) which would make using it even more costly than it is already.

2.3 - Conclusions

The synthesis of a variety of bisimidazolyl compounds was successfully achieved, and some of these were used to form palladium complexes that will be used as catalysts in later chapters. The method used can be further expanded on to change the substituents on the bridging carbon using the relatively easy to synthesise ligand **2** as a starting point, allowing further modification of the catalyst's properties. However, not all substituents are simple to use in a lithiation reaction, as shown by the difficulty faced in synthesising the previously used ligand **4** and its corresponding palladium complex.

Halide concentration was shown to increase the apparent pK_a of bisimidazolyl palladium catalysts, showing that these pK_a s are not pK_a s in the traditional sense at all. The observed pK_a s are in fact dissociation equilibria for the halides in solution, certainly for bromide ions at least. This finding has repercussions for the mechanism of the homocoupling reaction, especially in halide-containing surfactants as the concentration of the halide will affect the state of the catalyst in the reaction. The characterisation of the catalyst indicates that there is a potentially significant difference between complexes PdCl₂-**2** and PdCl₂-**4** due to the bite angle of the ligand. The larger bite angle appears to result in a lower apparent pK_a for PdCl₂-**2** compared to both PdCl₂-**4** and PdCl₂-**5**.

Both PdCl₂-**2** and PdCl₂-**5** were shown to catalyse the homocoupling reaction of boronic acids. Both PdCl₂-**2** and PdCl₂-**5** behave analogously to PdCl₂-**4** in CTAB, even if the observed reaction rate constants were lower. Therefore both PdCl₂-**2** and PdCl₂-**5** are suitable replacements for the more complex PdCl₂-**4** for kinetic experiments, even if the sulphur in PdCl₂-**4** does appear to accelerate the reaction when compared to PdCl₂-**2** and PdCl₂-**5**. What would be interesting to investigate would be the question of whether the thio ether group assists the reaction in the reductive elimination step (in the same way that hydroxyl groups are proposed to do by Amatore ^{12c}).

Laureth-10 can be used as a surfactant to support kinetic measurements of the homocoupling reaction, although the peroxidation of the surfactant leading to the decomposition of arylboronic acids to phenols is an issue even when stock solutions are freshly prepared. A solution to this problem could be found either by finding another surfactant that does not risk peroxidation, and does still allow for effective catalysis, or by finding a way to eliminate the peroxides in solution without hindering the homocoupling reaction.

Finally, it was shown that there is still a maximum in the pH-rate profile for the reaction in laureth-10 solutions in the absence of added halide, meaning that the pH maximum cannot be attributed just to the need to displace halides from the palladium and for the phenylboronic acid to exist in its acidic form. However, adding halide ions to this system affects the optimum pH in a manner that matches the effect that halide has on the pK_a of the catalyst, so it is safe to assume that in the presence of halides the equilibrium between the Pd-OH and Pd-X species does have a significant impact on the pH dependence.

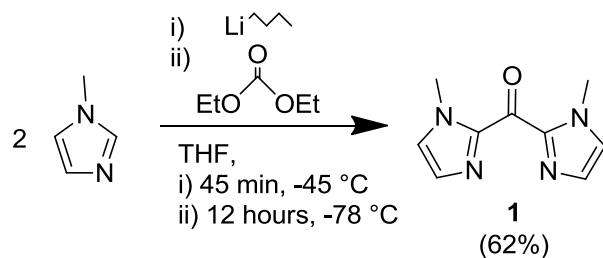
2.4 - Experimental

2.4.1 - General

Commercially available reagents were obtained from Sigma Aldrich, Fisher Scientific or TCI and were used without further purification unless otherwise stated. D₃-acetonitrile and D₂O were obtained from Fluorochem. Organic solvents were dried by standard procedures except DCM, THF, hexane and diethyl ether which were dried using an MBraun SPS-800 solvent purification system. Borate buffers were prepared by dissolving boric acid in water at a concentration of 0.1 M and adjusted to the appropriate pH using sodium hydroxide and sulphuric acid. Laureth-10 was prepared in darkened containers at a concentration of 100 mM and kept in a cool dark cupboard to minimise the peroxidation in solution. Flash column chromatography was carried out using Fischer 60Å silica, thin layer chromatography was carried out using aluminium-backed plates coated with silica. Gas chromatography was carried out using a Perkin Elmer Autosystem XL instrument equipped with a low resolution mass spectrometer Perkin Elmer Turbomass as detector and a Sigma-Aldrich SLB-5ms column. Nuclear magnetic resonance spectra were recorded at room temperature using either a Bruker Avance DPX400 instrument operating at 400 MHz for ¹H NMR or a Bruker Avance 500 operating at 500 MHz for ¹H-NMR or 125 MHz for ¹³C-NMR. Values for chemical shift are reported in ppm downfield from TMS, J values are reported in Hz and multiplicities are expressed in the normal manner (s=singlet, d=doublet,

t=triplet, q=quartet, m=multiplet, br=broad). High resolution mass spectra were measured on a Micromass LCT premiere XE mass spectrometer using electrospray ionisation.

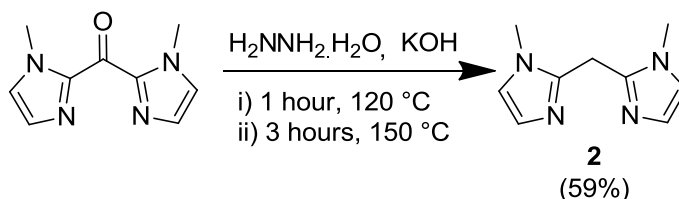
2.4.2 - Synthesis of Bisimidazole 1



1-Methylimidazole (3.95 g, 50 mmol) was placed in a dried schlenk tube with a magnetic stirrer to which dry THF (50 mL) was added and the whole tube was freeze-pump-thaw degassed. After degassing, the solution was cooled to -45 °C in a CO₂/acetone bath under a N₂ atmosphere and n-BuLi (2.5 M in hexanes, 20 mL, 50 mmol) was added dropwise using a syringe over thirty minutes. The solution was stirred for an additional thirty minutes at -45 °C, before additional CO₂ was added to the cooling bath to bring the temperature down to -78 °C. Diethylcarbonate (2.97 g, 25 mmol) in dry THF (10 mL) was added dropwise via a syringe which in some instances caused the orange reaction mixture to become deep purple. The reaction mixture was allowed to warm slowly to room temperature overnight and was then quenched with water (5 mL). Most of the solvent was removed under reduced pressure and dichloromethane (3 x 50 mL) was used to extract the product from the aqueous remainder. The pooled organic layers were dried over Na₂SO₄ and the solvent was evaporated to give small orange crystals. The crystals were recrystallised from acetone and washed on the filter with ice-cold acetone to yield pale

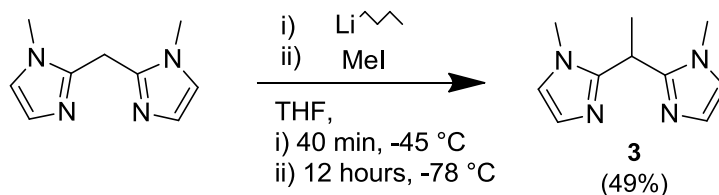
yellow crystals (2.96 g, 62%), ^1H NMR (400 MHz, CDCl_3) δ 7.25 (2H, s, imidazolyl), 7.00 (2H, s, imidazolyl) and 3.95 (6H, s, 2 x N-Me) as previously reported.⁸

2.4.3 - Synthesis of Ligand 2



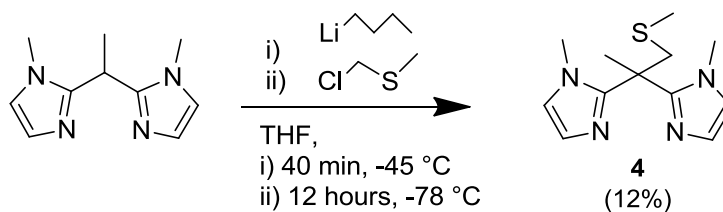
Bis(1-methylimidazolyl)ketone (2.96 g, 15.6 mmol) and powdered KOH (3.0 g, 53.6 mmol) were placed in a round-bottomed flask with a reflux condenser attached to a nitrogen inlet. Hydrazine monohydrate (28 ml, 0.1 mol) was added and the flask was heated on a dry heating block to $120\text{ }^\circ\text{C}$. The solution formed a yellow precipitate that eventually redissolved as the temperature rose. After stirring at $120\text{ }^\circ\text{C}$ for an hour, the temperature was raised to $150\text{ }^\circ\text{C}$ for 3 hours. The flask was cooled slowly to room temperature overnight and a white powder precipitated. The suspension was extracted three times with dichloromethane (3x40 ml) and the organic extracts were pooled. The organic layer was washed with water (2x10 mL), and the water washings were pooled and further extracted with DCM (6x20 mL). All the organic layers were pooled and dried with sodium sulfate, filtered and the solvent was evaporated under reduced pressure within a fume hood to yield white crystals (1.63 g, 59% yield), ^1H NMR (400 MHz, CDCl_3) δ 6.85 (2H, s, imidazolyl), 6.60 (2H, s, imidazolyl), 4.20 (2H, s, CH_2) and 3.60 (6H, s, 2xMe) as previously reported.⁸

2.4.4 - Synthesis of Bisimidazole 3



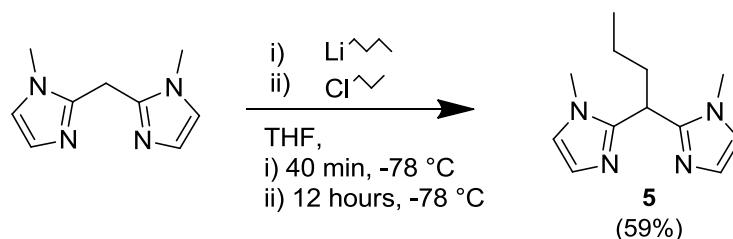
Bis(1-methylimidazol-2-yl) methane (1.0 g, 5.6 mmol) was placed in a dried schlenk tube with a magnetic stirrer to which dry THF (70 mL) was added and the whole tube was freeze-pump-thaw degassed. After degassing, the solution was cooled to $-45\text{ }^{\circ}\text{C}$ in a CO_2 /acetone bath under a N_2 atmosphere and n-BuLi (2.5 M in hexanes, 2.4 mL, 6 mmol) was added dropwise by syringe over twenty minutes. The reaction was stirred at $-45\text{ }^{\circ}\text{C}$ for a further twenty minutes before additional CO_2 was added to the cooling bath to bring the temperature down to $-78\text{ }^{\circ}\text{C}$. Iodomethane (0.85 g, 0.37 mL, 6 mmol) was added dropwise via a syringe at a rate of one drop every 30 seconds (or 0.05 mL per minute using a syringe pump). The reaction was allowed to warm slowly to room temperature overnight and then quenched with water (5 mL). Most of the solvent was removed under reduced pressure and dichloromethane (5 x 20 mL) was used to extract the product from the aqueous remainder. The pooled organic layers were dried over Na_2SO_4 and evaporated to dryness producing a yellow oil that eventually solidified as a yellow wax. The crude product was recrystallised from acetone to yield the product as light yellow crystals. (0.51 g, 48%), ^1H NMR (400 MHz, CDCl_3) δ 6.91 (2H, s, imidazolyl), 6.74 (2H, s, imidazolyl), 4.78 (1H, q $^3J_{\text{HH}}$ 7.38 Hz, apical H), 3.47 (6H, s, 2x N-Me) and 1.76 (3H, d $^3J_{\text{HH}}$ 7.2 Hz, Me) as previously reported.⁸

2.4.5 - Synthesis of Ligand 4



Bis(1-methylimidazol-2-yl)ethylene (400 mg, 2.1 mmol) was placed in a dried schlenck tube with a magnetic stirrer to which dry THF (40 mL) was added and the whole tube was freeze-pump-thaw degassed. After degassing the solution was cooled to -45 °C in a CO₂/acetone bath under a N₂ atmosphere and n-BuLi (2.5 M in hexanes, 1 mL, 2.5 mmol) was added dropwise by syringe over twenty minutes. The reaction was held at -45 ° for a further twenty minutes before cooling it to -78 °C by addition of more CO₂ to the cooling bath. Chloromethylmethylsulfide (241 mg, 0.21 mL, 2.5 mmol) was added dropwise via a syringe. The reaction mixture was allowed to warm to room temperature slowly overnight and then quenched with methanol (5 mL). The reaction mixture was reduced in volume on a rotary evaporator without warming, then water (10 mL) was added and dichloromethane (5 x 20 mL) was used to extract the product from the aqueous solution. The pooled DCM layers were dried over Na₂SO₄ and evaporated at room temperature to dryness to leave a yellow oil. The ligand was purified on a 40 cm silica column using a gradient of 2%-30% methanol and 1% triethylamine in ethyl acetate. The ligand eluted with an rf of 0.32. The solvent was evaporated to give a creamy crystalline solid (0.16 g, 12%, ¹H NMR (400 MHz, CDCl₃) 6.90 (2H, s, imidazolyl), 6.70 (2H, s, imidazolyl), 3.53 (3H, s, CH₂S), 3.00 (6H, s, 2x N-Me), 1.85 (3H, s, Me-S) and 1.65-1.80 (3H, m, Me) as previously reported.⁸

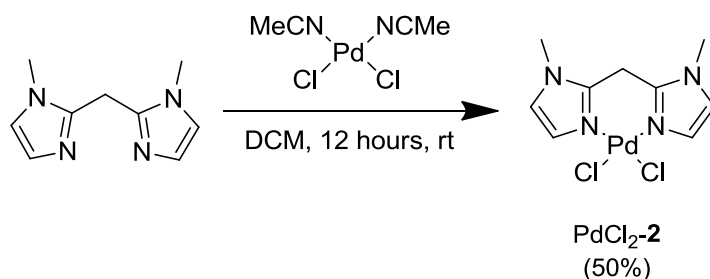
2.4.6 - Synthesis of Ligand 5



Bis(1-methylimidazol-2-yl) methane (1 g, 5.6 mmol) was placed in a dried schlenk tube with a magnetic stirrer to which dry THF (60 mL) was added and the whole tube was freeze-pump-thaw degassed. After degassing the solution was cooled to -78 °C in a CO₂/acetone bath under a N₂ atmosphere and n-BuLi (2.5 M in hexanes, 2.5 mL, 6.25 mmol) was added dropwise by syringe over twenty minutes. The reaction was held at -78 °C for a further twenty minutes. 1-Iodopropane (0.56 mL, 5.68 mmol) was added dropwise via a syringe. The reaction mixture was allowed to warm to room temperature slowly overnight and then quenched with water (5 mL). The reaction mixture was transferred to a separating funnel and chloroform (10 mL) was added. The aqueous layer was extracted with dichloromethane (3 x 50 mL). The pooled organic layers were dried over Na₂SO₄ and evaporated to dryness. The crude product was purified by flash column chromatography using a mixture of 84:15:1 ethyl acetate:methanol:triethylamine as the eluent. Evaporating the solvent yielded the product as a pale oil which, when dried in a vacuum dessicator, crystallised as pale glassy crystals (0.73 g, 59%, ¹H NMR (500 MHz, CDCl₃) δ 6.97 (2H, d, *J* 1.2 Hz, imidazolyl), 6.79 (2H, d, *J* 1.2 Hz, imidazolyl), 4.61 (H, t, ³*J*_{HH} 7.9 Hz, CHCH₂CH₂CH₃), 3.54 (6H, s, 2x N-Me), 2.22-2.34 (2H, m, CHCH₂CH₂CH₃), 1.30-1.46 (2H, m,

CHCH₂CH₂CH₃) and 0.98 (3H, t, ³J_{HH} 7.4 Hz, CHCH₂CH₂CH₃) ¹³C NMR (125 MHz, CDCl₃) δ 146.2, 126.3, 121.9, 38.1, 33.4, 33.1, 20.9, 13.7)

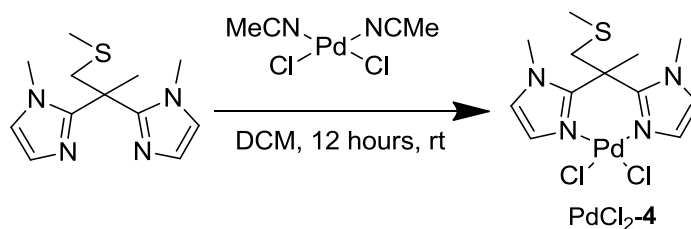
2.4.7 - Synthesis of Catalyst PdCl₂-2



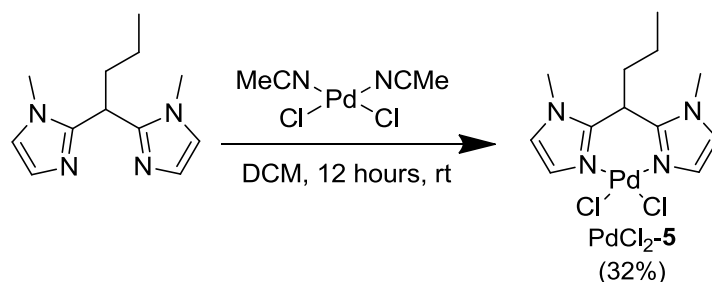
Bisacetonitrilepalladium dichloride (0.15 g, 0.55 mmol) was dissolved in dry dichloromethane (5 mL) and placed in a round-bottomed flask and stirred slowly under nitrogen. Bis(1-methylimidazol-2-yl)methylene (0.1 g, 0.6 mmol) was also dissolved in dry dichloromethane (10 mL) and slowly added to the solution containing the palladium precursor by syringe. The solution appeared unchanged upon completion of the addition, so was left stirring overnight under a nitrogen atmosphere. A cloudy precipitate formed during the reaction. The solvent was removed under reduced pressure to give an orange powdery precipitate. This was recrystallised from acetonitrile to yield the product as a pure powder. This powder was dissolved in acetonitrile and placed in an ultrasonicator for 30 minutes after which the solution was left to stand for several days to give large needle-shaped crystals (0.1 g, 50%) ¹H NMR (400 MHz, CD₃CN) δ 7.45 (2H, s, imidazolyl), 6.90 (2H, s, imidazolyl), 4.15 (2H, s, apical CH₂) and 3.60 (6H, s, 2x N-Me), ¹³C not obtained due to low solubility, crystal structure is presented in main text, HR-ESI-

MS from solution in acetonitrile (Molecular Ion = 358.0071 $[\text{C}_9\text{H}_{12}\text{N}_4+\text{Pd}+\text{MeCN}+\text{Cl}]^+$ expected 358.0051, expected for $[\text{C}_9\text{H}_{12}\text{N}_4+\text{Pd}+\text{Cl}_2]$ 351.9473).

2.4.8 - Attempted synthesis of Catalyst $\text{PdCl}_2\text{-4}$



Bisacetonitrilepalladium dichloride (0.1 g, 0.42 mmol) was dissolved in dry dichloromethane (5 mL) and placed in a round-bottomed flask and stirred slowly under nitrogen. 2,2-Bis(1-methylimidazol-2-yl)propyl methyl thioether (0.1 g, 0.42 mmol) was also dissolved in dry dichloromethane (10 mL) and slowly added to the solution containing the palladium precursor by syringe. The solution appeared unchanged upon completion of the addition, so was left stirring overnight under a nitrogen atmosphere. A cloudy precipitate formed during the reaction. The solvent was removed under reduced pressure to give an orange powdery precipitate. The ^1H NMR of the powder in acetonitrile was recorded as it was insoluble in chloroform which did not contain any imidazolyl protons and consisted of a single peak at δ 5.40 which is assumed to be the residue of the dichloromethane.

2.4.9 - Synthesis of Catalyst PdCl₂-5

Bisacetonitrilepalladium dichloride (0.1 g, 0.39 mmol) was dissolved in dry dichloromethane (10 ml) in a round-bottomed flask and stirred slowly under nitrogen. Bis(1-methylimidazol-2-yl)butane (0.1 g, 0.46 mmol) was also dissolved in dry dichloromethane (10 ml) and added slowly to the solution containing the palladium precursor by syringe. The orange solution appeared unchanged upon completion of the addition, so was left stirring overnight under a nitrogen atmosphere. The solvent was removed under reduced pressure to give a light brown powdery solid. This solid was recrystallised from acetonitrile to give the product as a pale brown powder. The powder was dissolved in acetonitrile and placed in an ultrasonicator for 30 minutes after which the solution was left to stand in acetonitrile for several days eventually forming long needle-like crystals (0.07 g, 0.14 mmol, 32%), ¹H NMR (400 MHz, CD₃CN) δ 7.36 (2H, d, ³J_{HH} 1.7 Hz, imidazolyl), 7.01 (2H, d, ³J_{HH} 1.7 Hz, imidazolyl), 4.48 (H, t, ³J_{HH} 7.3 Hz, CHCH₂CH₂CH₃), 3.74 (6H, s, 2x N-Me), 2.30-2.45 (2H, m, CHCH₂CH₂CH₃), 1.80 (2H, dt, ³J_{HH} 5.0 Hz, 2.4, CHCH₂CH₂CH₃) and 0.98 (3H, t, ³J_{HH} 7.3 Hz, CHCH₂CH₂CH₃), ¹³C not obtained due to low solubility, crystal structure is presented in main text.

2.4.10 - XRD crystallography

XRD Data were collected at 150 K on a Nonius Kappa CCD diffractometer using graphite monochromated Mo K α radiation ($\lambda(\text{Mo-K}\alpha) = 0.71073 \text{ \AA}$) equipped with an Oxford Cryosystems cooling apparatus. The structures were solved using direct methods and refined with SHELX-97.¹⁸ All non-hydrogen atoms were refined anisotropically, while the hydrogen atoms were inserted in idealised positions with Uiso set at 1.2 or 1.5 times the Ueq of the parent atom.

2.4.11 - NMR experiments

The NMR experiments were performed on the powder precipitated from acetonitrile prior to crystallisation (see Chapter 2). The powder was dried under reduced pressure on a drying line. The NMR samples were prepared by dissolving 10 mg of the dried orange powder in 1 mL of solvent, either D₃-acetonitrile or 1:1 D₃-acetonitrile:D₂O. If the powder did not fully dissolve, the tube was immersed in an ultrasound bath at 50 °C for twenty minutes to aid dissolution. The NMR spectra were recorded on a Bruker biospin operating at 250 MHz for ¹H.

2.4.12 – UV-visible titrations

UV-visible spectra were recorded using a Jasco V-630 spectrophotometer thermostatted at 30 °C using an air-cooled peltier cell-holder. The pH was controlled using a range of borate buffers that were adjusted to the appropriate pH. pH of the samples was measured in the quartz cuvettes

using a Hanna pH211 microprocessor pH meter equipped with a narrow VWR 662-1759 glass electrode. The surfactant solutions were prepared in 45 mL centrifuge tubes and covered in storage to limit photodegradation. Once the samples for pK_a analysis were prepared in vials they were transferred to a 1 cm path length quartz cuvette and the UV-visible spectrum was recorded between 200 and 600 nm with a resolution of ± 0.2 nm. Spectra were recorded once an hour for three hours to ensure that spectrum was reproducible and that equilibrium had been reached. pK_a s were calculated by fitting Equation 1 to a plot of k_{obs} against pH.

$$A_{obs} = \frac{1}{1 + 10^{(pH-pK_a)}} \cdot A_{low\ pH} + \frac{1}{1 + 10^{(pK_a-pH)}} \cdot A_{high\ pH}$$

Equation 1

2.4.13 - Kinetic experiments

The homocoupling reactions were performed in 10 mm path length cuvettes filled to a total volume of 2.5 mL (leaving approximately 1 mL head space above the water level). Laureth-10, Mega-10 or CTAB stock solutions were warmed to 30 °C and then added to the cuvette using a 200-1000 μ L Eppendorf micropipette (typically 250 μ L, 10 mM) followed by borate buffer at the appropriate pH (typically 250 μ L, to give 10 mM, *vide supra*). Water was added using a 1-5 mL Gilson pipette (typically 1.95 mL) and the UV spectrum was recorded in order to check the base line was suitably level. The catalyst in acetonitrile was then added using a 10-100 μ L Eppendorf micropipette (typically 20 μ L, to give 33.6 μ M) and the spectrum recorded again. Finally, the 4'carboxyphenylboronic acid was added a 10-100 μ L Eppendorf micropipette

(typically 37.5 μL , to give 150 μM) and the kinetic measurements started. Either the full spectrum was recorded every five minutes, or when performing simultaneous measurements the absorbance of each cuvette at 278 ± 2 nm was measured every thirty seconds. Once the reaction reached its end point a full spectrum of the contents of each cuvette was measured and then a second aliquot of 4-carboxyphenylboronic acid was added using a 10-100 μL Eppendorf micropipette (typically 37.5 μL , 150 μM) and the kinetic measurements of the second cycle started. Equation 3 was used to fit to the kinetic data to derive the observed pseudo-first-order rate constant. A is the absorbance at the λ_{max} of a given component, typically 253 nm for **7** and 278 nm for **8**.

$$A = A_{\text{final}} - \Delta A e^{-kt} \quad \text{Equation 3}$$

The k_{obs} values from equation 3 were plotted against the pH recorded using the pH probe to give the pH rate profile. Equation 4 was fitted to the data, with $\text{p}K_{\text{a}}$ for PhB ($\text{p}K_{\text{a}}\text{PhB}$) fixed to 8.0 in order to determine the pH maximum.

$$k_{\text{obs}} = k_{\text{catPd}} \left(\frac{1}{1+10^{(\text{pH}-\text{p}K_{\text{a}}\text{PhB})}} \right) \left(\frac{1}{1+10^{(\text{p}K_{\text{a}}\text{Pd}-\text{pH})}} \right) \quad \text{Equation 4}$$

2.5 - Bibliography

1. Matthey, J. *Platinum 2013*; 2013; pp 35-38.
2. (a) Peris, E.; Crabtree, R. H., Recent homogeneous catalytic applications of chelate and pincer N-heterocyclic carbenes. *Coordination Chemistry Reviews* **2004**, 248 (21–24), 2239-2246;

- (b) Kumar, A.; Kumar Rao, G.; K Singh, A., Organochalcogen ligands and their palladium(ii) complexes: Synthesis to catalytic activity for Heck coupling. *RSC Advances* **2012**, 2 (33), 12552-12574.
3. Aldrich, S. Tetrakis(triphenylphosphine)palladium (0). <http://www.sigmaaldrich.com/catalog/product/aldrich/216666?lang=en®ion=GB> (accessed July).
4. Othman, M. A. The palladium-catalysed aerobic oxidative homocoupling reaction of arylboronic acids in aqueous micellar medium kinetic and mechanistic studies. Cardiff University, Cardiff University, 2011.
5. Liu, C.; Ni, Q.; Hu, P.; Qiu, J., Oxygen-promoted PdCl₂-catalyzed ligand-free Suzuki reaction in aqueous media. *Organic & Biomolecular Chemistry* **2011**, 9 (4), 1054-1060.
6. de Vries, A. H. M.; Mulders, J. M. C. A.; Mommers, J. H. M.; Henderickx, H. J. W.; de Vries, J. G., Homeopathic Ligand-Free Palladium as a Catalyst in the Heck Reaction. A Comparison with a Palladacycle. *Organic Letters* **2003**, 5 (18), 3285-3288.
7. (a) Schmid, R.; Broger, E. A.; Cereghetti, M.; Cramer, Y.; Foricher, J.; Lalonde, M.; Muller, R. K.; Scalone, M.; Schoettel, G.; Zutter, U., New developments in enantioselective hydrogenation. *Pure Appl. Chem.* **1996**, 68 (1), 131-8; (b) RajanBabu, T. V.; Casalnuovo, A. L., Electronic effects in asymmetric catalysis: enantioselective carbon-carbon bond-forming processes. *Pure Appl. Chem.* **1994**, 66 (7), 1535-42.
8. Sidhu, M. Complexes of Imidazole Based Ligands. Cardiff University, Cardiff University, 2009.
9. Adamo, C.; Amatore, C.; Ciofini, I.; Jutand, A.; Lakmini, H., Mechanism of the Palladium-Catalyzed Homocoupling of Arylboronic Acids: Key Involvement of a Palladium Peroxo Complex. *Journal of the American Chemical Society* **2006**, 128 (21), 6829-6836.
10. Kuivila, H. G.; Armour, A. G., Electrophilic Displacement Reactions. IX. Effects of Substituents on Rates of Reactions between Hydrogen Peroxide and Benzeneboronic Acid1-3. *Journal of the American Chemical Society* **1957**, 79 (21), 5659-5662.
11. Reibold, M.; Paufler, P.; Levin, A. A.; Kochmann, W.; Patzke, N.; Meyer, D. C., Materials: Carbon nanotubes in an ancient Damascus sabre. *Nature* **2006**, 444 (7117), 286-286.

12. (a) Matos, K.; Soderquist, J. A., Alkylboranes in the Suzuki–Miyaura Coupling: Stereochemical and Mechanistic Studies. *The Journal of Organic Chemistry* **1998**, *63* (3), 461-470; (b) Nakai, H.; Ogo, S.; Watanabe, Y., pH-Dependent Cross-Coupling Reactions of Water-Soluble Organic Halides with Organoboron Compounds Catalyzed by the Organometallic Aqua Complex [(SCS)PdII(H₂O)]⁺ (SCS = C₆H₃-2,6-(CH₂SBut)₂). *Organometallics* **2002**, *21* (8), 1674-1678; (c) Amatore, C.; Jutand, A.; Le Duc, G., Kinetic Data for the Transmetalation/Reductive Elimination in Palladium-Catalyzed Suzuki–Miyaura Reactions: Unexpected Triple Role of Hydroxide Ions Used as Base. *Chemistry – A European Journal* **2011**, *17* (8), 2492-2503.
13. Buurma, N. J.; Serena, P.; Blandamer, M. J.; Engberts, J. B. F. N., The Nature of the Micellar Stern Region As Studied by Reaction Kinetics. 2[†],1. *The Journal of Organic Chemistry* **2004**, *69* (11), 3899-3906.
14. Aldrich, S. MSDS for chloromethylmethyl sulfide (2375-51-5). http://www.sigmaaldrich.com/MSDS/MSDS/PrintMSDSAction.do?name=msdspd_1405142135208145.
15. Covington, A. K.; Paabo, M.; Robinson, R. A.; Bates, R. G., Use of the glass electrode in deuterium oxide and the relation between the standardized pD (paD) scale and the operational pH in heavy water. *Analytical Chemistry* **1968**, *40* (4), 700-706.
16. de Jong, G. T.; Kovács, A.; Bickelhaupt, F. M., Oxidative Addition of Hydrogen Halides and Dihalogens to Pd. Trends in Reactivity and Relativistic Effects. *The Journal of Physical Chemistry A* **2006**, *110* (25), 7943-7951.
17. Amatore, C.; Jutand, A., Anionic Pd(0) and Pd(II) Intermediates in Palladium-Catalyzed Heck and Cross-Coupling Reactions. *Accounts of Chemical Research* **2000**, *33* (5), 314-321.
18. Sheldrick, G., A short history of SHELX. *Acta Crystallographica Section A* **2008**, *64* (1), 112-122.

Chapter 3

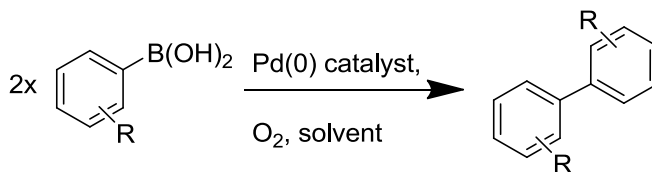
Kinetic Studies of the Homocoupling of Arylboronic acids by Pd-polypyrrole Nanocomposites

Abstract: A palladium-polypyrrole nanocomposite formed on the surface of 5.2 μm polystyrene microspheres was tested in the aerobic homocoupling reaction of arylboronic acids under aqueous conditions. With a catalyst palladium loading of 1.2 mol%, pH 8 and 70 $^{\circ}\text{C}$ the homocoupling reaction of 4-carboxyphenylboronic acid (150 μM) was completed in 24 hours with an observed rate constant of $1.8 \times 10^{-3} \text{ min}^{-1}$. There was a mild correlation between increased pH and increased rate constant for the reaction, with the highest rate constant of $1.87 \times 10^{-3} \text{ min}^{-1}$ recorded at pH 9. The product ratio determined using HPLC showed far less than stoichiometric production of the phenol byproduct. The catalyst activity was conserved by sedimentation (1/8th activity remaining after 3 cycles) or centrifugation (1/4th activity remaining after 4 cycles) of the reaction mixture to recover the immobilised catalyst. Addition of chloride to the homocoupling reaction mixture dramatically increases the rate constant of the reaction, with the reaction completing within three hours in the presence of $>0.05 \text{ M Cl}^{-}$. Addition of bromide further accelerates the reaction, with the reaction completing within 90 minutes in the presence of $>0.05 \text{ M Br}^{-}$. The product ratio determined using HPLC showed that for the reaction in the presence of halide far more phenol byproduct was produced relative to the biaryl product when compared to the reaction in the absence of halide. The pH rate profile was measured in the presence of 1 M Cl^{-} which showed a maximum rate constant at pH 8.4. Recovery of the catalyst by centrifugation after the addition of halide caused a much sharper drop in activity between cycles, particularly for added Br^{-} where concentrations $>0.5 \text{ M}$ caused no activity to be recovered after 2 cycles.

3.1 - Introduction

3.1.1 - The homocoupling reaction and homogeneous catalysts.

The homocoupling reaction of arylboronic acids (hereafter 'the homocoupling reaction') (Scheme 1). has been previously studied using molecular palladium catalysts (Chapter 2). Molecular catalysts, particularly palladium with phosphine ligands, are very commonly used in palladium-catalysed coupling reactions as they are typically more catalytically active than heterogeneous catalysts. Not only are the individual palladium atoms easy to modify with ligands to improve their catalytic activity, homogeneous catalysts have the virtue of the catalytic metal atom being extremely available for reaction. However these molecular catalysts are not without drawbacks - in order to be active they need to be homogeneous with the reaction medium. This means that the catalyst must be soluble in the same solvent as the reaction mixture and substrates. Also, since the catalyst is dissolved in the reaction mixture, it is not trivial to recover.



Scheme 1. The oxidative homocoupling reaction of arylboronic acids.

Water is a very attractive medium for synthetic reactions as it is typically cheap and plentiful, non-flammable, non-toxic and has a relatively low environmental impact (especially compared to DMF or toluene which are more typically used in palladium-catalysed coupling reactions). The problem with using water as a solvent for palladium-catalysed reactions is that many palladium compounds are insoluble in water. In Chapter 2 the use of surfactants to solubilise an otherwise insoluble catalyst in a primarily aqueous medium was described. Whilst the use of surfactants overcomes the solubility issue of the catalyst, at the end of the reaction the catalyst is still dissolved in the reaction mixture and separating the surfactant, catalyst and product can be difficult.

3.1.2 - Heterogeneous catalysts and nanoparticles

Heterogeneous catalysts are much easier to recover than homogeneous catalysts, since they exist in a separate phase to the reaction mixture. In many cases this means that the catalyst itself is solid which means the catalyst is easily separated from the reaction mixture by filtration, decantation, evaporation or even using magnets if the catalyst is magnetic or immobilised on a magnetic material. Industrial catalysis very often uses heterogeneous catalysts as they can be used in continuous processes by flowing the reaction mixture across the catalyst. However, reactivity in heterogeneous catalysts is constrained by surface area, since reactions can only occur at the surface of the structure. Due to the cubic-quadratic relationship between a structure's volume and surface area, the larger the structures become the less surface area they have (as a proportion of their size). In order to get high reactivities heterogeneous catalysts need to have

very high surface areas, which can either be achieved by having very small particles, or by having fine structures on the surface of particles that increase the surface area.

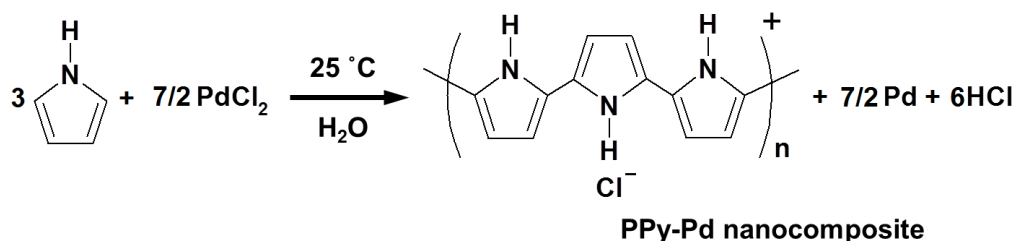
The term “nanoparticle” is a catch-all term that describes a number of different kinds of particle that are between 1-100 nm in size, and these nanoparticles typically have properties that are intermediate between individual molecules and bulk materials. Metallic nanoparticles are being heavily investigated for catalytic purposes because even with relatively simple spherical structures they have extremely high surface areas due to the small size of each particle (a 20 nm wide particle has a surface area $>1250 \text{ nm}^2$). As such nanoparticles can be very catalytically active, due to their high surface areas, whilst still existing as a separate phase in the reaction mixture that can be easily recovered by sedimentation or centrifugation. If the catalyst is particularly rare or valuable (such as palladium or platinum) then being able to obtain extremely high surface areas, and therefore reactivities, with less material is also quite attractive. Additionally, the electronic properties of nanoparticles can be very different to either the bulk material or the individual atoms since the surface represents a much larger proportion of the material (30% of atoms in a 20 nm particle exist on the surface as compared to 0.3% in a 2 μm particle).¹

Despite being much larger than individual atoms or molecules, true nanoparticles are still not simple to separate completely from solutions. However, there are ways to increase the size of particles without having to sacrifice the surface area of nanoparticles. By binding nanoparticles to a much larger support the reactivity of the nanoparticles can be conserved whilst making

recovery of the particles much easier.² Such a technique is commonly used by biochemists to immobilise enzymes on large bead supports so that they can be used for continuous flow catalysis.² The main concern with using such an immobilised nanoparticle as a catalyst is whether the nanoparticle remains bound to the support under reaction conditions, since any particles detached from the surface will not be recovered with the support.

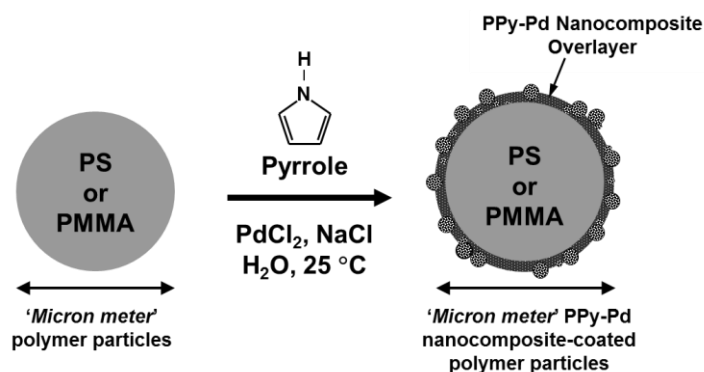
3.1.3 - Polystyrene-immobilised Pd-PPy nanocomposites

A nanocomposite is a mixture of multiple different phases to form a single material where one of the constituent materials is in the nanoscale.³ By forming a nanocomposite with Pd nanoparticles, the properties of the nanoparticles can be modulated to better suit their purpose. This is a similar principle as changing the ligands used in a molecular catalyst to modulate the properties of the metal centre to improve its catalytic characteristics. Using a conductive polymer to confine metallic nanoparticles is of interest because, unlike nanoparticles confined using insulating polymers, the individual nanoparticles are electronically connected which can affect the electronic state of the nanoparticle surfaces.⁴ Whilst these metal-conducting polymer nanocomposites can be synthesised using presynthesised polymers,⁵ both components of the nanocomposite can also be synthesised in one-pot under appropriate conditions.⁶



Scheme 2. The synthesis of the PPy-Pd nanocomposite by oxidative polymerisation.

The group of Professor Syuji Fujii at the Osaka Institute of Technology have been researching the field of catalytic nanoparticle synthesis and have synthesised a series of palladium nanocomposites immobilised on polystyrene beads.⁷ Oxidative polymerisation of pyrrole (Py) by PdCl₂ (Scheme 2) caused the formation of Pd nanoparticles in a nanocomposite with the polypyrrole (PPy). In the presence of micrometer-sized polystyrene (PS) particles this oxidative polymerisation causes the PPy-Pd nanocomposite to form as a thin layer on the surface of the PS particles (Scheme 3).



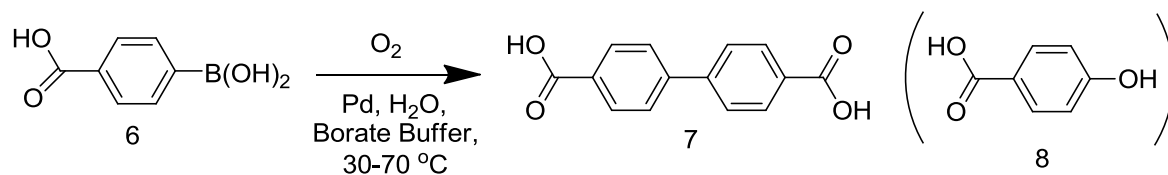
Scheme 3. Schematic representation of the formation of PPy-Pd nanocomposite as a thin layer on the surface of a micrometer-sized polystyrene particle.

These PS-PPy-Pd particles have already shown themselves to be an active catalyst for the Suzuki-Miyaura cross-coupling reaction in aqueous conditions.⁸ The particles would therefore be expected to make a good catalyst for the homocoupling reaction in aqueous conditions as well, negating the need for surfactants to solubilise the catalyst, making product work-up straightforward. Additionally, the particles should be easy to separate and reuse after the reaction is complete as all the Pd-PPy-PS particles were noted to sediment. Whilst most of the functionalised particles sedimented at a faster rate than the PS seed particles due to their increased density, the smallest 5.2 μm particles actually sedimented at a slower rate than the 5.2 μm seed particles. This is thought to be because the charge build up on the particles surface due to the PPy causes a stronger attraction to the vessel's walls than the increased rate of sedimentation due to the increased density on such a small particle.

3.2 - Results and Discussion

3.2.1 - Catalyst loading

The group at Osaka Institute of Technology kindly provided us with samples of the PS-PPy-Pd particles with a diameter of 5.2 μm and a palladium loading of 1.2 wt%. As before (Chapter 2) the reaction to be tested was the homocoupling of 4-carboxyphenylboronic acid **6** (Scheme 4).



Scheme 4 - The palladium catalysed oxidative homocoupling reaction of 4-carboxyphenylboronic acid (6) to form 4,4'-dicarboxybiphenyl (7) and 4-hydroxybenzoic acid (8).

Boronic acid **6** was selected as in the absence of any surfactants the product needed to be soluble in water to be quantified by UV-visible spectroscopy, and **6** is the most readily available arylboronic acid that forms a soluble biaryl product (**7**). The particles were tested under equivalent conditions as used in Chapter 4, *sans* surfactant, to see if the reaction could be followed in the same manner (Figure 1).

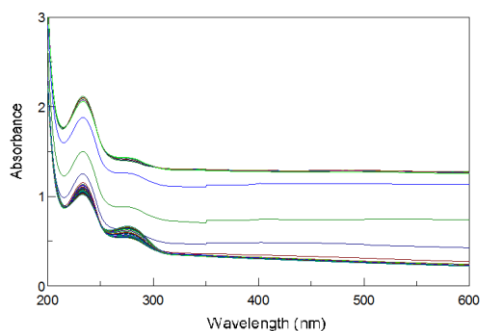


Figure 1. UV-visible spectra recorded during the course of the homocoupling reaction of **6** (150 μM) in water with pH 8 borate buffer (10 mM) and catalyst Pd-PPy-PS (67 μM Pd) over the course of 24 hours at 30 $^{\circ}\text{C}$.

The first conditions were selected to give a total Pd concentration of 67 μM , twice the standard concentration of PdCl₂-**2** used for the molecular catalyst studies (Chapter 2). At this concentration the suspension in the cuvette is an extremely dark black, and this is reflected by the high starting baseline of the absorbance at 1.5 AU (especially given that the maximum accurate absorbance that can be recorded is 3 AU). It was further observed that even with the reaction being stirred the particles sediment over time, reducing the baseline by two-thirds. Clearly, this changing baseline complicates the analysis of the kinetics since the decrease in baseline will also affect the apparent absorbance at the peaks. In addition, the sedimentation will likely affect the actual rate of the reaction as the sedimented particles become less well dispersed in the reaction. Nevertheless, even with the sedimentation, there is clearly development of a peak at 278 nm, the λ_{max} of the product **7**. In order to follow the reaction by UV-visible spectroscopy a

far lower concentration of nanoparticles should be used, both to decrease the height of the baseline, but also to reduce the effect of sedimentation of the particles. A concentration of 1.8 μM Pd was found to produce a suitably low baseline, and throughout the reaction there was no significant decrease in the baseline (Figure 2)

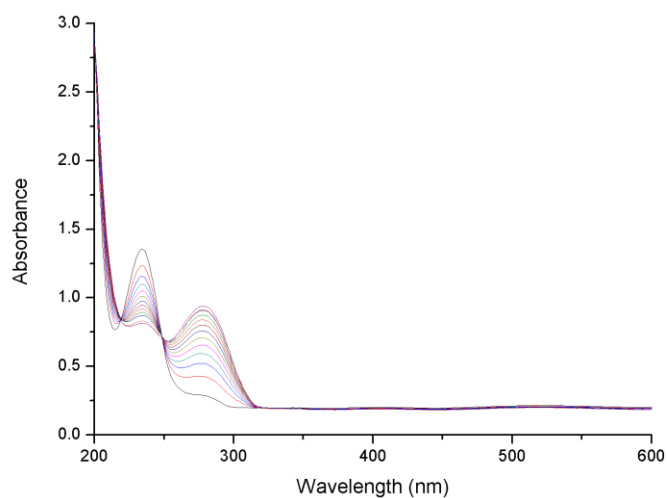


Figure 2. UV spectra recorded during the course of the homocoupling reaction of **6** (150 μM) in water with pH 8 borate buffer (10 mM) and catalyst Pd-PPy-PS (1.8 μM , 1.2 mol % Pd) over the course of 24 hours at 70 $^{\circ}\text{C}$.

Figure 2 shows that there is no appreciable reduction in the absorbance of the baseline over the course of the reaction, and there is a clear decrease in absorbance at 235 nm and an increase in absorbance at 278 nm (the λ_{max} of **6** and **7** respectively). Additionally, Figure 2 does not show a large increase in the absorbance at 253 nm (λ_{max} of **8**) relative to 278 nm, so there has not been a greater than stoichiometric formation of phenol **8** (as was often a problem in nonionic surfactants

in Chapter 4). However, in order for the reaction to complete in a reasonable time frame it was necessary to perform it at an elevated temperature. At 30 °C the reaction with 1.8 μM Pd took approximately three days to reach completion, which was too long a time for a single experiment, especially when considering that the observed rate constant is only likely to decrease during catalyst recovery experiments.

The reaction was followed using UV-visible spectroscopy at 278 nm at two different temperatures (Figure 3).

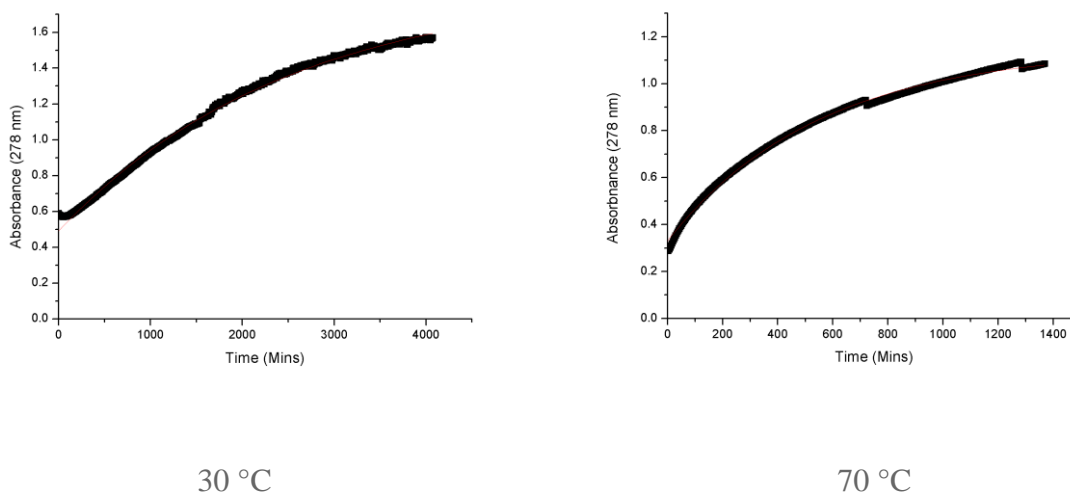


Figure 3. Absorbance at 278 nm recorded during the course of the homocoupling reaction of **6** (150 μM) in water with pH 8 borate buffer (10 mM) and catalyst Pd-PPy-PS (1.8 μM Pd) over the course of 72 hours at (left) 30 °C (right) 70 °C.

Figure 3 shows the homocoupling reaction takes nearly three days to complete at 30 °C, but raising the temperature to 70 °C causes the reaction to accelerate, completing within 24 hours.

Since the concentration of the catalyst is assumed to be constant and the reaction is assumed to be first order in the boronic acid, Equation 1 was fitted to the data to calculate observed pseudo-first order rate constants. Equation 1 takes the form of a first-order rate equation, where the absorbance measured by UV is used in place of the concentration and k is the pseudo-first order rate constant (which is the rate constant times the concentration of the palladium).

$$A = A_{\text{final}} - \Delta A e^{-kt} \quad \text{Equation 1}$$

The observed rate constant (k_{obs}) as determined by fitting Equation 1 to the data was $4 \times 10^{-4} \text{ min}^{-1}$ which, although far lower than k_{obs} found for molecular catalysts ($0.004\text{-}0.04 \text{ min}^{-1}$, Chapter 2), indicates a relatively fast reaction when considering the palladium concentration; there was at least 18x as much PdCl₂-2 used in the experiments described in Chapter 4 than the total Pd content used in this reaction, and a proportion of the palladium will be inaccessible to the reaction as it is not on a surface. At 70 °C the reaction reached completion after 24 hours with k_{obs} of 0.0018 min^{-1} . Whilst still not as quick as the molecular catalyst experiments (which could typically be finished in under 8 hours), 24 hours is a manageable experiment length. It should be noted that there is a slight amount of roughness to the data caused by bubbles forming in the cuvette under reaction conditions, although this was not usually significant to interfere with the kinetic analysis. The effect of pH on the reaction k_{obs} was tested in order to find the optimal pH to further accelerate the reaction (Figure 4).

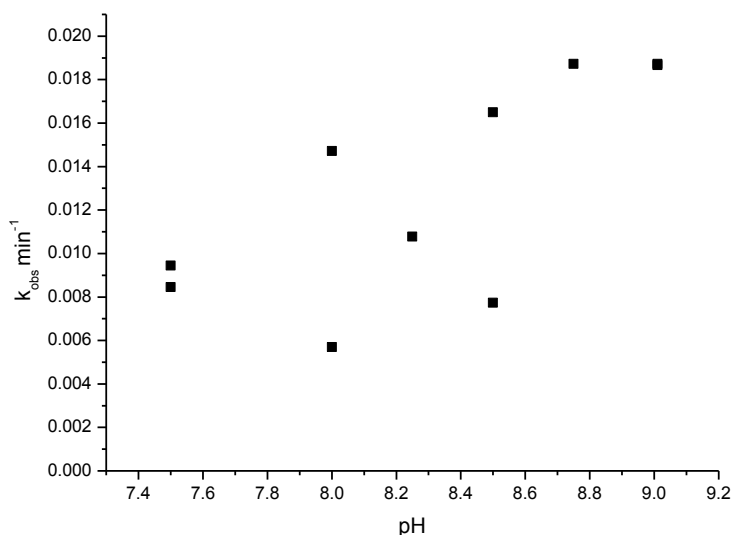


Figure 4. pH rate profile for the homocoupling reaction of **6** (150 μM) in water with borate buffer (10 mM) and catalyst Pd-PPy-PS (1.8 μM Pd) at 70 $^{\circ}\text{C}$.

Figure 4 shows that, unlike for the molecular catalysts in Chapter 2, the effect of pH on the reaction rate with Pd-PPy-PS particles was not well defined. There does appear to be a discernable trend towards higher k_{obs} at higher pHs, but the wide variance in k_{obs} makes it less conclusive. It may be that the absence of halide from the reaction eliminated the need for base (since there is no halide bound to the palladium that needs displacing). The highest k_{obs} value of 0.0187 min^{-1} was recorded at pH 9.

3.2.2 - Pd-PPy-PS particle recovery

The particles were then tested for recovery of activity by sedimentation of the particles at both pH 8 and pH 9 since these pHs were shown to give appropriately fast reaction rates (Figure 5).

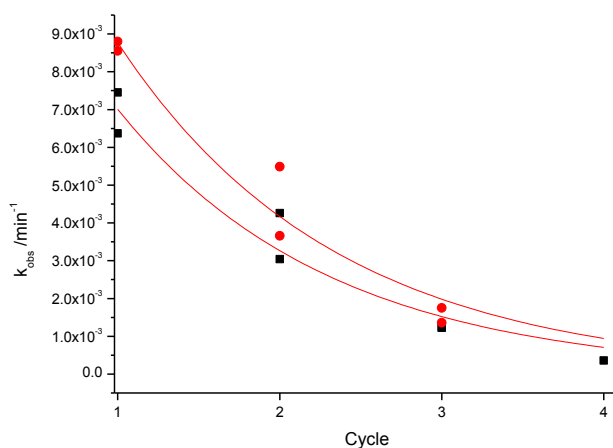


Figure 5. Observed first-order rate constants k_{obs} as a function of use cycle of the 5.4 μm Pd-PPy-PS catalyst at Pd concentration of 1.8 μM for the homocoupling reaction of **6** (150 μM) in water with pH 8 (■) and pH 9 (●) borate buffer (10 mM) at 70 °C with catalyst recovered by sedimentation under gravity for 60 minutes.

One would expect from the reported sedimentation rate observed in quartz cuvettes for the 5.4 μm particles (0.1% per minute) that the catalyst activity recovered by sedimentation would be very poor. Over the course of an hour only a recovery of 6% of the activity was expected, but the results were not as bad as initially feared. The rate of activity loss per cycle at both pHs is approximately 50%, which is far less than would have been expected from the sedimentation

rate. However, after the second recovery attempt the rate constant had dropped so low that the reaction could not be completed in a reasonable time frame. The k_{obs} calculated after three days for the fourth use of the particles at pH 8 was $3.6 \times 10^{-4} \text{ min}^{-1}$ which would require 7 days to reach completion. Since the recovery still took a considerable time to complete and did not achieve complete retention of activity recovery was repeated using centrifugation rather than using gravity. Immediately after the reaction 88% (2.2 mL) of the contents of the cuvette was removed and centrifuged at 13300 rpm for 10 minutes. The resulting pellet was resuspended and placed back in the cuvette for use in another reaction (Figure 6).

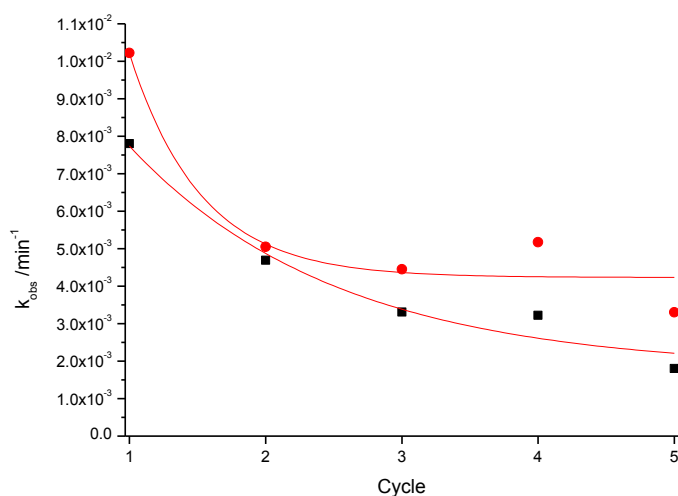


Figure 6. Observed first-order rate constants k_{obs} as a function of use cycle of the $5.4 \mu\text{m}$ Pd-PPy-PS catalyst at Pd concentration of $1.8 \mu\text{M}$ for the homocoupling reaction of **6** ($150 \mu\text{M}$) in water with pH 8 (■) and pH 9 (●) borate buffer (10 mM) at $70 \text{ }^\circ\text{C}$ with catalyst recovered by centrifugation at 13300 rpm for 10 minutes .

There was better retention of activity by centrifugation than by sedimentation at both pHs. The k_{obs} values no longer appear to trend towards 0 min^{-1} , with the reaction at pH 8 trending towards a low k_{obs} of 0.0018 min^{-1} and the reaction of pH 9 trending towards a k_{obs} of 0.0042 min^{-1} . There is, however, a large decrease in the rate constant for the reaction for the first centrifugation at pH 9, halving the observed rate constant between the first and second reaction cycles, at which point it remained relatively constant through the following four reaction cycles. At pH 8 the decrease is slower at first, but continues for at least the first two recovery cycles, resulting in a k_{obs} after the fifth cycle of a quarter of the initial rate. Since the recovery was most effective at pH 9, the recovery was further investigated at a range of catalyst concentrations at that pH (Figure 7).

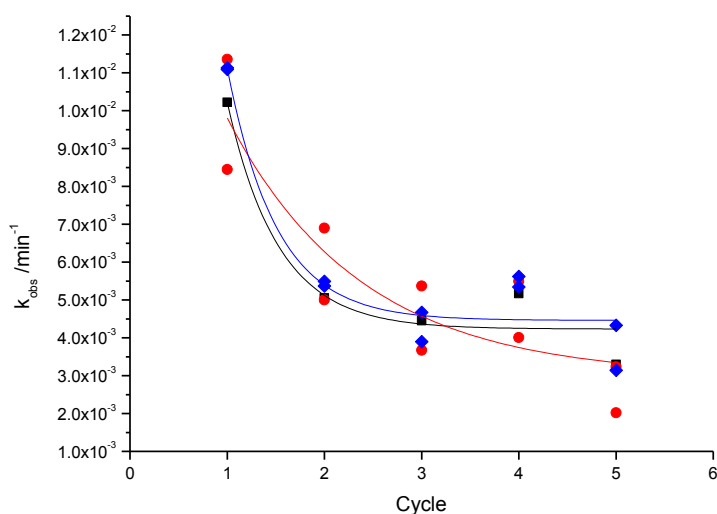
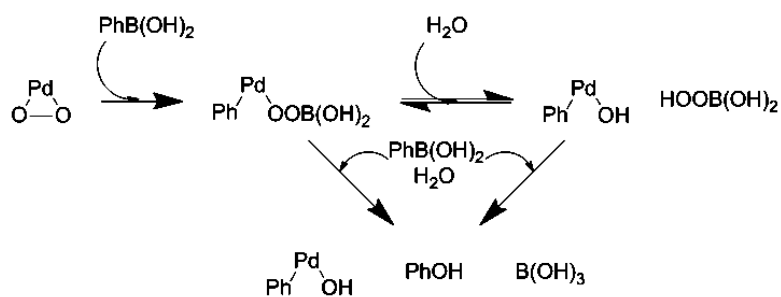


Figure 7 - Observed first-order rate constants k_{obs} as a function of use cycle of the catalyst Pd-PPy-PS at catalyst Pd concentrations of $1.8 \mu\text{M}$ (■), $3.6 \mu\text{M}$ (●) and $5.4 \mu\text{M}$ (◆) for the homocoupling reaction of **6** ($150 \mu\text{M}$) in water with pH 9 borate buffer (10 mM) over the course of 72 hours at $70 \text{ }^\circ\text{C}$.

Figure 7 shows that k_{obs} is not significantly affected by the initial concentration of the catalyst. Since increasing the initial concentration of the catalyst did not change rate constant, the reaction appears to be zero order in the catalyst. This means that the decrease in rate constant across the reaction cycles cannot be directly attributed to recovery of the microparticles, as the concentration of the catalyst does not directly affect the rate constant. This is further confirmed by the fact that the recovered activity of the particles decays on approximately the same order and to the same final value at all three catalyst concentrations. The loss of catalytic activity could therefore be due to a change in the nature of the nanoparticles rather than a change in the concentration of the nanoparticles. One possible explanation could be that the most weakly bound nanoparticles on the surface of the microparticles are lost into solution under the reaction conditions during the in the first reaction cycle, thus reducing the loading of palladium, but not the microparticles. However, this is not in agreement with the fact that increasing the concentration of microparticles does not increase the reaction rate constant, since then the rate constant should also not be affected by palladium loss either. Alternatively, the palladium nanoparticles in the nanocomposite may be coalescing under the reaction conditions, forming larger clusters, which reduces the total available surface area for the reaction and could alter the surface properties in the process. Both of these mechanisms would explain why the loss of activity appears quite pronounced after the first reaction cycle, and then later cycles show far less activity loss. If this is the case, it is likely that the same process is occurring in the particles recovered by sedimentation, and the reason that the k_{obs} trends towards zero rather than a higher k_{obs} is that the incomplete recovery of the particles is additionally greatly decreasing the observed rate constant.

Regardless, the activity is maintained quite well between the later reaction cycles at pH 9 and, even taking into account the initial loss in activity, the catalytic activity is quite good considering the low palladium concentration being used. Additionally, the microparticles appear extremely stable considering the reaction conditions meant that by the end of the fifth cycle they have been kept at 70 °C, pH 9 in aerobic aqueous conditions for a total of fifteen days and they are still catalytically active.

A high catalytic rate and catalyst recovery are not the only qualities an ideal catalyst requires. For good catalysis the reaction needs to reach completion and the yield of the product needs to be high. These two things would usually go hand in hand, but as previously mentioned in Chapter 4 there is a side reaction to the oxidative homocoupling reaction that creates phenol byproduct **8** which is thought to be due to stoichiometric formation of peroxy-borates during the catalytic cycle (Scheme 6).



Scheme 6 - The suggested mechanism for peroxide formation during the homocoupling reaction that results in conversion of phenylboronic acid into phenol.

Whilst a monoaryl phenol is relatively simple to separate from the biphenyl product, any formation of phenol does reduce the yield of the intended product. To determine the product ratio resulting from the use of the nanocomposites, after catalyst recovery the product ratio in the supernatant was measured by HPLC and in all cases the desired product **7** was found to be formed in greater than a 1:1 ratio relative to the byproduct **8** (Table 1).

Table 1. Product distribution after kinetic experiments of the homocoupling reaction of 6 (150 μM) by catalyst Pd-PPy-PS (1.8 μM) in water with pH 9 borate buffer (10 mM) over the course of 24 hours at 70 $^{\circ}\text{C}$.						
		Reactant	Products			Product ratio
	Cycle	[6] / μM	[7] / μM	[8] / μM	Completion	Biphenyl : Phenol
pH 8 Centrifuged	1	0.00	42.05	4.15	100.00 %	10.1:1
	2	5.28	45.25	8.46	94.93 %	5.3:1
	3	5.94	39.79	7.87	93.64 %	5.1:1
	4	16.84	40.53	10.55	84.47 %	3.8:1
pH 9 Centrifuged	1	0.00	42.37	9.76	100.00%	4.3:1
	2	0.00	50.39	12.69	100.00%	4.0:1
	3	0.00	45.41	12.73	100.00%	3.6:1
	4	4.54	48.94	17.03	96.20%	2.9:1
pH 9 Sedimented	1	0.00	45.05	6.29	100.00%	7.2:1
	2	0.00	52.83	10.45	100.00%	5.1:1
	3	0.00	46.85	10.26	100.00%	4.6:1
	4	4.99	45.85	11.78	95.40%	3.9:1
Product ratios in the supernatant after catalyst recovery at each stage as determined by HPLC. Completion is calculated as the ratio of phenol and twice the biphenyl to remaining borate.						

Table 1 shows that the **7:8** ratio was highest for the first use cycle of the catalyst and decreased in successive runs. The improved product ratio when compared to any of the molecular catalysts (Chapter 4) could either be due to the peroxoborate not being generated in the reaction, or the Pd-PPy nanocomposite decomposes the peroxide before it can react with **6**.

5.2.3 - Effect of added halide on the catalytic activity of Pd-PPy-PS nanocomposites

The pH rate profile for the reaction catalysed by the Pd-PPy-PS nanocomposites did not show a distinct maximum, unlike what was found for the reaction with the molecular catalyst. In Chapter 4 the pH maximum of the reaction was shown to be affected by the concentration of halide in the reaction mixture. The Pd-PPy-PS nanocomposites have no halide present at all, and so the absence of halide ions may mean that the halide-hydroxo exchange equilibrium responsible for the pH maximum is not active under the reaction conditions. Addition of halide to the reaction mixture may introduce an equivalent equilibrium and through that a pH-rate profile displaying a maximum. To test this hypothesis, the homocoupling reaction of **6** was carried out under the same conditions as before, but with the addition of various quantities of NaCl to the reaction mixture (Figure 8).

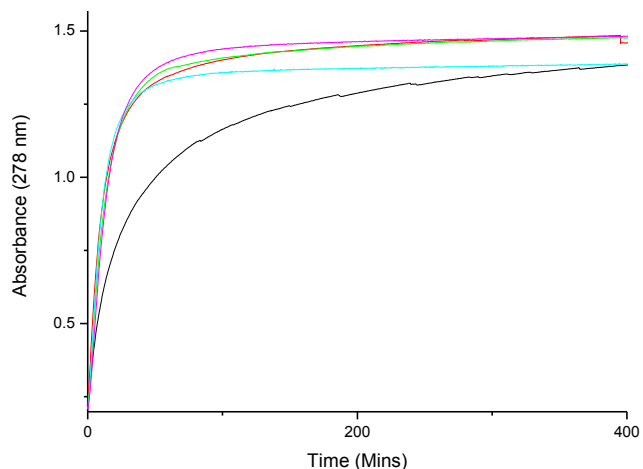


Figure 8. Absorbance at 278 nm recorded during the course of the homocoupling reaction of **6** (150 μM) in water with pH 9 borate buffer (10 mM) and catalyst Pd-PPy-PS (1.8 μM Pd) over the course of 7 hours at 70 $^{\circ}\text{C}$ in the presence of - 0 M, - 0.05 M, - 0.1 M, - 0.5 M and - 1 M of Cl^- .

Remarkably, Figure 8 shows that the addition of halide drastically increases the k_{obs} for the reaction (e.g. at pH 9 and 1 M $[\text{Cl}^-]$ the k_{obs} is 0.051 min^{-1} rather than 0.019 min^{-1} in the absence of halide). In fact, all the reactions are essentially complete within three hours in the presence of Cl^- . Testing under the same conditions with the addition of bromide instead of chloride gives a similar rate acceleration (Figure 9).

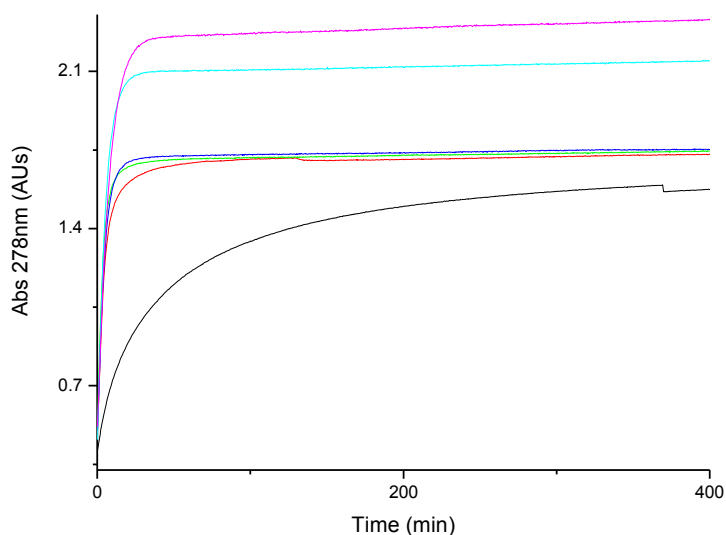


Figure 9. UV spectra recorded during the course of the homocoupling reaction of **6** (150 μM) in water with pH 9 borate buffer (10 mM) and catalyst Pd-PPy-PS (1.8 μM Pd) over the course of 7 hours at 70 $^{\circ}\text{C}$ at $[\text{Br}^-]$ - 0 M, - 0.05 M, - 0.1 M, - 0.25 M, - 0.5 M and - 1 M.

The rate amplification by bromide appears to be even greater than for chloride since all the reactions appear to be over by 90 minutes (at pH 9 and 1 M $[\text{Br}^-]$ the k_{obs} is 0.131 min^{-1} rather than 0.019 min^{-1} in the absence of halide). Plotting k_{obs} as a function of halide concentration illustrates the effect of halide addition on the observed reaction rate constant (Figure 10).

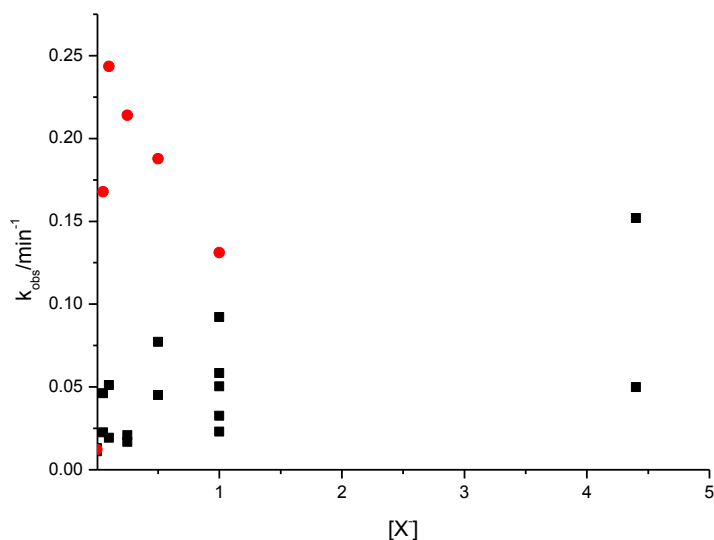


Figure 10 - k_{obs} for the homocoupling reaction of **6** (150 μM) in water with pH 9 borate buffer (10 mM) and catalyst Pd-PPy-PS (1.8 μM Pd) over the course of 7 hours at 70 $^{\circ}\text{C}$ at varying $[\text{Cl}^-]$ (\blacksquare) and $[\text{Br}^-]$ (\bullet).

Figure 10 shows that for the addition of chloride the trend is that k_{obs} increases as $[\text{Cl}^-]$ increases all the way to a concentration of 4.4 M. With bromide there is a turning point at 0.1 M $[\text{Br}^-]$ where the highest k_{obs} is found (0.244 min^{-1}), after which increasing the bromide concentration decreases the rate constant.

The observed increase in rate constants is unexpected since the proposed mechanism for the role of base in the Suzuki-Miyaura and the homocoupling reaction assumes that halide ions

deactivate the palladium and need to be displaced prior to the transmetallation step. One would therefore expect addition of halide to slow down the homocoupling reaction by introducing an equilibrium that inactivates the palladium.

There are two possible explanations for the observed increase in the rate constant for the homocoupling reaction upon the addition of halide ions. First, the halide ions could be helping leach palladium atoms into solution where they are more available to the reaction, and therefore lead to a faster reaction. If this is the case, the deceleration after 0.1 M $[\text{Br}^-]$ could be due to the equilibrium being in favour of the Pd-Br form inactivating the catalyst having a greater effect than the increase in availability of Pd after that bromide concentration. If this is the case, the reaction is not actually occurring on the surface of the nanoparticles, but rather in solution. Alternatively, the halide ions could have an activating effect on the Pd surface which is not observed in the molecular catalysts because of the different electronic properties of Pd atoms and Pd-PPy nanocomposites. Either way, the observed acceleration can be exploited to perform the reaction in a reasonable time of around 5 hours at a lower temperature of 30 °C (Figure 11).

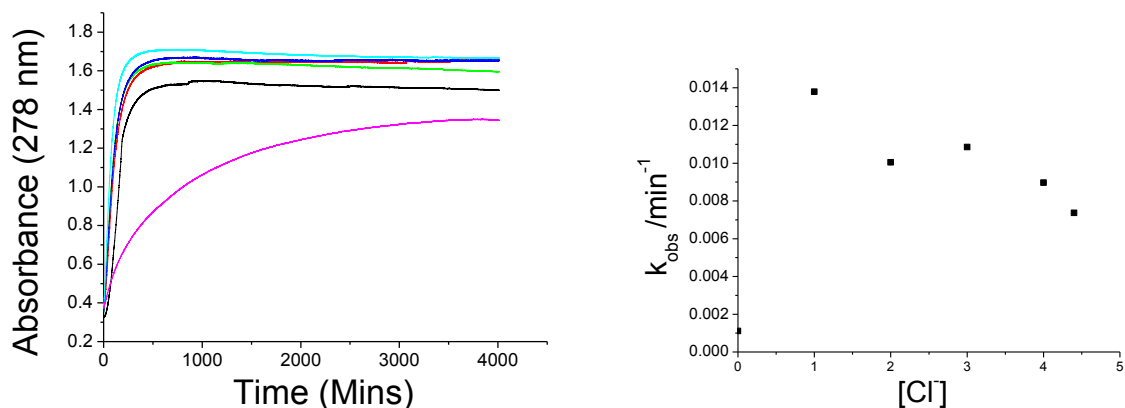


Figure 11. (l) UV spectra recorded during the course of the homocoupling reaction of **6** (150 μM) in water with pH 9 borate buffer (10 mM) and catalyst Pd-PPy-PS (1.8 μM Pd) over the course of 64 hours at 30 $^{\circ}\text{C}$ at $[\text{Cl}^-]$ - 0 M, - 1 M, - 2 M, - 3 M, - 4 M and - 4.4 M. (r) k_{obs} plotted against $[\text{Cl}^-]$ for the same reactions.

The addition of 1M chloride or more allows the reaction to reach completion by 12 hours at 30 $^{\circ}\text{C}$. The k_{obs} at 1 M Cl^- (0.014 min^{-1}) is of approximately the same order as for the reaction in the absence of halide at 70 $^{\circ}\text{C}$ (0.019 min^{-1}). The pH of the reaction mixture was varied at 30 $^{\circ}\text{C}$ in order to determine if the reaction displays a pH maximum (Figure 12).

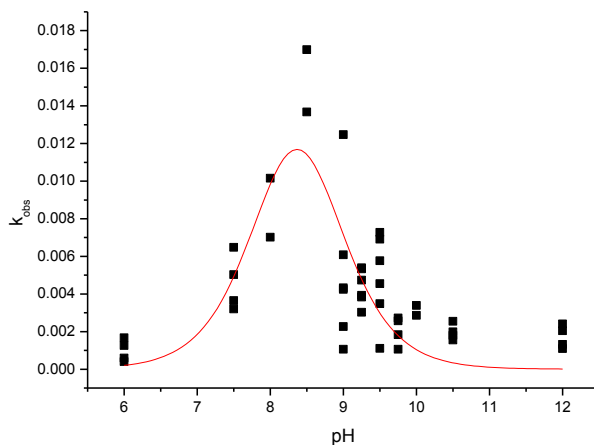


Figure 11. pH rate profile of the homocoupling reaction of **6** (150 μM) in water with borate buffer (10 mM) and catalyst Pd-PPy-PS (1.8 μM Pd) over the course of 64 hours at 30 $^{\circ}\text{C}$ with $[\text{Cl}^-]$ 1 M.

Unlike for the homocoupling reaction in the absence of added halide, in the presence of 1 M chloride there is now a distinct pH maximum at 8.4. This observation suggests that the mechanism of the transmetalation step is the same as for the reaction with the molecular catalysts involving an equilibrium between the Pd-X and Pd-OH forms. This still does not explain why introduction of halide causes an increase in k_{obs} as it is clear from the pH rate profile that displacing the halide with base is accelerating the reaction. If the decrease in rate is due to particles being leached into the solution from the nanoparticle surface, then one would expect to see a much faster loss of activity during catalyst recovery (as any particles in solution will be too small to sediment in a centrifuge). Alternatively, it could be that the nanoparticles are

functioning as a source of palladium atoms that leach off during the reaction, and the rate is limited by the solubility of the palladium atoms. In this case the halide ions could be raising the solubility of the palladium atoms in solution, leading to a higher rate of reaction, which would also mean that halide would deteriorate the particles more between use-cycles. The rate of activity recovery was therefore compared at different concentrations of chloride (Figure 12).

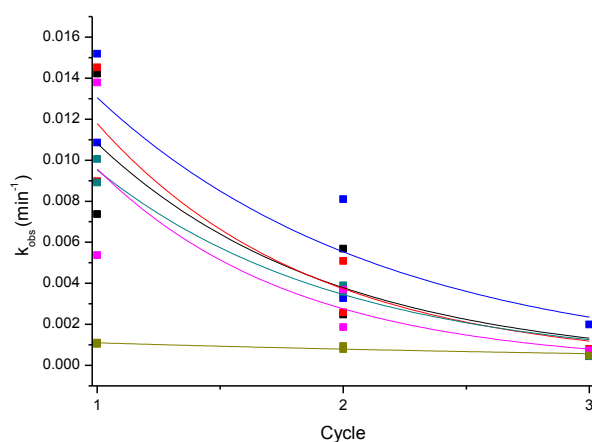


Figure 12. Observed first-order rate constants k_{obs} as a function of use cycle of the catalyst Pd-PPy-PS at catalyst Pd concentrations of $1.8 \mu\text{M}$ for the homocoupling reaction of **6** ($150 \mu\text{M}$) in water with pH 9 borate buffer (10 mM) over the course of 72 hours at $30 \text{ }^\circ\text{C}$ with $[\text{Cl}^-]$ - 4.4 M , - 4 M , - 3 M , - 2 M , - 1 M and - 0 M .

The rate of relative catalyst activity loss is much higher in the presence of halide than it is in the absence of halide, with a loss of just over half the activity per cycle. Unlike what was found for

the reaction in the absence of halide, the reactions in chloride-containing reaction mixtures trend towards 0 rather than to a retained level of activity. This puts a finite limit on the reusability of the catalyst, since after 3 cycles k_{obs} is essentially 0 min^{-1} making the catalyst unusable. This observation agrees with the idea that the halide is activating the catalyst by leaching particles or atoms into solution where they are more available to the reaction. This process is a double edged sword, since the addition of halide to the system has drastically improved the rate constant for the reaction for the first cycle, but by the third cycle the observed rate constant for the reaction was approaching that for the halide-free reaction.

The studies of the retention of catalytic activity by the Pd-PPy-PS particles in the presence of added bromide was carried out at $70 \text{ }^\circ\text{C}$ to see if the activity also decayed to 0 (Figure 13).

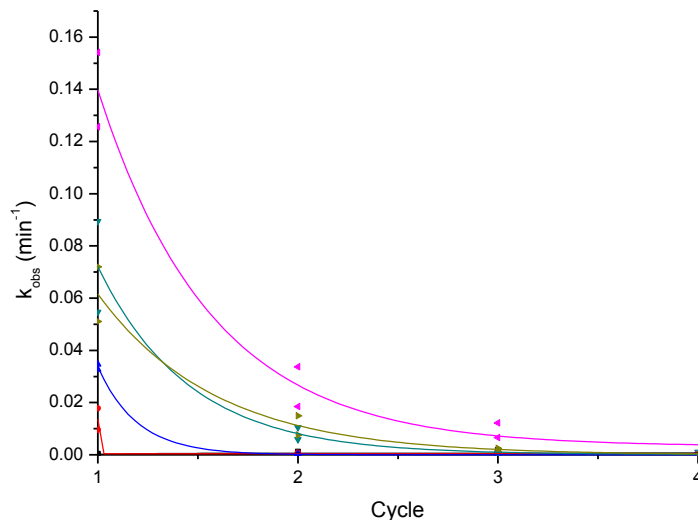


Figure 13. Observed first-order rate constants k_{obs} as a function of use cycle of the catalyst Pd-PPy-PS at catalyst Pd concentrations of $1.8 \mu\text{M}$ for the homocoupling reaction of **6** ($150 \mu\text{M}$) in water with pH 9 borate buffer (10 mM) over the course of 21 hours at 70°C with $[\text{Br}^-]$ - 4.45 M, - 4 M, - 2 M, - 1 M, - 0.5 M and - 0 M.

The highest k_{obs} was recorded at a $[\text{Br}^-]$ of 0.5 M, and the highest k_{obs} were obtained for those conditions for four reaction cycles, with the k_{obs} after four cycles still being high enough for the reaction to complete within 24 hours. Increasing $[\text{Br}^-]$ above 0.5 M seriously decreased k_{obs} at pH 9, with the rate constant at 4 M Br^- being much lower than in the absence of halide, and decaying to 0 after a single reaction cycle.

For both chloride and bromide the retention of activity decreases as halide concentration increases, with the bromide decreasing the retention of activity much more significantly than the chloride does.

The product ratios of the reaction carried out in the presence of chloride were measured using HPLC (Table 2). As one would expect from the greatly diminished rate constants determined from the UV data, the third reaction cycle at 4.4-3.0 mol dm⁻³ [Cl⁻] did not reach completion during the 64 hour reaction time. At chloride concentrations of 1-2 M the reaction did reach completion in all three cycles. The product ratio was typically between 1:1 and 3:1 in favour of **7**, and the excess of **7** over **8** decreased with reaction cycle (except in one result marked with an * where a comparatively low concentration of **8** results in an extremely high ratio). These product ratios in the presence of chloride are not as good as those found for the reaction in the absence of halide performed at 70 ° C at the same pH.

Table 2. Product distribution after kinetic experiments of the homocoupling reaction of **6 (150 μ M) by catalyst Pd-PPy-PS (1.8 μ M) in water with pH 9 borate buffer (10 mM) over the course of 64 hours at 30 $^{\circ}$ C with a range of [Cl].**

[Cl] / M	Cycle	Reactant	Products		Completion	Product ratio
		[6] / μ M	[7] / μ M	[8] / μ M		Biphenyl : Phenol
4.4	1	0.00	82.81	26.48	100%	3.13:1
	2	0.00	76.31	47.11	100%	1.62:1
	3	64.89	73.72	54.10	76%	1.36:1
4	1	0.00	86.17	28.92	100%	2.98:1
	2	0.00	81.55	39.66	100%	2.06:1
	3	62.40	82.01	52.17	78%	1.57:1
3	1	0.00	79.21	43.70	100%	1.81:1
	2	0.00	77.05	2.77	100%	55.63:1*
	3	68.60	69.60	67.18	75%	1.04:1
2	1	0.00	45.07	15.75	100%	2.86:1
	2	0.00	77.40	53.67	100%	1.44:1
	3	0.00	71.36	69.52	100%	1.03:1
1	1	0.00	86.46	0.00	100%	N/A
	2	0.00	79.16	47.31	100%	1.67:1
	3	0.00	74.46	64.59	100%	1.15:1
0	1	77.92	89.09	24.02	72%	3.71:1
	2	83.82	77.46	35.55	69%	2.18:1
	3	97.04	81.65	56.10	69%	1.46:1

Product ratios in the supernatant after catalyst recovery at each stage as determined by HPLC. Completion is calculated as the ratio of **8** and 2 x **7** divided by that + **6**.

The product distribution for the reactions performed in the presence of bromide at 70 °C determined using HPLC are listed in Table 3.

Table 3. Product distribution after kinetic experiments of the homocoupling reaction of 6 (150 μM) by catalyst Pd-PPy-PS (1.8 μM) in water with pH 9 borate buffer (10 mM) over the course of 21 hours at 70 °C with a range of [Br⁻].						
		Reactant	Products			Product ratio
[Br ⁻] M	Cycle	[6] / μM	[7] / μM	[8] / μM	Completion	Biphenyl : Phenol
4.45	1	254.71	13.50	31.79	19%	0.42
	2	283.33	11.07	28.84	15%	0.38
	3	351.12	1.14	18.10	5%	0.06
4	1	0.00	51.13	50.85	100%	1.01
	2	46.81	52.09	71.71	79%	0.73
	3	245.38	25.92	49.80	29%	0.52
2	1	0.00	62.25	62.15	100%	1.00
	2	0.00	30.85	133.10	100%	0.23
	3	167.38	31.62	78.59	46%	0.40
1	1	0.00	62.30	59.73	100%	1.04
	2	0.00	71.10	74.24	100%	0.96
	3	164.44	44.26	56.20	47%	0.79
0.5	1	0.00	77.52	65.70	100%	1.18
	2	0.00	73.76	72.61	100%	1.02
	3	0.00	76.92	81.40	100%	0.95
0	1	0.00	81.57	64.73	100%	1.26
	2	0.00	80.53	81.01	100%	0.99
	3	0.00	70.90	82.97	100%	0.85

Product ratios in the supernatant after catalyst recovery at each stage as determined by HPLC. Completion is calculated as the ratio of 8 and 2 x 7 divided by that + 6.

Table 3 shows, as would be expected from the rate constants shown in Figure 13, that as the concentration of bromide is increased, the percentage completion of the reaction after 21 hours decreases. The product ratio of 7:8 ranges between 0.06 and 1.18 which decreased after each

cycle of the catalyst, and where the lowest ratios were found for the reactions that did not reach completion.

3.3 - Conclusions

The Pd-PPy-PS microparticles have been shown to be remarkably active in catalysing the homocoupling reaction of **6**, with reactions being completed in under 24 hours at 70 °C at a catalyst loading of 1.2 mol-%. The microparticles are also recoverable by centrifugation, although it appears that particle loss is not the only factor affecting the reusability of the catalyst. Other factors affecting the reusability includes the concentration of halide ions. In the presence of chloride ions the particles display a pH rate profile with a maximum. Halide ions also influence the rate of the homocoupling reaction, with the addition of 0.5 M bromide causing a tenfold increase in the observed rate constant. The halide concentration does, however, appear to reduce the recoverability of the catalyst activity indicating that the activity boost may be due to removal of palladium atoms from the nanocomposite to form a homogeneous catalyst in solution.

3.4 - Experimental

3.4.1 - Chemicals

All chemicals were obtained from Sigma-Aldrich and were used as received unless noted. Water was purified using an ELGA option-R 7BP system. Sodium hydroxide and sulphuric acid were

purchased from Fisher. Borate buffers were prepared at a concentration of 0.1 M and adjusted to the appropriate pH using sodium hydroxide and sulphuric acid. 4-carboxyphenylboronic acid was purchased from Acros. The Pd-PPy-PS nanocomposites were transported from Osaka in a sealed aqueous suspension and kept in the dark until use.

3.4.2 - Techniques

UV-visible spectra were recorded using a Jasco V-650 spectrophotometer with a PAC-743R peltier thermostatted 6-cell changer. Quartz cuvettes with a path length of 1 cm were used with a magnetic stirrer bar added to reduce sedimentation. pH of the samples were measured using a Hanna pH211 microprocessor pH meter equipped with a narrow VWR 662-1759 glass electrode. HPLC analysis was carried out using an Agilent1200 instrument with a ZORBAY (Eclipse XDB-C18 4.6x150 mm, 5 μ m) column. Equation 1 was used to analyse the kinetic data to derive the observed pseudo-first-order rate constant. A is the absorbance at the λ_{max} of a given component, typically 253 nm for **7** and 278 nm for **8**.

$$A = A_{\text{final}} - \Delta A e^{-kt} \quad \text{Equation 1}$$

The k_{obs} values from equation 1 were plotted against the pH recorded by pH probe to give the pH rate profile. Equation 2 was fitted to the data, with the pK_a for phenylboronic acid (PHB) fixed to 8.0, in order to determine the pH maximum and the apparent pK_a of the catalyst.

$$k_{\text{obs}} = k_{\text{catPd}} \left(\frac{1}{1 + 10^{(\text{pH} - \text{pK}_a^{\text{PhB}})}} \right) \left(\frac{1}{1 + 10^{(\text{pK}_a^{\text{Pd}} - \text{pH})}} \right) \quad \text{Equation 2}$$

3.4.3 - Kinetic experiments

The homocoupling reactions were performed in 1 cm path length cuvettes filled to a total volume of 2.5 mL (leaving approximately 1 mL head space above the solution). Water was added to the cuvette using a 1-5 mL Gilson pipette (typically 2.2 mL) followed by borate buffer using a 200-1000 μL Eppendorf micropipette (typically 250 μL , resulting in 10 mM) and the UV spectrum was recorded in order to check the base line was suitably level. The stock catalyst suspension was shaken to disperse the nanoparticles and the required amount was then added using a 10-100 μL Eppendorf micropipette (typically 20 μL , resulting in 1.8 μM [Pd]) and a spectrum was recorded again. Finally, the 4-carboxyphenylboronic acid was added using a 10-100 μL Eppendorf micropipette (typically 37.5 μL , resulting in a boronic acid concentration of 150 μM) and the kinetic measurements were started. Either a full spectrum was recorded every five minutes or, when performing simultaneous measurements, the absorbance of each cuvette at 278 ± 2 nm was measured every thirty seconds. Once the reaction reached its end point a full spectrum for each cuvette was recorded.

3.4.4 - HPLC

HPLC analysis was carried out using an Agilent1200 instrument with a ZORBAY (Eclipse XDB-C18 4.6X150 mm, 5 μ m) column which was kept at a constant 40 °C and a DAD. The method used a gradient of three solvents, deionised water, 0.2% trifluoroacetic acid in water and acetonitrile. The gradient started at 65:30:5 and rose to 0:20:80 over the first seven minutes and then held at that level for the remaining three minutes. Concentrations were calibrated using purchased compounds and the retention times of **6**, **7**, and **8** were found to be 4.05, 4.45 and 5.95 minutes respectively. Concentrations were determined as the average of three runs separated by a two minute gap.

3.4.5 - Catalyst Recovery

At the end of the reaction the microcomposite was recovered either by sedimentation or centrifugation. Catalyst recovery by gravity-assisted sedimentation was achieved by allowing the particles to sediment in the cuvette for 1 hour following reaction, after which the supernatant was removed by glass pipette (leaving an amount of the reaction mixture together with the sedimented particles corresponding to a liquid column in the cuvette of approximately 4 mm, corresponding to approximately 0.3 mL). Catalyst recovery by centrifugation was achieved by transferring two aliquots of 1100 microlitres each into two eppendorf containers for each cuvette (i.e. 2200 microlitres for every cuvette). The solutions in the eppendorf containers were centrifuged at 13.3k rotations per minute for 10 minutes at 20 °C. A total of 1000 μ L of supernatant from each eppendorf container was combined to yield 2000 μ L of combined

supernatant. The sedimented particles were resuspended in $2 \times 850 \mu\text{L}$ of water, combined with the 0.3 mL remaining in the cuvette, and 250 μL of buffer stock solution was added. The recovered particles were then re-used in a homocoupling reaction under otherwise identical conditions as the first experiment.

3.5 - Bibliography

1. Constable, D. J. C.; Dunn, P. J.; Hayler, J. D.; Humphrey, G. R.; Leazer, J. J. L.; Linderman, R. J.; Lorenz, K.; Manley, J.; Pearlman, B. A.; Wells, A.; Zaks, A.; Zhang, T. Y., Key green chemistry research areas-a perspective from pharmaceutical manufacturers. *Green Chemistry* **2007**, *9* (5), 411-420.
2. Jaramillo, T. F.; Baeck, S.-H.; Cuenya, B. R.; McFarland, E. W., Catalytic Activity of Supported Au Nanoparticles Deposited from Block Copolymer Micelles. *Journal of the American Chemical Society* **2003**, *125* (24), 7148-7149.
3. Schadler, L. S., Polymer-Based and Polymer-Filled Nanocomposites. In *Nanocomposite Science and Technology*, Wiley-VCH Verlag GmbH & Co. KGaA: 2004; pp 77-153.
4. Selvan, T.; Spatz, J. P.; Klok, H.-A.; Möller, M., Gold-Polypyrrole Core-Shell Particles in Diblock Copolymer Micelles. *Advanced Materials* **1998**, *10* (2), 132-134.
5. Khan, M. A.; Perruchot, C.; Armes, S. P.; Randall, D. P., Synthesis of gold-decorated latexes conducting polymer redox templates. *Journal of Materials Chemistry* **2001**, *11* (9), 2363-2372.
6. Selvan, S. T.; Hayakawa, T.; Nogami, M.; Möller, M., Block Copolymer Mediated Synthesis of Gold Quantum Dots and Novel Gold-Polypyrrole Nanocomposites. *The Journal of Physical Chemistry B* **1999**, *103* (35), 7441-7448.
7. Fujii, S.; Matsuzawa, S.; Hamasaki, H.; Nakamura, Y.; Bouleghimat, A.; Buurma, N. J., Polypyrrole-Palladium Nanocomposite Coating of Micrometer-Sized Polymer Particles Toward a Recyclable Catalyst. *Langmuir* **2011**, *28* (5), 2436-2447.
8. Fujii, S.; Matsuzawa, S.; Nakamura, Y.; Ohtaka, A.; Teratani, T.; Akamatsu, K.; Tsuruoka, T.; Nawafune, H., Synthesis and Characterization of Polypyrrole-Palladium Nanocomposite-Coated Latex Particles and Their Use as a Catalyst for Suzuki Coupling Reaction in Aqueous Media. *Langmuir* **2010**, *26* (9), 6230-6239.

Chapter 4

Kinetic Studies of the Homocoupling and Cross Coupling Reactions of Arylboronic acids Catalysed by Paper-Immobilised Pd Nanoparticles

Abstract: Oleylamine-capped palladium nanoparticles with a diameter of 3.0 ± 1.0 nm immobilised in a filter paper support were investigated for their efficiency in the oxidative homocoupling reaction of 4-carboxyphenylboronic acid and in the Suzuki-Miyaura cross-coupling reaction of 4-carboxyphenylboronic acid and 4-iodoanisole, both in aqueous and ethanolic aqueous conditions. One of the paper strips appeared to have been affected by a currently unknown process and caused nearly total decomposition of 4-carboxyphenylboronic acid to 4-carboxyphenol. All other paper strips adequately catalysed the homocoupling reaction at pH 8.75 and 70 °C. Under all tested conditions the homocoupling reaction using the paper strips produced a stoichiometric or nearly-stoichiometric concentration of 4-carboxyphenol alongside the homocoupling product 4,4'-dicarboxybiphenyl. The rate constant for the homocoupling reaction of 4-carboxyphenylboronic acid (444 μM) (measured by HPLC) was not greatly altered by catalyst use cycle or the addition of ethanol, staying in the region of $(1.72 \pm 0.17) \times 10^{-3} \text{ min}^{-1}$. Changing the pH from 8.75 to 10 or 7 with 4-carboxyphenylboronic acid (444 μM), did not appear to significantly affect the rate constant measured by HPLC. The Suzuki-Miyaura cross-coupling reaction performed at pH 8.75 in mixtures of ethanol and water, and under atmospheric conditions, gave a mixture of cross-coupled and homocoupled product in a ratio of 2.74-5.24:1. The highest ratio of cross-coupled to homocoupled product was found at low ethanol concentration. The rate constant for the cross-coupling reaction increased linearly with ethanol concentration from $1.55 \times 10^{-3} \text{ min}^{-1}$ at 2.25% ethanol to $3.0 \times 10^{-3} \text{ min}^{-1}$ at 25% ethanol. Increasing the pH to 10.01 also increased the rate of the cross-coupling reaction to $3.4 \times 10^{-3} \text{ min}^{-1}$ whilst maintaining a product ratio of 5.12:1. With a tenfold excess of the iodoanisole the rate of the cross coupling increased to $9.44 \times 10^{-3} \text{ min}^{-1}$ and the product ratio increased to 21.8:1, showing that the initial oxidative addition is the rate-determining step.

4.1 - Introduction

4.1.1 - Nanoparticle Catalysts

Pd-polypyrrole nanocomposites immobilised on polystyrene microbeads have already shown promise as catalysts for the homocoupling reaction in aqueous media, and these nanocomposites enabled catalyst recovery by sedimentation and centrifugation (Chapter 5). However these microbeads are still not the easiest particles to handle and the catalytic activity was never fully recovered between reactions, indicating that some palladium was either lost from the microparticles or deactivated in the process. Immobilising palladium nanoparticles on a larger support, rather than on microscopic particles, would be synthetically useful as macroscopic supports can easily be manipulated by filtration or, if large enough, with tweezers. There are many other supports that can be used, such as microscopic bacterially-derived cellulose fibres supporting palladium nanoparticles roughly 40 nm in diameter, shown recently by Tang *et al.*¹ These microfibre-immobilised catalysts were found to be active in the Heck reaction and 90% of their activity was retained after four recovery cycles by filtration.

Alternatively, immobilised nanoparticles can be used in a flow catalytic system. Recently, Whitesides *et al.* described a method where a combination of layers of paper that had been laser-patterned with a hydrophobic polymer and layers of double-sided tape had been used to construct a three-dimensional microfluidics device.² The channels in the paper and the holes in the tape (which were filled in with powdered cellulose) created the route which allowed liquids to flow through capillary wicking and mix and react in a cheap and reliable microfluidic system.

Binding catalysts either to the paper before patterning or the cellulose powder filling the air gaps in the tape layers would allow for relatively simple design of a flow catalytic system. The concerns for such a system would be the same as for the polystyrene particles discussed in Chapter 5 - how active are the particles when bound to a support and how much (if any) palladium is leached into solution during the reaction.

4.1.2 - The Suzuki-Miyaura cross-coupling reaction

Which of these steps in the Suzuki reaction is the rate limiting one varies depending on the reaction conditions and the substrates involved.³ Since the homocoupling reaction of the arylboronic acids results in impurities in the cross-coupling reaction, there is much interest in mitigating this side-reaction. Whilst removing oxygen from the reaction is an obvious way to do this, it is not always possible to achieve this at an acceptable level to prevent the homocoupling reaction. If the oxidative addition step is the rate-limiting step then the yield can be improved by using an alternative borate source, such as a trifluoroborate⁴ that must first hydrolyse before reacting. This way, the concentration of the boronic acid at any point will be kept quite low as it will react as it is formed, reducing the likelihood of the boronic acids coming together and homocoupling. Also, by slowly-releasing the boronic acid then the rate acceleration of a higher halide concentration can be achieved, whilst having a stoichiometric quantity of each reactant, therefore meaning that less reactant is wasted. If however the rate limiting step is the transmetallation, then this step cannot be accelerated cleanly as increasing the concentration of the boronate would also accelerate the homocoupling reaction as well as the cross-coupling reaction.

4.1.3 - Previous Work

Our collaborators in the Colloid Chemistry Group at the Universidad de Vigo have been synthesising and studying nanoparticle systems for various purposes for many years, and recently have turned their attention towards catalysis by palladium nanoparticles.

Palladium nanoparticles with a diameter of 3.0 ± 1.0 nm were synthesised with oleylamine (Figure 1) as a capping agent to stabilise the nanoparticle according to the method reported by Sato *et al.*⁵

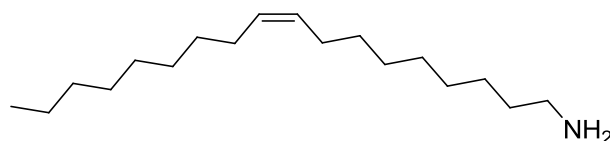


Figure 1 - The oleylamine capping agent.

Oleylamine was selected as a capping agent because the long hydrophobic chains will form very strong Van der Waals interactions with hydrophobic supports and between the capped particles themselves and so should help keep the nanoparticles tightly bound to the support. Standard laboratory filter paper was chosen as the support for a variety of reasons. Firstly, it is cheap, renewable and relatively inert. In addition filter paper is composed of strands of microfibrils that give it a very high surface area. Filter paper is further very porous allowing it to absorb fluids via capillary action, which is also of interest for application in paper-based microfluidics. Since the microfibrils are composed of cellulose, they also have a very high surface area for Van der Waals

interactions and so should be able to form persistent structures with the nanoparticles. Finally, once the catalyst is no longer useful, either due to poisoning of the metal or the degradation of the support the precious metal can be easily recovered by burning the support.

Oleylamine-stabilized palladium nanoparticles with an average diameter of 3.0 ± 0.4 nm were prepared and washed by precipitation with methanol to ensure elimination of excess oleylamine. The nanoparticle precipitate was redispersed in chloroform and the filter paper was loaded with nanoparticles by simply dipping the strips into the Pd nanoparticle dispersion for 2-3 seconds. The solvent was evaporated and the dipping was repeated up to four more times to maximise the nanoparticle loading. The loaded strips were then dried in a 70 °C oven, then washed in pH 8.6 aqueous borate buffer solution, then ethanol and then chloroform to remove any weakly bound nanoparticles or impurities (such as oleylamine or oleic acid), although no palladium was observed desorbing even in hexane or chloroform.⁶

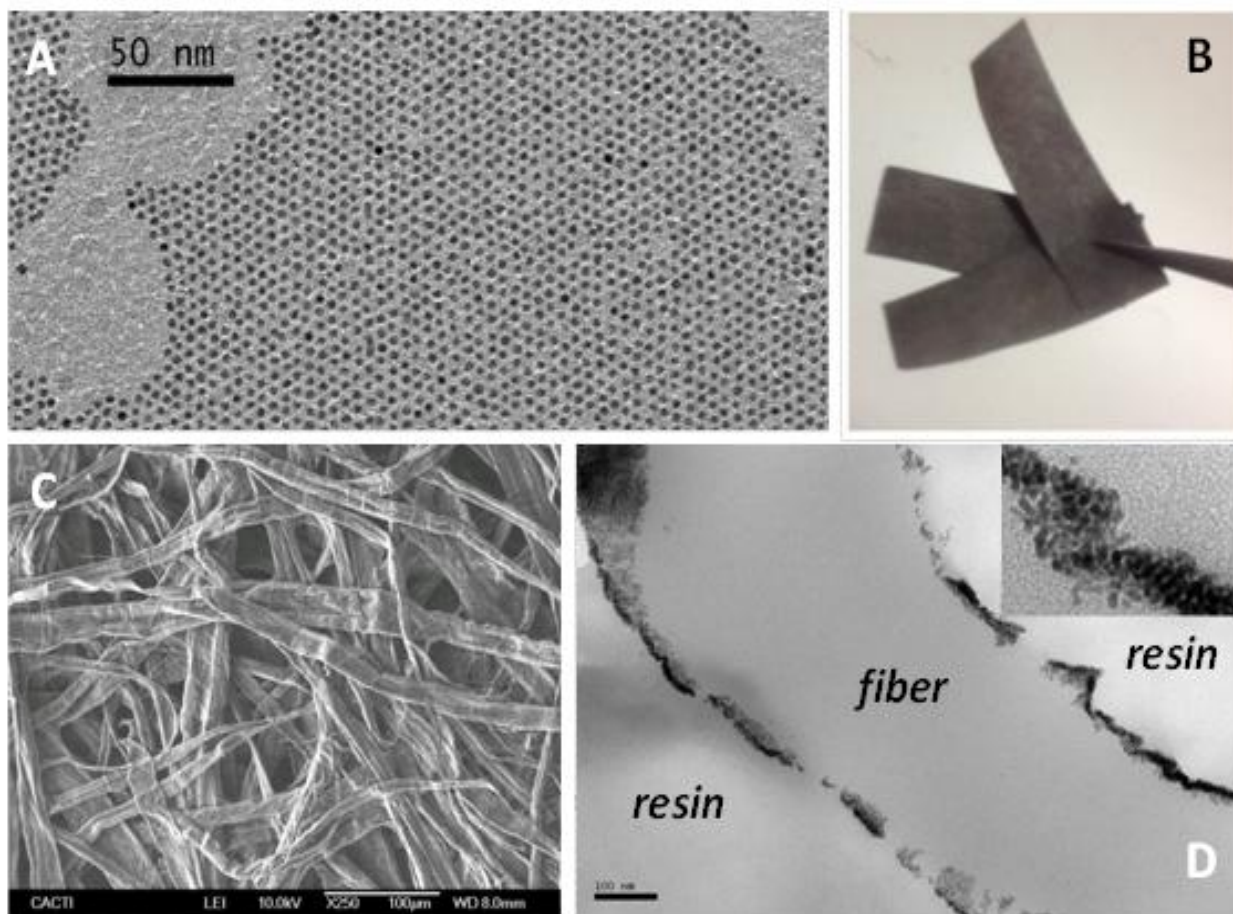
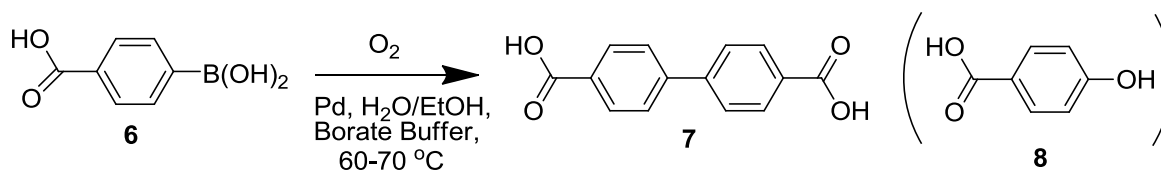


Figure 2 - A. TEM images of the 3.0 ± 1.0 nm palladium nanoparticles. B. Palladium doped filter papers cut to 4.0×1.3 cm strips. C. SEM image of the palladium doped filter papers. D. TEM image of a single cellulose fibre in the palladium doped filter paper embedded in an epoxy resin in order to visualise it, with inset showing a higher magnification of the palladium nanoparticles on the surface of the cellulose fibre.

The palladium-nanoparticle-doped filter paper was characterised by TEM and SEM to observe the palladium clusters in the cellulose matrix (Figure 2) and ICP-OES to determine the palladium loading as 0.167 ± 0.016 mg cm⁻² (or 1.57 ± 0.15 nm cm⁻²).

The palladium-doped paper was tested for activity and reusability in the oxidative homocoupling reaction of 4-carboxyphenylboronic acid **6** (Scheme 4) under the same conditions that were used for the polystyrene-immobilised nanoparticles (Chapter 5), i.e. with 10 mM borate buffer in aqueous conditions at 70 °C.



Scheme 4 - The palladium catalysed oxidative homocoupling reaction of 4-carboxyphenylboronic acid **6** to form 4,4'-dicarboxybiphenyl **7** and 4-hydroxybenzoic acid **8**.

The reaction was followed through the UV absorbance at 278 nm which was measured over time. Catalyst recovery was a simple matter of removing the palladium-doped paper from the reaction mixture and washing it in milli-Q water and then drying the strip. Not only were the palladium doped strips catalytically active, they were remarkably reusable (Figure 3).

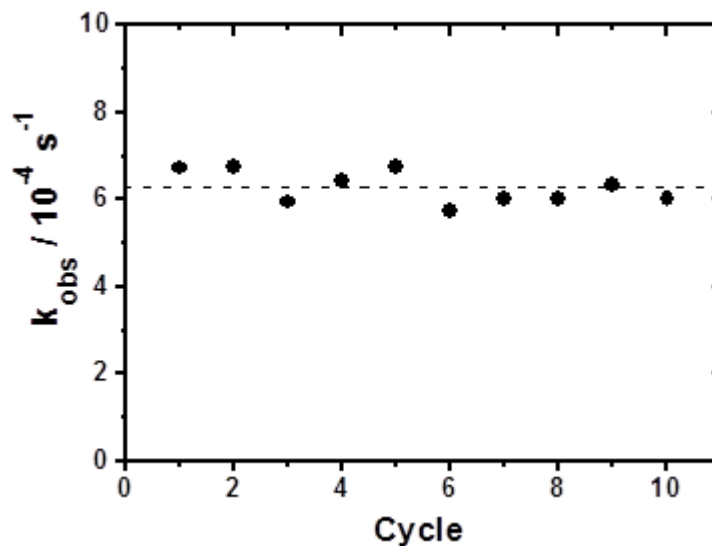


Figure 3 - Observed rate constants for the homocoupling reaction of **6** (150 μM) at pH 8 with three strips of paper-supported catalyst in 30 mL at 70 $^{\circ}\text{C}$ for multiple reuse cycles of the catalyst determined from UV absorbance at 278 nm as a function of time.

The rate constant for the homocoupling reaction was conserved for ten consecutive reaction cycles, each time with the reaction proceeding to completion within four hours. The retention of the reaction rate constant indicates that the particles are indeed well bound to the paper support, and the palladium is still catalytically active despite being buried in the paper's structure. Also, the product ratio of **7:8** (biphenyl:phenol) for the reaction, as determined using HPLC, was between 1-2:1.

4.1.4 - Objectives

Our goals were to reproduce the data using alternative conditions and analytical methods (due to equipment availability), so that any results found can be compared to those results found in Vigo. Once the results can be verified then the catalyst will be tested in new conditions, specifically in the presence of co-solvents and in the Suzuki-Miyaura cross-coupling reaction.

4.2 - Results and Discussion

4.2.1 - Reproducing Homocoupling data "shaken, not stirred"

The palladium-doped nanoparticle paper strips were received in a sealed container via mail from Spain. The first thing to be ascertained was that the results found by the group in Vigo could be reproduced. The reaction of **6** to form **7** (Scheme 3) using a single strip of catalyst was followed by UV-visible spectroscopy (Figure 4). Since the paper strips were unsuitable to be used in a cuvette, the reaction was carried out in a screw-top flask and samples were analysed by removing aliquots for analysis and then replacing these aliquots. In place of magnetic stirring (as used in Vigo) the reaction was homogenised using a lab shaker operating at 160 rpm, while the temperature was kept at 70 °C in line with the experiments carried out in Vigo.

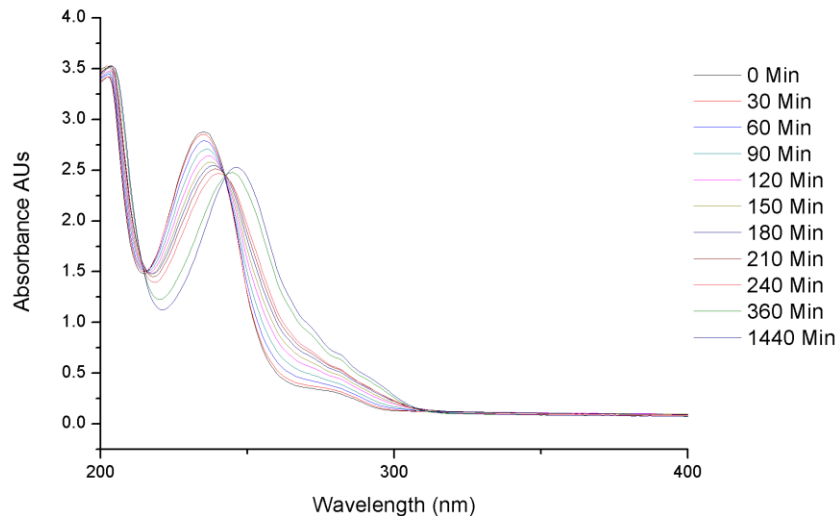


Figure 4 - UV spectra recorded in a 0.5 mL path length cuvette during the homocoupling reaction of **6** (444 μM) at 70 $^{\circ}\text{C}$ with one strip of palladium doped paper as a catalyst in water with pH 8.75 borate buffer (10 mM).

The initial results certainly did not replicate the results of the Vigo group (Figure 4). The reaction showed a significant increase in absorbance at 253 nm, and almost no change at 278 nm, indicating mainly conversion of **6** to phenol **8**, with very little homocoupling to form biphenyl **7**. The final product ratio determined using HPLC also reflects the predominant formation of phenol **8**; the reaction has proceeded to completion with respect to starting material **6**, but only 1% of the product was **7** (2.7 μM) and the remainder was **8** (411 μM).

The reaction was repeated using the same paper strip with immobilised catalyst, and this time the reaction was followed using both UV-visible spectroscopy (Figure 5) and HPLC (Figure 6).

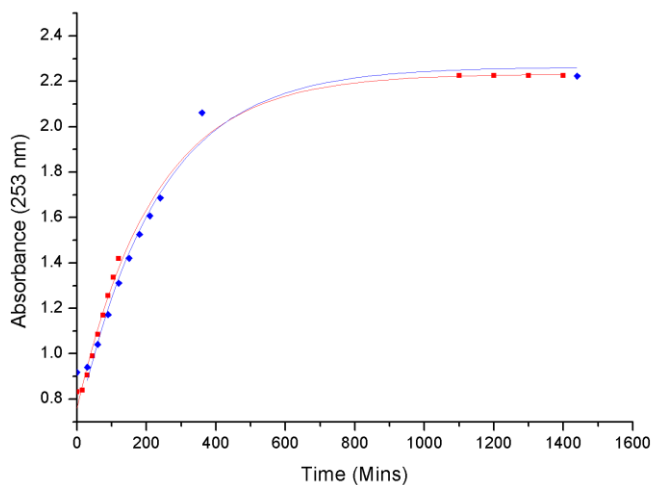


Figure 5 - Change in absorbance at 253 nm of 200 μL samples taken during the homocoupling reaction of 6 (444 μM) at 70 $^{\circ}\text{C}$ with the same strip of palladium-doped paper as a catalyst in water with pH 8.75 borate buffer (10 mM) for the first (◆) and second (■) use.

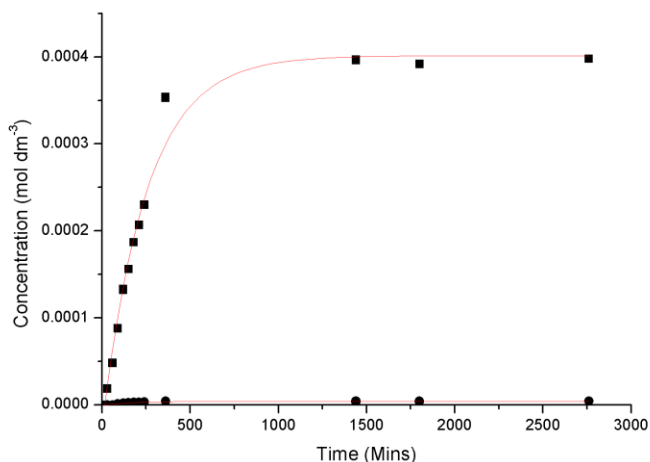


Figure 6 - Change in concentration of **7** (●) and **8** (■) recorded by HPLC of 200 μL samples taken during the homocoupling reaction of **6** (444 μM) at 70 $^{\circ}\text{C}$ with one strip of palladium-nanoparticle-doped paper as a catalyst in water with pH 8.75 borate buffer (10 mM).

To determine the rate constant for the reaction, a first-order rate law (equation 1 - *vide infra*) was fitted to the experimental results. Where the data did not match first-order kinetics at the start of the reaction, data points were disregarded until a good fit to the remaining data points was obtained. This treatment of the data essentially assumes that the catalytic reaction is subject to an induction period which is not reproduced by the first-order rate equation.

Analysis in terms of a first-order rate law of the UV-visible absorbance at 253 nm for both experiments gave very similar rate constants (0.00451 min^{-1} for the first, compared to 0.00517 min^{-1} for the first cycle), indicating that the corresponding reaction and the reaction kinetics were indeed reproducible. The rate constant was also determined from the HPLC trace of **8** as a

function of reaction time and was found to be 0.0039 min^{-1} ; the change in absorbance at 253 nm is a good way to determine the rate constant for this process (Figure 6).

To investigate the source of the unexpected reactivity, a control reaction where the reaction conditions were replicated, but without addition of the catalyst, was carried out simultaneously to see if **6** was stable under the reaction conditions. The control reaction was monitored using HPLC (Figure 7).

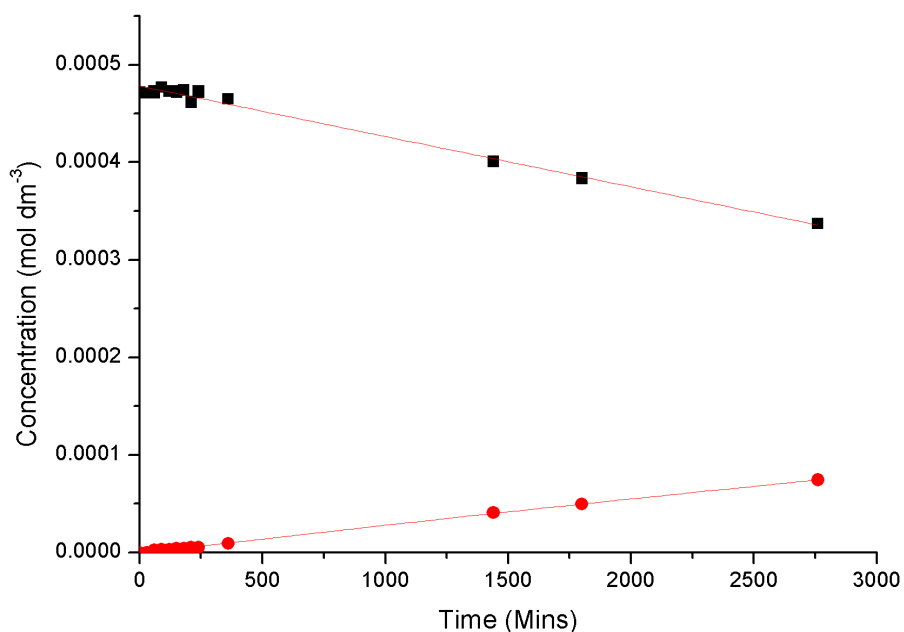


Figure 7 - Change in concentration of **6** (■) and **8** (●) recorded by HPLC of 200 μL samples taken during a control sample of **6** ($444 \mu\text{M}$) at $70 \text{ }^\circ\text{C}$ with no catalyst, in water with pH 8.75 borate buffer (10 mM).

Figure 7 shows that over the course of 45 hours approximately 1/6th of the present **6** decomposes to give **8**, and the rate at which it does so seems to be constant throughout the reaction at $5.16 \times 10^{-8} \text{ mol min}^{-1}$.⁷ Whilst the two rate constants are not directly comparable, the initial rates will be. The initial rate of **8** formation in the absence of catalyst is $5.16 \times 10^{-8} \text{ mol min}^{-1}$, and for the reaction in the presence of catalyst the initial rate is nearly two orders of magnitude higher ($1.622 \times 10^{-6} \text{ mol min}^{-1}$). The fact that the reaction in the absence of the catalyst is much slower means it cannot be solely responsible for the production of **8** in Figures 4-6. Why the hydrolysis of **6** to form **8** should be so pronounced in the presence of the paper-immobilised palladium catalyst was not certain, in particular because this behaviour had not been observed by our collaborators in Vigo. We therefore repeated the process with a different paper strip.

The repeat experiment with a different paper strip does not reproduce the behaviour observed for the first strip (*vide infra*). Nevertheless, the behaviour is reproduced by the same paper strip multiple times. The cause of this additional hydrolysis could be oxidation of the cellulose in the paper to form carbonyl compounds⁸ although whether carbonylated cellulose would react to hydrolyse phenylboronic acids is not certain. Also, given the basic nature of the reaction medium, one would expect that the paper would degrade over time if the cellulose was oxidised, and degradation of the paper was not observed despite storage of the strip in borate buffer at pH 8.75 for several weeks.

Since the unexpected results were not reproducible for other papers strips doped with catalyst, experiments were conducted to reproduce the results found by the group in Vigo using a second paper strip (Figure 8).

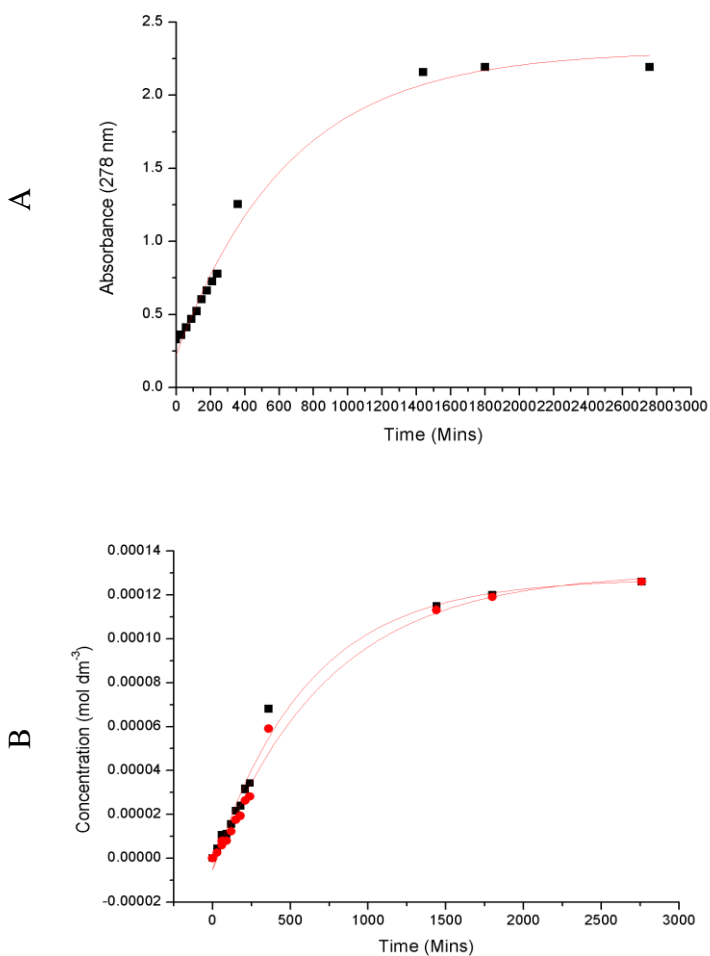


Figure 8 - Change in (A) absorbance at 278 nm and (B) concentration of **7** (●) and **8** (■) determined by HPLC analysis of 200 μL samples collected during the homocoupling reaction of 444 μM **6** at 70 $^{\circ}\text{C}$ with one strip of palladium-doped paper as a catalyst in 10 mM borate buffer, pH 8.75.

Figure 8 shows that following the experiment using UV-vis absorption at 278 nm and using HPLC give similar reaction profiles. These reaction profiles are more typical than those observed for the reaction catalysed by the first strip for the homocoupling reaction, as shown in Chapters 4 and 5 and the results from Vigo. The rate constant for formation of **7** determined using HPLC is much slower than the rate constant found using UV-visible spectroscopy in Vigo ($1.66 \times 10^{-3} \text{ min}^{-1}$ as opposed to $4 \times 10^{-2} \text{ min}^{-1}$). Analysis of the UV-visible data in terms of equation 1 does not reproduce the data perfectly but does give a similar rate constant ($1.53 \times 10^{-3} \text{ min}^{-1}$) to the HPLC data. The decreased rate constant compared to the data from Vigo could be due to the higher pH used (8.75 as opposed to the 8.00 used in Vigo) or due to the efficiency of stirring used previously compared to the shaking used in these experiments. The final product ratio **7:8** is exactly 1:1, indicating that the reaction likely follows the same mechanism as found for the molecular catalyst. This behaviour is different from the Pd-PPy nanocomposite that achieved very low phenol production. Also, the reaction using the paper-immobilised palladium catalyst is considerably slower than with the Pd-PPy nanoparticles, although this could be attributed to the lower concentration of palladium used. A single strip of palladium doped paper in an 18 mL reaction gives a palladium loading of $0.154 \mu\text{M}$, less than a tenth of the $1.8 \mu\text{M}$ typically used with the Pd-PPy-PS particles in Chapter 5. The same paper strip was used a second time under the same conditions to ascertain if the observed rate constant was conserved for a second cycle (Figure 9).

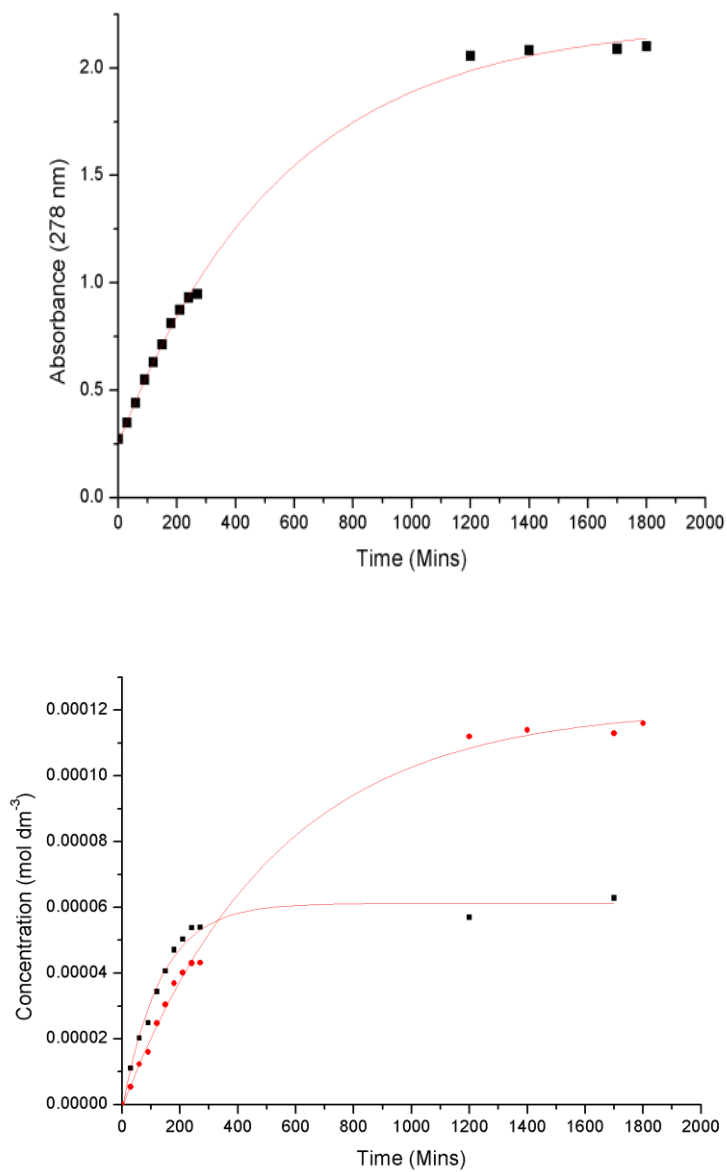


Figure 9 - Change in (A) absorbance at 278 nm and (B) concentration of 7 (●) and 8 (■) recorded by HPLC of 200 μL samples taken during the homocoupling reaction of 6 (444 μM) at 70 $^{\circ}\text{C}$ reusing one strip of palladium doped paper as a catalyst in water with pH 8.75 borate buffer (10 mM).

Repeating the homocoupling reaction under the same conditions with the same catalyst sheet yielded a similar reaction profile both in HPLC and UV. According to the analysis of the UV data, the rate constant was slightly higher for the reused strip ($1.79 \times 10^{-3} \text{ min}^{-1}$) and by HPLC the rate constant for the formation of **7** was also slightly higher ($1.90 \times 10^{-3} \text{ min}^{-1}$ compared to $1.66 \times 10^{-3} \text{ min}^{-1}$ for the unused strip). The biggest change, however, appears to be in the side reaction forming phenol **8**. Initially the rate of the side reaction appears faster than the reaction generating **7** but the side reaction reaction appears to stop at a lower endpoint leading to a final **7:8** ratio of 1.85:1, which is higher than for the first reaction. An observed rate constant of $7.60 \times 10^{-3} \text{ min}^{-1}$, which is 3x that of the previous reaction, is found but the side reaction also terminates much sooner than the homocoupling reaction, resulting in a much lower final concentration of **8** when compared to **7**. Unlike the previous reaction, the mass balance is noticeably low (final phenyl group concentration is $305 \mu\text{M}$, a third of the $444 \mu\text{M}$ starting concentration). If the missing mass is due to phenol evaporating out of the reaction overnight, it may be that the ratio was closer to 1:1, or even higher (up to a maximum **7:8** ratio of 0.54:1 if all of the missing mass is assumed to be **8**).

Using the same conditions a third paper strip was tested to see if the results were reproducible between separate paper strips with the first and second reaction cycles followed by HPLC (Figure 10).

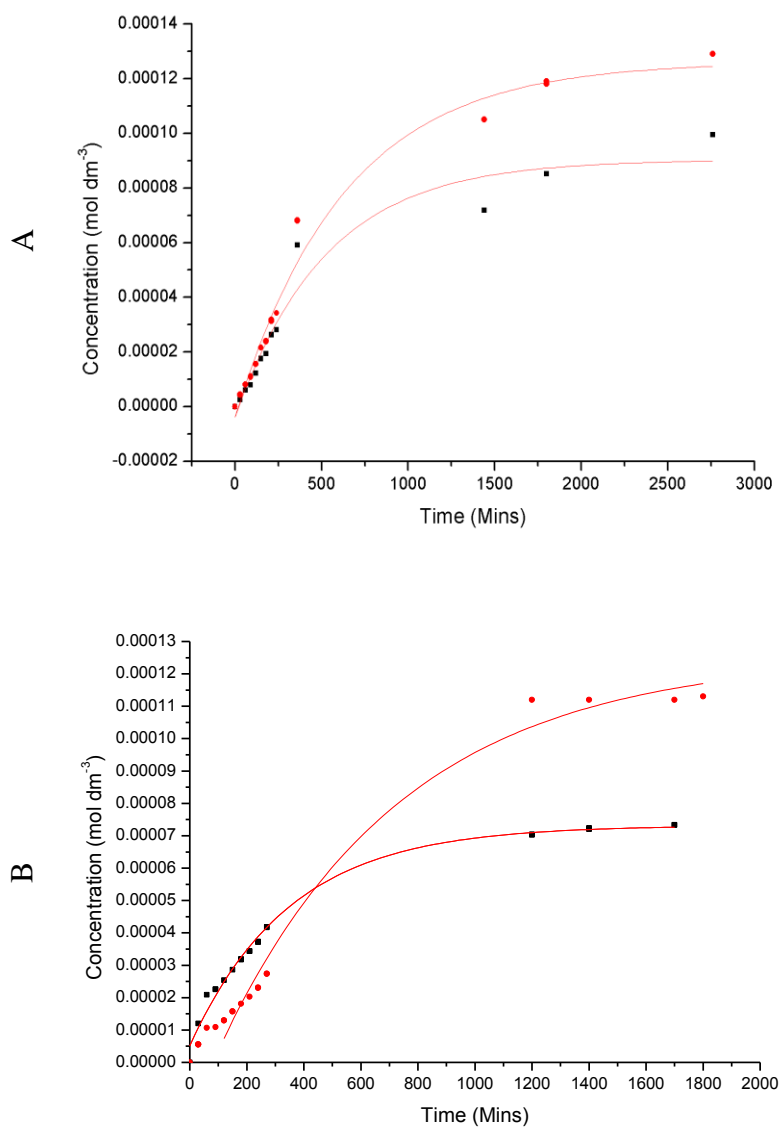


Figure 10 - Change in concentration of **7** (●) and **8** (■) recorded by HPLC of 200 μ L samples taken during the homocoupling reaction of **6** (444 μ M) at 70 $^{\circ}$ C using one strip of palladium doped paper as a catalyst for (A) the first and (B) the second time in water with pH 8.75 borate buffer (10 mM).

Repeating the reaction under the same conditions did not produce significantly different results by HPLC to those found for the second strip. The first use of the catalyst yielded a slightly higher concentration of **8** (**7:8** - 0.77:1) which indicates that the generation of phenol may not have been stoichiometric, but the rate constant of $1.90 \times 10^{-3} \text{ min}^{-1}$ for the formation of **7** was higher than the $1.66 \times 10^{-3} \text{ min}^{-1}$ that was previously found. The second use of the strip looks visually very similar as before, with a higher initial rate of **8** formation that caps out at a lower final value than for **7**, although the rate constants for both reactions are lower than before ($1.56 \times 10^{-3} \text{ min}^{-1}$ and $2.86 \times 10^{-3} \text{ min}^{-1}$ for **7** and **8**, respectively). Again the mass balance of the reaction is lower than expected, though the biphenyl always reaches the same end point, indicating that more phenol may have been generated than was detected at the end of the reaction. Collecting the data from UV-visible spectroscopy and HPLC analysis forming the formation of **7** gives a k_{obs} of $(1.72 \pm 0.17) \times 10^{-3} \text{ min}^{-1}$, which is approximately a 10% error margin.

4.2.2 - pH dependence of the homocoupling reaction

There is no halide present in the catalyst. The Pd-Py-PPS nanocomposite used in Chapter 5 also had no halide present and did not exhibit a clear pH maximum until halide was introduced. In order to test if pH has an effect on the rate of the homocoupling reaction using the paper-immobilised paper catalyst the reaction was followed at neutral pH (7.0) and more basic pH (10.0) (Figure 11).

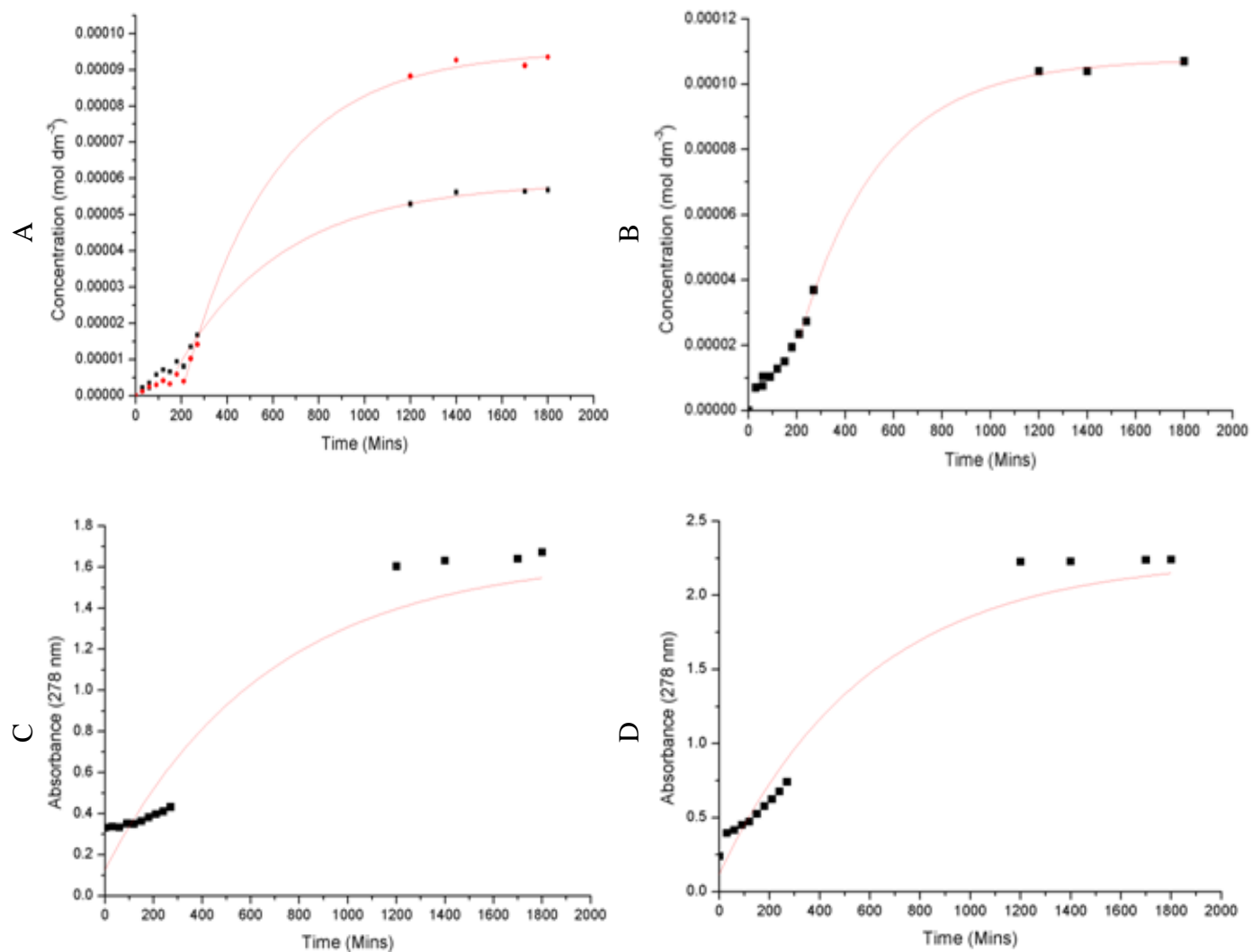


Figure 11 - Change in concentration of **7** (●) and **8** (■) recorded by HPLC of 200 μ L samples taken during the homocoupling reaction of **6** (444 μ M) at 70 °C using one strip of palladium doped paper as a catalyst for the first time in water with (A) pH 7.0 and (B) pH 10 borate buffer (10 mM) and change in absorbance at 278 nm recorded by UV-visible spectroscopy for the same reactions at (C) pH 7.0 and (D) pH 10.

Changing the pH of the reaction medium does not appear to appreciably affect the rate constant of the homocoupling reaction. Both at pH 7 and at pH 10 there appears to be a slow initial rate, but after this initially slow period the rate of generation of **7** is higher at both pHs than in the equivalent reaction at pH 8.75 ($2.53 \times 10^{-3} \text{ min}^{-1}$ and $2.95 \times 10^{-3} \text{ min}^{-1}$, respectively). The concentration of **7** reaches more-or-less the same endpoint as found at pH 8.75 of $1 \times 10^{-4} \text{ mol dm}^{-3}$ at both pH 10 and 7. At pH 10, phenol **8** was not visible at all in the early samples, but appeared in the final few samples taken the following morning, allowing a final concentration to be calculated, but not the rate constant. In the UV data the induction period is even more pronounced than in the HPLC data and the rate constant at pH 7 could not be calculated as the initial rate appeared flat due to the induction period. At pH 10 the rate calculated appears to be effectively unchanged, but is still dominated by the induction period, from the rate constant at pH 8.75 ($1.68 \times 10^{-3} \text{ min}^{-1}$, respectively, compared to $1.53 \times 10^{-3} \text{ min}^{-1}$ at pH 8.75). The ratio of product:byproduct is very favourable at pH 7 (1.65:1), but it also has the lowest mass-balance (which may be due to carboxyphenol **8** being more protonated and hence more volatile at low pHs). Since there is no halide present in the reaction at all, it is possible that the pH has no appreciable effect on the rate of the homocoupling reaction.

4.2.3 - Effect of ethanol addition on the homocoupling reaction

In order to study the kinetics of Suzuki-Miyaura cross-coupling reaction catalysed by the paper-immobilised paper catalyst, the solvent system has to be changed as most aryl halides are insoluble in water. Ethanol was chosen as the co-solvent to dissolve the aryl halide (*vide infra*), but before the SM reaction was attempted the homocoupling was tested in the presence of ethanol to see if and how it affects the catalysis or the catalyst (Figure 12). Addition of ethanol to the reaction medium of the homocoupling reaction does not appear to affect the reaction significantly. Following the reaction by HPLC produced a rate constant of the same magnitude when a quarter of the water was replaced with ethanol ($1.77 \times 10^{-3} \text{ min}^{-1}$). Unfortunately, the rate constant for formation of **8** could not be determined using HPLC as none was visible in any of the early samples. The rate constant determined from the UV data seemed drastically higher, viz. three times the rate constant found using HPLC ($4.21 \times 10^{-3} \text{ min}^{-1}$). Again, both the HPLC and UV traces show a slow initial rate for the reaction, but the reaction does proceed to completion (with a final concentration of $120 \mu\text{mol dm}^{-3}$). The final product ratio is approximately 1:1, as was found in the absence of ethanol. All of this data adds up to show that the presence of ethanol does not adversely affect the homocoupling reaction either in rate or yield.

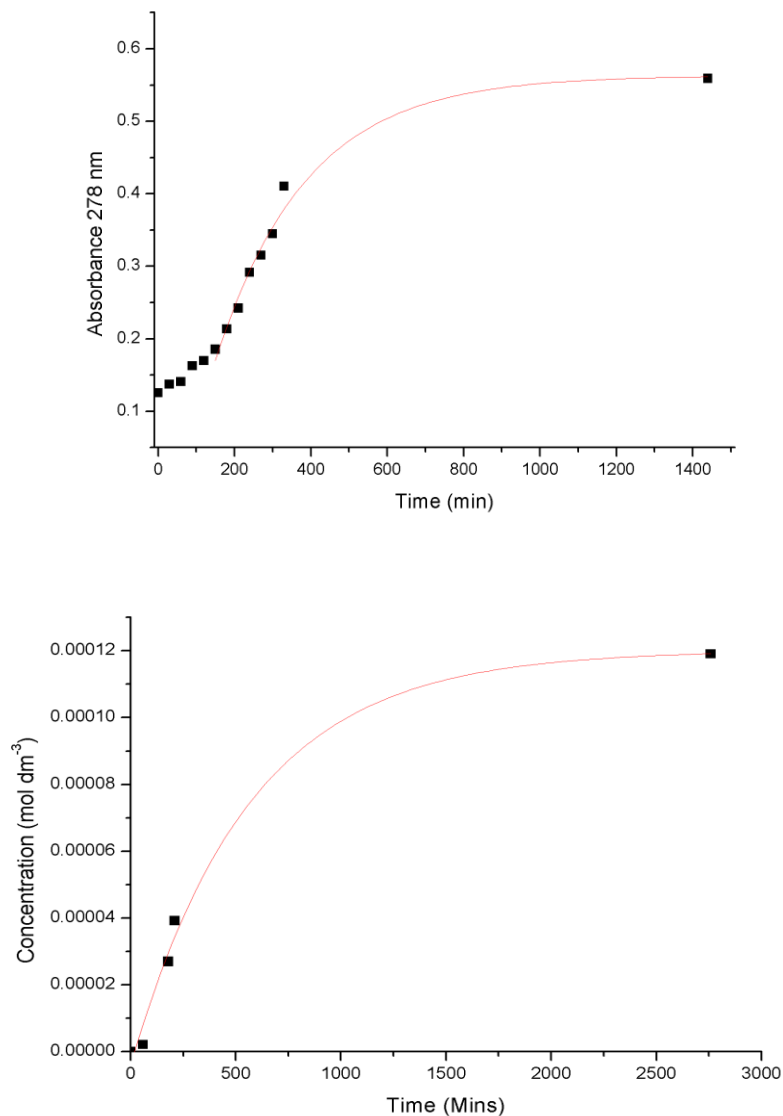


Figure 12 - Change in (A) Absorbance at 278 nm and (B) concentration of **7** recorded by HPLC of 200 μL samples taken during the homocoupling reaction of **6** (444 μM) at 70 $^{\circ}\text{C}$ using one strip of palladium-doped paper as a catalyst for the first time in 1:3 ethanol:water with pH 8.75 borate buffer (10 mM).

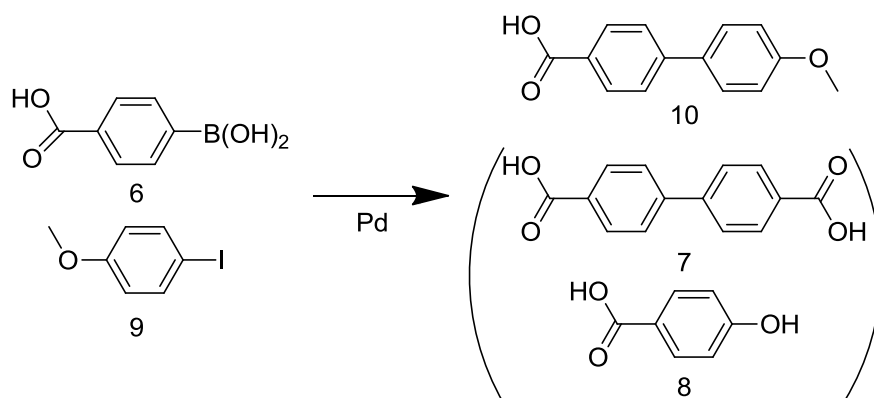
Why there should be a slow initial step in many of these reactions is unclear. It may be that the palladium becomes deactivated in storage and it takes time to reach its optimal rate under the reaction conditions. Alternatively, it could be a diffusion issue, if the shaking of the reaction is less efficient at homogenising the reaction. Since the reactants must diffuse into the cellulose matrix, and the products must likewise diffuse out, then poor homogenisation could lead to the samples being taken not accurately representing the reaction as a whole.

Data for all of these homocoupling reactions, including rate constants and final product concentrations, are collated in Table 1.

[6] (mol dm ⁻³)	pH	Catalyst Use	k_{obs} [7] (min ⁻¹)	k_{obs} [8] (min ⁻¹)	k_{obs} 278 nm	[7] _{final} (mol dm ⁻³)	[8] _{final} (mol dm ⁻³)	[7]:[8]	Mass Balance
4.44 x10 ⁻⁰⁴	8.75	1st	1.38 x10 ⁻⁰³	1.66 x10 ⁻⁰³	1.53 x10 ⁻⁰³	1.26 x10 ⁻⁰⁴	1.26 x10 ⁻⁰⁴	1.00	85.14%
4.44 x10 ⁻⁰⁴	8.75	2nd	1.90 x10 ⁻⁰³	7.60 x10 ⁻⁰³	1.79 x10 ⁻⁰³	1.13 x10 ⁻⁰⁴	7.34 x10 ⁻⁰⁵	1.54	67.43%
4.44 x10 ⁻⁰⁴	8.75	1st	1.90 x10 ⁻⁰³	1.58 x10 ⁻⁰³	[1.83E-04]	1.29 x10 ⁻⁰⁴	9.94 x10 ⁻⁰⁵	1.30	80.50%
4.44 x10 ⁻⁰⁴	8.75	2nd	1.56 x10 ⁻⁰³	2.86 x10 ⁻⁰³	1.81 x10 ⁻⁰³	1.16 x10 ⁻⁰⁴	6.28 x10 ⁻⁰⁵	1.85	66.40%
2.22 x10 ⁻⁰⁴	8.75	1st	2.07 x10 ⁻⁰³	1.20 x10 ⁻⁰³	1.41 x10 ⁻⁰³	4.97 x10 ⁻⁰⁵	3.82 x10 ⁻⁰⁵	1.30	61.98%
8.88 x10 ⁻⁰⁴	8.75	1st	8.36 x10 ⁻⁰³	1.05 x10 ⁻⁰³	1.05 x10 ⁻⁰³	2.13 x10 ⁻⁰⁴	2.11 x10 ⁻⁰⁴	1.01	71.73%
4.44 x10 ⁻⁰⁴	7	1st	2.53 x10 ⁻⁰³	2.12 x10 ⁻⁰³	1.49 x10 ⁻⁰³	9.36 x10 ⁻⁰⁵	5.67 x10 ⁻⁰⁵	1.65	54.93%
4.44 x10 ⁻⁰⁴	10	1st	2.95 x10 ⁻⁰³	N/A	1.68 x10 ⁻⁰³	1.07 x10 ⁻⁰⁴	1.08 x10 ⁻⁰⁴	0.99	72.52%
4.44 x10 ⁻⁰⁴	8.75*	1st	1.77 x10 ⁻⁰³	N/A	4.21 x10 ⁻⁰³	1.19 x10 ⁻⁰⁴	1.11 x10 ⁻⁰⁴	1.07	75.87%

4.2.4 - Suzuki-Miyaura Reaction

Given that the palladium-doped paper strips had performed effectively in the homocoupling reaction in mixtures of ethanol and water, it should be possible to carry out Suzuki-Miyaura cross coupling reactions in the same solvent mixture. The addition of ethanol will aid in the solvation of aryl halides which are typically insoluble in water, especially when compared to the arylboronic acids. If the Suzuki-Miyaura reaction could be carried out successfully it would further demonstrate the effectiveness of the paper-immobilised palladium nanoparticles as a reusable catalyst. The reaction chosen to test the SM reaction is that of **6** with 4-iodoanisole (**9**) (Scheme 5), since the byproducts of this cross coupling reaction, viz. homocoupled **7** and phenol **8** have already been studied previously.



Scheme 5 - The palladium-catalysed Suzuki-Miyaura crosscoupling reaction of 4-carboxyphenylboronic acid **6** and 4-iodoanisole **9** to form 4-methoxy-4'-carboxybiphenyl **10**, and impurities 4,4'-dicarboxybiphenyl **7** and 4-hydroxybenzoic acid **8**.

It was important that the aryl halide had a different functional group to the arylboronic acid so that the cross-coupled product can be distinguished from the homocoupled product (the production of phenol is not reproducibly measurable so is not a good way to measure the progress of the homocoupling reaction). Also, ideally, the aryl halide would be at least slightly soluble in water which would allow for lower ethanol concentrations and relatively unreactive, lest the functional group interfere with the catalyst or the reaction. The reaction was performed in the same way as the previously described homocoupling reactions, except with the addition of **9** in place of half of the boronic acid **6**. The reaction was followed using UV-visible spectroscopy and with a 1:1 ratio of ethanol:water (Figure 13).

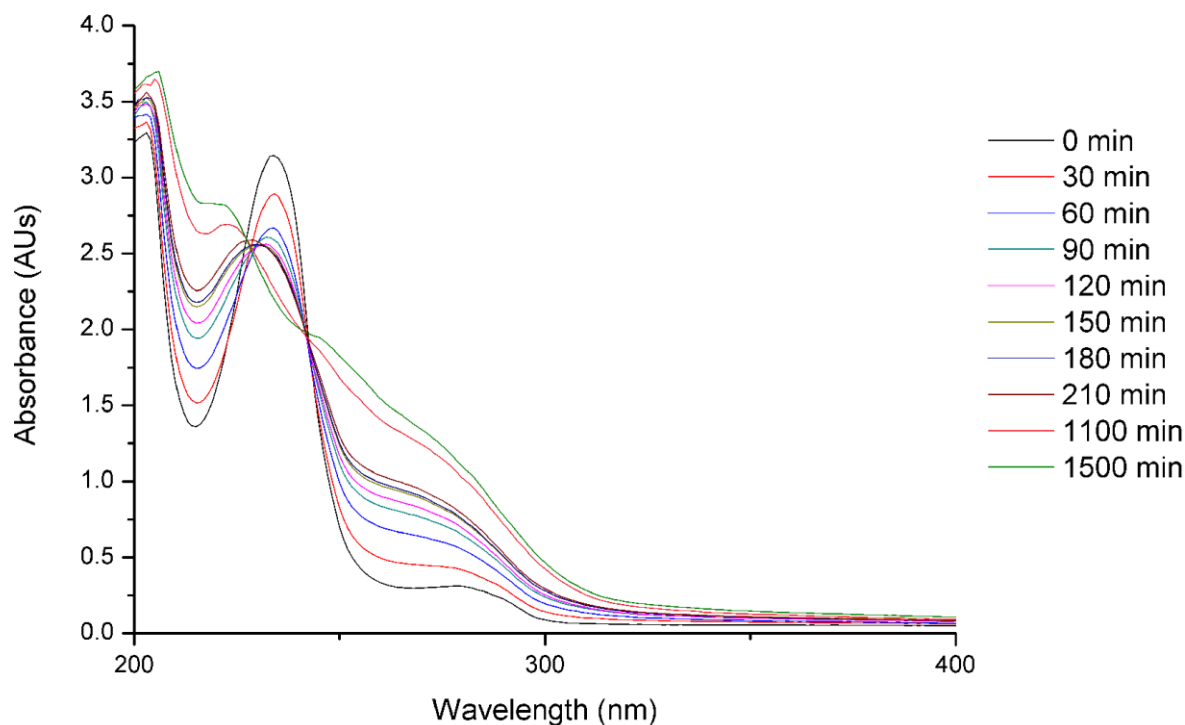


Figure 13 - UV spectra recorded in a 0.5 mL path length cuvette during the SM reaction of **6** (200 μM) and **9** (200 μM) at 70 $^{\circ}\text{C}$ with one strip of palladium-doped paper as a catalyst in 1:1 ethanol and water with pH 8.75 borate buffer (10 mM).

The reaction was performed at 70 $^{\circ}\text{C}$ and was followed by UV-visible spectroscopy at 30 minute intervals. At pH 8.75 the reaction took at least 1500 minutes to reach completion. The absorbance at 289 nm (the λ_{max} of **10**) showed a considerable change through the reaction, as did the absorbance at 278 nm, although the largest change was at 253 nm suggesting significant generation of phenol throughout the reaction. The changes in absorbance at these wavelengths,

and at 235 nm (the λ_{max} of **6**), were plotted against time in order to determine the observed apparent rate constants (Figure 14).

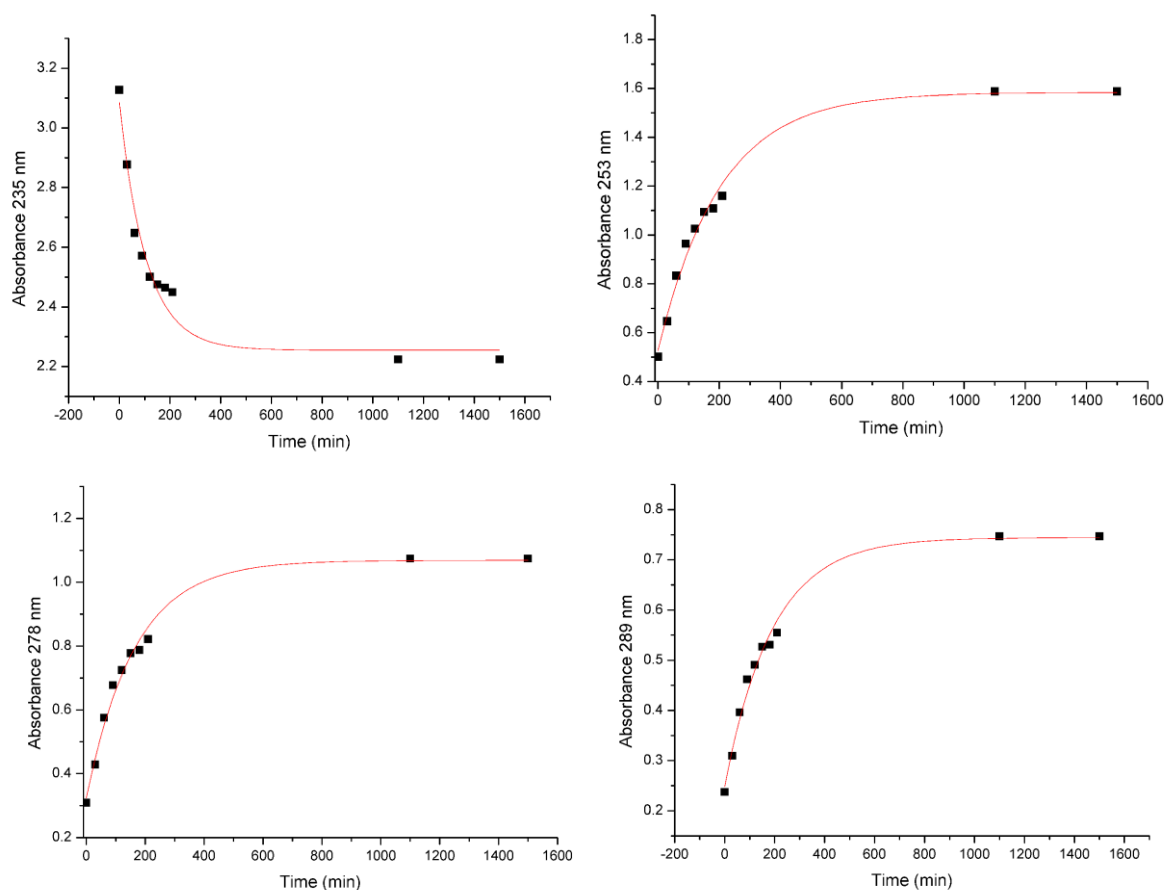


Figure 14 - Change in UV absorbance at a) 235 nm, b) 253 nm, c) 278 nm and d) 289 nm recorded in a 0.5 mL path length cuvette during the SM reaction of **6** (111 μM) and **9** (111 μM) at 70 $^{\circ}\text{C}$ with one strip of palladium doped paper as a catalyst in 1:1 ethanol and water with pH 8.75 borate buffer (10 mM).

Fitting Equation 1 to the absorbances at 253 nm, 278 nm and 289 nm as a function of time gives very reasonable first-order fits, however the fit for the 235 nm absorbance is less good. The rate constants derived from these plots are collated in Table 2.

Table 2 -. Changes in absorbance and observed rate constants recorded in a 0.5 mL path length cuvette during the SM reaction of 6 (400 μ M) and 9 (400 μ M) at 70 $^{\circ}$ C with one strip of palladium doped paper as a catalyst in 1:1 ethanol and water with pH 8.75 borate buffer (10 mM).				
	6	7	8	10
λ_{max}	235 nm	278 nm	253 nm	289 nm
$k_{\text{obs}} / \text{s}^{-1}$	$9.48 \times 10^{-03} \pm 1.36 \times 10^{-03}$	$6.07 \times 10^{-03} \pm 4.77 \times 10^{-04}$	$4.96 \times 10^{-03} \pm 3.97 \times 10^{-04}$	$5.24 \times 10^{-03} \pm 4.16 \times 10^{-04}$
$\Delta A / \text{a.u.}$	-0.83 ± 0.059	0.74 ± 0.029	1.06 ± 0.040	0.50 ± 0.019

Which wavelength is the best to follow for the reaction is hard to judge. Theoretically, the observed rate constant should be the same at all wavelengths, but the observed rate constant at wavelength at 235 nm (the λ_{max} of **6**) is nearly twice the observed rate constants at 253, 278 and 289 nm.

HPLC analysis of the products showed 44% completion of the reaction based on the large amount of **6** remaining (240 μ M out of 400 μ M). Curiously, the anisole seemed almost entirely absent; whilst one would expect the majority of the **9** to remain after such a low completion, only 11% was present (44 μ M). The cross-coupling product **10** only comprised 2% of the material at the end point (8.45 μ M out of a theoretical 400 μ M). The concentration of **7** and **8** at the end point (23.1 μ M and 82.0 μ M respectively) indicates that the homocoupling reaction was active,

probably contributing to most of the change in UV absorbance observed throughout the reaction. Since the reaction stopped despite having a large amount of borate remaining something must have shut down the reaction. Perhaps, the reaction was self poisoning. Since the same was not observed for the homocoupling reaction and very little of the SM reaction occurred one would doubt that this was the case. It is possible that iodide release by the cross-coupling was poisoning the catalyst, since the Pd mol% of 1% means that even a 2% conversion of **9** to **10** would release enough halide to bind to every Pd atom, and if the binding were irreversible under the reaction conditions it would leave the catalyst poisoned. Perhaps the high ethanol concentration itself was hindering the reaction or the combination of factors was causing the destruction or evaporation of the iodoanisole.

From the product ratio it is clear that the rates calculated from the UV data are likely to be mainly for the homocoupling reaction, since the absorbance at 289 nm will be mainly from **7** and not from **10** as there is 2.7 times more of the homocoupling product than of the cross-coupling product.

The best way to follow this reaction was to follow it more closely by HPLC. As was previously shown (*vide supra*) the palladium remains tightly immobilised in the cellulose support even in ethanol, and the reaction was shown to stop cleanly as soon as the catalyst strips are removed from the reaction by the group in Vigo. By removing samples from the reaction at regular intervals the reaction can be followed by HPLC as the concentrations of reactants and products in the samples should stop changing as soon as the samples are removed. Also, since the

palladium particles are not in solution, it should not be necessary to filter the samples before injection on the HPLC. Not requiring sample filtration allows smaller samples to be taken from the reaction without risking damage to the HPLC instrument.

The SM reaction was tested again, with a reduced concentration of ethanol (1:4 v/v EtOH:H₂O) to see if those conditions result in an increase in the rate of the cross-coupling reaction. The reaction was followed by UV spectroscopy (Figures 15 and 16) and by HPLC (Figure 17).

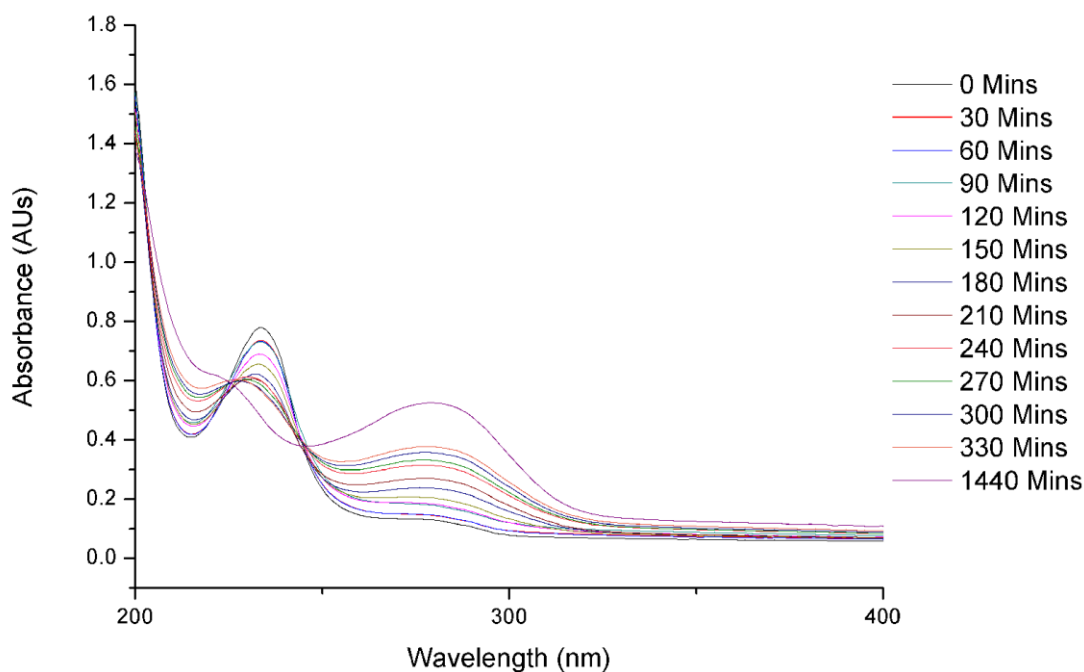


Figure 15 - UV spectra recorded during the SM reaction of **6** (222 μ M) and **9** (222 μ M) at 70 $^{\circ}$ C with one strip of palladium doped paper as a catalyst in 1:3 ethanol and water with pH 8.75 borate buffer (10 mM) for samples in a 0.1 mL path length cuvette.

The UV spectra showed much more change than the previous attempt did, with the wavelength of largest change being 281 nm, just above the λ_{max} of **7**, and also near the λ_{max} of **10** (Figure 15).

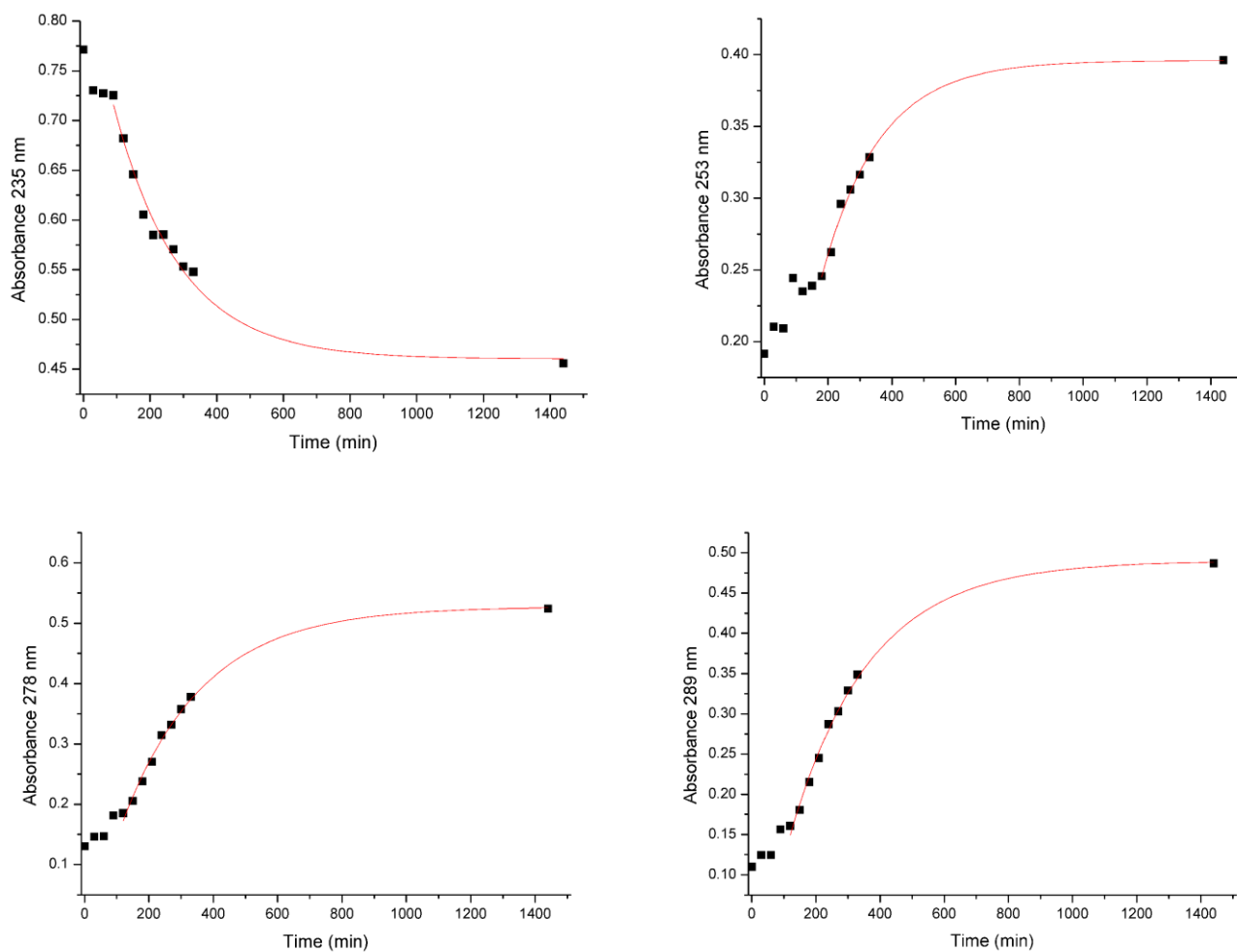


Figure 16 - Change in UV absorbance at a) 235 nm, b) 253 nm, c) 278 nm and d) 289 nm recorded for samples in a 0.1 mL path length cuvette during the SM reaction of **6** (222 μM) and **9** (222 μM) at 70 $^{\circ}\text{C}$ with one strip of palladium doped paper as a catalyst in 1:3 ethanol and water with pH 8.75 borate buffer (10 mM).

The spectra all exhibit an induction period for the first 200 mins and thereafter exhibit good first order kinetics. The rate constants derived from all four data sets (collated in Table 3) are all very similar ($0.00467 \pm 0.00078 \text{ min}^{-1}$). However, as before, the rate constants derived from UV spectra cannot necessarily be relied upon to distinguish the SM reaction from the homocoupling reaction. Samples were therefore also analysed by HPLC (Figure 17).

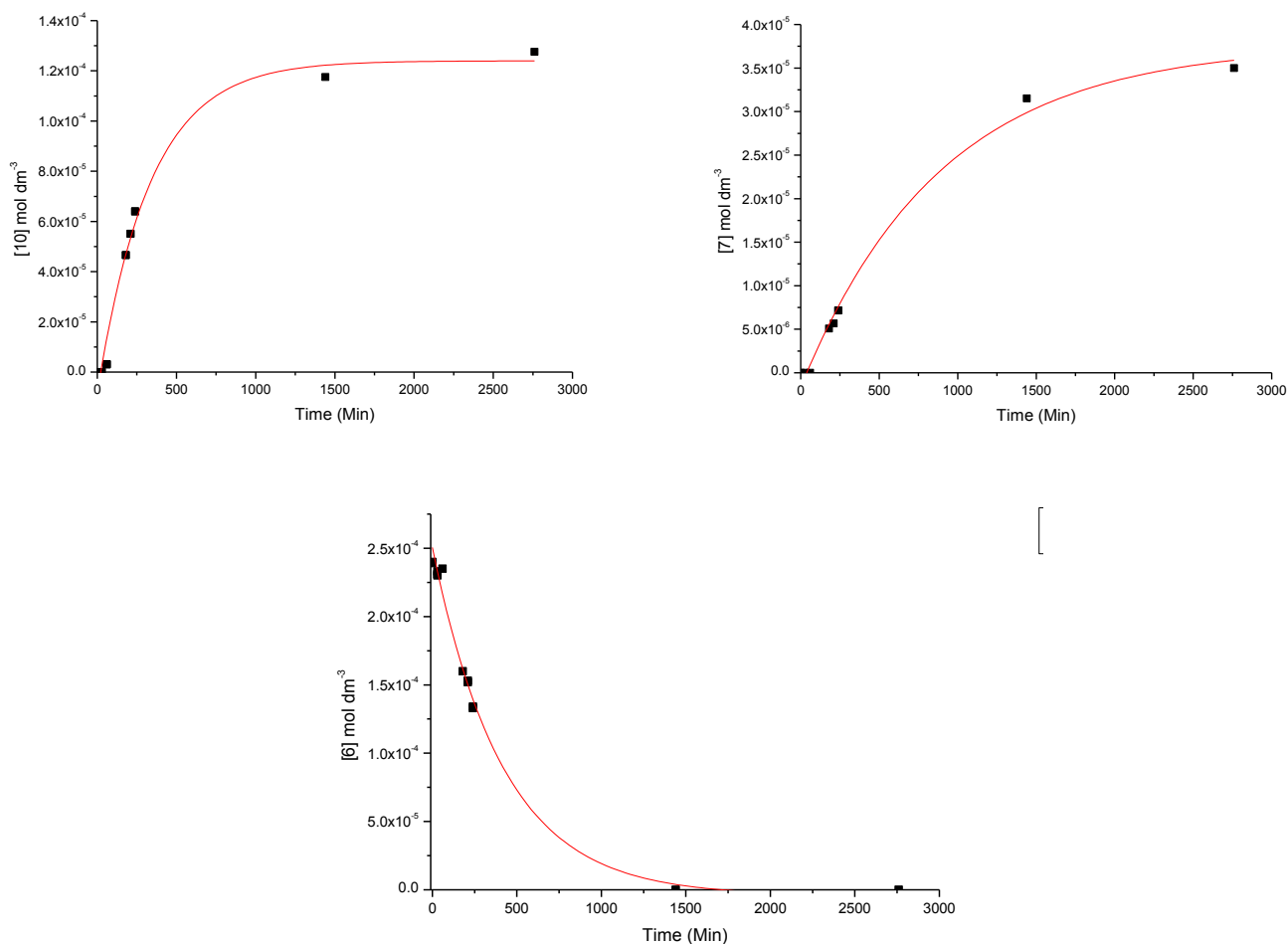


Figure 17 - Change in concentration of **10**, **7** and **6** recorded by HPLC of 200 μ L samples taken during the SM reaction of **6** (222 μ M) and **9** (222 μ M) at 70 °C with one strip of palladium-doped paper as a catalyst in 1:3 ethanol and water with pH 8.75 borate buffer (10 mM).

Unfortunately, the HPLC instrument failed to analyse some samples and as such the data is less comprehensive than that from the UV spectra. The HPLC traces (Figure 17) show that the reaction proceeds to completion with respect to 4-carboxyphenylboronic acid **6** by 1500 minutes

and follows good first-order kinetics. The traces for 4,4'-dicarboxybiphenyl **7** and 4-methoxy-4'-carboxybiphenyl **10** also both follow a first-order rate law with the rate of the SM reaction being roughly 3 times that of the homocoupling reaction leading to a final product ratio of 3.64:1 or 58% with respect to **6**. The traces for 4-iodoanisole **9** and 4-hydroxybenzoic acid **8** do not follow any appreciable pattern, indicating that the concentrations of **8** and **9** may not have remained constant in the sample vials prior to HPLC analysis. Due to a lack of data points in the early period of the reaction the same induction period seemingly observed in the UV spectra is not apparent, and the data appears to follow first-order kinetics from the start. However, if one takes only the UV data points that have corresponding HPLC data, the low initial rate is also not obvious, indicating that the rate constant calculated from the HPLC may underestimate the actual rate constant (Figure 18).

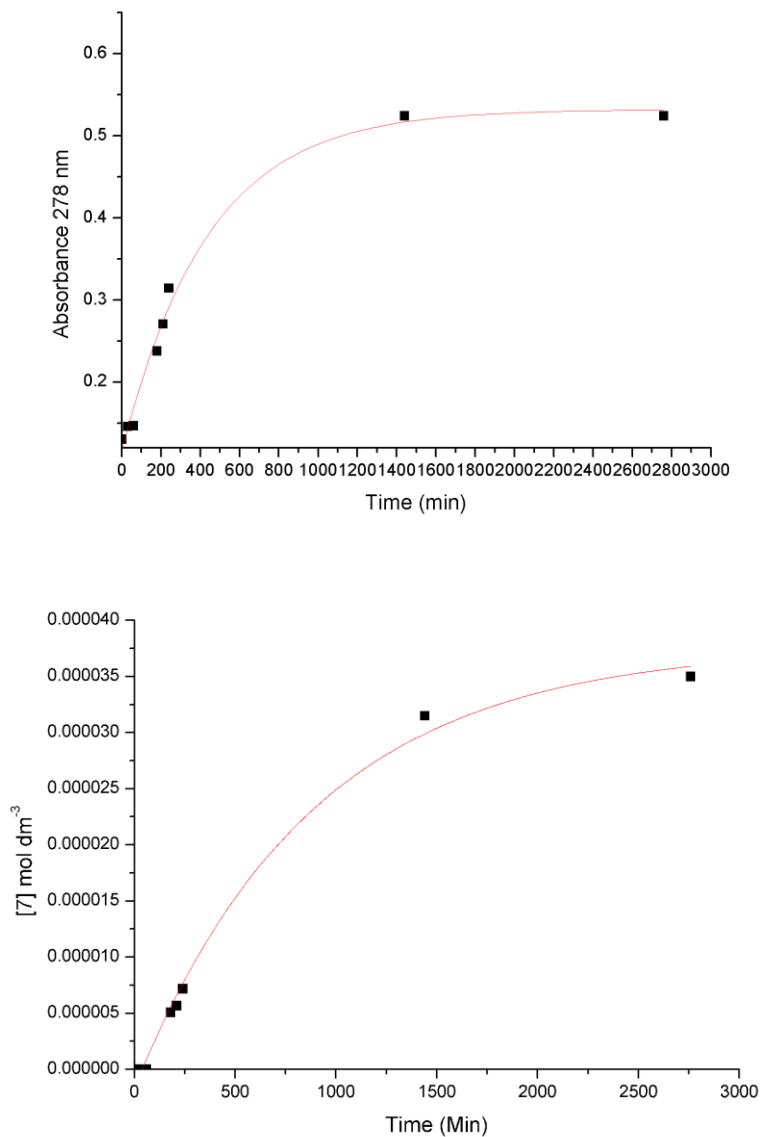


Figure 18 - Comparison of HPLC trace of **7** and UV absorbance at 278 nm from samples taken during the SM reaction of **6** (222 μM) and **9** (222 μM) at 70 $^{\circ}\text{C}$ with one strip of palladium doped paper as a catalyst in 1:3 ethanol and water with pH 8.75 borate buffer (10 mM).

Since at an ethanol:water ratio of 1:1 the cross-coupling reaction seems inhibited when compared to a 1:4 ratio, the reaction was tested with a reduced 1:7 (v/v ethanol:water) ratio to see if lower ethanol concentrations inhibit or accelerate the reaction. As before, the reaction was followed by HPLC (Figure 19).

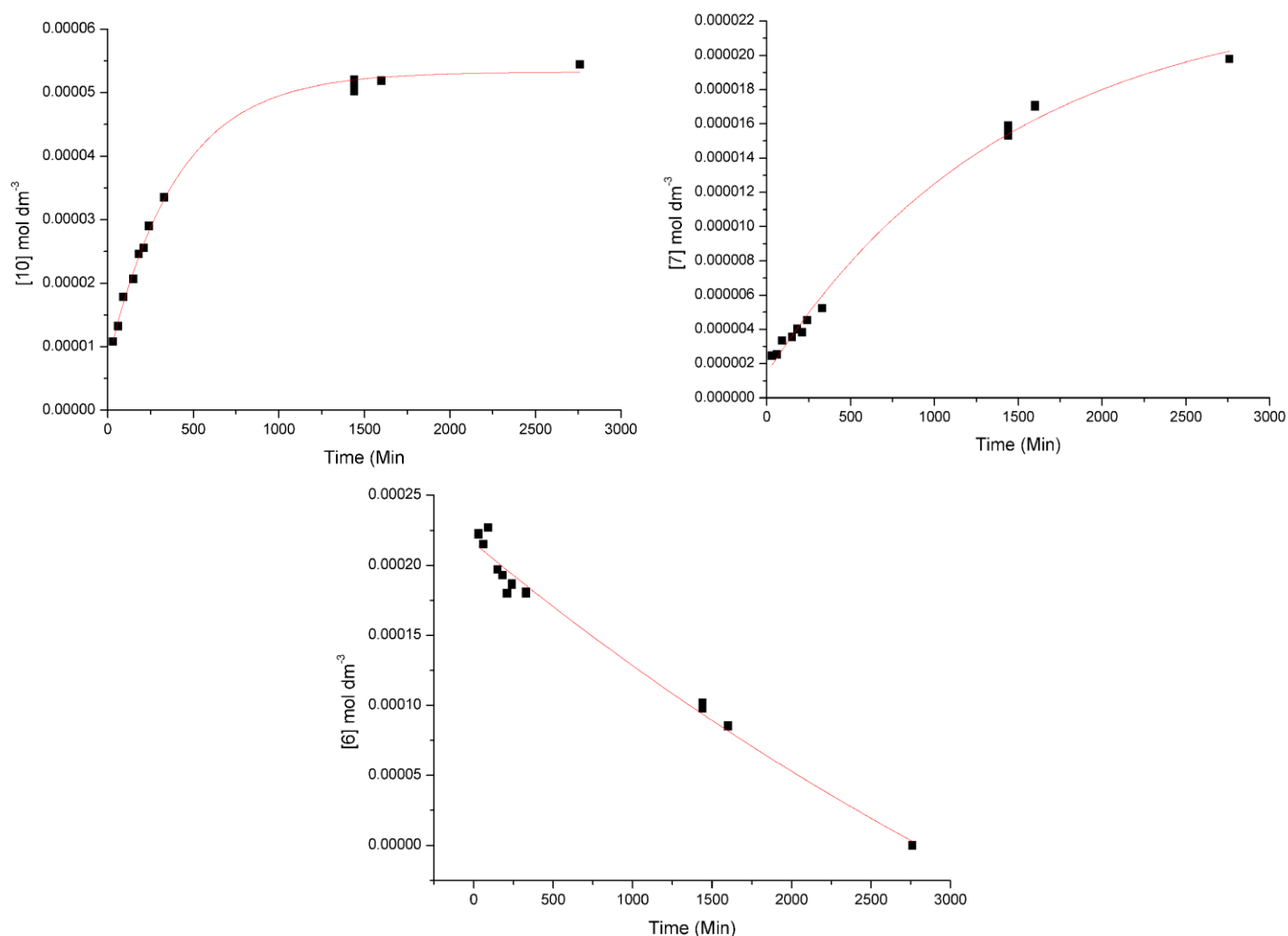


Figure 19 - Change in concentration of **10**, **7** and **6** recorded by HPLC of 200 μ L samples taken during the SM reaction of **6** (222 μ M) and **9** (222 μ M) at 70 $^{\circ}$ C with one strip of palladium doped paper as a catalyst in 1:7 ethanol and water with pH 8.75 borate buffer (10 mM).

Reducing the ethanol:water ratio to 1:7 did alter the rate compared to the reaction at a 1:4 ethanol:water ratio. From UV spectroscopy the rate constant was higher at 235 nm, 278 nm and 293 nm, but at 253 nm the rate constant was lower. From the HPLC data the rate constant for the SM reaction was calculated as being 3-fold that of the homocoupling reaction, however the final product ratio **10:7** was lower than for the higher ethanol concentrations at 2.74:1, however the yield with respect to **6** is only 25%. Looking at the trace for **7**, the data for the homocoupling product is not reproduced well by a first-order rate law and it may be that there is a slow start that has decreased the estimate of the overall rate constant. The actual rate constant for the homocoupling reaction may be higher than estimated, which would explain why the product:byproduct ratio is lower despite the rate constants seeming to be further in the product's favour.

Alongside the SM reactions, a homocoupling-only reaction was studied in 1:3 ethanol:water as a control, with iodide **9** replaced with an equal concentration of boronic acid **6**. The rate constant of the homocoupling was roughly double that of the homocoupling side reaction in the SM reaction (collated with the results for the cross-coupling reactions in Table 3). However, the rate constant is still less than the rate constant for the production of both biaryls in the SM coupling, which again shows that the SM reaction is faster than the homocoupling reaction under the same conditions.

Table 3 - Observed rate constants recorded by UV-visible spectroscopy and by HPLC and final concentrations of aryl species during the SM reaction of 6 (222 μM) and 9 (222 μM) at 70 $^{\circ}\text{C}$ with one strip of palladium-doped paper as a catalyst with pH 8.75 borate buffer (10 mM) in (A) 1:3 ethanol and water, (B) 1:7 ethanol and water and (C) the homocoupling of 6 (444 μM) at 70 $^{\circ}\text{C}$ with one strip of palladium-doped paper as a catalyst with pH 8.75 borate buffer in 1:4 ethanol and water.					
		6	7	8	10
	λ_{max}	235 nm	278 nm	253 nm	289 nm
	$k_{\text{obs}} \text{ UV} / \text{s}^{-1}$	5.06×10^{-03}	3.98×10^{-03}	5.57×10^{-03}	4.05×10^{-03}
(A)	$k_{\text{obs}} \text{ HPLC} / \text{s}^{-1}$	2.39×10^{-03}	1.12×10^{-03}	-	3.00×10^{-03}
	final conc (mol dm ⁻³)	0	3.50×10^{-05}	4.39×10^{-05}	1.28×10^{-04}
	$k_{\text{obs}} \text{ UV} / \text{s}^{-1}$	7.20×10^{-03}	4.23×10^{-03}	5.46×10^{-03}	4.46×10^{-03}
(B)	$k_{\text{obs}} \text{ HPLC} / \text{s}^{-1}$	1.52×10^{-03}	6.99×10^{-04}	-	2.51×10^{-03}
	final conc (mol dm ⁻³)	0	1.98×10^{-05}	3.02×10^{-05}	5.44×10^{-05}
	$k_{\text{obs}} \text{ UV} / \text{s}^{-1}$	3.42×10^{-04}	4.21×10^{-03}	5.08×10^{-03}	4.33×10^{-03}
(C)	$k_{\text{obs}} \text{ HPLC} / \text{s}^{-1}$	1.74×10^{-03}	1.77×10^{-03}	-	-
	final conc (mol dm ⁻³)	0	1.19×10^{-04}	1.11×10^{-04}	-

The UV data in Table 3 gives observed rate constants that are generally higher than those derived from the HPLC traces. Since the change in absorbance at any wavelength includes contributions from both the homocoupling and cross-coupling reactions, the observed rate constants from the UV data are probably not useful for distinguishing between the rates of the homocoupling and cross-coupling reactions.

To see if the reaction could be performed in the minimum possible amount of ethanol, a reaction involving only the ethanol from the stock solution of iodide **9** (giving an EtOH:H₂O ratio of 1:44) was followed by HPLC at pH 8.75, as before, but also at pH 10.01 (Figure 20).

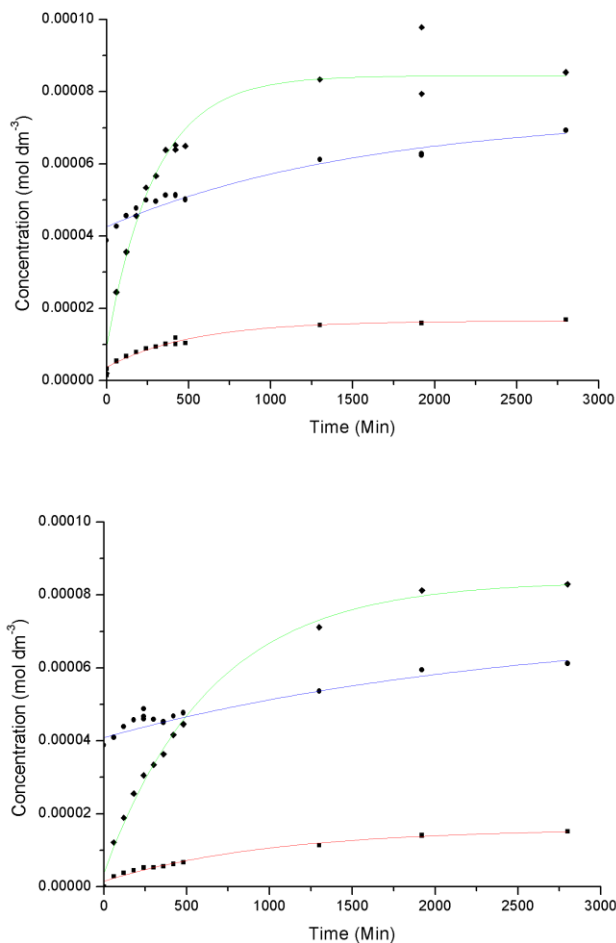


Figure 20 - Change in concentration of **10** \blacklozenge , **8** \bullet and **7** \blacksquare from HPLC analysis of 200 μL samples taken during the SM reaction of **6** (222 μM) and **9** (222 μM) at 70 $^{\circ}\text{C}$ with one strip of palladium doped paper as a catalyst in 1:3 ethanol and water with pH (A) 8.75 and (B) 10.01 borate buffer (10 mM).

The HPLC shows that there was a significant amount of phenol **8** present from the start, which likely is an impurity in the boronic acid solution that was used. The rate constant for the SM reaction determined from the HPLC data is again lower ($1.55 \times 10^{-3} \text{ min}^{-1}$) as the amount of ethanol was reduced. In fact, the observed rate constant for the cross-coupling appears to increase linearly with ethanol concentration (Figure 21).

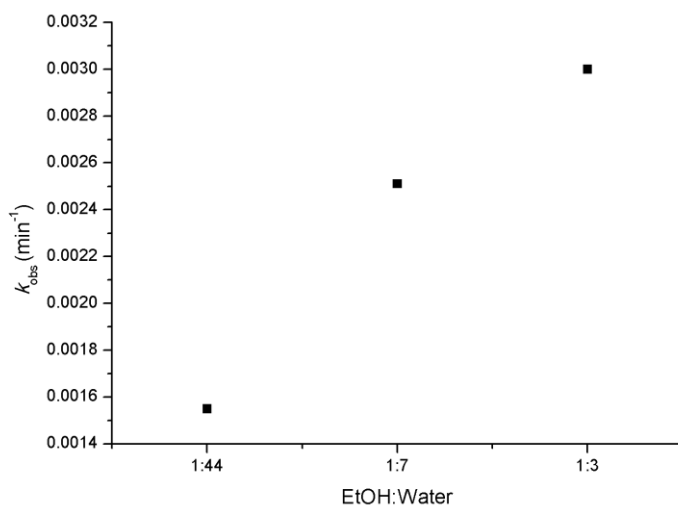


Figure 21 - Change in k_{obs} for the formation of **10** as ethanol:water ratio is changed for the SM reaction of **6** ($222 \mu\text{M}$) and **9** ($222 \mu\text{M}$) at $70 \text{ }^\circ\text{C}$ with one strip of palladium doped paper as a catalyst with pH 8.75 borate buffer (10 mM).

The decrease in rate constant could be attributed to the changing of the effect of pH on the reaction as the solvent becomes less of an aqueous environment. This trend may differ from the

homocoupling reaction which did not appear to react to changing pH (*vide supra*). However, the ratio of **10:7** of 5.24:1 at pH 8.75 and with 1:3 ethanol:water is higher than for the reaction with more ethanol. Increasing the pH to 10.01 (Figure 20) increases the rate constant of the SM reaction to the fastest so far ($3.39 \times 10^{-3} \text{ min}^{-1}$), but without a large drop in the ratio of **10:7** (5.12:1). Both reactions started with a high concentration of **8**, possibly due to decomposition in the stock solution of **6**, but the increase of **8** was far less than for the product **10**. Unlike the homocoupling reaction, which did not seem to show a trend with changing pH, the SM reaction by its nature involves the presence of halides. The higher rate constant at pH 10.01 is a good indicator that the reaction mechanism is unchanged from the commonly accepted mechanism for the SM reaction, which predicts that increasing the pH will favour the displacement of halides from the palladium.

The catalytic cycle has several steps in it (*vide supra*), and which step is rate-limiting varies with reaction conditions. In order to test if the oxidative addition was rate limiting the cross coupling was performed with a tenfold excess of iodoanisole **9** (Figure 22).

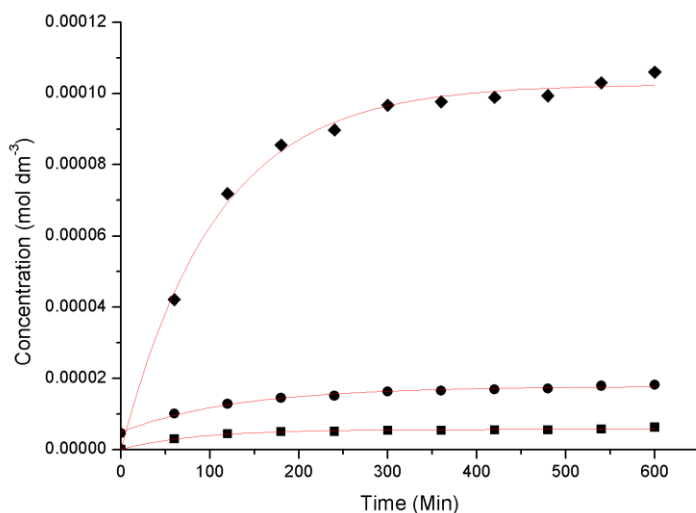


Figure 22 - Change in concentration of **10** \blacklozenge , **8** \bullet and **7** \blacksquare from HPLC analysis of 200 μL samples taken during the SM reaction of **6** (150 μM) and **9** (1.5 mM) at 70 $^{\circ}\text{C}$ with one strip of palladium doped paper as a catalyst in 1:1 ethanol and water with pH 8.75 borate buffer (10 mM).

Ethanol concentration was increased to 1:1 in order to ensure the iodoanisole did not precipitate. Figure 22 shows that the increased concentration of iodoanisole accelerated the reaction, with the reaction reaching completion by 300 minutes, rather than the roughly 24 hours that is common for the stoichiometric reactions. The observed rate constant for the formation of the product **10** is $9.44 \times 10^{-3} \text{ min}^{-1}$ which is over 3 times as high as for the stoichiometric experiment (albeit with a lower ethanol:water of 1:3). Since increasing the concentration of iodoanisole **9** has accelerated the reaction, then the oxidative elimination must be the rate-limiting step. The ratio of **10**:**7** is 21.8:1 indicating a very high preference towards homocoupling, and the yield of **10** at 300 minutes is 92% with respect to the initial concentration of **6**.

4.3 - Conclusions

Paper is a cheap and simple means of increasing the ease of handling and the ease of recovery of palladium catalysts. The paper-immobilised nanoparticles function as a homocoupling reaction catalyst under a variety of different conditions (including varied pH, ethanol content and reactant concentration). The paper strips were also shown to effectively catalyse the SM reaction giving reasonable product ratios despite the fact that the reactions were carried out under aerobic conditions. Overall, not only are paper-supported palladium nanoparticles very reliable catalysts, the paper does not appear to greatly affect the homocoupling reaction compared to molecular catalysts.

In the future the catalyst should be tested under anaerobic conditions to see if the homocoupling reaction can be further hindered, allowing the cross-coupling product to be synthesised in a high enough purity to make our paper-immobilised nanoparticles a viable synthetic laboratory catalyst. Additionally, the variance of catalyst strips should be verified to identify why some of the strips caused hydrolysis of the starting material rather than catalysis of the homocoupling reaction.

4.4 - Experimental

4.4.1 - Chemicals

All chemicals were obtained from Sigma-Aldrich and were used as received unless otherwise noted. Water was purified using an ELGA option-R 7BP system. Analytical grade ethanol, sodium hydroxide and sulphuric acid were purchased from Fisher. Borate buffers were prepared at a concentration of 0.1 M and adjusted to the appropriate pH using sodium hydroxide and sulphuric acid. Palladium-oleylamine nanoparticles were synthesised and used to create nanoparticle-doped paper strips by the group in Vigo University⁹ and transported dry in a sealed plastic container, and were kept in the dark and dry until use.

4.4.2 - Techniques

UV spectra were obtained using a Jasco V-650 spectrophotometer at ambient temperature. Quartz cuvettes with a path length of 0.1, 0.2 or 0.5 mm were used, depending on the concentration of starting materials used. pH of the samples were measured using a Hanna pH211 microprocessor pH meter equipped with a narrow VWR 662-1759 glass electrode. HPLC analysis was carried out using an Agilent1200 instrument with a ZORBAY (Eclipse XDB-C18 4.6X150 mm, 5 μ m) column. Equation 1 was fit to the kinetic data to derive the observed pseudo-first-order rate constant. A is either the absorbance at the given wavelength or the concentration from HPLC data.

$$A_t = A_{\text{final}} - \Delta A \times e^{-k \times t} \quad \text{Equation 1}$$

4.4.3 - Homocoupling and cross-coupling experiments

The homocoupling reactions were performed in a 20 mL screwcap vial filled to 18 mL. Phenylboronic acid **6** was prepared at a concentration of 1 mM in water and was added to the reaction vial using a 1000 μL Eppendorf micropipette (typical volume 800 μL giving a concentration of 444 μM). Borate buffer of the desired pH was added from the 100 mM stock solutions using a 1000 μL Eppendorf micropipette (typical volume 1.8 mL giving a concentration of 10 mM). The remaining volume of water or ethanol was added using a 5 mL Gilson pipette, and the absorbance and HPLC of samples corresponding to the reaction's starting point was measured. Measurements were performed by pipetting a 0.5 mL aliquot of the reaction mixture into a quartz cuvette and recording the UV-visible absorption spectrum. Afterwards, a 200 μL sample for HPLC analysis was taken from the cuvette using a 200 μL Eppendorf micropipette, and the remainder of the cuvette's contents was returned to the reaction vial. The reaction vials were kept at 70 $^{\circ}\text{C}$ using an aluminium dry heating block on a thermostatted hot plate, and were agitated by placing the hot plate atop a laboratory shaker operating at 160 rpm. The catalyst strips were soaked in borate buffer at the appropriate pH and buffer strength for 10 minutes prior to use and were added to the reaction vials using a pair of tweezers. Samples were taken at regular intervals, with breaks in the measurement overnight. After completion of the reaction the catalyst strip was removed and placed in clean deionised water and then stored in borate buffer at the appropriate pH in a cool, dark cupboard.

The Suzuki-Miyaura crosscoupling reactions were performed as described for the homocoupling reactions, except that an equal volume of a stock solution of **9**, also at a concentration of 1 mM in ethanol, was added at the same time as **6**.

4.4.4 - HPLC

HPLC analysis was carried out using an Agilent1200 instrument with a ZORBAY (Eclipse XDB-C18 4.6X150 mm, 5 µm) column which was kept at a constant 40 °C and a DAD. The method used a gradient of three solvents, deionised water, 0.2% trifluoroacetic acid in water and acetonitrile. The gradient started at 65:30:5 and rose to 0:20:80 over the first seven minutes and then held at that level for the remaining three minutes. Concentrations were calibrated using purchased compounds and the retention times of **6**, **7**, **8**, **9** and **10** were found to be 4.05, 4.45 and 5.95, 9.01 and 7.50 minutes respectively. Concentrations were determined as the average of three runs separated by a two minute gap.

4.5 - Bibliography

1. Zhou, P.; Wang, H.; Yang, J.; Tang, J.; Sun, D.; Tang, W., Bacteria Cellulose Nanofibers Supported Palladium(0) Nanocomposite and Its Catalysis Evaluation in Heck Reaction. *Industrial & Engineering Chemistry Research* **2012**, *51* (16), 5743-5748.
2. Martinez, A. W.; Phillips, S. T.; Whitesides, G. M., Three-dimensional microfluidic devices fabricated in layered paper and tape. *Proceedings of the National Academy of Sciences* **2008**, *105* (50), 19606-19611.
3. Lennox, A. J. J.; Lloyd-Jones, G. C., Transmetalation in the Suzuki–Miyaura Coupling: The Fork in the Trail. *Angewandte Chemie International Edition* **2013**, *52* (29), 7362-7370.
4. Butters, M.; Harvey, J. N.; Jover, J.; Lennox, A. J. J.; Lloyd-Jones, G. C.; Murray, P. M., Aryl Trifluoroborates in Suzuki–Miyaura Coupling: The Roles of Endogenous Aryl Boronic Acid and Fluoride. *Angewandte Chemie* **2010**, *122* (30), 5282-5286.
5. Sato, R.; Kanehara, M.; Teranishi, T., Homoepitaxial Size Control and Large-Scale Synthesis of Highly Monodisperse Amine-Protected Palladium Nanoparticles. *Small* **2011**, *7* (4), 469-473.
6. Guangchao Zheng, K. K., Stefanos Mourdikoudis, Azzedine Bouleghlimat, Niklaas J. Buurma, Polavarapu Lakshminarayana, Belén Vaz, Ángel R. de Lera, Luis M. Liz-Marzán, Isabel Pastoriza-Santos, and Jorge Pérez-Juste, Manuscript: Pd nanoparticle immobilization for Carbon-Carbon coupling reactions (Unpublished). a Departamento de Química Física, U. d. V., 36310 Vigo, Spain.; b Physical Organic Chemistry Centre, S. o. C., Cardiff University, Main Building, Park Place Cardiff, CF10 3AT, United Kingdom.; c Centre for Cooperative Research in Biomaterials (CIC biomaGUNE), P. d. M., 20009 San Sebastián, Spain; d Departamento de Química Orgánica, U. d. V., 36310 Vigo, Spain.; e Ikerbasque, B. F. f. S., 48011 Bilbao, Spain, Eds. 2014.
7. Only following a reaction 1/6th of the way to completion does not allow you to distinguish between zeroth and first order rate constants.
8. Knill, C. J.; Kennedy, J. F., Degradation of cellulose under alkaline conditions. *Carbohydrate Polymers* **2003**, *51* (3), 281-300.
9. Guangchao Zheng, K. K., Stefanos Mourdikoudis, Azzedine Bouleghlimat, Niklaas J. Buurma, Polavarapu Lakshminarayana, Belén Vaz, Ángel R. de Lera, Luis M. Liz-Marzán, Isabel Pastoriza-Santos, and Jorge Pérez-Juste, Supporting Information: Pd nanoparticle immobilization for Carbon-Carbon coupling reactions (Unpublished). a Departamento de Química Física, U. d. V., 36310 Vigo, Spain.; b Physical Organic Chemistry Centre, S. o. C., Cardiff University, Main Building, Park Place Cardiff, CF10 3AT, United Kingdom.; c Centre for Cooperative Research in Biomaterials (CIC biomaGUNE), P. d. M., 20009 San Sebastián, Spain; d Departamento de Química Orgánica, U. d. V., 36310 Vigo, Spain.; e Ikerbasque, B. F. f. S., 48011 Bilbao, Spain, Eds. 2014.

Chapter 5

Synthesis of gold nanoparticles for nitric oxide release

Abstract: Gold nanoparticles with a diameter of 15 nm were synthesised and were used as seeds to grow 60 nm nanoparticles in CTAB solution. The particles were used to release NO from S-nitrosopenicillamine (SPEN) and S-nitrosoglutathione (GSNO) in CTAB to ascertain if the release allowed for the reproducible measurement of NO release by NO-selective electrode without the nanoparticles damaging the electrode. Addition of SPEN to the 15 nm gold nanoparticles caused a release of NO that was proportional to 391-662 SPEN molecules binding to each nanoparticle, or a surface coverage between 8-13%, that did not appear to be greatly affected by CTAB concentration. Addition of GSNO to the 15 nm gold nanoparticles caused a release of NO that was proportional to 129-197 GSNO molecules binding to each nanoparticle, or a surface coverage between 9-14%, that did not appear to be greatly affected by CTAB concentration. Addition of SPEN to the 60 nm gold nanoparticles caused a release of NO that was proportional to 7624-91914 SPEN molecules binding to each nanoparticle, or a surface coverage between 10-115%. The unexpectedly high range of stoichiometry is due to the instability of SPEN which quickly decomposed in CTAB at pH 7 and higher to release NO even in the absence of gold. Addition of GSNO to the 60 nm gold nanoparticles caused a release of NO

that was proportional to 2356-6458 GSNO molecules binding to each nanoparticle, or a surface coverage between 10-28%.

5.1 - Introduction

5.1.1 - Applications of Nanoparticles

Chapters 5 and 6 described the use of nanoparticles and nanoparticle-based structures in catalysis. Particles and structures on the nanoscale are an area of great interest beyond their use in catalysis. In particular, the difference in properties and reactivity of nanoparticles from the bulk metal and from their molecular properties has opened up whole new categories of uses.

Biologically active nanoparticles are an extremely interesting field, since the very unique features and chemistry of nanoscale materials can be employed to open up entirely new approaches to problems.

Drug delivery with nanoparticles typically uses a nanoscale container to encapsulate a conventional drug. The properties of the nanoparticle can be modified to release the drug only when it reaches the desired area, whether that is to target only specific locations or merely to protect the payload from being decomposed (for example by the digestive tract or the liver). Liposomes are spherical containers constructed of a phospholipid bilayer, based on naturally occurring vesicles, and are already used in multiple drug formulations.¹ Unlike micelles they are persistent rather than transient structures and, more importantly, the water-filled central cavity is hydrophilic. Since the membrane of the vesicle is hydrophobic, hydrophilic payloads can be kept inside the liposome without risk of escaping in transit and the vesicles can then deploy the payload either by binding with the target cell or by slow diffusion of the payload from the

liposome. An example is AmBiosome, a formulation of Amphotericin B, an antifungal drug that can cause kidney damage, in a liposome that is preferentially attracted to the target cells, thus reducing the damage to the body by the treatment.²

Silver can be used as an antimicrobial agent. Silver has long been known for its antimicrobial properties by the alchemists and physicians of old (even if they did not understand the how or the why of it) being used for storing water safely and later in medicinal treatments.³ Ionic silver has been used in medicine and makes a good broad range antimicrobial agent with low bacterial resistance.⁴ However, there are debates about the efficacy of wound dressings that release silver ions⁵ and the potential for toxic effects, such as argyria - the discoloration of the skin caused by silver metal deposition - and in high concentrations nephrotoxicity.⁶ Recent studies have shown that silver nanoparticles can be effective antimicrobial agents and studying the mechanism of action is extremely interesting to distinguish between whether the nanoparticle itself is active or whether it is a delivery system for silver ions.^{4a, 7} A silver nanoparticle that was stable in vivo and active against microbes would be a much safer alternative to silver ions and could have a much longer lasting effect.

Another approach that has been demonstrated is using the nanoparticles as a targeted anti-cancer therapy. Nanoparticles can be heated using an external source, either by magnetism⁸ or IR/RF irradiation⁹ to cause localised cell death. The surface of the nanoparticle can then be functionalised with a variety of different biologically active groups that interact with the target cancer cells. Because of these interactions, the nanoparticles will accumulate in the tumor, and

irradiation with relatively harmless IR/RF radiation or application of magnetism will only cause heating in the desired location rather than across the whole body. Another similar approach uses a nanoparticle as a container for a photoactive compound that upon radiation generates singlet oxygen that diffuses out of pores in the NP and attacks the surrounding cells.¹⁰

5.1.2 - Nitric oxide release

Nitric oxide (NO) is an important neurotransmitter in biological systems. It had long been thought to stimulate the release/production of Endothelium Derived Relaxing Factor (EDRF), the neurotransmitter that causes vasodilation, but it is becoming increasingly clear that the factor is NO itself.¹¹ It is still possible there are other chemicals that are also the EDRF, but NO on its own does cause vasodilation.

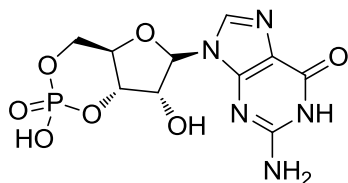


Figure 1. Cyclic guanosine monophosphate, one of the receptors of NO in the body.

In the body NO binds to cyclic guanosine monophosphate (cGMP, figure 1), which triggers the relaxation of smooth muscle, such as that found in the lining of veins and arteries, which causes them to expand. The expanded blood vessels carry more blood, an effect that is useful in treating a variety of conditions related to the supply of blood such as angina (the restriction of blood flow

in the coronary artery). Alternative methods to increase the blood flow such as by the installation of a stent to prevent the contraction are not always feasible or appropriate.

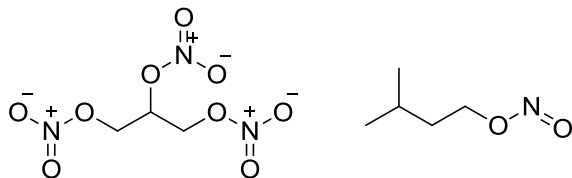


Figure 2 - Structure of vasodilatory agents nitroglycerin (Left) and amyl nitrate (Right)

The NO vasodilation mechanism is used medicinally with several pharmaceuticals. The most obvious target is for the treatment of angina and other heart problems by dilating the blood vessels supplying the heart. This is how drugs like nitroglycerin¹² and amyl nitrate¹³ (Figure 2) function in the treatment of cardiac issues. By dilating the coronary blood vessels they increase the blood flow to the heart which reduces the effect of angina and the risk of heart attacks. Additionally, other organs at risk of ischemia (the restriction of blood supply) can be protected by drugs utilising the NO vasodilation mechanism.

The main issue with this kind of vasodilatory agent is the blunt nature of the effect - the NO release is not localised so it tends to affect the whole body, even when the intended target is only a small area. This causes undesirable side-effects such as low blood pressure (as the volume of the circulatory system is greatly increased) and low heart rate which, whilst not problems in their own right, can cause complications. Since blood-vessel walls are not the only smooth muscles in the body, NO release can also affect these other involuntary muscles such as sphincters (a

common problem among recreational amyl nitrate users is the loss of bowel control).¹⁴ Additionally, being able to maintain a long lasting effect is difficult since the half life of NO and the NO-activated cGMP complex in the body is quite short (the former because it binds to cGMP quite rapidly, and the latter because enzymes start to break down the complex almost immediately after it forms). Being able to localise the release of NO, and therefore the vasodilatory effect, would reduce these kinds of side effects. However, targeting drugs in the body is not trivial as they usually spread themselves evenly throughout the bloodstream rather than concentrating at the target location.

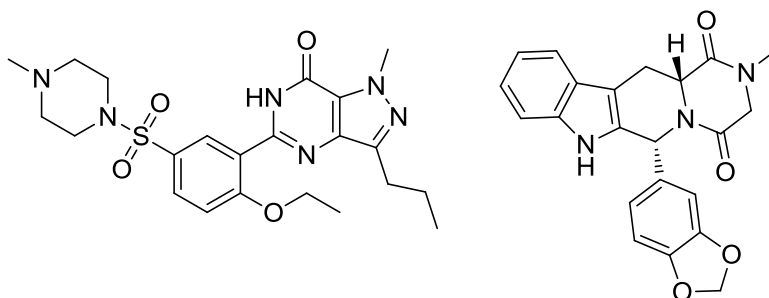


Figure 3 - Erectile dysfunction drugs sildenafil (L) and tadalafil (R).

One approach to targeting is used by erectile dysfunction drugs like sildenafil¹⁵ and tadalafil¹⁶ (figure 3) to localise the vasodilatory effect in the target area. Rather than release NO, like amyl nitrate and nitroglycerine, they inhibit the enzyme cGMP-specific phosphodiesterase type 5 which prevents the NO-activated cGMP complex from being broken down.¹⁷ This prolongs the vasodilatory effect from the naturally released NO in the body. Since the body naturally releases NO in the desired area the vasodilatory effect is localised to the target area, and should not normally affect other areas. The problem with this form of targeting is that it relies on specific

factors that are beyond our control. Unless the body would naturally release NO in the target area, these drugs cannot target vasodilation in that area.

A second approach to targeting NO release would be to use a pro-drug that releases NO in the body in a controlled manner. Then the pro-drug can be delivered normally (orally or directly into the bloodstream) but the effects would not be spread out across the body.

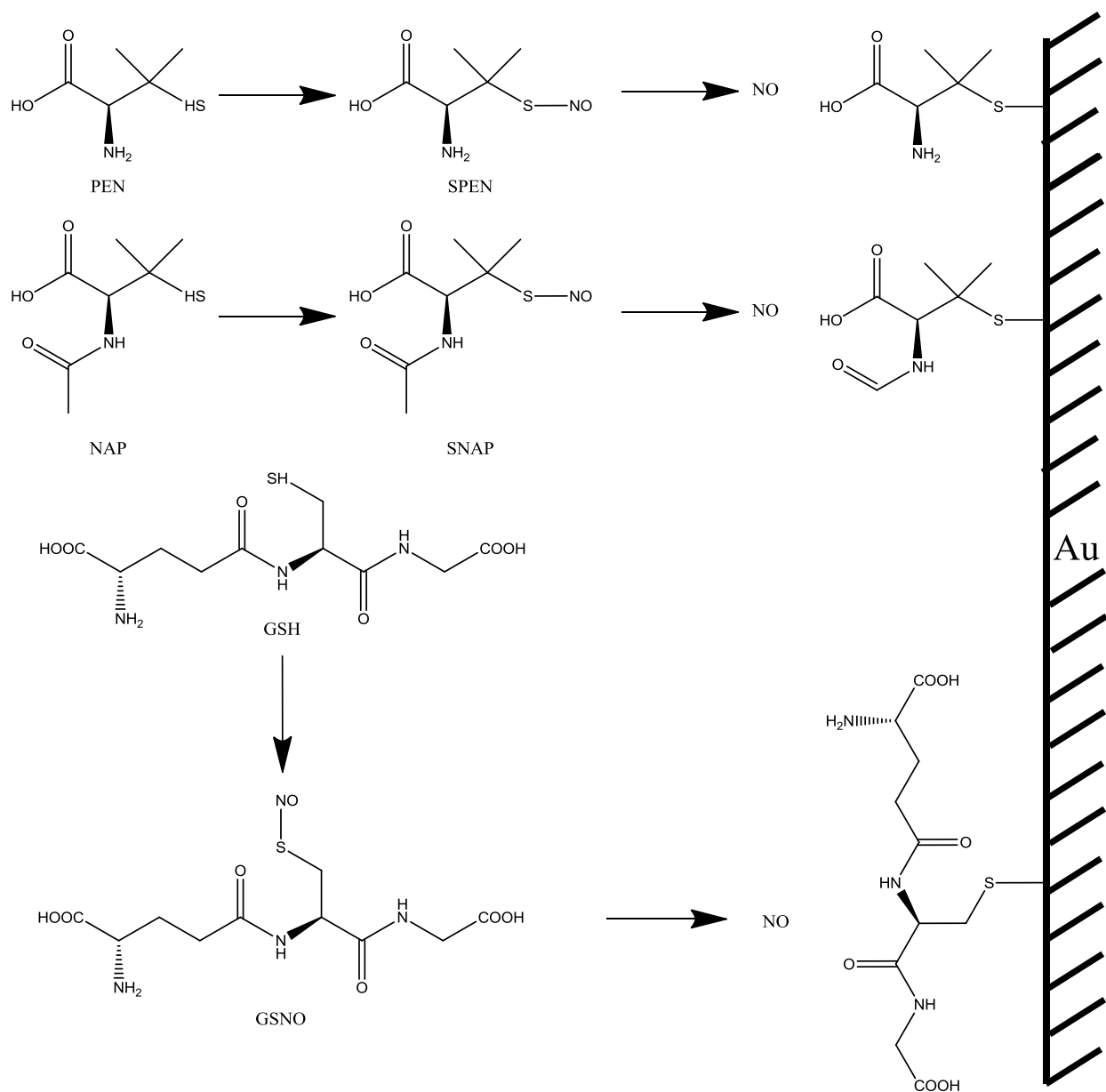
Using a metallic catalyst for the conversion of a pro-drug to NO could overcome the tolerance effect found when nitroglycerin is used in long term treatments, since one hypothesis for the tolerance is that the body interferes with the conversion of nitroglycerin to NO. If that were to be the major cause of tolerance in the body, then supplying a mechanism to convert the pro-drug into NO could limit the body's ability to become tolerant. Also, if the limiting release of NO to the target area could serve to limit other repercussions of the treatment if the tolerance derives from a localised desensitisation to NO. The rest of the body would not be as affected, as the NO release will only be induced in the target area, and should therefore respond normally to the body's own NO release.

Additionally, if the tolerance is due to a defensive response of the body against the externally introduced NO source, then perhaps by localising it to the target area and not the rest of the body, the response may be lessened since the overall quantity of extra NO could be much lower.

5.1.3 - Use of Nanoparticles for NO release

Thiols are of interest for NO release as the thiol can be functionalised with an NO group to form nitrosothiols. Nitrosothiols have been studied as a possible NO delivery system for some time.¹⁸ Commonly studied nitrosothiols include S-nitrosopenicillamine (SPEN) and S-nitroso-N-acetylpenicillamine (SNAP), both derived from the penicillin metabolite penicillamine, and S-nitrosoglutathione (GSNO) which is derived from the tripeptide glutathione.

Sulphur forms very strong bonds with gold surfaces. Therefore, the nitrosothiols bind to gold particles, releasing NO into solution in the process (Scheme 1). GSNO is in fact one of the compounds the body uses for transporting NO in the body (since NO is too reactive to transport neat) so NO and its metabolite would not pose a high toxicity risk in the body.¹⁹ SPEN and SNAP, both being metabolites of penicillin, do not occur normally in the body, but nevertheless do not appear to be toxic.²⁰ Due to the binding affinity of sulphur and gold it is unlikely that the thiol will become free from the gold particle's surface, but even if it were to desorb penicillamine can be broken down by the body, although it may trigger penicillin allergies.²¹



Scheme 1 - S-Nitrosopenicillamine (SPEN), S-Nitroso-N-acetylpenicillamine (SNAP) and S-Nitrosoglutathione (GSNO) compounds and their Au catalysed NO release

Gold nanoparticles would make a very good agent for releasing NO in a targeted area as the nanoparticles could be placed in the desired area, perhaps bound to a larger structure placed in

the blood vessel. The interaction nitrosothiol and gold is stoichiometric as the thiol remains bound to the gold surface so the release of NO is limited by the available surface area of gold. Nanoparticles are in a 'sweet spot' for such a stoichiometric reaction as they are large enough to be physically held in place, but with a very high surface area for the amount of gold being used which allows for a high amount of NO to be released. However, before using gold nanoparticles for NO release is clinically feasible, it is important to understand the interaction of the gold and the nitrosothiol to work out whether the release of NO can be regulated at all, let alone under physiological conditions.

5.1.4 - Previous Work and outline of Study

Previous work in the Vigo Colloids group²² used 15 nm gold nanospheres synthesised by the chloroauric acid/citrate method described by Jana²³ and measured the release of NO from the nitrosothiols SNAP, SPEN and GSNO. NO release was monitored using an NO-selective electrode. Whilst very effective at monitoring the NO release, the protective membrane became quickly contaminated by the gold nanoparticles which affected the accuracy of further studies using the same membrane. Changing the membrane between each experiment was both time- and-cost-prohibitive. To mitigate this it was thought that changing from citrate-stabilised to cetyltrimethylammonium bromide(CTAB)-stabilised gold nanoparticles could reduce the contamination of the sleeve by better keeping the particle in suspension/solution. In addition, this change would allow for the effect of nanoparticle size on NO release to be easily studied, since the protocol used to grow larger nanoparticles is performed in CTAB and displacing the CTAB

afterwards without causing particle aggregation is not trivial.²⁴ In fact, the nanoparticles are typically capped with sulphides in order to remove the CTAB, which would be completely counter-productive for studying NO release from nitrosothiols. However, it is possible that the inclusion of more components to the system could hinder the NO release by competing with the nitrosothiols for the nanoparticle surface, as the Vigo group noticed when they performed binding studies in foetal bovine serum rather than water.²²

5.2 - Results and Discussion

5.2.1 - Effect of CTAB concentration on NO release from 15 nm gold nanoparticles

If CTAB-stabilisation of nanoparticles interfered with the release of NO, then clearly the system would not be suitable for these studies, and instead an alternative method for synthesising larger nanoparticles would need to be used. To evaluate the possible inhibition of NO release by CTAB, 15 nm particles were used to make a series of samples with a gold concentration of 0.45 mM and different CTAB concentrations between 1 and 10 mM. It appears that 1 mM CTAB is not concentrated enough to stabilise the 15 nm particles, but is enough to displace the citrate that stabilised them previously, as the particles quickly aggregated and sedimented, leaving a pale purple solution.

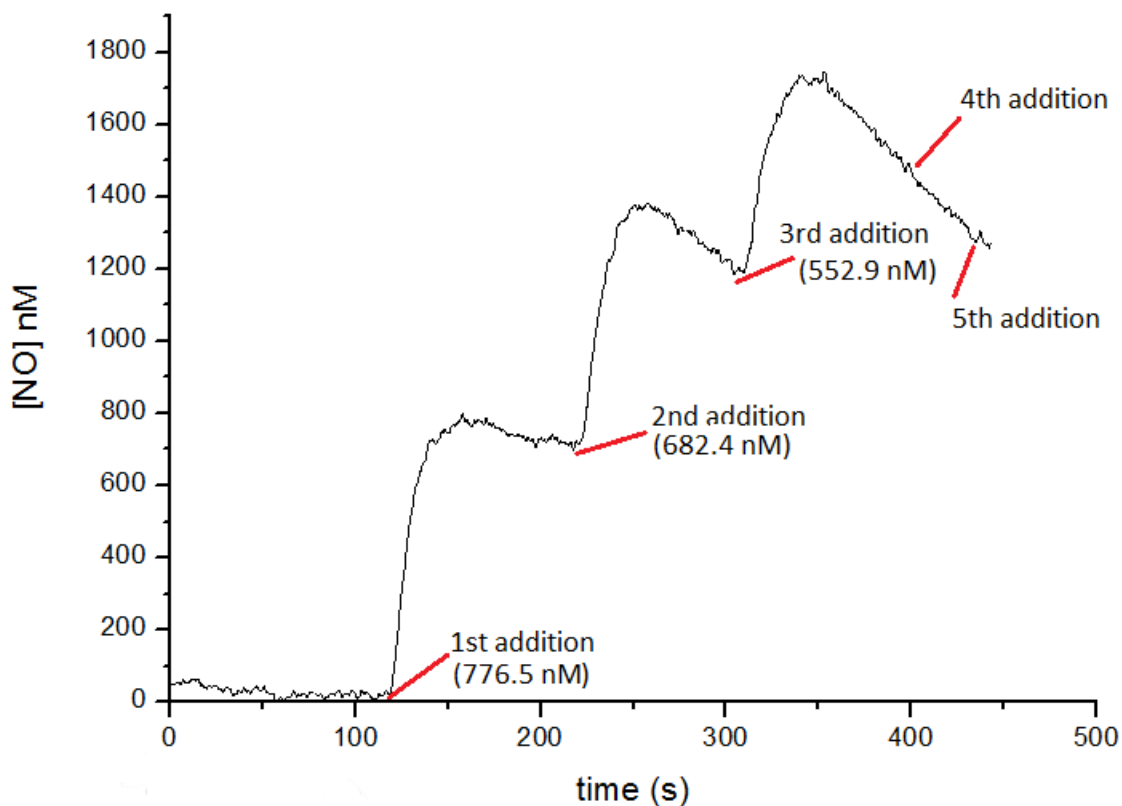


Figure 4 - A typical NO release trace for an Au concentration of 4.475×10^{-4} M with 15 nm particles in 10 mM CTAB.

The efficiency of NO release by the particles was quantified through rate of NO release measured using an ISO-NO electrode while pipetting SPEN into the samples until there was no further NO release from the sample. Each addition contained 1 μ mol of SPEN, and in all cases the NO release was less than the theoretical maximum release of 1 μ mol of NO. An example trace is shown in Figure 4 showing the immediate response to the SPEN addition in a sample

with 10 mM CTAB and the fact that the final two additions (4th and 5th) elicited no further NO release, indicating that the gold surface is fully saturated. UV measurements of the samples before and after NO release were used to verify that the particles' structure was not changed by the experiment and that the gold concentration remained as expected (although it was obvious by visual inspection when sedimentation had happened).

The stoichiometry of release was measured over a range of CTAB and [Au] concentrations. The data for NO release from the 15 nm gold nanoparticles with SPEN is presented in Table 1. The NO release is normalised for nanoparticle size and concentration giving the stoichiometry both per nanoparticle and per surface area.

Table 1

NO release from SPEN and 15 nm gold particles in varying CTAB concentrations.

[Au] (mM)	[CTAB] (mM)	[NO] (nM)	Stoichiometry /nm ⁻²	Stoichiometry /NP	% coverage
0.3125	2	2115±167	0.94±0.14	662±101	13%
0.46	5	2050±57	0.66±0.02	465±13	9%
0.32222	5	1416±172	0.65±0.08	459±56	9%
0.32222	10	1379±219	0.63±0.10	447±71	9%
0.46	10	1975±37	0.63±0.01	448±8	9%
0.32222	15	1208±119	0.55±0.06	391±39	8%
0.32222	20	1298±33	0.60±0.02	421±11	8%
0.32222	100	2024±235	0.93±0.11	656±76	13%
-*	-	-	7.04	4978.17	100%
0.4†	0	7814	2.87	2040	41%
<p>* is the theoretical maximum given that each PEN molecule occupies 0.142 nm² of the surface area, and † is a reference for the 15 nm molecules without CTAB from previous work²²</p>					

Table 1 shows that the observed stoichiometries for all of the CTAB-containing systems are far lower than those found for the previously studied systems without CTAB. In all cases the NO release appeared to be limited to a quarter of the surface coverage recorded in the absence of CTAB. The effect of CTAB concentration on NO release is not entirely clear, however. Between 5 and 20 mM CTAB the stoichiometry is around 450 thiols per nanoparticle while for the very low and very high CTAB concentrations (2 and 100 mM CTAB systems) a stoichiometry of

around 660 thiols per nanoparticle is found (although these results have markedly poor reproducibility - the error is about 1/6th of the value).

The release of NO from GSNO using the 15 nm gold particles was measured over a range of CTAB concentrations and the surface coverage calculated, and the results are presented in Table 2.

Table 2

NO release from GSNO and 15 nm gold particles in varying CTAB concentrations.

[Au] (mM)	[CTAB] (mM)	[NO] (nM)	Stoichiometry /nm ²	Stoichiometry /NP	% coverage
0.32222	5 mM	553	0.94±0.14	179	13%
0.32222	10 mM	543	0.66±0.02	176	12%
0.32222	15 mM	399	0.65±0.08	129	9%
0.32222	20 mM	493	0.63±0.10	160	11%
0.32222	100 mM	609	0.63±0.01	197	14%
-*	-	-	2.02	1428	100%
0.48†	0	2392	0.73	518	36%
* is the theoretical maximum given that each GS molecule occupies 0.494 nm ² of the surface area, and † is a reference for the 15 nm molecules without CTAB from previous work ²²					

NO release from the same system using GSNO as the NO source results in a similar pattern as observed for SPEN. As expected the stoichiometry is lower relative to SPEN because the

glutathione molecule occupies much more space on the nanoparticle's surface (about 3.5x more than penicillamine). There is less variance in NO release with changing CTAB concentration than was observed for SPEN, and the average stoichiometry was closer to that found in previous work in the absence of CTAB (1/3, rather than the 1/4 for SPEN). Again, the stoichiometry was larger at the lowest and highest CTAB concentrations than for the intermediate CTAB concentrations.

The fact that the stoichiometries are so different compared to those observed in the absence of CTAB would be troubling but for two things. First, the fact that the stoichiometry is lower than would be expected indicates that it is not caused by the stability of the nitrosothiol in the solution (instability would lead to an increase in the observed stoichiometry), so the observation must be related to the binding of the nitrosothiol to the gold surface. Second, the fact that the stoichiometry for the GSNO binding has dropped by a third relative to the stoichiometry observed for SPEN binding indicates that it is the surface that the nitrosothiol is interacting with, and the surface is reaching saturation. If this were not the case (and the nitrosothiol was instead reacting with the CTAB) then one would not anticipate such a marked difference in NO release between the nitrosothiols as the size difference of the nitrosothiols would not have as large an effect on the S-NO bond strength. Changes in NP structure and concentration can be ruled out as UV spectra before and after nitrosothiol additions indicate no change in the absorbance resulting from nitrosothiol addition. One possible reason for the reduced stoichiometry in the presence of CTAB could be that CTAB is binding to the surface and preventing the nitrosothiol from binding. However, the CTAB concentration would then be expected to affect the total NO

release as the position of the nitrosothiol/CTAB equilibrium would shift. Another reason for the lower observed stoichiometry in the presence of CTAB could be that gold particles are micellised by the CTAB and this is limiting their availability to react with the nitrosothiols, or worse is limiting the availability of the released NO to the electrode. However, it is unlikely that this is the case as this would be expected to result in a slower reaction (as it is diffusion-limited) rather than a lower stoichiometry.

Whilst the system does appear to be far less available for nitrosothiol binding than the CTAB-free system, it does appear to work in principle, and the benefits of being able to study NO release in CTAB do make up for this.

5.2.2 - Nitrosothiol binding with 60 nm gold nanoparticles

One of the advantages of studying NO release in the presence of CTAB is that it is very easy to modify the nanoparticle size in CTAB solutions. To study the effect of particle size on NO release, 60 nm gold particles were grown in CTAB using ascorbic acid from the 15 nm seed particles. A diameter of 60 nm was chosen because that results in a surface area that is a fifth of the surface area offered by 15 nm particles at the same total gold concentration. The concentration of the stock solution was determined to be 1.79 mM from UV-visible spectroscopy, which was less than the intended 2.5 mM (five-fold the concentration of the 15 nm particles, which should lead to the same maximum NO release). Table 3 shows the results from binding tests for the 60 nm particles with SPEN.

Table 3

NO release from SPEN and 60 nm gold particles in varying CTAB concentrations.

[Au] (mM)	[CTAB] (mM)	[NO] (nM)	Stoichiometry /nm-2	Stoichiometry /NP	% coverage
0.358	20 mM	1097	1.81	20463	26%
0.358	20 mM	1734	2.86	32353	41%
0.358	20 mM	4306	7.10	80346	101%
0.358	20 mM	4925	8.13	91914	115%
1.79	20 mM	6096	2.01	22751	29%
1.79	20 mM	2043	0.67	7624	10%
1.79	20 mM	3017	1.00	11261	14%
1.79	100 mM	8718	2.88	32538	41%
1.79	100 mM	2834	0.94	10577	13%
1.79	100 mM	2220	0.73	8286	10%
-*	-	-	7.04	79671	100%
* is the theoretical maximum given that each PEN molecule occupies 0.142 nm² of the surface area²²					

Table 3 shows that the release of NO from the 60 nm nanoparticles is not as reproducible as for the 15 nm particles; supposedly identical systems have resulted in different NO release, even resulting in NO releases that (slightly) exceed the theoretical maximum. A hint of what may be occurring is that the coverage percentage seems to be a lot higher at the low gold concentration than at the high gold concentration. The lowest stoichiometries found are 10%, which is in agreement with what was found for the 15 nm particles. If the release of NO is not linearly

related to the concentration of gold surface in otherwise identical conditions, there must be another factor causing the change in NO release. One possibility is that the SPEN is not stable in the solution and is decomposing to release NO without interacting with the gold particles.

There is less available data for the interaction of GSNO with the 60 nm particles, but it does show some interesting results (Table 4).

Table 4

NO release from GSNO and 60 nm gold particles in CTAB. * is the theoretical maximum given that each GS molecule occupies 0.494 nm^2 of the surface area.²²

[Au] (mM)	[CTAB] (mM)	[NO] (nM)	Stoichiometry /nm-2	Stoichiometry /NP	% coverage
1.79	20 mM	642	0.2121	2398	11%
1.79	20 mM	631	0.208318	2356	10%
0.358	20 mM	346	0.571096	6458	28%
0.358	20 mM	267	0.44101	4987	22%
-*	-	-	2.02	22845	100%

At the higher gold concentration the stoichiometry indicates a surface coverage of 10%, which is in agreement with what was found for the 15 nm particles and also with the lowest stoichiometries of the SPEN addition to the 60 nm particles. However, there is still no explanation for why the stoichiometry is so much higher for the lower gold concentrations.

5.2.3 - Effect of Gold Particle concentration on NO release

To study the effect of the gold concentration on NO release, the gold concentration was systematically varied. By successively diluting the gold nanoparticles it becomes clear there is more afoot (Figure 5).

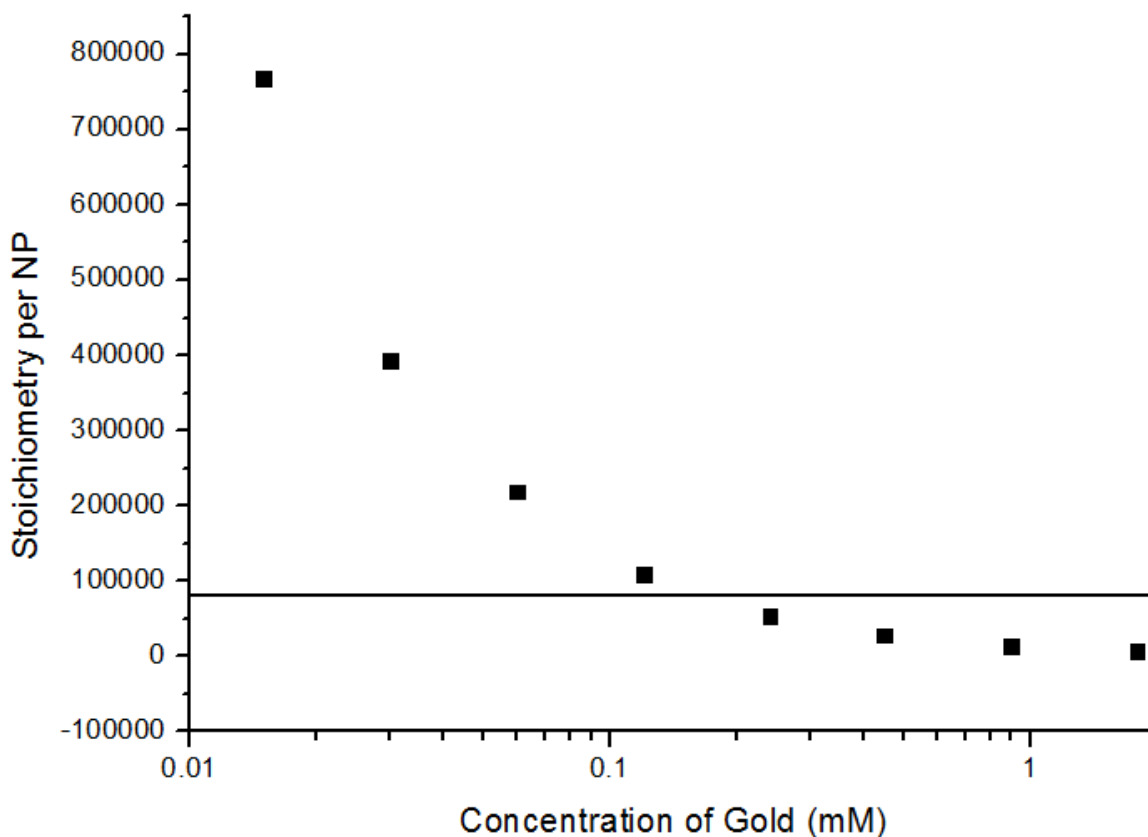


Figure 5 - Change in observed stoichiometry of NO release against gold concentration for the 60 nm nanoparticles in 20 mM CTAB. The black line represents the theoretical maximum stoichiometry.

Figure 5 shows that as the concentration of gold decreases so too does the total NO release, but it is not proportional. At the lowest gold concentration (15 nM total gold, particle concentration of 0.002 nM) the amount of NO released was 1609 nM and would correspond to a stoichiometry of 770000 or 960% of the theoretical maximum. This makes it clear that somehow this system is different to the 15 nm system previously studied, and there is only one obvious way this could be the case - the pH. The pH of the 60 nm gold particle stock solution is possibly different from the 15 nm gold particle stock solution as a result of the work up procedure. A difference in pH could account for the different NO release. Either the pH is causing displacement of the thiol from the gold surface, thus allowing more nitrosothiol to bind, or the nitrosothiol is decomposing in solution to give NO. Recording the pH of the stock solutions was not feasible since the nanoparticles appeared to interfere with the pH electrode, so instead the stability of the nitrosothiol in the absence of gold was investigated.

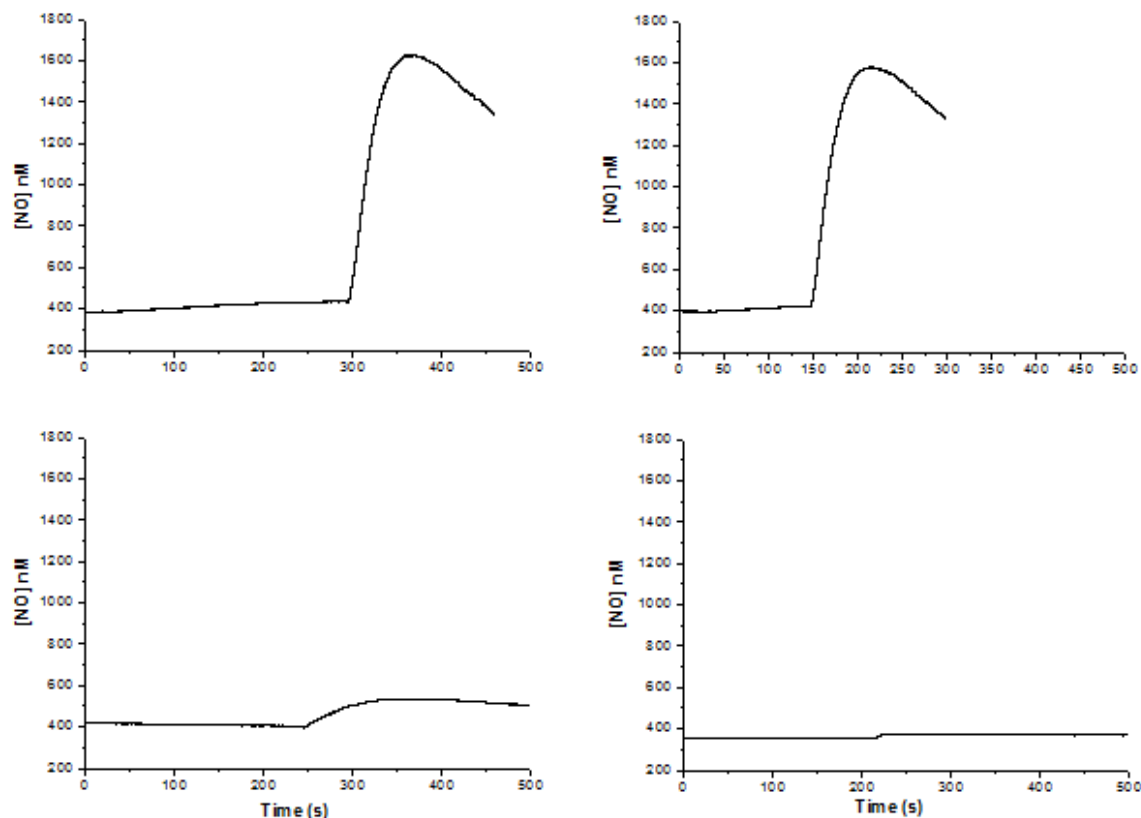


Figure 6 - Observed NO release upon the addition of SPEN in the absence of nanoparticles in CTAB (10 mM) and phosphate buffer (1.5 mM) at (1) pH 8, (2) pH 7, (3) pH 6 and (4) pH 4.

In the absence of any gold there is NO release upon the addition of SPEN and the release increases with pH (Figure 6). This observation is unfortunate, as it indicates that some of the results observed for the 60 nM particles cannot be interpreted in a straightforward manner because some, or most, of the NO release may not relate directly to the reaction between the nitrosothiol and the gold nanoparticles in this system. Even for the lowest recorded stoichiometries it may well be that some of the NO release is due to the nitrosothiol decaying,

and as such the stoichiometry cannot be trusted. However, it is not clear why the release should be higher than expected with the 60 nm particles, since the stock solution of the 60 nm particles should be more acidic than the stock solution of the 15 nm particles (as more acid has been added to it during the growth procedure). Testing with pH paper puts the pH of the 60 nm stock solution around pH 4, whilst the pH of the 15 nm stock solution is around pH 6.

5.3 - Conclusions and future work

The study of nitrosothiol addition to the 15 nm gold particles in the presence of CTAB show some promise, even if the stoichiometry of the addition was far lower than in the absence of CTAB. For mechanistic studies, reproducibility and the ability to gather more measurements can be more important than getting the most promising result, and in this respect the 15 nm system does reliably and easily give reproducible results. The same cannot be said for the 60 nm particles, which did not yield particularly reliable results as it appears that there may be a large degree of nitrosothiol decomposition during the measurements. If the pH of the system can be easily controlled and measured then it would be possible to more clearly study the effect of pH on the reaction, which may give clues as to why the results were so varied.

5.4 - Experimental

5.4.1 - Chemicals

All chemicals were obtained from Sigma Aldrich besides DL-penicillamine which was obtained from Fluka and were used as received. Milli-Q water was distilled in the laboratory and used in all preparations.

5.4.2 - Techniques

UV spectra were recorded with an Agilent 8453 UV-visible spectrophotometer, NO release was measured using a World Precision Instrument ISO-NO electrode with an NO selective membrane based on direct amperometric detection of diffused NO.

5.4.3 - Synthesis of 15 nm Nanoparticles

Chloroauric acid stock solution in water (0.1359 mM stock solution, 919.79 μL , 0.125 mmol) was diluted to 250 mL in water and was stirred and brought to the boil. Once the solution was a clear pale yellow, citric acid (0.125 g) was dissolved in water (12.5 mL) and added to the boiling solution. The solution immediately darkened to black, and grew lighter over fifteen minutes giving a deep wine red colour when it was removed from the heat. After a further ten minutes of

stirring without heat the flask was sealed and covered in foil until it had cooled to room temperature. Once at room temperature water was added to bring the total volume back to 250 mL, and the UV-visible spectrum was recorded to ascertain the diameter and concentration of the nanoparticles ($\lambda_{\max} = 520$ nm, Abs at λ 400 nm = 1.17 AUs, Au concentration of 0.49 mM).

5.4.4 - Growth of 60 nm Nanoparticles

$$R = R_{\text{seed}} \left(\frac{M_{\text{added}} + M_{\text{seed}}}{M_{\text{seed}}} \right)^{\frac{1}{3}} \quad \text{Equation 1}$$

The ratio of seed particles to chloroauric acid used to create the desired nanoparticle size was calculated according to *Equation 1*.²⁴ A solution of CTAB in water (250 mL, 15 mM) was placed in a conical flask, to which chloroauric acid (0.1359 mM stock solution, 1.84 mL, 0.250 mmol) was added and warmed to 36 °C in a water bath until the solution became orange. Ascorbic acid (88 mg, 5 mmol) was added which caused the solution to discolour. Finally the 15 nm gold seed particles (0.49 mM stock solution, 8.8 mL, 0.016 mmol) were added. The solution was left to react for 45 minutes at a constant temperature of 36 °C during which time the solution darkened to a bluish red. The nanoparticle size of 60 nm was verified by UV ($\lambda_{\max} = 540$ nm). The solution was split into 10 mL centrifuge tubes and centrifuged at 4000 rpm for 30 mins. The pellets of nanoparticles were combined in a glass boiling tube and suspended in CTAB solution (10 mL, 0.1 M) and heated in a boiling water bath for 10 minutes. The tube was then removed from the

heat and allowed to gradually cool to room temperature over the course of 12 hours. A golden precipitate (the impurities of gold nanorods and other non-spherical particles) formed at the base of the tube and the solution was gently pipetted out to yield the purified 60 nm nanoparticle solution ($\lambda_{\text{max}} = 540$, 1.79 mM concentration).

5.4.5 - NO release experiments - General procedures

After changing the NO permeable membrane on the ISO-NO electrode it was left to stand in milli-Q water until the current dropped to a low stable value (<20 mA). The electrode was calibrated by titrating several volumes of a solution of NaNO_2 (50 μM) into a vial of 0.1 M potassium iodide in 0.1 M sulphuric acid. Once the calibration gave consistent results the electrode was considered ready for use and was not recalibrated until the sleeve was changed (as the gold particles interfere with the calibration process).

Both nitrosothiols SPEN and GSNO were prepared on the morning of the experiment from either PEN or GSH (0.1 mM) and KNO_2 (0.4 mM) and HCl (50 mM) and kept refrigerated until use. The gold samples were prepared in glass vials to a volume of 10 mL from mixing the gold stock solution, CTAB solution and water and a magnetic stirring bar was added. The electrode was placed in the vial and once the current gave a stable reading phosphate buffer (50 μL of 0.3 M, pH 7.4) and the nitrosothiol were titrated in using Gilson pipettors giving an immediate rise in current from the NO release. The nitrosothiol titration was continued until addition of

nitrosothiol gave no further response and the NO release was calculated by adding the recorded increases in current.

5.5 - Bibliography

1. Balakrishnan, V. K.; Han, X.; VanLoon, G. W.; Dust, J. M.; Toullec, J.; Buncel, E., Acceleration of Nucleophilic Attack on an Organophosphorothioate Neurotoxin, Fenitrothion, by Reactive Counterion Cationic Micelles. Regioselectivity as a Probe of Substrate Orientation within the Micelle†. *Langmuir* **2004**, *20* (16), 6586-6593.
2. Moen, M.; Lyseng-Williamson, K.; Scott, L., Liposomal Amphotericin B. *Drugs* **2009**, *69* (3), 361-392.
3. Murr, L. E., Nanoparticulate materials in antiquity: The good, the bad and the ugly. *Materials Characterization* **2009**, *60* (4), 261-270.
4. (a) Kim, J. S.; Kuk, E.; Yu, K. N.; Kim, J.-H.; Park, S. J.; Lee, H. J.; Kim, S. H.; Park, Y. K.; Park, Y. H.; Hwang, C.-Y.; Kim, Y.-K.; Lee, Y.-S.; Jeong, D. H.; Cho, M.-H., Antimicrobial effects of silver nanoparticles. *Nanomedicine : nanotechnology, biology, and medicine* **2007**, *3* (1), 95-101; (b) Crabtree, J.; Burchette, R.; Siddiqi, R.; Huen, I.; Hadnott, L.; Fishman, A., The efficacy of silver-ion implanted catheters in reducing peritoneal dialysis-related infections. *Peritoneal Dialysis International* **2003**, *23* (4), 368-374.
5. Silver dressings – do they work? *Drug and Therapeutics Bulletin* **2010**, *48* (4), 38-42.
6. Okan, D.; Woo, K.; Sibbald, R. G., So What If You Are Blue? Oral Colloidal Silver and Argyria Are Out: Safe Dressings Are In. *Advances in Skin & Wound Care* **2007**, *20* (6), 326-330
10.1097/01.ASW.0000276415.91750.0f.
7. Rai, M.; Yadav, A.; Gade, A., Silver nanoparticles as a new generation of antimicrobials. *Biotechnology Advances* **2009**, *27* (1), 76-83.
8. Shinkai, M.; Yanase, M.; Suzuki, M.; Hiroyuki, H.; Wakabayashi, T.; Yoshida, J.; Kobayashi, T., Intracellular hyperthermia for cancer using magnetite cationic liposomes. *Journal of Magnetism and Magnetic Materials* **1999**, *194* (1–3), 176-184.
9. Cherukuri, P.; Glazer, E. S.; Curley, S. A., Targeted hyperthermia using metal nanoparticles. *Advanced Drug Delivery Reviews* **2010**, *62* (3), 339-345.

10. Roy, I.; Ohulchansky, T. Y.; Pudavar, H. E.; Bergey, E. J.; Oseroff, A. R.; Morgan, J.; Dougherty, T. J.; Prasad, P. N., Ceramic-Based Nanoparticles Entrapping Water-Insoluble Photosensitizing Anticancer Drugs: A Novel Drug–Carrier System for Photodynamic Therapy. *Journal of the American Chemical Society* **2003**, *125* (26), 7860-7865.
11. Griffith, T. M.; Lewis, M. J.; Newby, A. C.; Henderson, A. H., Endothelium-derived relaxing factor. *Journal of the American College of Cardiology* **1988**, *12* (3), 797-806.
12. Dahl, A.; Russell, D.; Nyberg-Hansen, R.; Rootwelt, K., Effect of nitroglycerin on cerebral circulation measured by transcranial Doppler and SPECT. *Stroke* **1989**, *20* (12), 1733-1736.
13. MASON, D. T.; BRAUNWALD, E.; Bullock, F. A.; King, C. V., The Effects of Nitroglycerin and Amyl Nitrite on Arteriolar and Venous Tone in the Human Forearm. *Circulation* **1965**, *32* (5), 755-766.
14. Haley, T. J., Review of the physiological effects of amyl, butyl, and isobutyl nitrites. *Clinical toxicology* **1980**, *16* (3), 317-329.
15. Schwartz, E. J.; Wong, P.; Graydon, R. J., Sildenafil Preserves Intracorporeal Smooth Muscle After Radical Retropubic Prostatectomy. *The Journal of Urology* **2004**, *171* (2, Part 1), 771-774.
16. Brock, G. B.; McMahon, C. G.; Chen, K.; Costigan, T.; Shen, W.; Watkins, V.; Anglin, G.; Whitaker, S., Efficacy and safety of tadalafil for the treatment of erectile dysfunction: results of integrated analyses. *The Journal of urology* **2002**, *168* (4), 1332-1336.
17. Lau, L.-C.; Adaikan, P. G., Mechanisms of direct relaxant effect of sildenafil, tadalafil and vardenafil on corpus cavernosum. *European Journal of Pharmacology* **2006**, *541* (3), 184-190.
18. Singh, R. J.; Hogg, N.; Joseph, J.; Kalyanaraman, B., Mechanism of Nitric Oxide Release from S-Nitrosothiols. *Journal of Biological Chemistry* **1996**, *271* (31), 18596-18603.
19. Lipton, A. J.; Johnson, M. A.; Macdonald, T.; Lieberman, M. W.; Gozal, D.; Gaston, B., S-Nitrosothiols signal the ventilatory response to hypoxia. *Nature* **2001**, *413* (6852), 171-174.

20. Aldrich, S. MSDS for S-Nitroso-N-acetyl-DL-penicillamine (N3398). http://www.sigmaaldrich.com/MSDS/MSDS/PrintMSDSAction.do?name=msdspdf_13102931629548.
21. Caron, G. A., The Role of Penicillenic Acid and Penicillamine in Contact-Type Sensitivity to Penicillin. *Immunology* **1963**, *6* (1), 81-93.
22. Taladriz-Blanco, P.; Pastoriza-Santos, V.; Pérez-Juste, J.; Hervés, P., Controllable Nitric Oxide Release in the Presence of Gold Nanoparticles. *Langmuir* **2013**, *29* (25), 8061-8069.
23. Jana, N. R.; Gearheart, L.; Murphy, C. J., Evidence for Seed-Mediated Nucleation in the Chemical Reduction of Gold Salts to Gold Nanoparticles. *Chemistry of Materials* **2001**, *13* (7), 2313-2322.
24. Jana, N. R.; Gearheart, L.; Murphy, C. J., Seeding Growth for Size Control of 5–40 nm Diameter Gold Nanoparticles. *Langmuir* **2001**, *17* (22), 6782-6786.

Chapter 6

Epilogue

No research project is truly over, and this is no exception. There are many experiments that could not be completed and some that could be improved upon, and those will be discussed here.

Through the course of the studies the main focus has been the homocoupling reaction of arylboronic acids, which was studied using a variety of catalysts and solvent systems. Using simpler analogues to the previously used catalyst, a thiol-containing bisimidazolylpalladium catalyst, the effect of pH on both the catalyst and the homocoupling reaction was probed, and the main effect was found to be in the displacement of halides from the palladium which occurs prior to the transmetallation. This was confirmed by the fact that the optimum pH for the reaction increased with halide concentration, indicating that the base was in equilibrium with the halide. This effect is observed both in CTAB which already has a high halide concentration and in Laureth-10 when halide is added to it. The error margins in some of the pH rate profile fits are quite large so in the future those should be bolstered with more data points to further define the profile and reduce the error margins. Additionally, the effect of chloride on the reaction should be further investigated in order to understand why increasing the chloride concentration lowers the optimum pH - the opposite of what one would expect, and what was found for the bromide concentration. Also, there is always value in synthesising additional catalysts or testing new surfactant systems. Mega-10 did not perform well in the homocoupling reaction, but an alternative non-ionic surfactant that did not cause excessive peroxidation would be extremely useful.

The homocoupling was also studied using two different nanoparticle catalysts. The first was immobilised on polystyrene beads and could be recovered by centrifugation. The recovery of

activity was never 100%, but it is unclear if this was down to recovery of the particles or another process that deactivates the palladium. Perhaps using the larger beads would improve this reaction, as they should be easier to recover. If the activity recovery still remains poor with larger beads, then that would imply that the palladium is being deactivated. Since halide appears to deactivate these particles, they may not be suitable for the Suzuki-Miyaura cross-coupling reaction, but it would be interesting if the reaction could be tested.

The second nanoparticle system is a paper-immobilised palladium nanoparticle system. The group in Vigo that created it showed that it had remarkable re-usability in the homocoupling reaction - not appearing to lose any of its activity over several use cycles. It was unusual that the reaction was much slower under the reaction conditions employed here than under the similar conditions employed in Vigo. Also, due to time and resource constraints it was not possible to fully test the recovery of catalytic activity over as many cycles as was previously shown. The final experiment, the cross-coupling reaction with an excess of iodoanisole yielded an interesting result, it would be interesting to see how it performed with a slow release borate, such as a trifluoroborate, which could allow for a stoichiometric reaction with much reduced opportunity for the homocoupling side product. Another test would be to see if the presence of halide from the cross-coupling causes a reduction in the recovered activity as was found for the palladium polypyrrole nanocomposite. If so, that would limit the usefulness of the catalyst. Also, more investigation of the affect of ethanol concentration and pH on both the homocoupling and cross-coupling reaction would be beneficial, since the trends so far are not clear (and the cross-coupling should exhibit a preference for high pH).

Finally, whilst in Vigo the release of NO from CTAB capped gold nanoparticles was investigated. The release of NO from this system did not appear to be controllable, which was a shame, since tolerance for CTAB would have made experimenting with different sizes and shapes of nanoparticle easier and would possibly have protected the NO selective electrode from damage by the nanoparticles, which had previously been observed with citrate capped nanoparticles. However, it may still be that the pH was responsible for the non-stoichiometric release of NO, and this could be investigated it a pH probe that was not affected by the high concentration of gold nanoparticles, or some other means of measuring the suspension's pH could be employed.

Appendix

Appendix**A.1 - Crystallographic data for PdCl₂-2**Table 4. Bond lengths [Å] for PdCl₂-2.

C(1)-N(2)	1.462(5)
C(3)-C(4)	1.352(5)
C(3)-N(2)	1.374(5)
C(4)-N(5)	1.385(4)
C(6)-N(5)	1.334(4)
C(6)-N(2)	1.351(4)
C(6)-C(7)	1.479(5)
C(7)-C(8)	1.487(5)
C(8)-N(9)	1.327(4)
C(8)-N(12)	1.355(4)
C(10)-C(11)	1.351(5)
C(10)-N(9)	1.389(5)
C(11)-N(12)	1.367(5)
C(13)-N(12)	1.462(5)
C(14)-C(15)	1.453(6)
C(15)-N(15)	1.136(6)
N(5)-Pd(1)	2.032(3)
N(9)-Pd(1)	2.034(3)
Cl(1)-Pd(1)	2.3117(9)
Cl(2)-Pd(1)	2.2964(9)

Table 5. Bond angles [°] for PdCl₂-2.

C(4)-C(3)-N(2)	106.6(3)
C(3)-C(4)-N(5)	109.1(3)
N(5)-C(6)-N(2)	110.0(3)
N(5)-C(6)-C(7)	129.3(3)
N(2)-C(6)-C(7)	120.7(3)
C(6)-C(7)-C(8)	116.1(3)
N(9)-C(8)-N(12)	109.6(3)
N(9)-C(8)-C(7)	129.7(3)
N(12)-C(8)-C(7)	120.7(3)
C(11)-C(10)-N(9)	108.2(3)
C(10)-C(11)-N(12)	107.3(3)
N(15)-C(15)-C(14)	179.5(5)
C(6)-N(2)-C(3)	107.9(3)
C(6)-N(2)-C(1)	125.6(3)
C(3)-N(2)-C(1)	126.5(3)
C(6)-N(5)-C(4)	106.4(3)
C(6)-N(5)-Pd(1)	127.1(2)
C(4)-N(5)-Pd(1)	126.1(2)
C(8)-N(9)-C(10)	107.0(3)
C(8)-N(9)-Pd(1)	127.0(2)
C(10)-N(9)-Pd(1)	125.8(2)
C(8)-N(12)-C(11)	107.8(3)
C(8)-N(12)-C(13)	125.7(3)
C(11)-N(12)-C(13)	126.5(3)
N(5)-Pd(1)-N(9)	90.00(12)
N(5)-Pd(1)-Cl(2)	176.09(8)
N(9)-Pd(1)-Cl(2)	91.00(9)
N(5)-Pd(1)-Cl(1)	91.81(8)
N(9)-Pd(1)-Cl(1)	175.91(8)
Cl(2)-Pd(1)-Cl(1)	87.43(3)

A.2 - Crystallographic data for PdCl₂-5Table 6. Bond lengths [Å] for PdCl₂-5.

C(1)-C(2)	1.353(5)
C(1)-N(1)	1.378(4)
C(1)-H(1)	0.9500
C(2)-N(2)	1.374(4)
C(2)-H(2)	0.9500
C(3)-N(1)	1.332(4)
C(3)-N(2)	1.344(4)
C(3)-C(4)	1.506(5)
C(4)-C(5)	1.500(5)
C(4)-C(9)	1.547(5)
C(4)-H(4)	1.0000
C(5)-N(3)	1.334(4)
C(5)-N(4)	1.351(4)
C(6)-C(7)	1.339(5)
C(6)-N(4)	1.381(5)
C(6)-H(6)	0.9500
C(7)-N(3)	1.377(4)
C(7)-H(7)	0.9500
C(8)-N(2)	1.456(4)
C(8)-H(8A)	0.9800
C(8)-H(8B)	0.9800
C(8)-H(8C)	0.9800
C(9)-C(10)	1.517(5)
C(9)-H(9A)	0.9900
C(9)-H(9B)	0.9900
C(10)-C(11)	1.529(5)
C(10)-H(10A)	0.9900
C(10)-H(10B)	0.9900
C(11)-H(11A)	0.9800
C(11)-H(11B)	0.9800
C(11)-H(11C)	0.9800
C(12)-N(4)	1.469(5)

C(12)-H(12A)	0.9800
C(12)-H(12B)	0.9800
C(12)-H(12C)	0.9800
N(1)-Pd(1)	2.002(3)
N(3)-Pd(1)	2.035(3)
Cl(1)-O(1)	0.688(19)
Cl(1)-Pd(1)	2.374(4)
Cl(2)-O(3)	0.73(3)
Cl(2)-Pd(1)	2.3229(19)
Pd(1)-O(4)	1.91(2)
Pd(1)-O(2)	1.957(17)
O(1)-O(2)	1.10(3)
O(3)-O(4)	1.13(4)

Table 7. Bond angles [°] for PdCl₂-5.

C(2)-C(1)-N(1)	108.5(3)
C(2)-C(1)-H(1)	125.8
N(1)-C(1)-H(1)	125.8
C(1)-C(2)-N(2)	106.7(3)
C(1)-C(2)-H(2)	126.6
N(2)-C(2)-H(2)	126.6
N(1)-C(3)-N(2)	109.5(3)
N(1)-C(3)-C(4)	126.3(3)
N(2)-C(3)-C(4)	124.2(3)
C(5)-C(4)-C(3)	110.7(3)
C(5)-C(4)-C(9)	112.4(3)
C(3)-C(4)-C(9)	113.5(3)
C(5)-C(4)-H(4)	106.6
C(3)-C(4)-H(4)	106.6
C(9)-C(4)-H(4)	106.6
N(3)-C(5)-N(4)	109.7(3)
N(3)-C(5)-C(4)	126.5(3)
N(4)-C(5)-C(4)	123.8(3)
C(7)-C(6)-N(4)	106.7(3)
C(7)-C(6)-H(6)	126.6
N(4)-C(6)-H(6)	126.6
C(6)-C(7)-N(3)	109.5(3)
C(6)-C(7)-H(7)	125.3
N(3)-C(7)-H(7)	125.3
N(2)-C(8)-H(8A)	109.5
N(2)-C(8)-H(8B)	109.5
H(8A)-C(8)-H(8B)	109.5
N(2)-C(8)-H(8C)	109.5
H(8A)-C(8)-H(8C)	109.5
H(8B)-C(8)-H(8C)	109.5
C(10)-C(9)-C(4)	116.2(3)
C(10)-C(9)-H(9A)	108.2
C(4)-C(9)-H(9A)	108.2
C(10)-C(9)-H(9B)	108.2

C(4)-C(9)-H(9B)	108.2
H(9A)-C(9)-H(9B)	107.4
C(9)-C(10)-C(11)	112.0(3)
C(9)-C(10)-H(10A)	109.2
C(11)-C(10)-H(10A)	109.2
C(9)-C(10)-H(10B)	109.2
C(11)-C(10)-H(10B)	109.2
H(10A)-C(10)-H(10B)	107.9
C(10)-C(11)-H(11A)	109.5
C(10)-C(11)-H(11B)	109.5
H(11A)-C(11)-H(11B)	109.5
C(10)-C(11)-H(11C)	109.5
H(11A)-C(11)-H(11C)	109.5
H(11B)-C(11)-H(11C)	109.5
N(4)-C(12)-H(12A)	109.5
N(4)-C(12)-H(12B)	109.5
H(12A)-C(12)-H(12B)	109.5
N(4)-C(12)-H(12C)	109.5
H(12A)-C(12)-H(12C)	109.5
H(12B)-C(12)-H(12C)	109.5
C(3)-N(1)-C(1)	107.2(3)
C(3)-N(1)-Pd(1)	125.1(2)
C(1)-N(1)-Pd(1)	127.7(2)
C(3)-N(2)-C(2)	108.1(3)
C(3)-N(2)-C(8)	127.7(3)
C(2)-N(2)-C(8)	124.2(3)
C(5)-N(3)-C(7)	106.6(3)
C(5)-N(3)-Pd(1)	124.0(2)
C(7)-N(3)-Pd(1)	129.1(2)
C(5)-N(4)-C(6)	107.5(3)
C(5)-N(4)-C(12)	127.1(3)
C(6)-N(4)-C(12)	125.2(3)
O(1)-Cl(1)-Pd(1)	171.5(8)
O(3)-Cl(2)-Pd(1)	171.3(13)
O(4)-Pd(1)-O(2)	89.3(9)
O(4)-Pd(1)-N(1)	177.8(8)

O(2)-Pd(1)-N(1)	90.8(5)
O(4)-Pd(1)-N(3)	92.6(8)
O(2)-Pd(1)-N(3)	177.8(5)
N(1)-Pd(1)-N(3)	87.22(11)
O(4)-Pd(1)-Cl(2)	1.0(9)
O(2)-Pd(1)-Cl(2)	90.2(5)
N(1)-Pd(1)-Cl(2)	178.03(10)
N(3)-Pd(1)-Cl(2)	91.73(10)
O(4)-Pd(1)-Cl(1)	90.8(8)
O(2)-Pd(1)-Cl(1)	1.4(6)
N(1)-Pd(1)-Cl(1)	89.41(12)
N(3)-Pd(1)-Cl(1)	176.51(13)
Cl(2)-Pd(1)-Cl(1)	91.61(11)
Cl(1)-O(1)-O(2)	5.6(11)
O(1)-O(2)-Pd(1)	177.4(16)
Cl(2)-O(3)-O(4)	4.7(15)
O(3)-O(4)-Pd(1)	177(3)

A.3 Absorbances at 223 nm for Figure 16 - pK_a of catalyst PdCl₂-2 (10 μ M) in laureth-10 (100 mM), NaBr (50 mM) and borate buffer (10 mM) at 30 °C.

pH	Absorbance (AUs)
4.42	2.151
5.14	2.19894
7.37	1.99921
7.94	1.89533
8.47	1.77867
8.92	1.69319
9.34	1.61684
10.24	1.59674

A.4 Absorbances at 212 nm for Figure 19 - pK_a of catalyst PdCl₂-2 (10 μ M) in laureth-10 (100 mM), NaCl (50 mM) and borate buffer (10 mM) at 30 °C.

pH	Absorbance (AUs)
4.53	0.71172
5.43	0.71942
7.73	0.63142
8.47	0.56804
9.33	0.55348
10.23	0.53749

A.5 Rate constants for Figure 34 - pH rate profile for the homocoupling of 6 (150 μ M) with unactivated (l) and activated (r) catalyst PdCl₂-2 (10 μ M) in laureth-10 (10 mM), NaBr (10 mM) and borate buffer (10 mM) at 30 °C.

pH	k_{obs} (unactivated) min ⁻¹	k_{obs} (activated) min ⁻¹
7.28	0.00353	5.2×10^{-4}
7.93	0.0092	--
8.46	0.022	0.01594
8.89	0.02232	0.01241
9.86	0.018	0.00972
10.19	0.01552	0.00161

A.6 Rate constants for Figure 35 - pH rate profile for the homocoupling of 6 (150 μM) with unactivated (l) and activated (r) catalyst $\text{PdCl}_2\cdot 2$ (10 μM) in laureth-10 (10 mM), NaBr (50 mM) and borate buffer (10 mM) at 30 $^\circ\text{C}$.

pH	k_{obs} (unactivated) min^{-1}	k_{obs} (activated) min^{-1}
7.35	0.003	2.7×10^{-4}
7.94	0.00612	0.00265
8.48	0.01091	0.00826
8.94	0.01539	0.01037
9.38	0.02452	0.00875
9.89	0.02659	0.00461
10.26	0.01194	--

A.7 Rate constants for Figure 36 - pH rate profile for the homocoupling of 6 (150 μM) with unactivated (l) and activated (r) catalyst $\text{PdCl}_2\cdot 2$ (10 μM) in laureth-10 (10 mM), NaBr (250 mM) and borate buffer (10 mM) at 30 $^\circ\text{C}$.

pH	k_{obs} (unactivated) min^{-1}	k_{obs} (activated) min^{-1}
7.16	0.00272	7×10^{-5}
7.74	0.0046	7.6×10^{-4}
8.25	0.0062	0.00234
8.69	0.01027	0.00287
49.16	0.01013	0.00416
9.61	--	0.00259

A.8 Data for Figure 37 - pH optimum and $\text{p}K_{\text{a}}$ against bromide concentration for the homocoupling reaction of 6 (100 mM) with unactivated and activated catalyst $\text{PdCl}_2\cdot 2$ (10 μM) in laureth-10 (10 mM) and borate buffer (10 mM) at 30 $^\circ\text{C}$.

$[\text{Br}^-]$ mmol	Optimum pH (unactivated)	Optimum pH (activated)
10	9.15 ± 0.13	8.83 ± 0.7
50	9.43 ± 0.15	8.95 ± 0.45
250	9.13 ± 0.27	9.1 ± 0.54

$[\text{Br}^-]$ mmol	$\text{p}K_{\text{a}}$ (unactivated)	$\text{p}K_{\text{a}}$ (activated)
10	10.29769 ± 0.13569	9.63626 ± 0.26334
50	10.88829 ± 0.89018	9.89843 ± 0.29408
250	10.30947 ± 1.08539	10.18399 ± 0.54879

A.9 Rate constants for Figure 38 - pH rate profile for the homocoupling of 6 (150 μM) with unactivated (l) and activated (r) catalyst $\text{PdCl}_2\cdot 2\text{H}_2\text{O}$ (10 μM) in laureth-10 (10 mM), NaCl (10 mM) and borate buffer (10 mM) at 30 $^\circ\text{C}$.

pH	k_{obs} (unactivated) min^{-1}	k_{obs} (activated) min^{-1}
7.46	0.00512	7.8×10^{-4}
8.01	0.0133	-
8.62	0.02054	0.00794
8.97	0.02976	-
9.51	0.03088	0.00466
10.33	0.02568	0.00213
7.46	0.00512	7.8×10^{-4}

A.10 Rate constants for Figure 39 - pH rate profile for the homocoupling of 6 (150 μM) with unactivated (l) and activated (r) catalyst $\text{PdCl}_2\cdot 2\text{H}_2\text{O}$ (10 μM) in laureth-10 (10 mM), NaCl (50 mM) and borate buffer (10 mM) at 30 $^\circ\text{C}$.

pH	k_{obs} (unactivated) min^{-1}	k_{obs} (activated) min^{-1}
7.32	0.00317	-
7.95	0.0078	0.00386
8.48	0.0155	0.01019
8.93	0.01692	0.01193
9.36	0.01601	0.00568
9.82	0.01992	0.00166

A.11 Rate constants for Figure 40 - pH rate profile for the homocoupling of 6 (150 μM) with unactivated (l) and activated (r) catalyst $\text{PdCl}_2\cdot 2\text{H}_2\text{O}$ (10 μM) in laureth-10 (10 mM), NaCl (250 mM) and borate buffer (10 mM) at 30 $^\circ\text{C}$.

pH	k_{obs} (unactivated) min^{-1}	k_{obs} (activated) min^{-1}
7.19	0.0023	-
7.72	0.0071	0.00284
8.28	0.01406	0.0095
8.73	0.01753	0.00841
9.2	0.0183	0.00557
9.89	0.01395	0.0029

A.12 Data for Figure 41 - pH optimum and pK_a against chloride concentration for the homocoupling reaction of **6 (100 mM) with unactivated and activated catalyst PdCl₂-2 (10 μ m) in laureth-10 (10 mM) and borate buffer (10 mM) at 30 °C.**

[Cl ⁻] mmol	Optimum pH (unactivated)	Optimum pH (activated)
10	9.59 \pm 0.45	8.77 \pm 0.23
50	9.83 \pm 21.4	8.63 \pm 0.29
250	9.11 \pm 0.03	8.58 \pm 0.21

[Cl ⁻] mmol	pK_a (unactivated)	pK_a (activated)
10	11.17031 \pm 0.44594	9.57637 \pm 0.2318
50	12.46134 \pm 21.42557	9.29238 \pm 0.2924
250	10.17698 \pm 0.03487	9.16112 \pm 0.20495